Institut für Landtechnik

der Rheinischen Friedrich-Wilhelms-Universität Bonn

In-Soil Measuring of Sugar Beet Yield Using UWB Radar Sensor System

Inaugural-Dissertation

zur

Erlangung des Grades

Doktor der Agrarwissenschaften

(Dr.agr.)

der

Hohen Landwirtschaftlichen Fakultät

der

Rheinischen Friedrich-Wilhelms-Universität

zu Bonn

vorgelegt im Mai 2007

von

Dipl.-Ing. M.Sc.mech.eng. Miodrag Konstantinović

aus

Novi Sad, Serbien

Referent:	Prof. Dr.-Ing. Peter Schulze Lammers
1. Korreferent	Prof. Dr.-Ing. Benno Kunz
2. Korreferent:	Prof. Dr. Milan Martinov
Tag der mündlichen Prüfung:	03. Juli 2007

D 98

Bezugsquelle: Institut für Landtechnik
Rheinische Friedrich-Wilhelms-Universität
Nussallee 5
53115 Bonn

Vervielfältigt und gedruckt mit Unterstützung des Deutschen Akademischen Austauschdienstes

Abstract

Yield mapping is a basic entity of the Precision Farming concept and provides crucial information about the success of cultivation. Several approaches to site-specific yield recording during the sugar beet harvest are known. Most of them are based on the weighing of sugar beets together with soil tare. Another real-time yield mapping approach with the option of plant population counting is based on estimating the mass of individual sugar beets on the basis of their maximal diameter.

The main goal of the research was to develop and evaluate a yield recording procedure based on radar technology, which will provide non-invasive in-soil detection and identification of single sugar beets in order to enable the counting of individual sugar beets and determining of the single sugar beet root mass. Further goals were to enhance the radar technology for other applications in the agriculture, as a general goal, and to define applicability restrictions of practical utilisation of the system for the sugar beet and similar crops.

The research activities have been divided into laboratory and field experiments. The results of the laboratory experiments have provided valuable information about the measuring system's behaviour, which enabled the successful field measurements.

The used method allowed the identification and detection of 90% to 96% of sugar beets under test in the various field conditions, with correlation coefficients between real sugar beet positions and detected positions of about 99%, and average positioning error from 1,1 to 3,6 cm. The correlation coefficients between single sugar beet root masses and recorded reflected energy amounts were for the majority of tests over 70%, and the best results have been on the level close to 90%.

This project was a joint venture of the Institute for Agricultural Engineering from Bonn and the Technical University of Ilmenau.

Kurzfassung

Die Ertragskartierung ist ein wesentlicher Bestandteil des Konzeptes „Precision Farming“. Die Erntemasse von Kulturpflanzen ist für den Landwirt eine elementare Information über den Erfolg pflanzbaulicher Maßnahmen. Es sind mehrere Verfahren zur Ertragsermittlung von Zuckerrüben während der Ernte mit dem Bezug auf Teilflächen bekannt. Ein sensorischer Ansatz besteht in der Pflanzenzählung und Ermittlung der Masse der einzelnen Zuckerrüben über den maximalen Durchmesser.

Das Hauptziel dieser Forschungsarbeiten war die Entwicklung und Bewertung eines berührungslosen Ertragserfassungssystems für Zuckerrüben, das teilflächenbasiert eine Zählung und Massebestimmung der Einzelrüben ermöglicht. Die weiteren Ziele bestanden in der Weiterentwicklung der Radartechnologie für andere Einsatzgebiete der Landwirtschaft und in der Bestimmung der Anwendbarkeitsgrenzen des Systems für Zuckerrüben und ähnliche Wurzelfrüchte.

Die Forschungsaktivitäten fanden im Labor und unter Feldbedingungen auf Versuchsparzellen eines typischen Zuckerrübenstandortes statt. Die Ergebnisse unter Laborbedingungen lieferten wertvolle Informationen, die erfolgreiche Feldmessungen ermöglicht haben.

Die angewendete Methode hat in unterschiedlichen Messbedingungen eine 90% bis 96% erfolgreiche Zuckerrübenidentifikation ermöglicht, mit Korrelationskoeffizienten zwischen tatsächlichen und detektierten Zuckerrübenpositionen von um 99% und einem durchschnittlichen Positionierungsfehler von 1,1 bis 3,6 cm. Die Korrelationskoeffizienten zwischen der Einzelrübenmasse und der gemessenen reflektierten Energiemenge lagen im Bereich von über 70% und die besten Ergebnisse erreichten Werte von 90%.

Das Projekt wurde in der Zusammenarbeit des Instituts für Landtechnik Bonn und des Instituts für Kommunikations- und Messtechnik der Technischen Universität Ilmenau durchgeführt.

Acknowledgments

My mother and brother I thank you for your love, for your support, and endless patience.

I would like to express my gratefulness to Prof. Martinov and Prof. Schulze Lammers for believing in me and for providing this opportunity, which enabled my professional advancement and allowed me to experience Germany, its culture and people in the best possible manner. I would also like to thank my dear friends and colleagues, especially Ms Beeken and Mr Lutz, for providing pleasant living and working atmosphere and being wonderful company during last several years, and Mr Düerkop and other members of the Technology of Crop Farming Department for their technical support and help.

I thank Mr Woeckel and Mr Sachs from Technical University of Ilmenau for the fruitful and pleasant cooperation, and Mr Dreesen and the whole staff of the Institute's workshop for their efforts and numerous useful advices during the project.

Special thanks to Mr Pätzold from the Institute for Soil Science (Institut für Bodenkunde) in Bonn for his advices and valuable soil analyses, Mr Ulbrich and the staff of the research station Marhof of the Agricultural Faculty in Bonn for growing of sugar beets in their greenhouses, and Mr Griese from the research station Frankenforst of the Agricultural Faculty in Bonn and Mr Hecker from Cologne for the readiness to allow the excavation of the soil in their fields.

Bonn, April 2007

Mom ocu za sve

Table of contents

1. Introduction

The data concerning the yield of crops are the main information which indicate the level of cultivation success. Natural and human-induced spatial and temporal variability of fields and yields determines economical and environmental sustainability of the production. The determination of spatial and temporal variability and in turn economical and environmental sustainability are the basis of the future-oriented agriculture and the general subject of this research venture.

Yield mapping, as one of the basic components of the Precision Farming concept, provides the crucial information about the success of cultivation. Several approaches to site-specific yield measuring during the sugar beet harvest are known today. Most of them are based on the weighing of sugar beets together with soil tare. One real-time yield mapping approach with the option of plant population counting is based on estimating the mass of individual sugar beets in the soil on the basis of their maximal diameter (Schmittmann 2002). The subsequent and improving idea was to develop a non-invasive yield mapping system for sugar beets based on radar technology.

The research venture described within this dissertation deals with the development and evaluation of a site-specific yield measuring radar sensor system designed to identify individual sugar beets and to estimate their size, i.e. mass by comparing the measured backscattered signal with signals stored in a databank.

The research activities have been conducted from the second half of 2004 to the begging of 2007 at the Institute for Agricultural Engineering, University of Bonn and at the Institute for Information Technology, Technical University Ilmenau. The venture was a part of the DFG (Deutsche Forschungsgemeinschaft – German Research Foundation) research project on precision farming and crop yield monitoring with the title “Teilflächespezifische Ertragmessung von Zuckerrüben im Boden mittels UWB Radarsensorsystems” (In-Soil Site-Specific Measuring of Sugar Beet Yield Using UWB Radar Sensor System).

2. State of the art – science and technology

2.1 Precision Farming

Precision Farming (PF) or Precision Agriculture (PA), as its known today, started in the late 1980s with the introduction of the global positioning system (GPS) into the agricultural sector, when it was realised how much farming data were spatially related. PF is defined as the management of arable variability to improve the economic benefit and reduce environmental impact (Blackmore 2003, Ludowicy et al. 2002). It is a systems approach to managing crops and land selectively, according to their needs. It utilizes expertise from many disciplines and integrates the advanced information technology tools and techniques to enable farm managers to get a better understanding and control of their fields (Blackmore 2003).

PF consists of three components: acquisition of data at an appropriate scale and frequency, interpretation and analysis of these data, and implementation of a management response at an appropriate scale and time. The most significant impact of PF is likely to be on how management decisions address variability in crop production systems (National Research Council 1997). Three types of variability have been identified: spatial variability, temporal variability and predictive variability (Blackmore 2003). The first type can be seen as changes across the field. According to Werner (Werner et al. 2002) spatial variability within a field is caused by small scale effects (soil, relief, lateral impacts, depth of water Table etc) or by anthropogenic impacts (land use, crop management, technical measures etc). Temporal variability is identified when parameters change over time. Predictive variability is the difference between what the manager assumed would happen and what actually happened. Each type of variability must be measured, assessed and possibly influenced, according to how significant it is (Blackmore 2003).

The ultimate goal in precision farming research is to understand and manage the variability found on most farms. This may not be realistic in the short to medium term but farm managers always have to make decisions in the face of uncertainty, i.e.

decisions have to be made even when some important information is not available (Blackmore 2003). To improve the decision making process, mathematical methods and simulation procedures (Seidl et al. 2004) have been developed to extract significant characteristics from data sets and present them in such a way as to be useful to the farm manager (Blackmore 2003). Managers should identify their own strategies and practices that allow them to deal effectively with the variability found on their farm (Blackmore 2003). The chosen management strategies and practices are defined by Diercks & Heitefuss (1994) as Integrated Farming, which has to ensure yields and provide economical success on a long term basis.

2.1.1 Yield mapping

Yield mapping and soil sampling are unavoidable starting points of any PF system (Ehrl et al. 2002, Fountas 2004). The average soil properties could be used to find parameters linked to yield variability and as a start to determine causes of variability in crop growth and yield, using a broader knowledge on the soil-plant interaction (Vrindts et al. 2003). High resolution soil maps are the best solution (Boess et al. 2003), but the cost of detailed soil sampling is a considerable obstacle (Fountas 2004).

Yield maps are produced by processing data from a harvesting machine, which has a *yield recording sensor system* integrated with a *positioning system* (GPS or dGPS) (Auernhammer et al. 1994, Ludowicy 2002). The principle and function of the GPS/DGPS are not going to be elaborated within this work. Yield maps provide the manager with a quantifiable picture of the yield and the variability within the yield. Other maps can be derived from yield maps to give temporal and spatial variability of yield as well as gross margins to help quantify the variability (Blackmore 2003). The yield recording system is equipped with one or more sensors and it is usually used only for the data acquisition. In some case acquired data are used for supervision and control (Schön 1993). In general, yield recording system provides two information: flow-rate of the biomass and at least one important biomass-specific value (e.g. moisture content, bulk density, non-biomass shares) (Schmittmann 2002). A general systematisation of yield recording principles is given in Table 1.1.

The first yield mapping systems were introduced in combine harvesters (Searcy et al. 1989). After only few years of development different yield mapping systems become commercially available for every new combine harvester (Demmel 1997). One general systematisation of the yield recording procedures after principle of measurement from tab. 2.1 was given by Schmittmann (Schmittmann 2002). According to this systematisation three basic measuring procedures could be identified as:

1. Measuring of physical values which are directly related to the yield mass.
2. Measuring of properties which are indirectly related to the yield mass.
3. Estimation of the yield mass.

Table 2.1 Systematisation of yield mass recording principles

Systematisation background	*Procedures*	*Measuring methods*	*Some method features*
Principle of measurement	*Direct*	Energy flow, Load change, Impulse	Directly connected to yield
	Indirect	Electromagnetic waves attenuation, Volume flow	Indirectly connected to yield
	Estimation	Counting, Sampling, Remote sensing	Correlation functions connected to yield
Chronology of recording	*Before the harvest*	Sampling probes and estimation	Possible site-specific information
	During the harvest	Different direct/indirect/ estimation procedures	Provide site-specific information
	After the harvest	Different weighing procedures	Cumulative information
Recorded physical property	*Energy*	Fuel consumption flow or torque change	Direct measuring principles
	Mass	Mass flow or cumulative mass weighing	Direct and indirect measuring principles
	Volume	Volume flow or volume change measuring	Indirect measuring principles
Spatial-temporal relationship	*Site-specific*	Possible by procedures before and during harvest	During the harvest, positioning necessary
	Cumulative	Procedures after the harvest	Shows average for a field/part of a field

The first group of measuring procedures is based on physical properties/values of the harvesting process which are directly connected to the harvested mass. These measuring systems are technically simple, but inaccurate and ambiguous. In this case three subgroups could be identified (Schmittmann 2002, Schmittmann & Schulze Lammers, 2003):

a) Measuring of the energy flow
The energy flow can be recorded over the fuel consumption of the harvester, or the torque change on parts of harvester's transportation system.

b) Measuring of the load change
The change of the weight of transport elements, the axle load, or the total weight of the harvester during the harvest is directly connected to the mass flow of the harvested material.

c) Measuring of the impulse
An impulse is defined as the integral of force over time. The integral of force and the mass flow are directly proportional if there is a constant velocity difference before and after the impact (Ehlert, 2000).

The second group of measuring procedures use some of measurable physical properties of the harvesting process which are indirectly related to the yield mass. The data acquired with this group of measuring principles has to be mathematically converted in order to give information about the harvested mass. In this case two subgroups could be identified (Schmittmann 2002, Schmittmann & Schulze Lammers, 2003):

a) Measuring of the attenuation of electromagnetic waves
The mass flow could be indirectly measured over the attenuation magnitude of radioactive waves, e.g. Cs and Am isotopes, (Kromer & Degen 1998), passing through the harvested material. This measuring procedure shows good results,

but it can not be accepted for biomass yield mapping because of its environmental and health hazards.

b) Measuring of the volume flow

The volume flow measuring is achieved by connecting the two-dimensional cross-section profile of the biomass flow with the speed of flow. The second possibility is to record the biomass level in the bunker. For these kinds of indirect measuring it is necessary to know the bulk biomass density, which has to be stable during the recording.

The third group of measuring procedures is using empirical estimation function for the yield mass estimation, and it is used if there are no applicable yield recording methods. These methods are used e.g. for predicting of the yield and are not influenced by mechanisation performance or ambiguous data interpretation. The disadvantage is the reliability and the accuracy of the estimation function. There are three basic method of yield estimation (Schmittmann 2002):

a) Single plant counting

This method estimates the yield by multiplying the number of plants with the empirical average mass of a single plant.

b) Single plant sampling

This procedure is the upgraded method of the single plant counting. In this procedure some other yield significant property/ies is recorded and put in the estimation function, which provides more accuracy in comparison with the original method.

c) Remote sensing

The mass estimation principle of remote sensing is based on recording some properties of the observed object without physical contact and is more comprehensive described in the Chapter 1.2.

2.1.2 Yield mapping systems for sugar beet and root crops

The advanced, environment friendly and sustainable sugar beet production, with increasing utilisation of the yield potentials, has to include several site-specific influencing factors (topographical characteristics, regional weather conditions, local soil types) on sugar beet yield and quality (Kromer & Degen 1998). Although the sugar beet yield and sugar content are not the only goals of the sugar beet production, they are its most important attributes (Winner 1981).

Since it is not possible to correlate the yield variation of other crops, e.g. grains (Fisher et al. 1997), and sugar beets, the yield mapping of sugar beets represents a necessary link in the Precision Farming chain. Therefore, the yield mapping of sugar beet represents a tool for: the variability measuring, the reduction of production costs, the decrease of harvesting losses, the increase of quality (Kromer et al. 2001), the enhanced logistic support, useful information for the harvester adjustments (Kromer & Degen 1998), and for the increase of efficiency of crop rotation (Isensee & Lieder 2001).

A yield mapping system for sugar beet harvesters has to deliver following three values/data (Schmittmann & Schulze Lammers, 2003):

1. The total mass of *harvested material*
2. The mass of *soil tare* and other *unwanted objects* (stones, sugar beet tops and foliage) or the mass of *clean sugar beets*
3. The *harvester's position* during harvesting

Measuring the mass of soil tare and other unwanted objects

There are no conventional recording systems which reliably distinguish the clean sugar beets from the soil tare and other unwanted objects (Schmittmann 2002). The ratio *clean/unwanted* (clean sugar beets/soil tare+unwanted material) can be only better or worse approximated using different estimation approaches. A systematisation according to the theoretical background of each estimation principle is shown in Table 2.2.

The following list contains a brief description and evaluation of known and tested estimation procedures:

1. Different gravimetric estimation procedures of the ratio clean/unwanted according to probe results after washing (Hien 1994), which are technically simple, but show low accuracy and depend on the estimator (Schmittmann 2002). For example: estimation procedure based on the density differences between clean sugar beets and other material called *Bonn soil tare information system* (BEIS – Bonner Erdanteil-Informationsystem) for the material in a transport vehicle/trailer (Hien 1994), and the procedure according to same principle for the material flow e.g. on a conveyor (Kromer 1999).
2. Optical principle based on image analysis with the aid of neural networks (Leppelmann et al. 1998). This optical approach also shows low estimation accuracy, most of all because the colour of soil is constantly changing its with water content, and because a soil-covered sugar beet could be classified as pure soil (Schmittmann 2002).
3. Radiometric procedure using γ waves for distinguishing between sugar beets and soil, which showed very good results with an error of ±2%, should be carefully utilised because of its environmental and health hazards (Hien 1994).

Beside the low accuracy and low reliability, in the list presented theoretical approaches for estimation of the ratio clean/unwanted usually deliver general, cumulative information about the harvesting results from one field or one part of the field, and do not deliver any usable site-specific information.

Table 2.2 Systematisation of the ratio clean/unwanted estimation principles (Hien 1994)

Theoretical background of the estimation principle	*Used physical property/ies*	*Known procedures*
Geometric	Size Form	Washing, Sieving, Pattern detection, Form detection
Gravimetric	Bulk density Gross density Water content	Weighing and volume measuring
Electric	Conductivity	Conductometry, TDR (time domain reflectometry)
Magnetic	Susceptibility Resonance	NMR (nuclear magnetic resonance), Gouy's balance
Acoustic	Absorption Characteristic impedance Wave speed	Reflection, Transmission
Optic	Reflection Remission Absorption Transmission	Reflectometry, Spectrometry
Radiometric	Attenuation	γ – transmission, Tomography, Radiography

Measuring of the total mass of harvested material

The material properties of sugar beets are considerably different from the properties of the grains or silage. Because of that it is not possible to apply the same yield recording principles used in grain or forage harvester (Demmel & Auernhammer 1998). In the following chapters several yield recording systems for root crops, primarily for sugar beet, but also for potatoes, sweet potatoes and peanuts are described and analysed. The recording systems are classified and evaluated according to the measurement principle into three general groups.

2.1.2.1 Direct yield recording procedures

Sugar beet

One yield recording system based on the measuring of the energy flow was developed at the Institute for Agricultural Engineering (Institut für Landwirtschaftliche

Verfahrenstechnik) in Kiel, Germany and it was tested during the sugar beet harvest in the year 1999 (Isensee & Lieder 2001). The measuring principle is based on the difference in in/out pressure of the hydraulic system of the elevator. The results of the tests with correctly adjusted sensors and not overloaded bunker showed the discrepancy of only few percent between the measured value and the real value of the sugar beet with soil tare.

The measuring principle of the load change was used in several sugar beet yield recording systems. A weighing system on the elevator of the sugar beet harvester used weighing rolls and showed a measuring error of 3,8% to 16%, depending from harvesting conditions and harvester type (Demmel & Auernhammer 1998). Two other weight-sensing systems were developed, tested, and evaluated on a laboratory test conveyor (Walter & Backer 2003). One system used 152 mm idler wheels attached to load cells. The instrumented idlers replaced an existing chain supporting idler on each side of the harvester outlet conveyor. The second system replaced two existing idlers on each side of the harvester outlet conveyor with slide bars covered with plastic. A mass flow rate was obtained from the combined load cell outputs and conveyor speed. Laboratory tests to predict accumulated weight showed a 2,5% error for the slide bar system and a 3,5% error for the idler wheel system.

The principle of impulse measuring on the last third of the cleaning turbine uses tangential acceleration of the rotating sugar beets to accomplish the constant speed of impact (Boos et al. 1998). This yield recording method is classified in indirect measuring by some authors (Demmel & Auernhammer 1998) because some of sugar beets never reach the impact point, which is corrected by system calibration.

Other root crops

The measuring principle of the load change was used in several *potato* yield recording systems and there are no substantial differences in comparison with the described systems for sugar beets. The elevators with load cells were comprehensively investigated (Campbell et al. 1994, Demmel & Auernhammer 1998) and the results show maximum error of about 5% (Kromer & Degen 1998).

Another yield recording system for *potato* uses the principle of impact on a bounce plate at the end of the conveyor belt (Ehlert 1996, Ehlert 1998a, Ehlert 1998b). Under laboratory conditions, a rubber coated plate with a force measuring instrument was placed in different positions in the discharge trajectory of a conveyor belt. For simulation of mass flow different masses of potatoes were placed on the conveyor belt. The results showed a linear relationship between the mass flow and the force. For some parameter combinations, the regression coefficient was even more than 0,99 and, in some cases, standard error was less than 0,083 kg/s (Ehlert 2000).

The yield recording systems based on mass flow, i.e. measuring of the mass increment with a load cell under the collecting basket of the *peanut* harvester (Thomas et al. 1997, Vellidis et al. 2001) showed good results and it was taken into consideration for the development of a comparable sugar beet yield recording system (Kromer & Degen 1998, Demmel & Auernhammer 1998). The general idea was to split the firm linkage between the bunker and chassis frame and to place a load cell, which would be a technologically bad solution. The second disadvantage of this system was the measuring principle. The information about the mass increment was relaying on the mass increase in short time intervals, which would be a lot less than the total measured weight (empty bunker + bunker content) and therefore required very sensitive and precise weighing equipment (Demmel & Auernhammer 1998).

The so far described systems based on the direct measuring principle do not give information about the amount of clean sugar beets.

2.1.2.2 Indirect yield recording procedures

Sugar beet

In last two decades several indirect continual yield mass recording systems on the basis of volume flow measurement in combination with the bulk density were developed at the Institute for Agricultural Engineering (Institut für Landtechnik) in Bonn, Germany. One stationary test facility on the conveyor of a cleaner-loader for testing of indirect sugar beet yield recording systems with laser scanner, ultrasound sensors, and mechanical sensors is shown in the Figure 2.1 (Schmittmann et al. 2001). The test of these three systems showed the best results for laser scanner

(error <4%) (Kromer & Degen 1998). The second best results, in the similar accuracy level with the laser scanner, showed the mechanical finger-sensing system, which recommended this principle for future low-cost solutions (Schmittmann 2002). The accuracy of ultrasonic device was about ±15%, which disqualified this measuring system for application (Schmittmann 2002).

Figure 2.1 Positions of the indirect sugar beet yield recording systems on the elevator: 1. laser system, 2. ultrasonic system, 3. mechanical finger-sensing system (Schmittmann et al. 2001)

Other root crops

The laser system and the mechanical finger-sensing system for sugar beet yield recording were tested for indirect continual yield mass recording for *potato* with comparable results (Schmittmann 2002).

As in the case of systems based on the direct measuring principles, previously described indirect measuring methods also do not give information about the amount of clean sugar beets.

2.1.2.3 Yield estimation procedures

Sugar beet

There were two sugar beet yield estimation systems developed at the Institute for Agricultural Engineering in Bonn. The first measuring principle is based on *counting*

of *sugar beets* in the soil (before lifting) and multiplying the number of sugar beets with the empirically determined *average mass of a single sugar beet* for the mapped field (Kromer & Degen 1998, Schmittmann & Hien 2001). The second system is the upgrade of the first one and the improvement is based on additional information on *biotechnological properties of single sugar beets*, which delivers the site-specific dimension (Schmittmann & Hien 2001, Schmittmann 2002).

The first method of sugar beet yield recording can be mathematically described as (Schmittmann & Hien 2001):

$$m' = \frac{n \cdot m_{single}'}{l_{DD} \cdot s_d} \qquad 2.1$$

m'	yield mass, t/ha
n	number of sugar beets, -
m_{single}'	empirical average mass of a single sugar beet for the whole field, kg
l_{DD}	measured length in the driving direction, m
s_d	distance between sugar beet rows, m

According to tests made with mechanical finger-sensing system and laser scanner, the in-soil sugar beet counting accuracy is very high from 95% (Schmittmann & Hien 2001) to 98% (Schmittmann 2002). The accuracy of this method depends on the approximated average single sugar beet mass. These data are normally distributed and according to measurements in the period from 1992 to 1998 the arithmetical mean values were between 710 g and 961 g (Schmittmann 2002).

The second, enhanced method can be mathematically described as (Schmittmann 2002):

$$m'' = \frac{\sum m_{single}''}{l_{DD} \cdot s_d} \qquad 2.2$$

The general correlation function between the maximum diameter of a single sugar beet and its mass, which showed the best correlation results, was the power function:

$$m_{single}'' = f(d_{max}) = a \cdot d_{max}^{\ b} \qquad 2.3$$

d_{max} maximum diameter of the single sugar beet, mm

a, b empirically determined coefficients, -

This general correlation function represents the additional measurable biotechnological property used for upgrading of the first simple system. It correlates with the empirical data with around 90% accuracy ($0,87 < R^2 < 0,94$).

The method used for sugar beet diameter measuring during the harvest, allowed only the measurement in the driving direction. The system is schematically shown in Figure 2.2 (Schmittmann & Hien 2001). In this case, the correlation coefficient between the mass of a single sugar beet and the *diameter in the driving direction* was 2 to 4% lower than in the case of the maximum diameter (Schmittmann & Hien 2001). The relationship between the diameter of a single sugar beet in the driving direction and its mass, shown in Figure 2.3 was (Schmittmann 2002):

$$m_{single}'' = 0,0084 \cdot d_{DD}^{\ 2,4433} \qquad 2.4$$

d_{DD} diameter of the single sugar beet in the driving direction, mm

This function has been calculated for the data taken in this period from 1992 to 1998 from 4 different fields and 4 different sugar beet varieties. The correlation coefficient of the function was $R^2 = 0,88$.

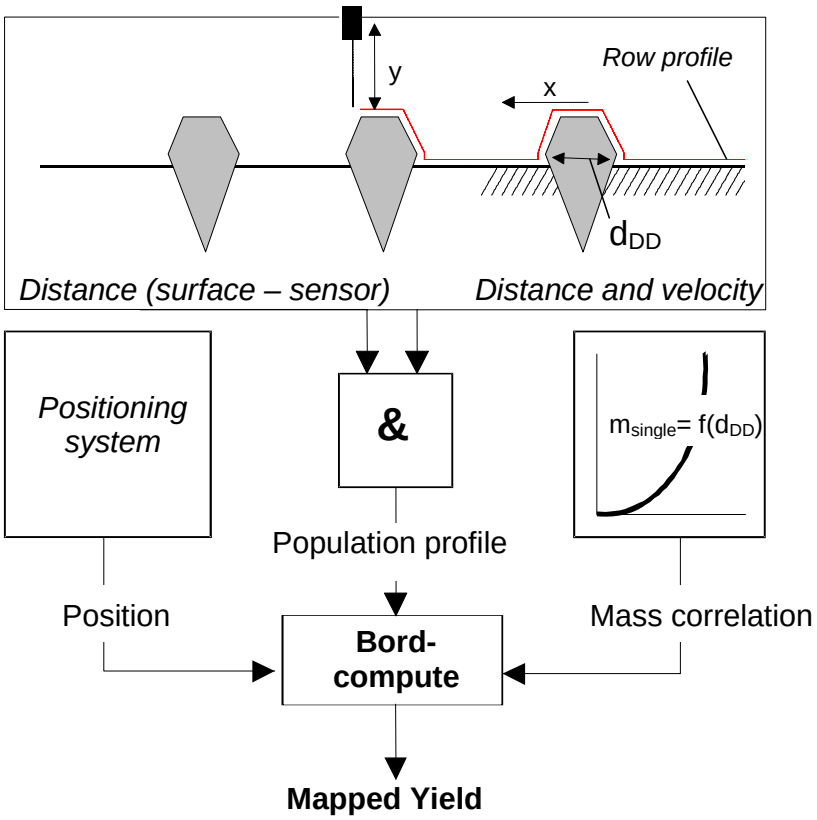

Figure 2.2 Sugar beet yield mapping system based on single sugar beet mass estimation according to the maximum diameter in the driving direction (Schmittmann & Hien 2001)

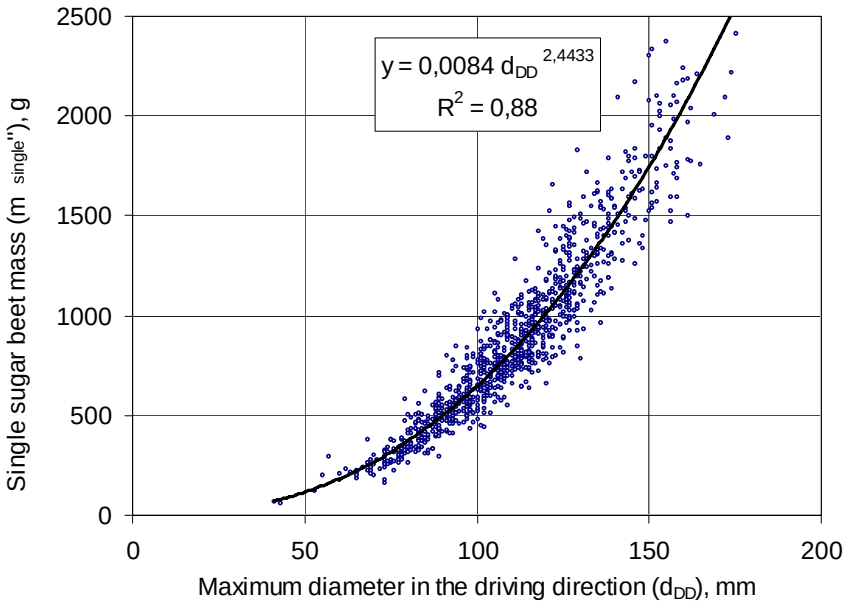

Figure 2.3 Relationship between the diameter in the driving direction of a single sugar beet and its mass (Schmittmann 2002)

Both previously described systems approximate the clean sugar beet mass up to certain level and therefore is the success of the harvester's cleaning system less significant, which represents the biggest advantage of these yield estimation systems.

Other root crops

The optical sensor system, which consists of a digital camera and LED light bar that illuminates the camera field of view with light in the red and near infrared (NIR) wavelengths was used for yield mapping of *potatoes* (Persson et al. 2004). The system was placed above the hopper on a potato harvester. In the hopper, a bin placed on load cells weighed the amount of potatoes that passed the sensor. Objects passing between the light bar and the camera shade or obscure parts of the structured light for a certain period of time. In the resulting image, the number of shaded pixels is used to calculate the object's cross-sectional area. The image is processed in real time, and a calculation of the object size is obtained using general linear model of variance. The results showed that this sensor system is suitable for distinguishing tuber size classes in both the laboratory and the field. Field tests with the sensor in a yield monitoring system showed low deviations from load cell measured weight and good consistency. The errors had an absolute mean of 1,3% (Persson et al. 2004).

Similar to the previous system, a machine vision system was developed for mass estimation of *potatoes* based on 2D information from a line scan camera placed above a transport belt of a potato harvester (Hofstee & Molema 2002). Different dimensions (mass and volume) of two potato varieties, different shapes and size classes were measured by hand and image processing to develop different models. Regression analysis was used to determine relations between potato volume and potato dimensions. The average prediction error of the best model was 0,27%. This model was used to estimate potato volume from line scan images of harvested potatoes on a moving transport belt. Applying the model to this dynamic situation showed an average deviation on batch level ranging from 1,5 to 2,6%. This gives, together with an estimated error of 2% for potato density, a mass estimation error between 3,5% and 4,6%. The authors noticed the need to improve the system by

introducing one correctional algorithm (approximate the shape of potatoes with ellipsis) for the soil tare estimation (Hofstee & Molema 2003), which slightly increased the error of the estimation model to 1% and caused some data processing problems.

A image-based system for *sweet potato* yield mapping (Gogineni et al. 2002) was equipped with a progressive-scan camera and illumination system, mounted at the top of the harvester's conveyor to block ambient light. The rest of the conveyor's opening was covered with flexible canvas door in order to block the ambient light and let sweet potatoes through. The estimation of the yield weight was based on multiple-linear regression and neural networks. The grade classifications were based on linear discriminant analysis and neural networks. The system was tested in laboratory and in field conditions. The laboratory results of sweet potato weights were highly correlated (R^2 = 0,96) with actual weights, and grade classifications of sweet potatoes were over 90% accurate. The system was also tested on sweet potatoes moving on a harvester's conveyor belt in the field, which also showed highly correlated weights (R^2 = 0,91). Grade classifications during harvesting were less accurate than in the laboratory (R^2 = 0,73 in the best case). The problem of soil tare was also identified. The authors suggested the harvest in dry conditions and the data processing algorithm enhancement, similar to correctional algorithm from Hofstee & Molema (Hofstee & Molema 2003).

2.1.2.4 Problems of sugar beet yield recording procedures

The system analysis of known procedures for sugar beet and root crops yield recording gives the following list of problems or incomplete solutions (Schmittmann & Schulze Lammers, 2003):

1. The mass of soil tare and *unwanted objects* (stones, sugar beet tops, foliage) are recorded together with the sugar beet yield.
2. There are various technical problems like swinging of the whole harvester or irregular oscillations/vibrations, which influence measuring errors.
3. A part of sugar beet stays uncollected in the field because of insufficient harvesting quality (to low-irregular topping and root-tips brakeage), and it is not included in the recording.

In addition to the list given by Schmittmann & Schulze Lammers the general lack of homogeneity of the material in the field causes several error sources as follows:

4. Season-dependant, site-specific and unreliable approximation/correlation functions, based on data gained by time-consuming empirical procedures e.g. the arithmetical mean value of the single sugar beet mass.
5. Deviations from mean values of relevant sugar beet properties e.g. variable bulk density on a conveyor.
6. Misinterpretation of measured data e.g. the reliability that the detected object in the sugar beet row and its diameter belong to a sugar beet (and not stone, leaf or soil lump).

Table 2.3 Significance analyse of observed problems for one representative yield recording method of each recording principle

Yield recording problems	*Recording procedure*		
	Direct Load cell measuring system on the harvester elevator	*Indirect* Laser scanner system for volume flow measuring	*Estimation* *Approximation based on the diameter in the driving direction*
1. Soil tare and other unwanted objects	2	2	*1*
2. Technical problems	2	1	*1*
3. Uncollected sugar beet parts	2	2	*0*
4. Approximation/ correlation functions	0	2	*2*
5. Large deviations from mean values	1	2	*2*
6. Misinterpretation of measured data	2	1	*2*
Total of problem-points	9	10	*8*

The assessment scale: 0 = no influence, 1 = moderate influence, 2 = strong influence

The influences of the listed problems on the typical representatives of all three yield recording principles are summarised in Table 2.3. The most independent yield recording method according to this comparative analysis would be the sugar beet yield mapping system based on single sugar beet mass estimation according to the diameter in the driving direction. The most important reason for the system's success is its independence from the soil tare and other unwanted objects as well as insignificance of the uncollected material, due to in-soil (before lifting) measuring of sugar beet properties.

2.2 Radar and radar applications

The German high frequency technician Christian Hülsmeyer invented in the year 1904 the „Telemobiloskop" for traffic supervision on the water pathways. He measured the running time of electromagnetic waves to a metal object (ship) and back, and calculated the distance using the constant wave speed. The first public demonstration of this device took place on the 18th May 1904 at the Hohenzollern Bridge in Cologne, Germany. This was the first *radar* test, and Hülsmeyer patented his invention in Germany with the title "*Verfahren, um entfernte metallische Gegenstände mittels elektrischer Wellen einem Beobachter zu melden*" and in the United Kingdom with the title "*Hertzian-wave projecting and receiving apparatus to indicate or give warning of the presence of a metallic body, such as a ship or a train, in the line of projections of such waves*". The term "RADAR" exists since the 1930s and it is an acronym for RAdio Detection And Ranging. (Anonymous 2006c, Anonymous 2006i).

The principle on which radar operates is very similar to the principle of sound-wave reflection. If the speed of sound in air is known, it is possible to estimate the distance and general direction of the object. The time required for the echo to return can be roughly converted to distance if the speed of sound is known. Radar uses electromagnetic energy pulses in the same manner. The electromagnetic energy in the form of radio waves is transmitted, and a part of this energy is reflected and returns to the radar, i.e. its antennas. This returned energy is called echo, just as it is in sound terminology. Radar uses the echo to determine the direction and distance of

the reflecting object. The Doppler Effect (apparent shift in the observed frequency of a wave) is used for measuring of the target/object speed and for differentiation between moving and fixed targets (Anonymous 2006c).

In the course of time, and especially during the Second World War, the development of the radar technology reached its peak primarily for military purposes (Anonymous 2006c). The results of this intensive development fortunately reached also some other spheres of life beside missile and weapon control, and delivered to the world many applications important for every day use:

- *Weather radar* or *Doppler Weather Radar* is able to detect the changes in frequency/wavelength resulting from storm motions toward or away from the radar (Anonymous 2006d).
- *Air traffic control radar, navigation* for ships and *surface surveillance* are invaluable for the today's World (Anonymous 2006c).
- *Speed gauges* also use the Doppler Effect for measurement of the object's speed with CW (Continuous Wave) radar signal using 24,125 GHz radar signals (Anonymous 2006g).
- *Speed Wedge* for ground speed measuring with 24,125 GHz radar signals (Schmitt 1986, Anonymous 2006e).
- *Driving assistance* like the Distronic distance-regulating braking and engine management control systems with a 77 GHz radar sensor, which ensures the vehicle maintains the cruising speed the driver has selected, while simultaneously keeping it at a safe distance from the vehicle in front (Anonymous 2006f).
- *Satellite and airborne remote sensing* for number of application in agriculture, forestry, geology and hydrology (Anonymous 2006h).
- *Non-invasive material tests* like the material structure test in civil engineering (Maierhofer et al. 1999).
- *GPR* (Ground Penetrating Radar) uses electromagnetic waves (generally from 10 MHz to 1 GHz) to acquire subsurface information (Anonymous 2006c).

Beside the known values of correct weather forecasts for successful planning in agriculture and introduction of ground speed radar sensor in various machines, according to Kühbauch (Kühbauch 2002), the remote sensing represents the future Precision Farming technology.

Remote Sensing refers to instrument-based techniques used in the acquisition and measurement of spatially organized data on some property/ies of an array of target points within the sensed scene that correspond to features, objects, and materials, doing this by applying one or more recording devices not in physical contact with the item/s under surveillance at a finite distance from the observed target, in which the spatial arrangement is preserved. Techniques involve gathering knowledge related to the sensed scene (target) by utilizing electromagnetic radiation, force fields, or acoustic energy through employing cameras, radiometers and scanners, lasers, radio frequency receivers, radar systems, sonar, thermal devices, seismographs, magnetometers, gravimeters, and other sensing instruments (Anonymous 2006a).

One detailed analysis of the principles and applications of GPR subsurface information acquisition and non-invasive measuring procedures, as subjects of the special interest for this work, is given in the following chapters.

2.2.1 Principle of GPR

The *Ground Penetrating Radar* (GPR) is a geophysical non-invasive method of soil subsurface information acquisition. According to general definition of the *Board on Earth Sciences and Resources*, USA (National Research Council 2000), the non-invasive methods are methods, involving little or no disruption of surface materials, able to: 1) sense and record the location of buried objects, 2) determine geological, geochemical and geobiological properties, 3) detect and map contaminants and monitor their movement, and 4) assess structural, lithologic, stratigraphic, and hydrogeologic conditions.

In general terms, the *GPR working principle* is similar to conventional air control radar. It is based on spreading of the electromagnetic wave radiated from the transmitter antenna through the material at a velocity which is determined primarily

by the *permittivity* (*dielectric constant*) of the material (usually soil) until it reaches a boundary layer (or other object) that has different electrical properties from the surrounding medium (host material). The boundary layer causes a reflection of electromagnetic wave and backscattering of a certain part of its energy, which is detected by a receiving antenna (Anonymous 2006j). Beside reflection, the principle of transmission could be also employed for GPR measurement (Annan 2002).

If the same antenna is used for transmitting and receiving the signal, then the antenna system is called a *monostatic* system. If the transmit and receive GPR antennas are separate entities (one transmitter or transmitter array and one receiver or receiver array), then this system is called a *bistatic* antenna arrangement (Anonymous 2006j).

Behaviour pattern of an electromagnetic wave

When a radar wave strikes the land (or some other surface and an object thereon), the partition into three modes of energy-interaction response occurs (Anonymous 2006a):

1. *Transmittance (T_r)* - some fraction (up to 100%) of the radiation penetrates into certain materials and passes through, generally with some diminution.
2. *Absorptance (A_b)* - some radiation is absorbed through electron or molecular reactions within the medium and a portion of this energy is then re-emitted, usually at longer wavelengths, and some of it remains and heats the target.
3. *Reflectance (R_e)* - some radiation (sometimes even 100%) reflects (moves away from the target) and scatters away from the target at various angles, depending on the surface roughness and the angle of incidence of the rays.

Because they involve ratios (to irradiance), these three parameters are dimensionless numbers (between 0 and 1), but are usually expressed as percentages. Following the Law of Conservation of Energy, these three modes represent the whole sent energy amount:

$$T_r + A_b + R_e = 1 \qquad 2.5$$

A fourth situation, when the emitted radiation results from internal atomic/molecular excitation, usually related to the heat state of a body, is a thermal process, which is not treated in this analyses.

In general GPR terms, if a portion of the wavefront (surface surrounding the advancing wave) encounters an object with a permittivity ε_2 different from the permittivity ε_1 of the surrounding material (host media), then that portion changes direction by a process that is called *scattering*. Scattering at the interface (boundary) between an object and the host material is of four main types illustrated in Figure 2.4 (Anonymous 2006j): a) specular reflection scattering, b) refraction scattering, c) diffraction scattering, and d) resonant scattering.

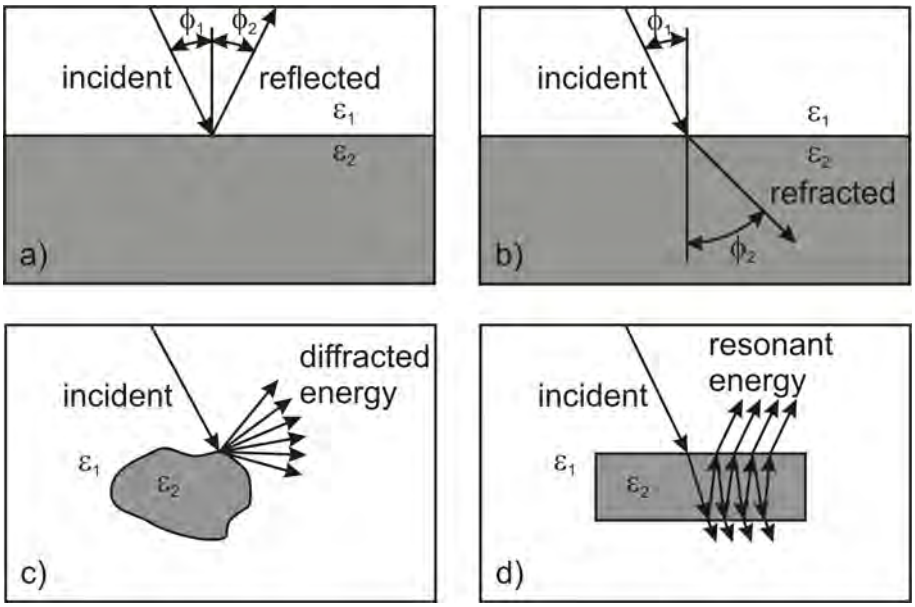

Figure 2.4 Scattering mechanisms: a) specular reflection scattering, b) refraction scattering, c) diffraction scattering, and d) resonant scattering (Anonymous 2006j)

Specular scattering, Figure 2.4 a), is based on the Law of Reflection, where the angle of reflection is equal to the angle of incidence:

$$\phi_1 = \phi_2 \qquad 2.6$$

When a wave reaches the object's surface, it scatters the energy according to the shape and roughness of the surface and the contrast of electrical properties between the host material and the object. Part of the energy is scattered back into the host material, while the other portion of the energy may travel into the object. The portion of the wave that propagates into the object is said to be *refracted*, Figure 2.4 b) (Anonymous 2006j). The angle under which the wave enters into the object is determined by Snell's law, which can be stated as follows:

$$\frac{v_1}{v_2} = \frac{\sin \phi_1}{\sin \phi_2} \qquad 2.7$$

Where v_1 and v_2 are the velocities of the wave through the upper and lower materials, respectively, and ϕ_1 and ϕ_2 are the angles of the path for the incident and refracted waves, respectively.

If the surface is smooth and continuous (e.g. a layer boundary), and velocity of the wave in the lower boundary is greater than velocity in the host material, then the wave will travel along the boundary with a velocity that is equal to velocity of wave in the object. The angle where this occurs is called *critical angle*, and can be determined by the following equation:

$$\frac{\varepsilon_2}{\varepsilon_1} = \frac{v_1}{v_2} = \sin \phi_1 \quad (\phi_2 = 90°) \qquad 2.8$$

The minimal distance between a receiver and a transmitter necessary in order to receive a refracted wave is called the critical distance. Refracted waves are uncommon as a propagation path for GPR, since the electromagnetic wave velocity tends to decrease with depth. This is a consequence of the fact that seismic and electromagnetic wave velocities in partially saturated and unconsolidated materials are affected primarily by the water content (Anonymous 2006j).

Diffraction scattering, Figure 2.4 c), occurs when a wave is partially blocked by a sharp boundary. Huygen's Principle of spherical spreading applies, but since the wave scatters off of a point, the wave spreads out in different directions. The nature of the diffracted energy depends upon the sharpness of the boundaries and the shape of object relative to the wavelength of the incident wave (Anonymous 2006j).

Resonant scattering occurs when a wave impinges on a closed object (e.g. a cylinder), and the wave bounces back-and-forth between different points of the boundary of the object. Every time the wave hits a boundary, part of the energy is refracted back into the host material, and part of the energy is reflected back into the object. This causes the electromagnetic energy to resonate (also called *ringing*) within the object, Figure 2.4 d). The resonant energy that is trapped inside of the object dissipates because part of it is re-radiated to the outside of the object. Closed objects are said to have a resonant frequency, which is based on the size of the object, the electrical properties of the object, and the surrounding material. However, the ability of an object to resonate depends on the wavelength with respect to dimensions of the object. The length of time that an object resonates is determined by the permittivity contrast between the object and the surrounding material (Anonymous 2006j).

GPR data visualization and interpretation

The objective of GPR data presentation is to provide a display of the acquired data that closely approximates an image of the subsurface, with the anomalies that are associated with the objects of interest located in their proper spatial positions. Good data display is an integral part of interpretation (Anonymous 2006j).

There are three types of displays - *radargrams* of surface data, including: 1) a one-dimensional trace (A-scan), 2) a two dimensional cross section (line scan or B-scan), and 3) a three dimensional display (C-scan or radar volume), shown in Figure 2.5 (Ulaby et al. 1981, Daniels 2004, Anonymous 2006j). Borehole data can be displayed as a two-dimensional cross section, or processed to be displayed as a velocity tomogram. A one-dimensional trace is not of very much value until several traces are

placed side-by-side to produce a two dimensional cross section, or placed in a three dimensional block view (Anonymous 2006j).

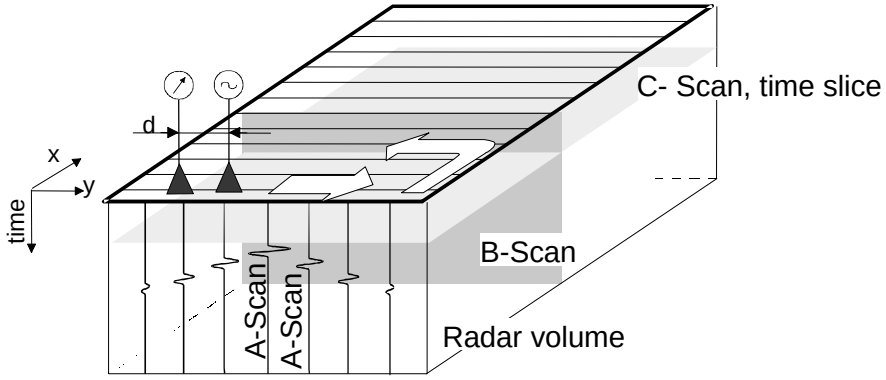

Figure 2.5 GPR data visualization (Ulaby et al. 1981)

A radargram is obtained by simply assigning a colour (or a variation of colour intensity) to amplitude ranges on the trace. There are several forms of radargrams a) gray-scale display ranging from black to white, b) colour intensity display using a single colour ranging from white (or black) to the pure form of the colour, and c) colour spectrum as shown in the radargram in Figure 2.6.

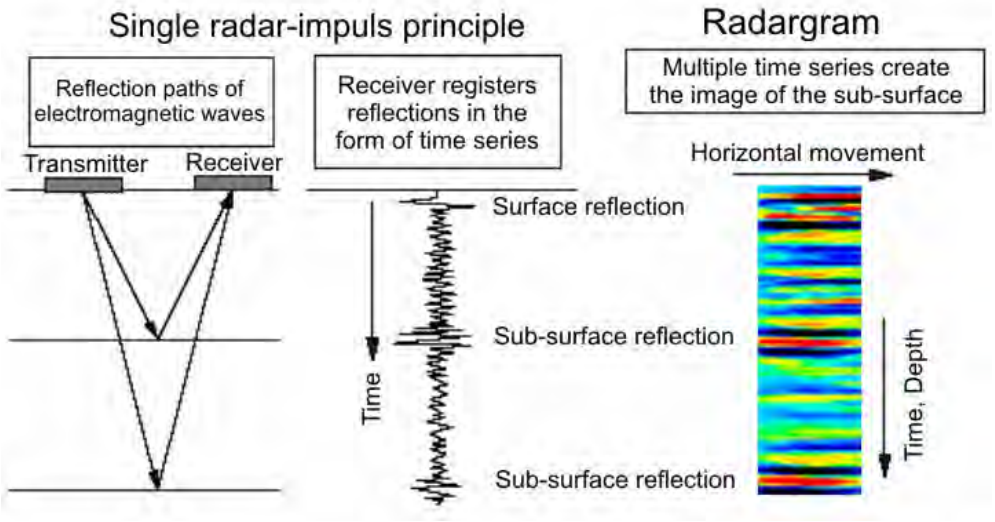

Figure 2.6 Single signal impulse behaviour and the GPR image of the sub-surface (Petersen et al. 2005)

The result of a single radar impulse transmitting, backscattering and receiving on two subsoil layers is shown in the Figure 2.6 in the middle in the form of time series

(Petersen et al. 2005). One example of a *radargram*, which is the collection of several single radar impulses recorded during the B-scan (horizontal movement), is shown on the right side of the Figure 2.6.

GPR object detection principle

The GPR detection principle is shown in Figure 2.6. The GPR performs object/target detection by sounding electromagnetic waves (E_i, g(t)) and measuring the reflected signal (E_r, s(t)) by a set of antennas, using several consecutive single signals like in Figure 2.7 a) and b).

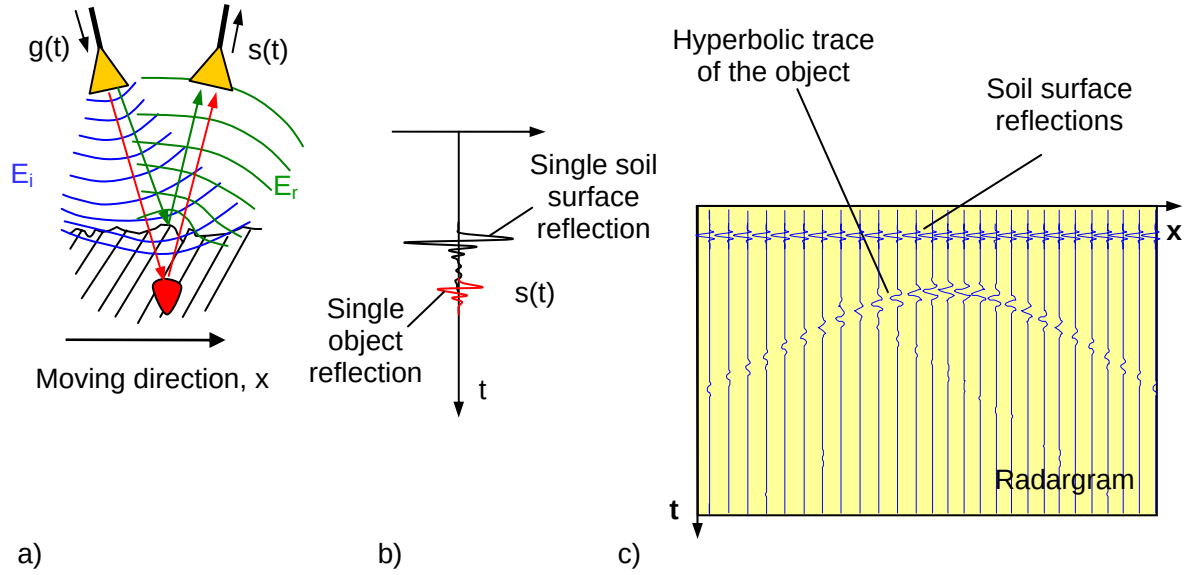

Figure 2.7 GPR detection principle: a) measured scenario and basic wavefront behaviour, b) reflections from the soil surface and an underground object, c) radargram with a hyperbolic trace of an underground object (Konstantinović et al. 2005)

Every obstacle with a permittivity different from the surrounding medium leads to the refraction and reflection of the incident wave. Thus, the measured signal s(t) is the sum of all reflections and scatterings from the rough surface as well as from all objects within the beam of the antenna, Figure 2.7 b).

The *roundtrip time* (antenna – object – antenna) provides data about the object distance to the antennas by the known wave velocity. This time interval is also called

the *travel time*. Electromagnetic waves travel at a specific velocity that is determined primarily by the permittivity of the material. The relationship between the velocity of the wave and material properties is the basis for using GPR to investigate the subsurface, i.e. the velocity is different between materials with different electrical properties. The basic unit of electromagnetic wave travel time is the nanosecond (1 ns = 10^{-9} s). Since the velocity of an electromagnetic wave in air is 3 x 10^{8} m/s (0,3 m/ns), then the travel time for an electromagnetic wave in air is approximately 3,33 ns per travelled meter (Anonymous 2006j).

The wave velocity is proportional to the inverse square root of the relative permittivity of the material (Daniels 2004). Since the permittivity of earth materials is always greater than the of the air, the travel time of a wave in a material other than air is always greater than 3,33 ns/m, i.e. the velocity is always smaller than 0,3 m/ns (Anonymous 2006j). More comprehensive analysis of the electromagnetic wave propagation behaviour is presented in the subsequent chapter.

In order to gain an image of the underground and to detect an underground object, the antennas are swept along the surface while they continuously gather the backscattered signals and form B-scan. The juxtaposed presentation of these time signals in a so-called *radargram* gives an impression of the distribution of materials and objects within the investigated soil, Figure 2.7 c). In this case, every *sufficiently large* obstacle with different permittivity in the beam of the antenna produces a hyperbolic trace in the radargram. Reflections from planar interfaces, e.g. from the soil surface, appear as a constant line. The surface reflections can be very strong, and they often cover small objects (Konstantinović et al. 2005).

2.2.2 Analysis of external and internal influential parameters on GPR measurements

The physical approaches which are used to explain the propagation of electromagnetic waves in dielectric materials have two main sources: electromagnetic wave theory and geometrical optics. The theory of geometrical optics is relevant only in cases when the wave length is shorter then the dimensions

of the object/medium under test or when involved materials can be considered as insulators (Daniels 2004).

Table 2.4 Properties of various materials measured at 100 MHz (Daniels 2004)

Material/Soil	*Relative permittivity range*	*Electrical conductivity, S/m*	*Attenuation, dB/m*
Clay (dry)	2 - 6	10^{-1} - 1	10 - 50
Clay (wet)	5 - 40	10^{-1} - 1	20 - 100
Fresh water	81	10^{-6} - 10^{-2}	0,01
Sand (dry)	2 - 6	10^{-7} - 10^{-3}	0,01 - 1
Sand (wet)	10 - 30	10^{-3} - 10^{-2}	0,5 - 5
Soil clay (dry)	4 - 10	10^{-2} - 10^{-1}	0,3 - 3
Soil clay (wet)	10 - 30	10^{-3} - 1	5 - 50
Soil loamy (dry)	4 - 10	10^{-4} - 10^{-3}	0,5 - 3
Soil loamy (wet)	10 - 30	10^{-2} - 10^{-1}	1 - 6
Soil sandy (dry)	4 - 10	10^{-4} - 10^{-2}	0,1 - 2
Soil sandy (wet)	10 - 30	10^{-2} - 10^{-1}	1 - 5

The energy of reflected electromagnetic waves - and, by implication, object detection - corresponds to the dielectric contrast between the target and the surrounding medium. This means that GPR indirectly measures the dielectric constant (permittivity) of the material through which the energy propagates. The dielectric constant measures the ability of a material to polarize or store energy through separation of bound charges. In the ground, the major effect in dielectric contrast is caused by water. Water has a high dielectric constant of about 80, air has a dielectric constant of ≈1 and dry soil materials and sediments between 3 and 10 (clays and silts as high as about 30 to 40) (Clement & Ward 2003). Further, the *permittivity* (dielectric constant) of the material determines the *propagation velocity* of the waves and it primarily depends upon water content (Daniels 2004). The apparent dielectric constant (complex value of dielectric constant) is almost independent of soil density, texture, salt content, and temperature changing (Topp et al. 1980). The *electrical conductivity* of soils caused by moisture, salinity and soil type influences the wave *attenuation*, which is usually strongly connected to the frequency. The most important

dialectical properties of water and some soil types are shown in Table 2.4 (Daniels 2004).

Propagation of electromagnetic waves in dielectric materials

The starting points of consideration of the propagation electromagnetic waves are Maxwell's equations. In the free space the magnetic susceptibility and electrical permittivity are constant (independent of frequency), and the medium is not dispersive. In a perfect dielectric medium there are no propagation losses and hence there is no consideration of the attenuation like in real dielectric media (Daniels 2004).

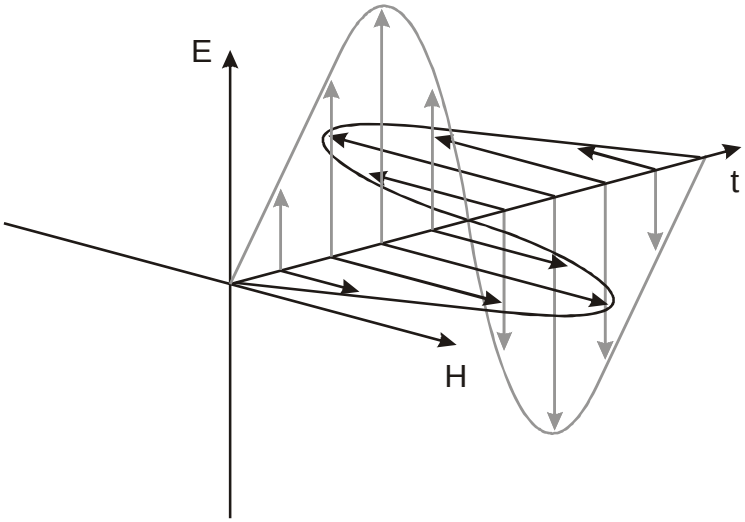

Figure 2.8 Propagation of electromagnetic waves in free space (Daniels 2004)

The electromagnetic wave propagation can be presented by a one-dimensional wave equation for propagation along z-axis, with perpendicular electric (E) and magnetic (H) fields as shown in Figure 2.8 (Daniels 2004).

$$\frac{\partial^2 E}{\partial z^2} = \mu\varepsilon \frac{\partial^2 E}{\partial t^2} \qquad 2.9$$

The velocity of wave propagation and velocity of light are respectively:

$$v = \frac{1}{\sqrt{\mu\varepsilon}} \qquad 2.10$$

$$c = \frac{1}{\sqrt{\mu_0\varepsilon_0}} \qquad 2.11$$

μ_0 absolute magnetic susceptibility of free space, $\mu_0 = 1{,}26 \cdot 10^{-6}$ Hm^{-1}

ε_0 absolute electrical permittivity of free space, $\varepsilon_0 = 8{,}86 \cdot 10^{-6}$ Fm^{-1}

μ absolute magnetic susceptibility of medium ($\mu = \mu_0 \cdot \mu_r$), Hm^{-1}

ε absolute electrical permittivity of medium ($\varepsilon = \varepsilon_0 \cdot \varepsilon_r$), Fm^{-1}

μ_r relative magnetic susceptibility, -

ε_r relative permittivity of medium, -

The relative permittivity ε_r has a value in the range from 1 to 80 for most geological materials, Table 2.4, and relative magnetic susceptibility μ_r has a value 1 for nonmagnetic geologic materials. Hence, the electromagnetic wave velocity in medium is proportional to the inverse square root of the relative permittivity of the material (Daniels 2004).

$$v_r = \frac{c}{\sqrt{\varepsilon_r}} \qquad 2.12$$

Electromagnetic waves propagating through *natural media* experience losses, to both the electric and magnetic fields, which causes attenuation of the original wave. In Equation 2.13 the complex permittivity of material is presented, where the imaginary part ε'' is related to the losses associated with both conductivity and frequency, and the nature of the parameter ε' relates to the relative permittivity (dielectric constant) (Daniels 2004).

$$\varepsilon = \varepsilon' - j\varepsilon'' \qquad 2.13$$

ε' real part of complex permittivity, -

$j\varepsilon''$ imaginary part of complex permittivity ($j = \sqrt{-1}$), -

For practical purposes at frequencies above 1 GHz the effect of the ε'' part of complex permittivity is low and is commonly disregarded by using time domain reflectometry (TDR) technology (Rial & Han 2000). The increase of frequency also causes the decrease of the dielectric constant of water (Harmsen et al. 2003). The phenomena of water permittivity changing with frequency changing is shown in Figure 2.9

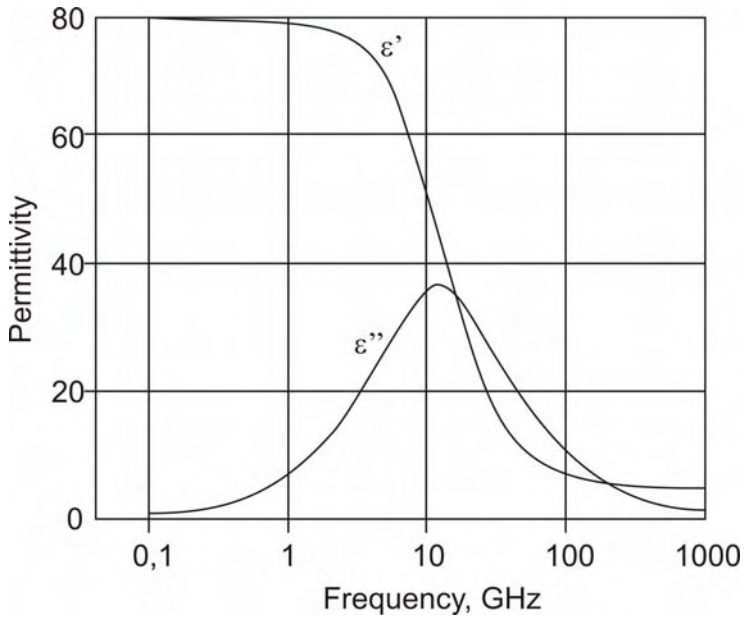

Figure 2.9 Relationship between frequency and permittivity of water (Paul & Speckmann 2004b)

When measurements are made on conducting materials, the measured parameter is the *apparent permittivity*:

$$\bar{\varepsilon} = \varepsilon_e' - j\varepsilon_e'' \qquad 2.14$$

ε_e' real part effective permittivity, -

ε_e'' imaginary part of effective permittivity, -

Penetration depth of GPR

Classical GPR devices operate with the centre frequency of their sounding signals below 1 GHz, which can promote penetration depth of few meters *under suitable conditions*, but it prevents a high image resolution and the detection of small objects (Konstantinović et al. 2005). On the other hand, a common concern of GPR service providers is whether or not GPR will be able to achieve the desired depth of penetration in the soils in the measured scenario (Anonymous 2006k). The penetration depth of GPR is determined by *antenna (working) frequency* and the *electrical conductivity* (moisture, soil type and salinity) of the earthen materials being profiled (Daniels 2004).

In many soils, high rates of signal attenuation severely restrict penetration depths and limit the suitability of GPR for a large number of applications (Anonymous 2006k). In saline and sodic soils, where penetration depths are often less than 25 cm (Daniels 2004), GPR is unsuited to most applications. In wet clays, where penetration depths are typically less than 1 m (Doolittle et al. 2002), GPR has very low potentials for many applications. However, GPR is highly suited to most applications in dry sands and gravels, where penetration depths can exceed 4 m with low frequency antennas (Smith & Jol 1995).

An illustration of the wide spectrum of *skin depths* as a function of soil volumetric water content and soil type (as *external* influences), and electromagnetic wave frequency (as the only *internal* factor in this analysis) is shown in Figure 2.10 (Ulaby et al. 1981). Skin depth provides an indication of the *penetration depth* of a GPR system.

The penetration depth is proportional to the inverse value of attenuation of the material (Daniels 2004) and it is directly connected to the wave frequency. For the frequency 1,4 GHz the penetration depths vary between 10 cm (water saturated soil) and 1 m (dry soil), for frequency 6 GHZ, the depths fluctuate between 1 cm and 10 cm, and for 30 GHz between 1 mm and 1 cm (Paul & Speckmann 2004b). The *sampling depth* on the other hand is the layer that is responsible for the reflection. Theoretically is this layer few tenths of the wave length, e.g. the sampling depth

using 1,4 GHz radar signal (wave length in air 21 cm) was between 2 and 5 cm, depending on the water content (Paul & Speckmann 2004b).

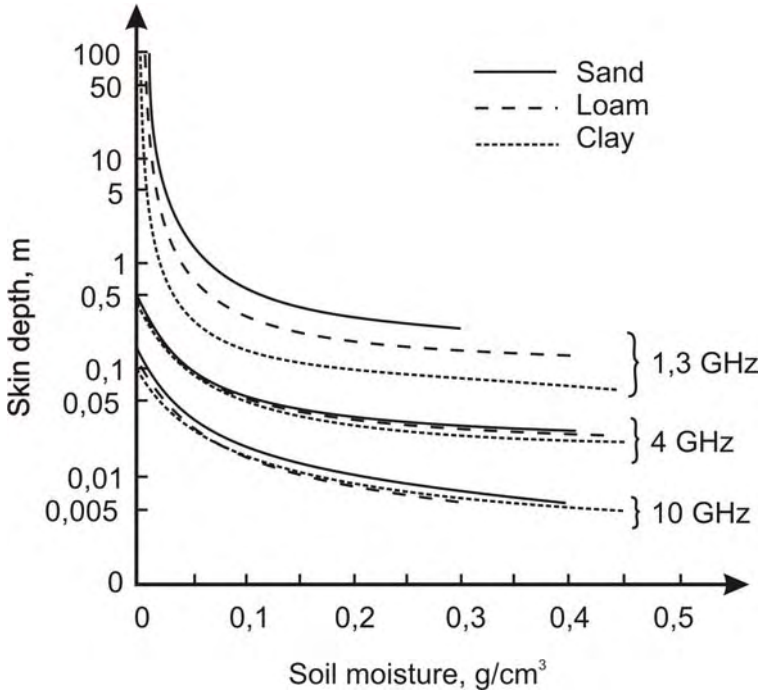

Figure 2.10 Skin depths as a function of soil volumetric water content, frequency and soil type (Ulaby et al. 1981)

Soils having high electrical conductivity rapidly attenuate radar energy, restrict penetration depths, and severely limit the effectiveness of GPR. The electrical conductivity of soils increases with increase in a) *water*, b) *clay* content and c) *soluble salt* content (Anonymous 2006k). Electrical conductivity is directly related to the amount, distribution, chemical composition, and phase (liquid, solid, or gas) of the *soil water*. At a given frequency, the attenuation of electromagnetic energy increases with increasing water contents (Daniels 2004).

Clays have greater surface areas and can hold more water than silt and sand fractions at moderate and higher water tensions. Because of their high adsorptive capacity for water and exchangeable cations, clays produce high attenuation losses (Daniels 2004). As a consequence, the penetration depth of GPR is inversely related to clay content. While soils with more than 35 percent clay are restrictive, soils with less than 10 percent clay are generally favourable to deep penetration with GPR (Anonymous 2006k).

Soils contain various proportions of different *clay minerals* (kaolin, mica, chlorite, vermiculite, smectite). The size, surface area, cation-exchange capacity (CEC), and water holding capacity of clay minerals vary greatly. Variations in electrical conductivity are attributed to differences in the CEC associated with different clay minerals (Saarenketo 1998). Electrical conductivity increases with increasing CEC (Saarenketo 1998). Soils with clay fractions dominated by high cation exchange capacity clays (smectite and vermiculite) are more attenuating to GPR than soils with an equivalent percentage of low cation exchange capacity clays (kaolin, gibbsite, and halloysite). Soils classified as kaolinitic, gibbsitic, and halloysitic characteristically have low cation-exchange capacity and low base saturation. As a general rule, for soils with comparable clay and water contents, greater depths of penetration can be achieved in soils of tropical and subtropical regions that have kandic or oxic horizons than in soils of temperate regions that have argillic horizons. Compared with argillic horizons, kandic and oxic horizons have greater concentrations of low activity clays (Anonymous 2006k).

Electrical conductivity is directly related to the concentration of *dissolved salts* in the soil solution at higher frequencies (Hook et al. 2004), as well as the type of exchangeable cations and the degree of dissociation of the salts on soil particles (Anonymous 2006k). The concentration of salts in the soil solution is dependent upon the degree of water-filled porosity, the soil texture, and the minerals found in soils. In semi-arid and arid regions, soluble salts and exchangeable sodium accumulate in the upper part of some soil profiles. These salts produce high attenuation losses that restrict penetration depths. Because of their high electrical conductivity, saline and sodic soils are considered unsuited to GPR (Anonymous 2006k).

Calcareous and gypsiferous soils are characterized by layers with secondary accumulations of calcium carbonate and calcium sulfate, respectively. These soils mainly occur in base-rich, alkaline environments in semi-arid and arid regions. High concentrations of calcium carbonate and/or calcium sulfate imply less intense leaching, prevalence of other soluble salts, greater quantities of inherited minerals from parent rock, and accumulations of specific mineral products of weathering. A

reduction in the depth of GPR signal penetration in soils that have high concentrations of calcium carbonate has been observed (Anonymous 2006k).

Prediction of propagation behaviour

The lack of adequate measuring methods for soil moisture and the high spatial and temporal variations in the degree of water content within most soils have important implications for the performance of a GRP system. This material parameters and geological conditions variability creates a situation with many degrees of freedom, and difficulties in accurate prediction of propagation behaviour (Daniels 2004), i.e. in correct interpretation of GPR acquired data.

In general there are two most influential spatially variable parameters on in-situ GPR measurements: *geological condition* (soil type and contents, which is temporally stable) and *water content* (temporally unstable).

The *first parameter* (or set of parameters) has very complex influence on electromagnetic wave behaviour because of both dielectric and conducting properties. The determination of the dielectric properties of earthen materials remains experimental and in-situ, although a large number of researchers sought to develop suitable models to link the properties of the material (physical, chemical and mechanical) to its electromagnetic parameters. In general it is not possible to make a reliable estimate of propagation velocity (relative permittivity) in a medium from a single measurement without supplementary information (Daniels 2004).

Since there is a limited knowledge of soils and it is not possible to forecast attenuation rates, penetration depths, and the general suitability of the soils to GPR, knowledge of the probable penetration depth and the relative suitability of soils would help to assess the appropriateness of using GPR and the probability of achieving acceptable results (Doolittle & Collins 2004, Anonymous 2006k). Soil attribute data have been used to develop thematic maps showing the relative suitability of soils for GPR applications in the USA. The GPR soil suitability map of the conterminous United States was complied at a scale of 1:250.000. However, as soil delineations are not homogenous and contain dissimilar inclusions, on-site investigations are

needed to confirm the suitability of each soil polygon for different GPR applications (Doolittle & Collins 2004, Anonymous 2006k).

An additional ambiguity factor in this analysis that is always important for any agricultural application is the soil surface roughness (Paul & Speckmann 2004b). The surface roughness causes electromagnetic surface scattering, which is difficult to predict and to model because of the complexity of natural surfaces and the difficulty in estimating appropriate input roughness parameters for agricultural fields having different tillage (roughness) states (Davidson et al. 2000).

The *second parameter* is more ambiguous, since even small amounts of water with relative permittivity of 80 cause significant increase of relative permittivity of the material (Daniels 2004). Many theoretical, or semi-theoretical and empirical models were developed to approximate the relationship: water content-dielectric properties (Weiler et al. 1998). The development of empirical models was based on measurement results of Time Domain Reflectometry with several frequency ranges, e.g. from authors Topp et al., Alharthi & Lange, Miller & Gaskin, Benedetto & Benedetto, Hallikainen et al., Wang & Schmugge (Harmsen et al. 2003) and similar procedures, like 50 MHz commercial soil-moisture probe “Hydra” (Rial & Han 2000).

The Time Domain Reflectometry (TDR) is a method with parallel rod type probe, which was in the past a wide-spread method for water content measurement especially for soil and grains, and it is still used for some measurement procedures. It measures water content in a wide range from the wave reflected from a probe inserted in the material under test. The water content of a material is measured from the attenuation or phase shift of the wave, or both of the parameters (Okamura 1999). The main disadvantages of TDR in comparison with the GPR moisture measurement are: it is a destructive method, it can not measure large volumes (Weiler et al. 1998), and it needs individual calibration for the measurement in porous materials such as coal (Zegelin et al. 1992).

The dielectric properties of soil have been comprehensively studied and there are numerous both empirical and theoretical models available. Systematic attempts have

been made to produce models of the dielectric behaviour of soils which use parameters obtained independently of the dielectric properties to be predicted. A number of models are believed to show reasonable agreement with experimental values over certain frequency range. Considerable difficulties are posed by the variability of the material, and none of the models developed is universally applicable. Simple models tend to be deficient, with the major discrepancy between theory and experiment being the frequency dependence of the observable effects. The principle errors are understood to relate to the representation of the energy absorption by moisture, although there are numerous other factors which have an impact on the matter (Daniels 2004).

2.2.3 GPR applications

Ground penetrating radar is widely used by a diverse group of service providers that include agronomist, archaeologists, criminologists, engineers, environmental specialists, foresters, geologists, geophysicists, hydrologists, land use managers, and soil scientists. In recent years, GPR has even gained recognition in the search for terrorism and military hazards (Anonymous 2006k).

Table 2.5 Systematisation of GPR applications according to the data extraction complexity

			GPR Applications				
			Level 1	*Level 2*	*Level 3*	*Level 4*	*Level 5*
Host material	geological condition	Known	√	√		√	
		Unknown			√		√
	water content	Known	√			√	
		Unknown		√	√		√
Object/ target	material/ properties	Known	-	-	-	√	
		Unknown	-	-	-		√
	form/size	Known	-	-	-	**(√*)**	
		Unknown	-	-	-	√	√

* Sometimes is the general form of an object known, e.g. one dimension of a drainage pipe is a lot larger than the other two (pipe diameter)

In Table 2.4 most of the wide range of GPR applications are systematised according to the *data extraction complexity level* in 5 groups. The level 1 represents the least complex group of methods and the level 5 the group with the highest data extraction complexity. This systematisation has been developed to give a general overview of the known applications. The first 3 levels represent methods applied in order to measure some of material properties, and the levels 4 and 5 represent target detection methods.

Level 1

Methods in this group are dealing with measurement of some object features in *known material with known material properties*, e.g. measurement of snow thickness (Annan 2002, Manacorda 2004) or extraction of crop density information from radar data (Paul & Speckmann 2002, Paul & Speckmann 2004c, Wild et al. 2003).

The *SnowScan* system for snow thickness measurement is also a good example of development and automation of one GPR method (Annan 2002). In the initial measurement process, the data were displayed as radar sections. Within months the application had auto picking and tracking capability which displayed a snow depth profile and could output the information as a single depth number vs. position (using GPS data). In its current version the system no longer needs to display radar data, but registers snow thickness along with the GPS coordinates and automatically transforms the data into a map. This kind of automated measurement is possible because of stabile dielectric properties of snow.

The attenuation level of radar signal was used to measure the crop density. The intensity of a reflected signal over the distance can be recorded for both pulsed and FMCW (frequency modulated continuous wave) radar. This is done by measuring the signal's time of flight and by recording the relative weakening of the echo compared to the original transmitted signal and plant material densities were classified as „weak, middle and dense" (Paul & Speckmann 2002). For this measurement it is necessary to have the information about biomass water content. Several related but more developed variants of this procedure are described in the level 2.

Level 2

The second level of complexity investigates *known materials with unknown properties* in order to extract some object features/properties, e.g. biomass estimation (Wild et al. 2003), water content in green tea leaves (Okamura 1999), soil water content (Clement & Ward 2003, Paul & Speckmann 2002, Paul & Speckmann 2004a, Paul & Speckmann 2004b, Weiler et al. 1998), or soil contamination (van Deen 2004).

In measurements, similar to the previous method for crop density determination, two pulse radar systems (5,8 GHz and 26,0 GHz respectively), originally designed to measure the level of solids or liquids in tanks, were used on biomass layers in order to measure the mass of a grass layer (Wild et al. 2003). The water content had a very high influence, e.g. the radar with a working frequency of 26,0 GHz was able to penetrate through only approximately 100 g of grass (water content of about 79%). For hay with water content of 11,1%, the maximum mass was 2500 g. A comparable procedure is commercially used for the water content measurement of green tea leaves on the band transporter in a layer with known thickness (Okamura 1999).

Several authors (Clement & Ward 2003, Paul & Speckmann 2002, Paul & Speckmann 2004a, Paul & Speckmann 2004b, Weiler et al. 1998, Redman et al. 2003) present a method of converting the data (dielectric constant) measured with GPR into information about water content in known material (concrete, sand, asphalt, soil, etc) using the empirical equation from Topp et al. (1980), or different semi-theoretical and empirical equations.

According to Redman et al. (2003), the observed variability in the GPR data can be attributed to true spatial variability in water content, GPR measurement error, and antenna orientation effects. The major source of error is believed to be related to surface scattering and spatial variability within the GPR sampling volume. The numerical modelling has shown that the GPR measured water content can be strongly influenced by stratification of the water content distribution. Further modelling is required to analyse the effects of surface scattering and to investigate the effects of spatial variability in water content within the sampling volume.

Clement & Ward (2003) and Paul & Speckmann (2004b) suggested that GPR moisture measuring method has many advantages over traditional methods for the determination of 3-dimensional distribution of the soil water content in the subsurface most of all because it is relatively inexpensive, it has a higher data acquisition speed, provides greater coverage by the large spatial sampling density, and it is a non-invasive method.

Freeland et al. (1998) had researched the relations of the data from radargrams with properties important for site-specific agricultural production: detection of soil horizons, perched water (episaturation), fragipans, hydrological preferential flow paths, and soil compaction. The enhancement step of the same team of researchers was the introduction of GIS (Geographic Information System) and dGPS technologies in order to investigate whether and how GIS, dGPS, and GPR can be linked to provide greater efficiency in data collection and image post–processing. This study demonstrated that the use of DGPS positioning increased survey efficiency with little loss in survey accuracy when compared to a traditional GPR procedures. Although susceptible to the various positioning errors, it was confirmed that the use of dGPS is more robust, efficient, and reliable than using survey wheels and manual positioning markings for surveying large open areas that require geospatial analysis and mapping.

The dielectric permittivity is largely determined by the water content and the composition of the soil. This means that the primary information is on layering and heterogeneity of soil strata. In principle the presence of organic contaminants (dense non-aqueous phase liquid - DNAPL as well as light non-aqueous phase liquid - LNAPL) will change the water content or influence the shape and thickness of the vadose zone. Therefore the presence of these substances could in some cases be visible in the radargrams. The second electric parameter that influences GPR is the electrical conductivity. It is generally this parameter that limits the application of the method because of the signal attenuation. On the other hand conductive polluting substances in ground water may give themselves away by the attenuation they generate in GPR signals (van Deen 2004).

Level 3

In the third Level of data extraction complexity researchers are dealing with *unknown properties of unknown materials* in order to extract some object features, e.g. soil water content and soil type (Ziekur & Schuricht 2002), or geologic structure and shape of an unknown area (Meier et al. 2002).

Authors Ziekur & Schuricht (2002) present a method of recognising the soil type on an agricultural land according to the intensity of reflected signals (weak = clayly-silty, strong = sandy soil), and propose the water content approximation method by comparing radargrams from dry (summer) period with the wet (spring) period.

A 100 MHz radar antenna was applied on moor area in order to measure the thickness of a peat layer (Meier et al. 2002). It was unknown which kind of geological material is under the peat layer, but the surrounding grounds were covered with ground moraine. The measurement showed that only casual correction of mechanical hand-sounding was needed (5 to 10% of usual hand sounding) in order to record the shape of the moor bottom.

The method of fuzzy-neural networks was proposed for the ambiguity problem of soil type classification from a radargram by Odhiambo et al. (2004a and 2004b). The feasibility of using textural features extracted from GPR data to automate soil characterizations was examined. The textural features were matched to a "fingerprint" database of previous soil classifications of GPR textural features and the corresponding ground truths of soil conditions. Four textural features (energy, contrast, entropy, and homogeneity) were selected for inputs into a neural-network classifier. This classifier was tested and verified using GPR data obtained from two distinctly different field sites. In choosing the type of network for soil classification, two limiting conditions were considered: 1) the characteristics of radargram, and 2) the soil variability. The characteristics of the radargram depend upon a number of variable factors, such as the frequency of the transmitted electromagnetic waves, the type of antenna, the antenna speed on the ground surface, the climate, the soil-water content, etc. Therefore, the characteristics of a radargram are likely to have

variations owing to different surveying conditions and equipment. As such, there are no fixed input-output examples for use in neural training. Furthermore, soil variation is more continuous than discrete; therefore, it calls for a continuous classification. With no fixed input-output examples and continuous soil variation, unsupervised classification and a system that is able to handle fuzzy boundary conditions are required. Such a neural network classifier was used to assign data to the known soil categories. The results of soil characterization using extracted textural features was found to be in close agreement with results obtained by careful visual interpretation of the radargrams (93,6% correct classified for site 1 and 90% correct classified for site 2).

Level 4

The fourth Level represents the simpler of two detection procedures. The data extraction consists of detecting objects made of known (usually man-made) material in more or less known form in the known medium, e.g. drainage pipes in soil (Allred et al. 2005, Meier et al. 2002, Youn et al. 2003), soil hard pan (Raper et al. 1990), rows detection in vineyards (Da Costa et al. 2003), or root biomass measuring (Butnor et al. 2003).

The use of GPR for detection of pipes in agricultural soil (Allred et al. 2005, Youn et al. 2003) and on a waste site (Meier et al. 2002) showed very good results. The dielectric properties of pipes (plastic or metal) are considerably different from the surrounding material, and the form is known: one dimension (length) is much larger than the other two (diameter). Results from initial research found GPR with 250 MHz antennas to be successful in locating 72% of the total amount of pipes present at 13 test plots on average (Allred et al. 2005). Shallow hydrologic conditions with a saturated soil surrounding a water-filled drainage pipe produce the poorest GPR drainage pipe detection response, but the shallow hydrologic conditions with a wet/saturated soil surrounding an air-filled drainage pipe produce the best detection response, especially if the ground surface is frozen. The type of drainage pipe present, either clay tile or plastic does not seem to impact the GPR response. The neural network method is also proposed for automatic pipe detection (Youn et al. 2003).

The GPR system with 500 MHz antenna was used to determine the depth and density of hard pans in two soil types with different clay and water contents (Raper et al. 1990). The tests were performed on sandy loam soil (71,6%, 17,4%, and 11,0% sand, silt, and clay, respectively) and clay loam soil (26,9%, 43,4%, and 29,7% sand, silt, and clay, respectively). The experiments showed that the depth of the hard pan in two soils could be closely estimated by using a GPR. Although water content had been thought to be a very important variable in the use of this device, different water contents when water was uniform throughout the soil profile did not affect GPR results. However, the authors concluded that the presence of a wetting front and moisture bands could complicate the use of GPR. Soil water content near field capacity could also cause problems, but the soil probably would not be trafficable to obtain GPR readings under this condition. Relationship between hard pan depths predicted by GPR and by penetrometer method were very linear and with correlation coefficients near 1.

The utility of GPR with 1,5 GHz antennas to measure tree root biomass in situ within a replicated, intensive culture forestry experiment planted with loblolly pine (Pinus taeda L.) has been studied as possible substitution for traditional labour-intensive and destructive methods (Butnor et al. 2003). The study site was in an area with different soil types. The measured data on root biomass to a depth of 30 cm were correlated to harvested root samples using soil cores. Significant effects of fertilizer application on signal attenuation were observed and corrected. The correlation coefficient between actual root biomass in soil cores and GPR estimates with corrections for fertilizer application were highly significant (R = 0,86). If the site conditions are favourable to radar investigation, the use of GPR can be a powerful and cost-effective tool, which considerably reduces the number of soil cores needed to assess tree root biomass and biomass distribution.

Level 5

On the highest Level of the data extraction complexity and interpretation ambiguity are archaeological, mine detection and forensic (Dittmer 2004) applications.

Archaeological radar data are difficult to interpret and many surveys in archaeology are analysed manually and this manual approach typically involves the visual inspection of data from each transect (with or without reference to its neighbouring transects). Significant features are picked out by the analyst and plotted on a site plan, which is an error-prone and time consuming technique. The quality of the results often depends heavily on the experience of the analyst as it is a very subjective procedure (Barker et al. 1998).

The difficulty with finding buried mines is that there is no single type of ‘‘target’’ and the surrounding background varies enormously from site to site. The soil surrounding the mine often strongly absorbs penetrating waves, and the site may be littered with irrelevant clutter objects such as buried rocks, moisture pockets, tree roots, bits of metal scrap (especially in a former battlefield). A random soil surface roughness is a significant noise source, which is impossible to avoid because demining systems have to be elevated from the soil surface. In addition, objects too close to the surface pose a problem in discrimination of the target from the ground surface itself (Rappaport et al. 2001). The problems in the field of mine detection appear like “to look for a needle in a haystack”. On the other hand, the vital demands to any GPR system for landmine detection are 99,6% probability of detection (UN criteria, Chignell et al. 2000) and low false alarm rate (Yarovoy et al. 2000).

Mine detection systems are limited both in terms of the type of soil and the type of mine (Daniels 1998). Plastic anti-personnel mines buried up to 50 mm can be detected in many, but not all grounds with a certain confidence. Plastic anti-personnel mines are typically 75 to 100 mm in diameter and between 25 and 50 mm thick. There are some smaller diameter types and some larger types. They are typically circular objects but other shapes are common. The bulk of their material is explosive (TNT) typically with a dielectric constant of around 3,5 (Chignell et al. 2000), which is practically the same as for dry soil (Rappaport et al. 2001). Plastic anti-tank mines buried up to 200 mm can be detected in most soils, with some confidence. Metallic mines can be detected at deeper depths with a higher confidence level (Daniels 1998).

Any GPR system will find it difficult to distinguish between a mine and an object of similar size and dielectric properties. Different authors have presented a number of landmine detection sensors and it is a common anticipation that a successful detection system will require a fusion of data from a number of different sensor types. In offering the potential of both rapid search and significant ground-penetration, a GPR sensor has potentially the most important part to play. However, in order to realise this potential in attenuating soil containing significant clutter, major improvements to GPR are needed (Craddock et al. 2001).

In general there are two possibilities for the development of mine detection systems: the hardware and the software development. For example, the RASOR (Real Aperture Synthetically Organized Radar) technique has been proposed for the GPR component of such a system (Craddock et al. 2001). An additional possibility is application of the UWB technology (Scheers 2000), which is going to be more comprehensive described in the subsequent chapter.

It is principally not possible to satisfy all requirements to GPR dedicated to landmine detection only in hardware. Requirements such as very fine cross-range resolution and efficient clutter reduction can be achieved mainly in dedicated software. However, this software should be hardware specific. It should take into account the specific antenna configuration, performance of hardware and data acquisition parameters. Both hardware and software contribute to the performance of the whole system and to the final result: 3-dimensional images of the subsurface (Groenenboom & Yarovoy 2002). The next significant software requirement is the target recognition. The most promising and to substantial extent confirmed technology is the fuzzy technology, e.g. fuzzy set-based information fusion algorithms (Gader et al. 2001).

With the introduction of the dynamic dimension in the system, the systematisation above would have one additional level, which would make the information extraction even more difficult and ambiguous. A good example comes from the field of forensics, where forensic targets change over time – during the process of decomposition (Freeland et al. 2003). Another example is so called through-wall

radar (Sachs et al. 2005a) for different police, intelligence or military employment, e.g. object surveillance, anti-terrorist employment and hostage situations.

2.2.4 UWB radar technology

The term ***U**ltra **W**ide **B**and* (*ultrawideband, ultra wideband, ultra-wideband* or *ultra wide-band*) or UWB signal includes a number of synonymous terms such as: impulse, carrier-free, baseband, time domain, nonsinusoidal, orthogonal function and large-relative-bandwidth radio/radar signals (Barrett 2000).

The origin of UWB technology stems from work in time-domain electromagnetics began in 1962 to fully describe the transient behaviour of a certain class of microwave networks through their characteristic impulse response. Instead of characterizing a linear time-invariant (LTI) system by the more conventional means of a swept frequency response (i.e. amplitude and phase measurements vs. frequency), an LTI system could alternatively be fully characterized by its response to an impulsive excitation - the so-called impulse response (Fontana 2000, Anonymous 2006l).

UWB radar systems have been in the commercial world since the 1970s. Currently developed and future applications include: ground-, wall- and foliage-penetration, position-location, collision warning for avoidance, fluid level detection, intruder detection radar, vehicle radar measurements, moisture and liquid sensing.: high speed LAN/WANs (local-/wide-area network), various tags (intelligent transportation systems, electronic signs, smart appliances), industrial RF (radio frequency) monitoring systems, RFID (radio frequency identification), breathing and heart monitoring, camera auto-focus, etc (Barrett 2000, Anonymous 2006l, Sachs et al. 2001, Sachs et al. 2005a).

Since UWB waveforms are of such short time duration, they have some unique properties. In communications, for example, UWB pulses can be used to provide extremely high data rate performance in multi-user network applications. For radar applications, the same pulses can provide very fine range resolution and precision distance increasing positioning measurement capabilities, and increase informational

capacity (Immoreev 2000, Immoreev 2002). These short duration waveforms are relatively immune to multipath cancellation effects as observed in mobile and in-building environments. Multipath cancellation occurs when a strong reflected wave (e.g. off of a wall, ceiling, vehicle, building, etc) arrives partially or totally out of phase with the direct path signal, causing a reduced amplitude response in the receiver. With very short pulses, the direct path has come and gone before the reflected path arrives and no cancellation occurs. As a consequence, UWB systems are particularly well suited for high-speed, mobile wireless applications. In addition, because of the extremely short duration of waveforms, packet burst and TDMA (time division multiple access) protocols for multi-user communications are readily implemented (Anonymous 2006l).

Among the most important advantages of UWB technology, however, are those of low system complexity and low cost. Because of the inherent RF simplicity of UWB designs, these systems are highly frequency adaptive, enabling them to be positioned anywhere within the RF spectrum. This feature avoids interference to existing services, while fully utilizing the available spectrum. The development of obstacles and limitations of the UWB technology can be summarised in two points. The first is very strong competition of high capacity optical fibre or optical wireless communications systems, and the second limitation is the physical nature of the UWB as a RF technology, which calls for tradeoffs (e.g. in signal-to-noise ratio vs. bandwidth, range vs. peak and average power levels, etc) (Anonymous 2006l).

UWB principles for GPR

Ultra-wideband (UWB) devices are considered as any devices where the *fractional bandwidth* b_f is grater than 25% **or** occupies 1,5 GHz or more of spectrum (Anonymous 2006m, Barrett 2001). The fractional bandwidth is defined as:

$$b_f = \frac{f_u - f_l}{\frac{1}{2} \cdot (f_u + f_l)} \cdot 100\% \qquad 2.15$$

in which f_u and f_l refer to the upper and lower bound of the occupied spectrum respectively. However it should be noted that practically all audio measurement systems having a bandwidth between 20 Hz and 20 kHz ($b_f \cong 200\%$) belong by definition to UWB-systems, because of that Sachs et al. (Sachs et al. 2001) proposed to replace the **or** by an **and** within the above UWB definition.

In the following analysis the GPR device will be considered as an LTI-system (Sachs et al. 2000). In order to gather information from an object under test, the object is touched by a wave and its reaction to this wave is measured. In the simplest case, two antennas are used (the use of one antenna is rare because of antenna mismatch). The application of antenna arrays is also possible. From the point of view of a GPR user and a simple interpretation of the images, the radiators are referred to virtual point sources, like in Figure 2.11, which are considered as sources of spherical waves. In contrast to that, the measurement plane, to which the further consideration is restricted, is more common from the standpoint of the radar electronics, and it is defined by the input/output channels 1 and 2.

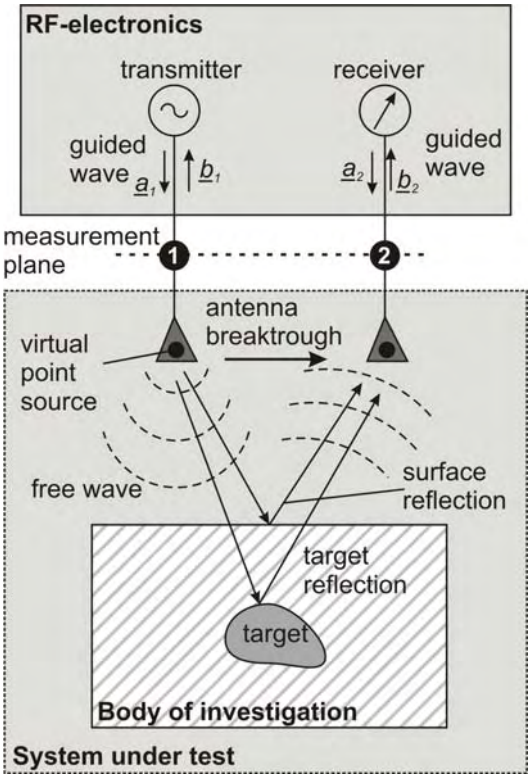

Figure 2.11 Basic GPR arrangement for air launching (Sachs et al. 2000)

Regarding the measurement plane, the radar electronics represent a two-port measurement device (N-port in case of an array) and the body under test plus its embedding (further called system under test) may be looked upon as a linear two-port. Assuming the antenna displacement during the measurement time T_{obs} (observation time) is negligible time independent behaviour can be supposed and classical network theory can be applied:

$$T_{obs} < \frac{c}{2 \cdot v_{max} \cdot B} \qquad 2.16$$

In Equation 2.16 c represents the propagation velocity of the wave, v_{max} the maximum displacement speed of the antennas and B is the bandwidth of the sounding wave (Sachs et al. 2000).

At fixed antenna positions, the system under test is completely determined by its N by N scattering matrix S (Sachs et al. 2000):

$$\underline{b}(f) = \underline{S}(f) \cdot \underline{a}(f) \text{ for the frequency domain} \qquad 2.17$$

or

$$b(t) = S(t) * a(t) \text{ for the time domain} \qquad 2.18$$

Herein *a(f)* is a column vector of the normalised guided waves incident to the antenna feeds, *b(f)* is a column vector of the normalised guided waves leaving the antenna feeds and *S* is the scattering matrix of the system under test. $\underline{S}(f)$ represents a set of Frequency Response Function (FRF) and *S(t)* a set of Impulse Response Functions (IRF). They are interconnected by the Fourier Transform. Underlined symbols mean complex valued functions and symbol * refers to the convolution.

The individual functions of the S-matrix will permanently change through the moving of the antennas over the ground. They represent the reflection behaviour (monostatic

mode) $\underline{S}_{ii}(f,r_i,r_i)$ or $S_{ii}(t,r_i,r_i)$ of the antenna *i* at position r_i and the behaviour of the transmission path $\underline{S}_{ij}(f,r_i,r_j)$ or $S_{ij}(t,r_i,r_j)$ between the antennas *i* and *j* (bistatic mode) at positions r_i and r_j. These functions form radargrams and/or radar volumes which serve to interpret the inner structure of the body under test. Generally the time representation of the measurement results is preferred because it is more accessible to human imagination. The Fourier transformation however permits the change of the domains, so that software procedures may also work in the frequency domain if advantageous.

The key features describing the performance of the radar electronics in an GPR device refer to its spatial resolution in range δ_r and cross range δ_{cr}, to the observation range *R* (unambiguity range), its sensibility for detecting weak reflecting objects and to the measurement rate r_m. These parameters have to be transformed to corresponding properties of the IRF or FRF measured by the radar electronics (Sachs et al. 2000).

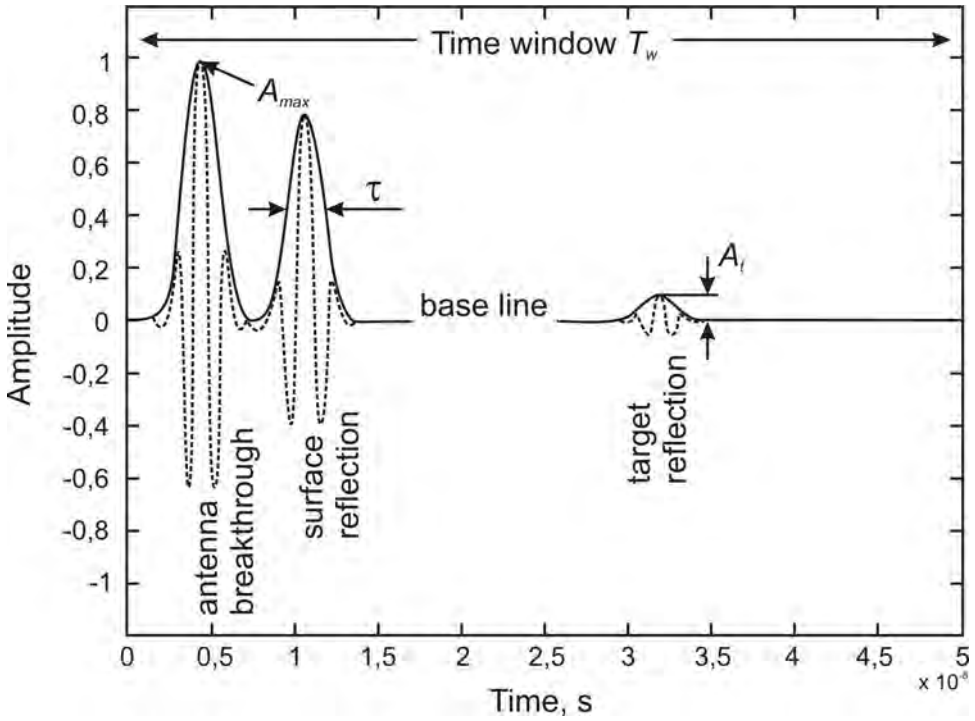

Figure 2.12 Idealised IRF $S_{21}(t)$ according to Figure 2.11 (Sachs et al. 2000)

To illustrate the facts, Figure 2.12 indicates an idealised curve of the IRF $S_{12}(t)$ of the transmission path 1 → 2 resulting from the simple situation in Figure 2.12. Pulse like sections appear and provide clues as to overall length and attenuation of the individual propagation paths. These results are finally used to reconstruct the inner structure of the body. The first two impulses in Figure 2.12 will merge if the antennas are in contact with the surface.

The spatial resolution in range δ_r depends upon the capability to distinguish between two closest pulses of equal amplitude. According to Figure 2.12 this can be expressed as:

$$\delta_r \cong \frac{1}{2} c\tau \cong \frac{c}{2 \cdot B} \qquad 2.19$$

where τ is the half-value width of the pulse envelope and B is the corresponding bandwidth. The effective usable bandwidth B of a GPR device is not only determined by the bandwidth of the stimulus signal and the antennas but also from the time jitter arising from instabilities in the transmitter and receiver circuit.

The cross range resolution δ_{cr} also strongly depends upon the pulse width if synthetic aperture processing is applied as well as the beamwidth 2Θ of the antennas.

$$\delta_r \cong \frac{c \cdot \tau}{2 \cdot \sin\Theta} \qquad 2.20$$

The observation range R (unambiguous range) depends upon the length of the time window T_w for which the impulse response is measured. In the case of periodical stimulation signals, it is limited to its period T to avoid time aliasing.

$$R = \frac{1}{2} c \cdot T_w \leq \frac{1}{2} c \cdot T \qquad 2.21$$

The time which is needed to gather all the data included in a complete IRF or FRF will be called observation time T_{obs}. As such, the repetition rate r_m for the measurement (measurement rate) is:

$$r_m \leq T_{obs}^{-1} \qquad 2.22$$

The detection limit describes the capability to find small scattering amplitudes in the IRF that are caused either from small scatterers with poor dielectric contrast or by propagation losses (Sachs et al. 2000).

The advantage of the UWB system important for this research is the high spatial resolution of the radargrams. The distance estimation with UWB radar in relationship with its bandwidth for propagation in several materials is shown in Figure 2.13 (Sachs & Peyerl 2003). In this illustration the approximate values of dielectric constants of materials are shown without taking into account the influence of different frequencies. According to the presented diagram, it is possible to achieve spatial resolution of the radargram up to the mm-level (for material with appropriate properties).

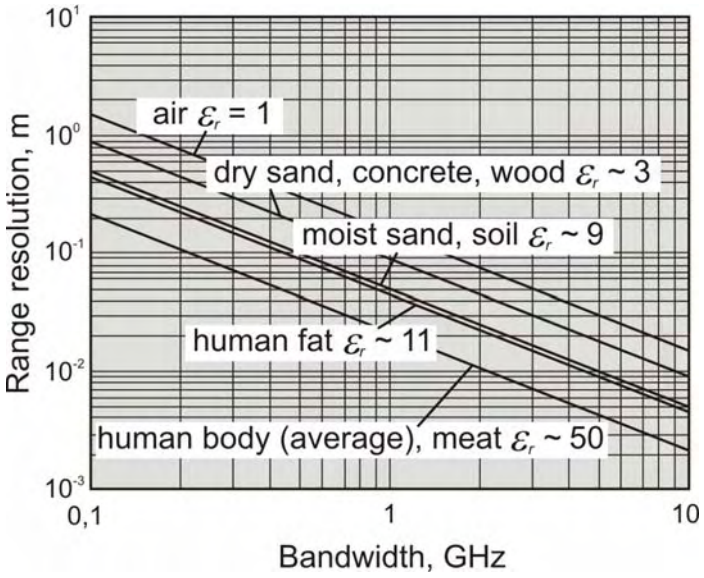

Figure 2.13 Distance estimation with UWB radar in relationship with its bandwidth for propagation in several materials (Sachs & Peyerl 2003)

UWB measurement techniques

Three basic measurement principles are known which are mainly distinguished by the kind of stimulus signal that is applied: Impulse-, Sine Wave- and Correlation-technique.

The *impulse technique* uses the fact that the convolution (Equation 2.18) will be needless, if very short pulses stimulate the sensor. Since the sensor reaction can be measured by an oscilloscope, the image of its screen represents immediately the sensors IRF. A classical device applying *sine-wave* excitation and operating over a large bandwidth is the network analyser i.e. stepped sine-wave source and a heterodyne vector receiver. The FMCW-principle (Frequency-modulated continuous-wave) represents an attractive alternative to the stepped frequency approach because of its simplicity (cost and size) and measurement speed. From the theoretical point of view, the *correlation technique* is the most flexible method of system identification since it is not fixed to a certain kind of test signal. The consequence is the wideband stimulus signals may be applied, which have high (mean) power but low peak voltages (compared to an impulse) (Sachs et al. 2001). The correlation technique opens the possibility to freely choose the test signal to be used (Sachs et al. 2000), e.g. random signal radar (Daniels 2004) or M-sequence radar (Sachs 2004). The last correlation technique is used within this research and it is going to be more closely described in the following chapters.

3. Definition of problems and instrumentation demands

The concept of precision farming and its connection to yield mapping with emphasis on sugar beet yield recording procedures have been thoroughly analysed in Chapter 2.1. Several researched and developed yield recording systems based on direct, indirect and estimation measuring procedures for sugar beet and similar root crops have been presented. The results of analyses of the state of the art showed manifold problems of known procedures. Within the comparative analyse in Table 2.3 the estimation recording procedures showed the least problems.

The representative example of the estimation procedure is the real-time yield mapping approach developed at the Institute for Agricultural Engineering (Schmittmann 2002). This results and experience obtained during the R&D activities on this system has been chosen to be the guidelines and the starting point of this research. Since the limits of this system have been reached, the necessity to develop a new yield recording system for sugar beets has been subsequently noticed. The new system should be able to partially or completely solve the problems of existing sugar beet yield recording procedures (see Chapter 2.1.2.4). Therefore the following solutions of the problems have been defined as demands put in front of the new system:

1. Recording of the sugar beet yield independent of the soil tare and other objects.
2. Avoiding measuring errors caused by swinging of the whole harvester or irregular oscillations/vibrations and various similar technical problems.
3. Measuring of the whole sugar beet mass independent of the harvesting quality.
4. Avoiding unambiguous approximation/correlation functions.
5. Eliminating errors caused by deviation from mean values of relevant sugar beet properties.
6. Preventing the misinterpretation of measured data.

The new sugar beet yield recording system should have features presented in Table 3.1 in order to comply with the above listed demands.

Table 3.1 Features of the measuring system solution complying with system demands

System demands		*Measuring system features*
1.	Independent recording	Differentiation between sugar beets and other material
2.	Measuring errors	Measurement independent of external influences (e.g. light, speed changes, bulk density etc)
3.	Measuring of the whole sugar beet	In-soil measuring before lifting
4.	No approximation functions	Direct measuring method
5.	No errors caused by deviations from mean values	Direct measuring method
6.	No misinterpretation of measured data	The measuring system is able to differentiate sugar beet from other material

4. Concept of the proposed measuring system

The basic concept of the measuring solution chosen for in-soil sugar beet yield recording has been presented in Figure 4.1. The measuring solution consists of a radar device and its peripheries. This system can be applied before or during the harvest; in Figure 4.1 the radar antennas (transmitter and receiver) are recording the scenario after topping or defoliating. The other option is to apply the system through the foliage, during growth for example.

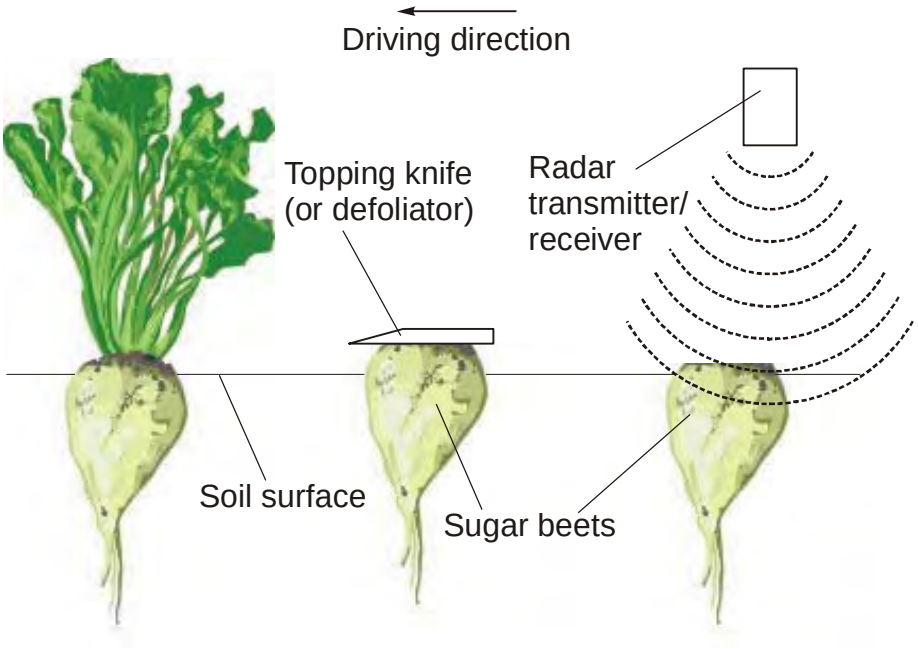

Figure 4.1 Basic concept of the proposed measuring system for in-soil sugar beet yield recording

The radar measuring principle has been chosen because it partially or entirely complies with the most of the listed demands from Table 3.1:

1. 3. and 6. Radar systems allow non-invasive in-soil differentiation between sugar beet and soil and recording the whole sugar beet before lifting.
2. External influences should have less influence in comparison to the internal influences within the radar-scenario system.

4. and 5. Recording result is in general case a radar image corresponding to the scenario and it is in that sense direct measuring method.

More thorough analysis of the chosen system is given in Chapter 6.

5. Goals of the research and research hypotheses

Goals of the research venture

The following goals of the research venture are as follows:

1. To develop and evaluate a yield recording procedure which will provide:
   - non-invasive in-soil identification of single sugar beets with sufficient reliability in order to enable
   - the counting of individual sugar beets and in turn
   - determining the single sugar beet root mass

2. To enhance the radar technology for further application in the agriculture and

3. To define applicability limitations for practical purposes for sugar beet relevant utilisation and for agriculture in general.

Research hypotheses

According to the listed goals and taking under consideration the list of problems and the capabilities of the UWB radar technology chosen for the measuring tasks, the following list of hypotheses has been defined:

1. The measuring system enables the differentiation of sugar beet roots from the soil independent of scenario properties.

2. The measuring system enables identification and counting of
   a. sugar beets with foliage
   b. sugar beets with leaves brush
   c. topped or defoliated sugar beets

   in the agricultural soils independent of scenario properties.

3. The measuring system enables root mass determination of
   a. sugar beets with foliage

b. sugar beets with leaves brush

c. topped or defoliated sugar beets

in the agricultural soils independent of scenario properties.

6. Material and methods

6.1 Biotechnological properties of sugar beets

Sugar beet (*Beta vulgaris* L. *ssp. Vulgaris* var. *Altissima*) belongs to the family Chenopodiaceae. The cultivated fodder and sugar beets originate from the Middle East and Mediterranean areas. It is a biennial plant, which is essentially vegetative during the first years of growth and requires over-wintering to induce reproductive development in the following year. Normally sugar beets are harvested at the end of the first growing season (Anonymous 2004).

Sugar beet morphology

The mature, vegetative sugar beet plant consists of a rosette of leaves, borne on erect petioles subtended from a compressed stem. In commercial practice, the compressed stem is referred to as the crown. The upper part of the root is derived from the seedling hypocotyl and the lower part, the true storage root, is developed from a series of secondary cambial rings that arise in the root pericycle. The main morphological parts of sugar beets are shown in Figure 6.1 (Anonymous 2004).

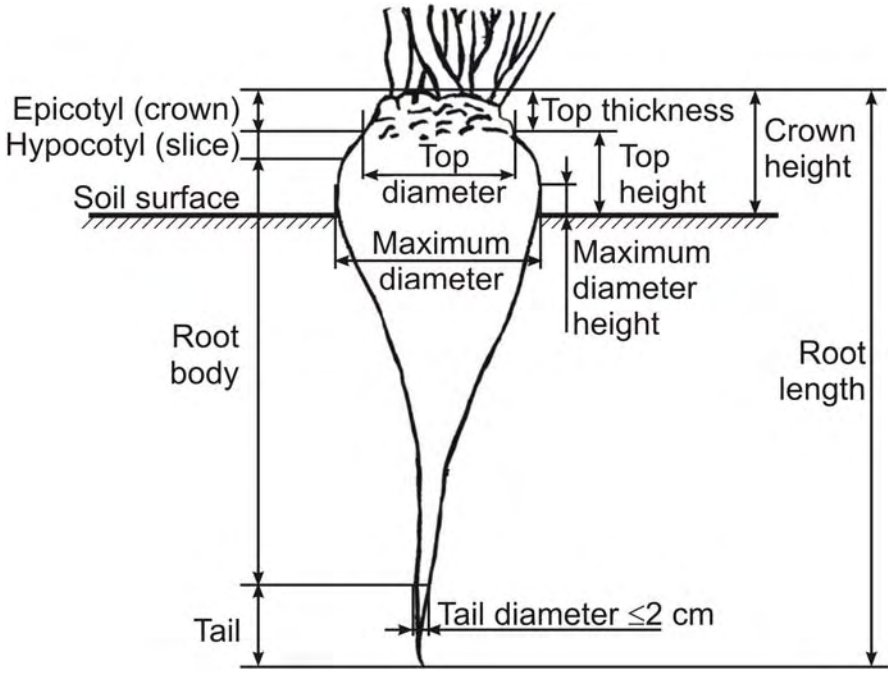

Figure 6.1 Morphology of sugar beets (Schmittmann 2002, Anonymous 2004)

Biotechnical characteristics of sugar beets

The root body contains the highest concentrations of sucrose (*c*. 16-20%), and concentrations progressively decline in the hypocotyl (*c*. 15%) and the lower (*c*. 13%) and upper (*c*. 7-9%) parts of the crown. The decrease in sucrose concentration is accompanied by increases in the concentrations of potassium, sodium, amino-nitrogen compounds and invert sugars. These melassigenic substances interfere with the crystallisation of white sugar in the factory, making sugar-beet crowns costly to process for small yields in sugar (Anonymous 2004).

Table 6.1 Biotechnical characteristics of sugar beets (Anonymous 2004)

Properties	*Unit*	*Average value*	*Value range*
Technical length	mm	220	100 – 340
Weight	kg (50 t/ha)	0,8	0,14 - 3
Maximum beet diameter	mm	120	40 –300
Top diameter	mm	80	40 – 160
Vertical height	mm	45	0 – 150
Top thickness	mm	30	5 – 100
Beet Density	kg/dm^3	1.07	1,00 – 1,14
Bulk Density	kg/m^3	635	580 – 690
Bulk Angle	degree	40,5	35 – 46
Dry matter content (*water content*)	%	22 *(78)*	18 – 26 *(74 – 82)*
Surface area	cm^2	350	10 – 700

The harvesting of sugar beet is usually completely mechanised. The first procedure, typical for European conditions, is topping. Plants are topped in the field to remove as much green shoot material as possible, but some crown tissue is left to avoid over-topping beet and removing part of the root. This is to ensure that the full yield of roots is delivered to the factory. The proportion of crown left on the beet after machine topping, the crown tare, depends on variation in plant size, the initial size of the biological crown, harvesting conditions, and the skills of the operator in adjusting and operating the harvesting machinery. Machine topping of field-grown beet is rarely

uniform, so delivered loads contain different proportions of over-, under- and correctly-topped beet, like in Figure 6.1, and different amounts of crown, leaf material, soil and stones (Anonymous 2004).

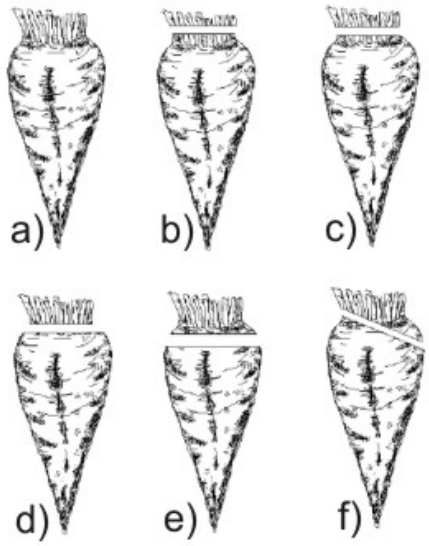

Figure 6.2 Assessment classes for topping quality; a) Untopped with petioles longer than 2 cm, b) Under topped with petioles shorter than or equal to 2 cm, c) Under topped with no petioles, d) Correctly topped, e) Over topped with under half of maximum diameter of bundle rings visible, f) Angled topped (Anonymous 2004)

6.2 UWB Radar system

The UWB radar system used in this research is based on the so called M-sequence approach. The term M-sequence is a short name of “maximum length binary sequence” (MLBS) and the device is sometimes called MBC-Radar (Maximum length Binary sequence Correlation Radar). The M-sequences are the special kind of pseudo-random binary sequence (PRBS). The PRBS signals are periodic and as such they are not really random. They have, however, properties which are very similar to the random sequences; the PRBS signals consist of elementary impulses (chips), which are apparently randomly distributed within a signal period. (Sachs et al. 2000, Sachs 2004).

The M-sequence technique is closely related to the impulse technique but it joins the advantage of that technique (simple layout, high measurement speed) with those of the sine wave approach (high stability, high energy signals with low amplitudes). It also applies periodic signals having a large instantaneous bandwidth and the data are captured by under sampling in order to reduce hardware costs and data throughput. However, there are two decisive differences compared to the impulse technique: they concern the type of stimulus signal and the method to control the sampling instant (Sachs et al. 2003).

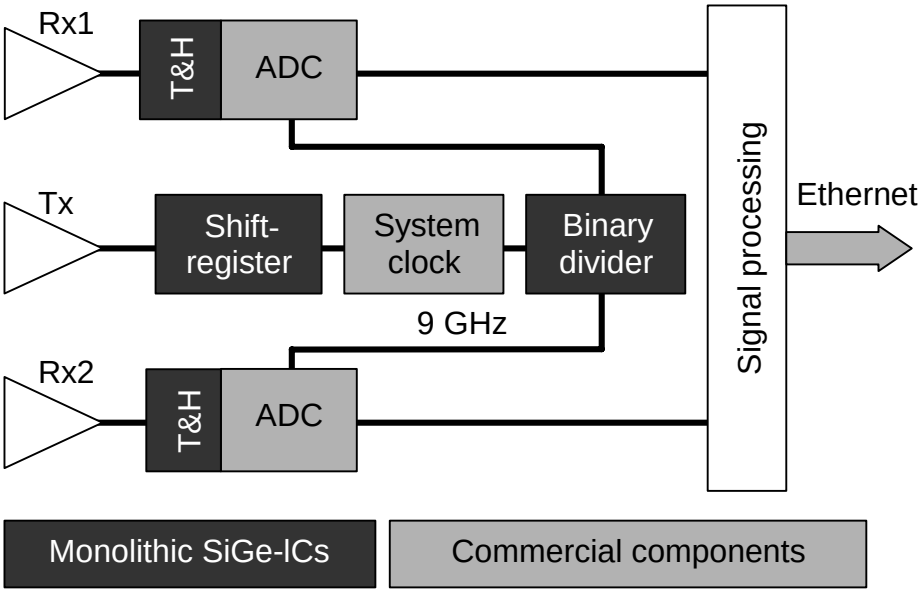

Figure 6.3 Scheme of M-sequence radar components (Woeckel et al. 2005)

Figure 6.3 shows the elementary structure of a wideband M-sequence device, which consists of three antennas: one transmitting Tx and, optionally, one or two receiving Rx. The M-sequence – the stimulus signal sent by transmitting antenna Tx – is generated by a digital shift register, which is pushed by a stable RF-clock frequency f_c. The stimulus response is received by receiving antenna Rx1 and/or receiving antenna Rx2. The used design permits the clock rate of 9 GHz. This results in a maximum usable bandwidth of about 4,5 GHz depicted later in Figure 6.5 c). One of the most important features of the M-sequence approach is that the actual sampling rate f_s can be derived by a simple and stable method (i.e. by a binary divider) from the RF-master clock $f_c = 2^n f_s$. The digital signal processing can be freely adapted to

the actual need, so that the provided data can be given in the frequency domain or the time domain (i.e. impulse or step response) or in other form (Sachs et al. 2005b).

The data gathering is based on sub-sampling in order to reduce the throughput. The sub-sampling is realised through the binary divider, which does this in a stable way by keeping an absolute linear (equivalent) time base of the captured signal. The divided pulse directly pushes the ADC (analog-digital converter) and the T&H-circuit (track and hold circuit). The T&H captures the wideband input signal and provides it to the ADC, which can work at a suitable sampling rate f_s (Sachs et al. 2002, Sachs et al. 2005a).

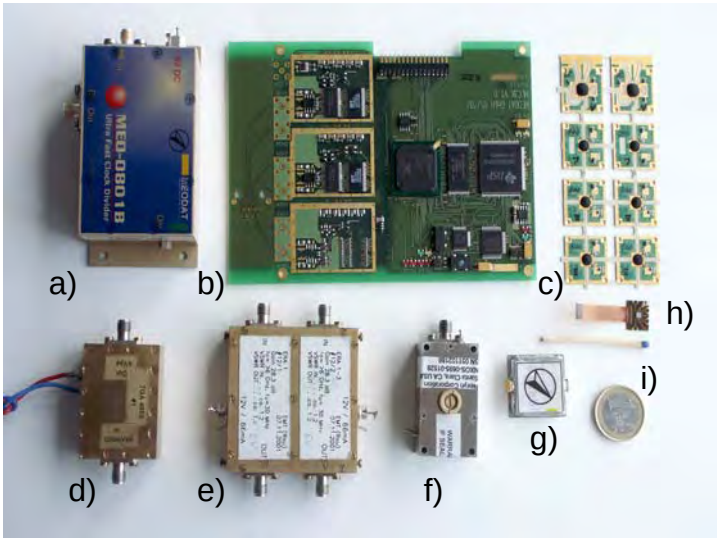

Figure 6.4 M-sequence UWB radar components: a) divider, b) digital unit, c) HF-chip (High Frequency-chip) carrier, d) impulse power divider, e) two amplifiers (LNA – low noise amplifier), f) oscillator (DLO – digital local oscillator), g) T&H-circuit, h) divider on carrier, i) match and one euro coin for size comparison (Sachs et al. 2005a)

The core elements of the radar device are shown in Figure 6.4 (Sachs et al. 2005a). The RF-modules are mounted on carriers. All modules are mutually shielded resulting in an excellent suppression of crosstalk. The shift register, T&H and the synchronisation unit are manufactured in a low cost SiGe-semiconductor technology (Sachs et al. 2005a, Sachs et al. 2005b).

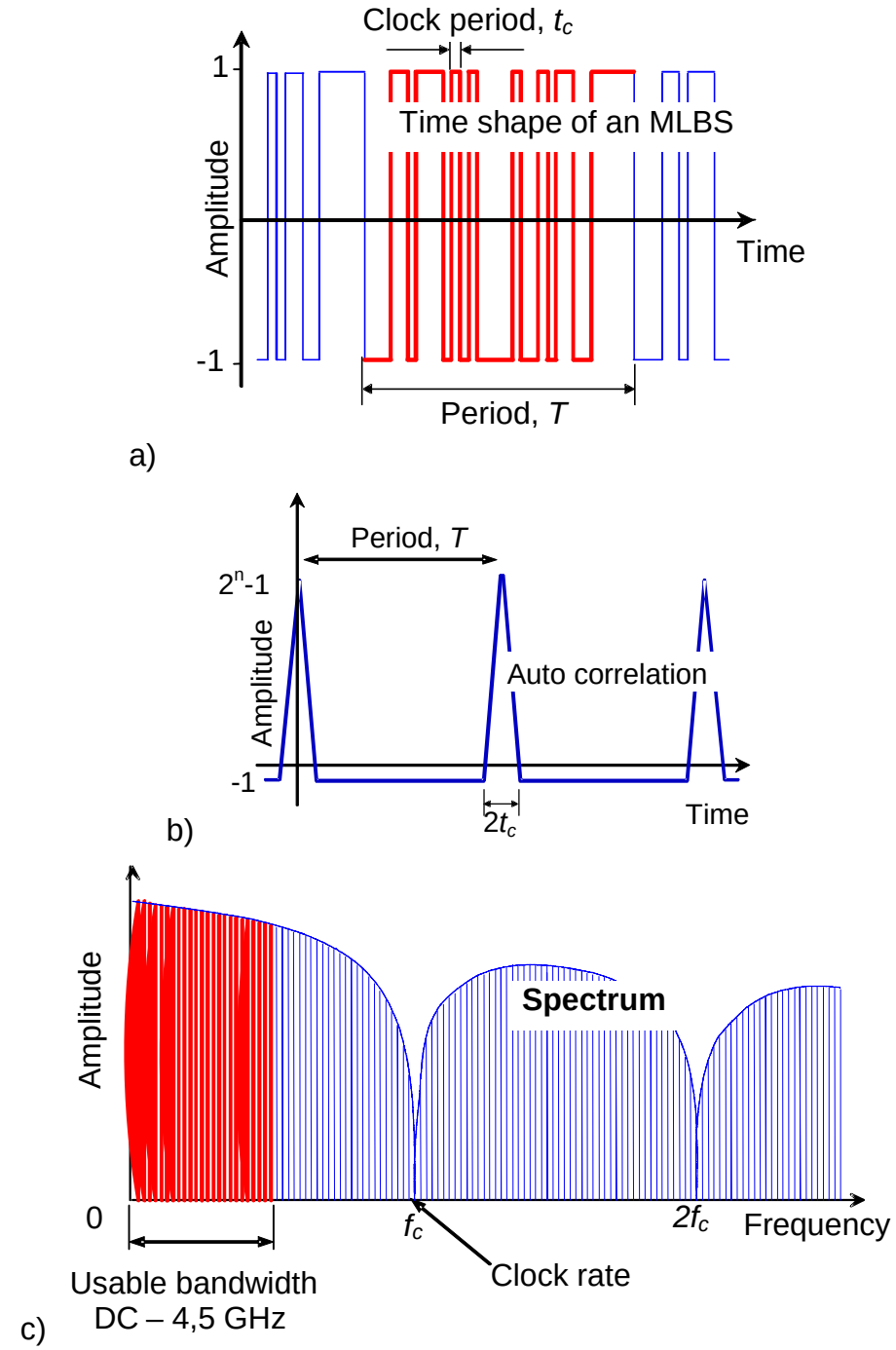

Figure 6.5 Time shape, auto correlation function and spectrum of a MLBS (Sachs et al. 2000)

Figure 6.5 shows the typical (idealised) time shape, autocorrelation function (measure of how well a signal matches a time-shifted version of itself) and spectrum of a MLBS of *n* order, generated by an n-stage shift register using an appropriate feedback. The MLBS period is $T = (2^n - 1)t_c$, where t_c is the period of the system

clock. Regarding the spectrum in Figure 6.5, it is useful to fix the equivalent sampling frequency of the receiver circuit to the clock frequency $f_c = 1/t_c$ that means one sample per elementary pulse of the sequence. Thus the usable bandwidth B_u is limited to the range $0 \leq f < f_c/2$ of the MLBS-spectrum. In Figure 6.5 c) the sequences of higher order than in the diagrams a) and b) are used in order to provide a better graphical representation of the shown spectrum (Sachs et al. 2000, Sachs 2004).

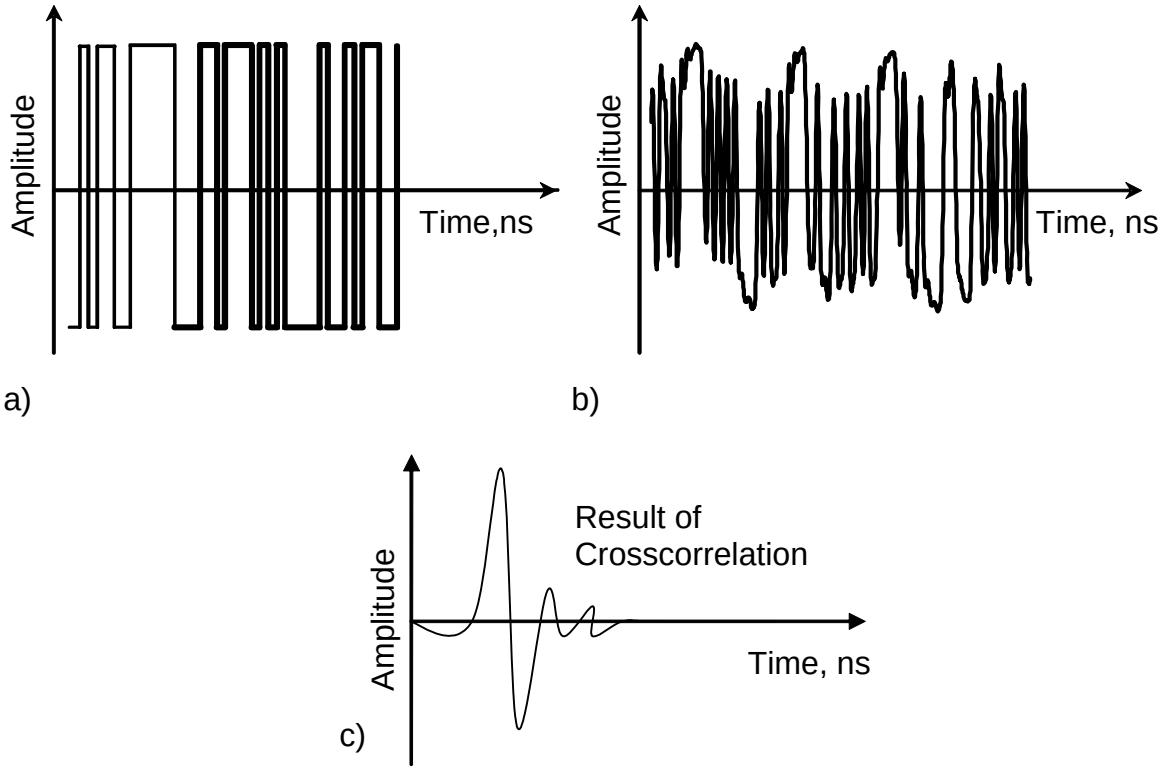

Figure 6.6 Result of crosscorrelation; a) transmitted ideal M-sequence signal, b) received signal, c) displayed time signal; correlation between a) and b)

A signal with a short autocorrelation function has a large bandwidth and it is, in principle, used as a stimulus in high-resolution radar technology. It is, however, not beneficial to consider the stimulus response, i.e. the backscattered signals, immediately as they cannot be interpreted due to their random nature. The situation changes by examining the crosscorrelation function between originally transmitted stimulus and received stimulus response, like in Figure 6.6. Therefore, the information of interest is the shape of the impulse response function (IRF) *h(t)* between the transmitting Tx and receiving antennas Rx. The IRF contains the

scattering behaviour of the targets. The IRF and auto- and crosscorrelation function are related by a convolution (convolution is a function that expresses the amount of overlap of one function as it is shifted over another one; the symbol $*$ stand for convolution operation). For comparison, the direct relation between stimulus *x(t)* and the response *y(t)* is (Sachs 2004):

$$y(t) = h(t) * x(t) \qquad 6.1$$

Further issues connected to signal acquisition, analysis and processing are described in the Chapter 6.4.

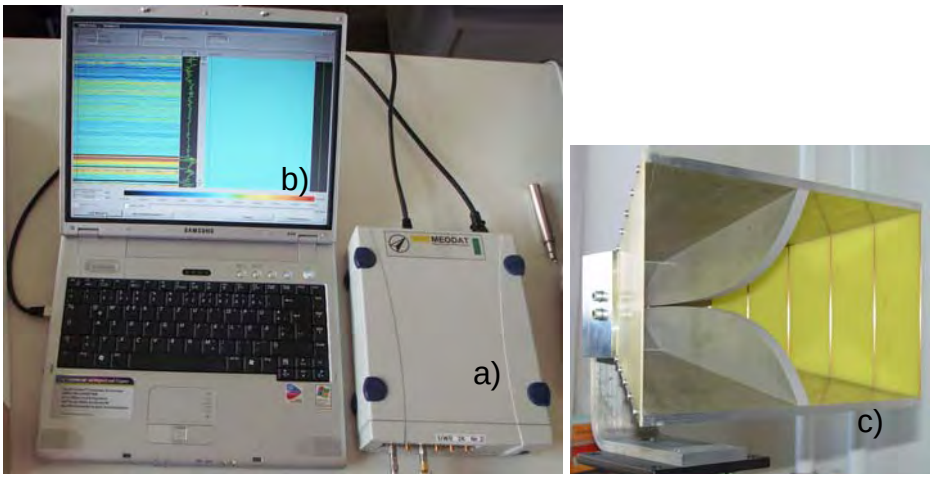

Figure 6.7 M-sequence measuring system used in the research: a) M-sequence unit, b) acquisition unit (PC) with software, c) horn antenna (Woeckel et al. 2006)

The measuring system used in this research is shown in Figure 6.7. The M-sequence unit has been developed and manufactured in the Meodat company in Ilmenau (www.meodat.de) according to the requirements of the project and project objectives. The described features of this unit have been defined by Technical University Ilmenau, Electronic Measurement Research Lab (www-emt.tu-ilmenau.de). The horn antennas used during the measurements have been manufactured and tested in the workshop of the Electronic Measurement Research Lab in Ilmenau. The whole system is easily mountable and portable, which enables its utilisation in conditions of different agricultural scenarios. It is also interesting to note that this radar emits a

radio power of about 1 mW, which is more than 1000 times lower than the radiation of a mobile phone and therefore there are no health hazards (Konstantinović et al. 2006).

6.3 Experimental facilities

6.3.1 Experimental environment and experimental accessories – laboratory

Experimental stand features

The test facility has been designed in order to comply with radar technology requests. The vast majority of the used elements are made of wood or plastic, as materials with appropriate dielectric properties and low reflection, and thus sufficiently "invisible" during radar measurements. The facility shown in Figure 6.8 consists of three basic parts:

- Soil box with three sections
- Measuring system carrier
- Driving unit of the carrier

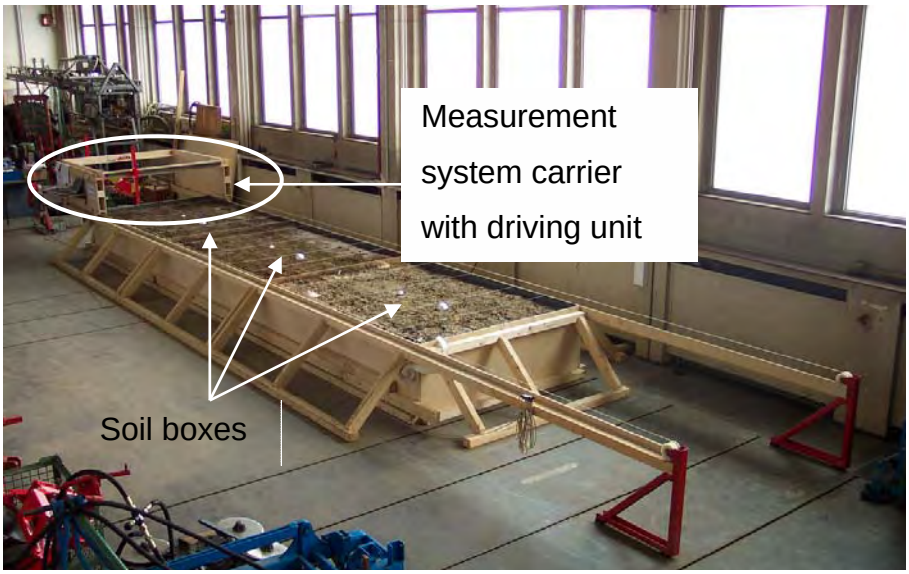

Figure 6.8 Photo of the laboratory test stand

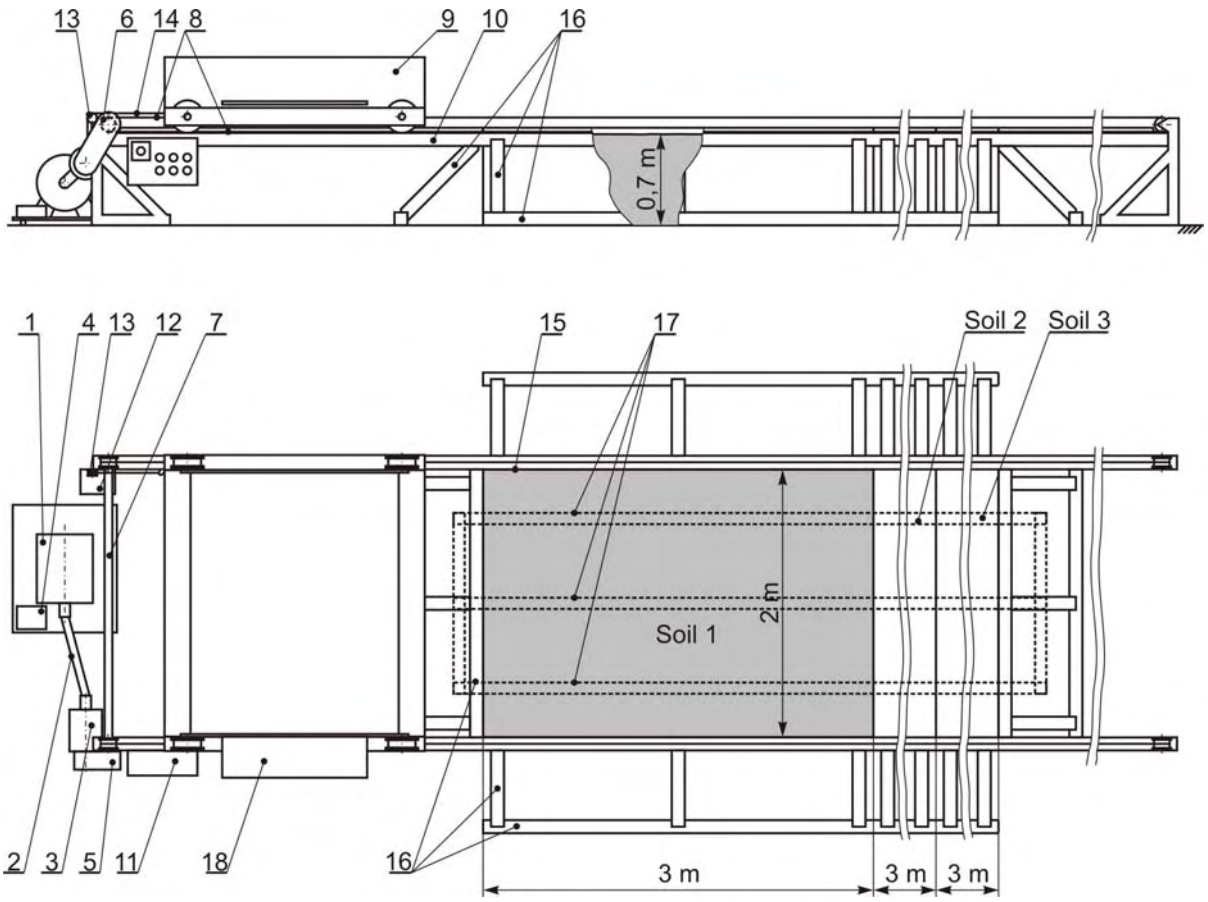

Figure 6.9 Laboratory test stand: 1– electromotor with variable transmission system, 2– fully suspended drive, 3– coupling, 4– RPM meter, 5– belt drive, 6– drive roll, 7– drive shaft, 8– plastic rope, 9– carrier of the measuring system, 10– wooden tracks, 11– control board, 12– path meter, 13– roll, 14– path meter's cable, 15– wooden walls, 16– wooden reinforcing elements, 17– drainage pipes/drainage system, 18– platform for PC and UBW radar

The dimensions of soil boxes have been also adjusted to the requests of radar technology. The technical drawing in Figure 6.9 shows a detailed layout of the laboratory test stand. The width of each soil box is 2 m and the length 3 m, which enables the extraction of the reflection from soil, without interference of side objects. There are three sections within the soil box, for three chosen soil types with the total length of 9 m. The height of the soil box's walls is 75 cm, which allowed the thickness of soil layer of about 70 cm. The walls are made of wood plates and reinforced with wooden elements. On the top of the longitudinal walls the wooden tracks are

mounted. The tracks are designed for the wooden cart with plastic wheels, carrier of the measuring system. The cart is driven by the electro motor with variable transmission system over fully suspended drive, coupling, and belt drive. The RPM meter is also integrated in the driving system enabling carrier speed measuring. The variable transmission drive allows different driving speeds in the range from 0,14 m/s to 2,2 m/s. The carrier is pulled in both directions by drive rolls connected with drive shaft over double plastic cable. On the bottom of the soil boxes a drainage system consisting of 3 longitudinal pipes is intended to remove possible redundant watering amounts.

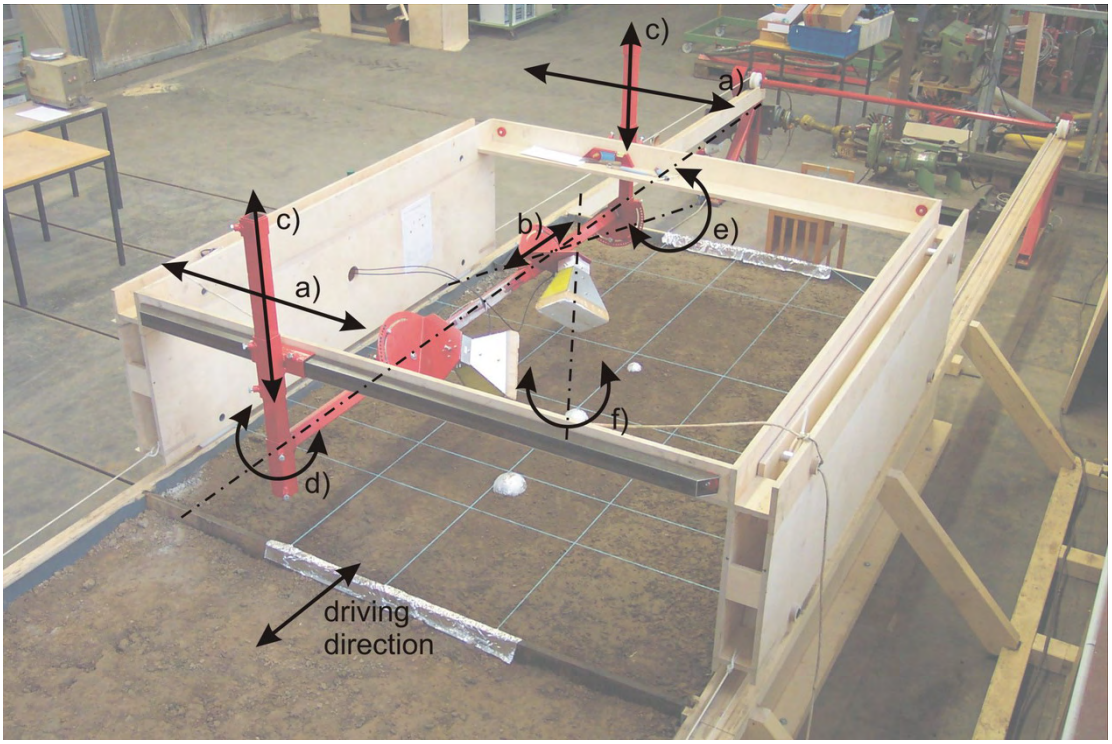

Figure 6.10 Laboratory measuring system carrier and adjustment possibilities of radar antennas; a) perpendicular adjustment of the antennas set, b) longitudinal adjustment of each antenna separately, c) vertical adjustment of the antennas set, d) antennas set angle adjustment in the perpendicular plane, e) antenna angle adjustment in the longitudinal plane of each antenna separately, f) antenna polarisation adjustment of each antenna separately

In Figure 6.10 the measuring system carrier is presented, which allows 6 degrees of freedom; three linear and three angular adjustments of antenna's position. The system carrier has been designed for two antennas and for the lateral scanning in the driving direction according to the measurement results from the initial phase of the project. In the initial phase of the project both scanning principles (laterally saddled and above the row) have been tested. More about the choosing of system parameters can be found in the Chapter 6.5.

Geophysical soil properties

For planned experiments it was necessary to cover typical soil types. Since the palette of different soil types is unlimited, three boundary soil types are chosen – sand, silt and clay soil from real agricultural locations. The choice was made according to similar experimental environments (Harmsen 2003, Daniels 2004).

The soil has been loaded into the soil box in the period winter/spring 2005. The soil was very moist, from 20%vol to over 50%vol, with very different moistures throughout the depth. The detailed description of the taking of soil probes and the excavation and the loading method can be taken from the Appendix in Chapter 10.4. Since it was needed to replicate natural conditions in the laboratory environment and it was not possible to cut out around 4,5 m^3 (2 x 3 x 0,75 m) large soil cube and to move it to the laboratory, the following method was chosen in order to provide field-near laboratory conditions. The soil layer was divided into two areas, above and below the depth of 30 cm. A digger was used for excavating and loading of two different layers into trailers: upper layer up to the depth of 30 to 35 cm was transported to the laboratory in one trailer and further 30 cm deep layer in the second trailer.

The lower layer in the sand box was 40 cm thick consisted of the "lower layer soil" from the field. The upper layer in the sand box, consisted of "upper layer soil" from the field, added 30 cm to the total depth of 70 cm in the soil boxes. This method enabled approximate field conditions without intention or potential to replicate it entirely.

The soil probes were taken from each layer in order to determine the soil water content as a volume fraction and the dry bulk density. The volume of the layer was defined by the size of the soil boxes (width and length) and the layer height. The mass of the trailer was measured before and after reloading in order to determine the total mass of reloaded soil. The scale for vehicles with accuracy of 10 kg was used. Soil properties in the soil boxes on the day of reloading were determined according to these measured data and shown in Table 6.2.

Table 6.2 Soil types; soil water content in the soil box on the day of transporting

		Soil 1: Sand soil		*Soil 2: Silt soil*		*Soil 3: Clay soil*	
Layer*		U	L	U	L	U	L
Soil water content, % vol	Mean value	38,8	22,4	34,6	27,5	42,9	50,6
	Standard deviation	0,88	0,99	1,55	1,15	4,77	1,79
Dry bulk density, g/cm^3		1,6	1,2	1,4	1,2	1,0	0,8

*U = Upper layer, which is the first 30 cm in the soil box, L = Lower layer, which is the depth from 30 to 70 cm

The data about soil water content in the sand box on the day of transporting serve only as information about the starting conditions in the soil boxes. Water content was one of the most important and controlled variables often changed during the experiments. The data about dry bulk density (dry matter) are more helpful, since they were constant during the whole project.

Separate soil probes were taken for soil particle distribution analysis and soil type determination from each layer. The probes were analysed in the Institute for Soil Science (Institut für Bodenkunde) in Bonn (Anonymous 2005). The method of analysis was according to the standard DIN ISO 11277 (Soil quality; Determination of particle size distribution in mineral soil material; Method by sieving and sedimentation following removal of soluble salts, organic matter and carbonates; 1994.) (Blume et al. 2000). The results of the analysis are shown in Table 6.3.

Big characters show the soil type according to German taxonomy and the small letters are adjectives showing which other fraction has the biggest share. The numbers (from 2 to 4) show the amount of this by-fraction (Scheffer & Schachtschabel 2002). The content of removed soluble salts, organic matter and carbonates is shown at the bottom of Table 6.3.

Table 6.3 Soil types; particle size distribution and soluble salts, organic matter and carbonates content measured according to DIN ISO 11277

		Soil 1: Sand soil		*Soil 2: Silt soil*		*Soil 3: Clay soil*	
Layer*, like in Figure 10.4		1_U	1_L	2_U	2_L	3_U	3_L
Soil type according to:	German taxonomy**	Sl3	Sl3	Ut	Ut	Tu3	Tu2
	US taxonomy***	Sandy loam	Sandy loam	Silt loam	Silt loam	Silty clay loam	Silty clay
Soil particle distribution (mean values)	Sand, %	56,9	56,7	10,7	10,6	16,1	12,3
	Silt, %	34,5	34,8	71,8	72,3	52,6	42,1
	Clay, %	8,6	8,5	17,5	17,1	31,2	45,6
Removed content (mean values)	Organic matter, %	1,4	0,6	1,33	0,2	2,0	0,3
	Salts and carbonates, %	2,9	5,8	0,1	0,1	-	-

*Index U = Upper layer (0-30 cm), Index L = Lower layer (30-70 cm)

**S, s = Sand, sandy (Sand, sandig), U, u = Silt, silty (Schluff, schluffig), T, t = Clay, clayey (Ton, tonig), L, l = Loam, loamy (Lehm, lehmig), the numbers 2 to 4 show the amount of the by-fraction, (Scheffer and Schachtschabel, 2002)

*** US taxonomy grading for sand and silt is different from German one (Silt: 2-63 µm by German and 2-50 µm by US taxonomy and sand: 63-2000 µm by German and 50-2000 by US taxonomy) and here given soil types according to US taxonomy are usable only for approximate soil type description, (Scheffer and Schachtschabel, 2002)

The graphical illustration of the particle size distribution analysis from Table 6.3 is shown in Figure 6.11. The shaded areas are representing the basic three soil types according to German taxonomy sand, silt and clay, and a mixture called loam in the middle of the diagram. Shown points 1_U, 1_L, 2_U, 2_L, 3_U and 3_L are marking used soil types during the research, better described in Table 6.3.

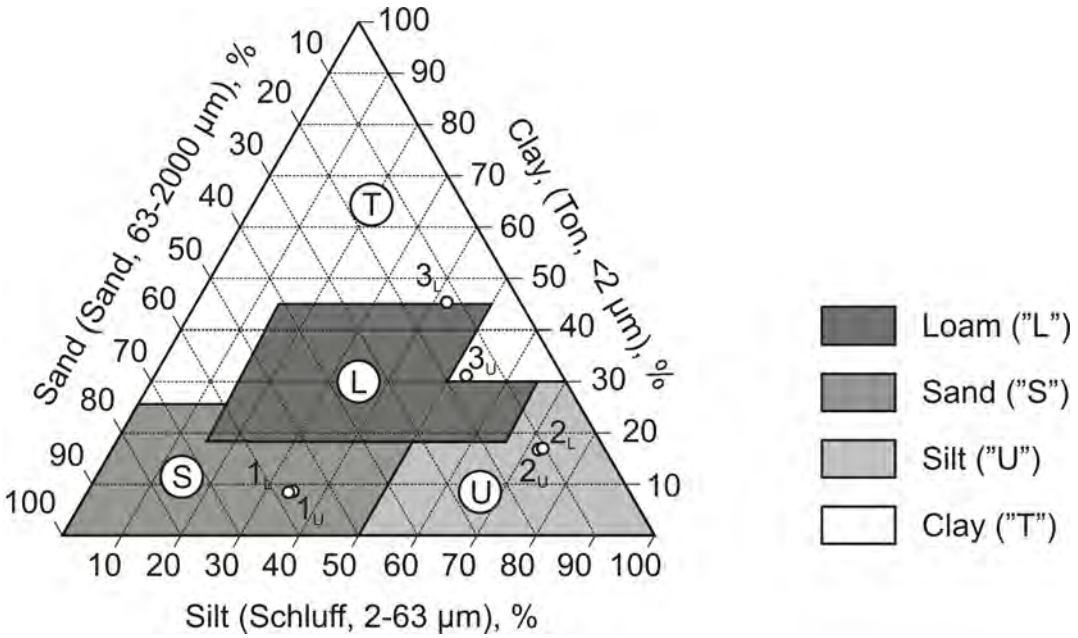

Figure 6.11 Soil types in triangular co-ordinate system, German taxonomy (Scheffer & Schachtschabel 2002)

Soil water content measurements

The soil water content, as one of most important and influential parameters of radar measuring was changed and monitored. For this purpose soil probes were taken with the horizontal soil sample cylinder of 100 cm^3 volume designed and manufactured according to DIN 19671 (Blume et al. 1997*)*. In laboratory conditions three levels of soil water content were used in the approximate range from 20%vol to 40%vol, depending on the soil type and water content level. More about the selection of water content levels is given in Chapter 6.5.0.

Soil surface properties

As already emphasised in Chapter 2.2.2, the soil surface roughness is an important ambiguity factor in the analysis of radar data. This factor is always present in any agricultural application (Paul & Speckmann 2004b). A soil surface roughness is a significant noise source, which is impossible to avoid because the used UWB system have to be elevated from the soil surface. The surface roughness causes electromagnetic surface scattering, which is difficult to predict and to model because of the complexity of natural surfaces and the difficulty in estimating appropriate input

roughness parameters for agricultural fields having different tillage (roughness) states (Davidson et al. 2000). Because of that the soil surface roughness is changed and measured. Three levels of soil surface roughness are established. More about the selection of soil surface roughness levels can be found in Chapter 6.5.

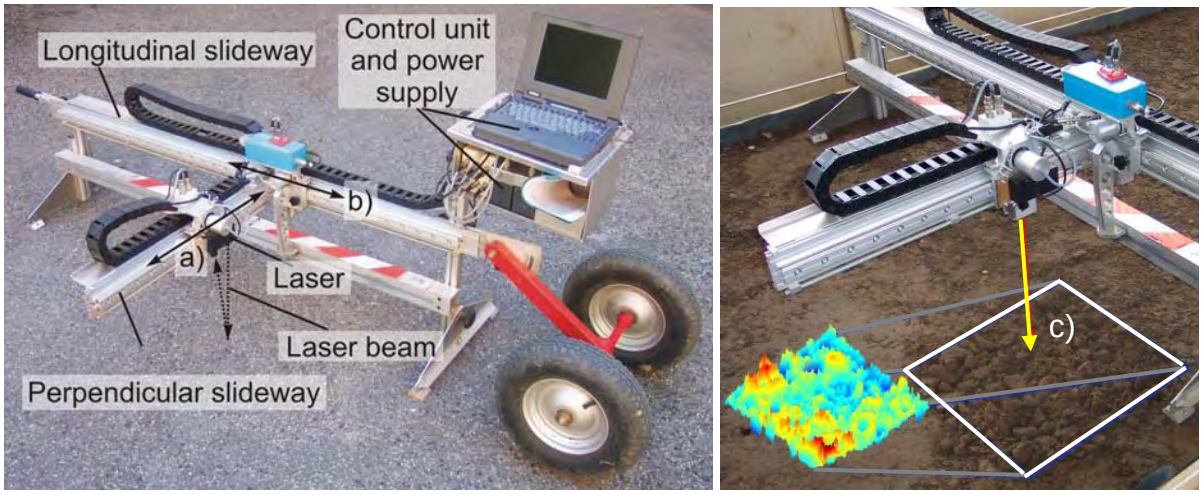

Figure 6.12 Profilometer, a) perpendicular moving direction of the laser head, b) longitudinal moving direction of the laser head, c) example of a scanned soil surface

The profilometer shown in Figure 6.12 is used for three-dimensional measuring of soil surface profile. This is a mobile device developed at the Institute for Agricultural Engineering in Bonn with optional measuring resolutions of 1 x 1 mm (the highest resolution), 2 x 2 mm, 5 x 5 mm, 10 x 10 mm and 20 x 20 mm, tested and described by Damerow (1998). The device consists of two slideways, for scanning of the 0,75 m^2 large area. The length in the longitudinal direction is 1500 mm and the length in the transversal direction is 500 mm. The laser is mounted on the carrier driven by step motor along transversal slideway. The whole transversal slideway is moved by the second step motor in the longitudinal direction. Both directions are indicated in Figure 6.12 with arrows. The drive and the laser are controlled and powered by the control unit and power supply, which enable mobility of the device and scanning independent of the power source for several hours.

The profilometer, equipped with the laser M5/200 produced by the company MEL Mikroelektronik (Anonymous 1998), uses the triangulation principle. The light source

is a diode, laser or LED. In the case of used M5/200 distance sensor it is laser with 675 mm wave length. The beam is vertically directed to the surface. The reflection from the surface is received by the position sensor. There are two different position sensors, which could be used: PSD (Position Sensing Device) or CCD element (Charge Coupled Device). These sensors measure the angle of the reflected beam, which provides the information about the distance of the object according to triangulation principle. The measuring range of the M5/200 is 200 mm, i.e. between two planes located at 200 and 400 mm from the sensor. The analogue output sends signals between 0 and 10 V and the sensor measurement resolution reaches 0,048 mm by 12 Bit conversion (Anonymous 1998).

Soil and air temperature and air humidity measurements

The data about air temperature and the relative air humidity are measured with the device TFM 100 shown in Figure 6.13 produced by the company *ELV Elektronik AG*. The most important technical data of this device are (Anonymous 2006n):

Temperature range:	from -40 to +120° C
Temperature accuracy:	±0,5° C
Moisture range:	from 0 to 99,5%
Moisture accuracy:	±3,5%

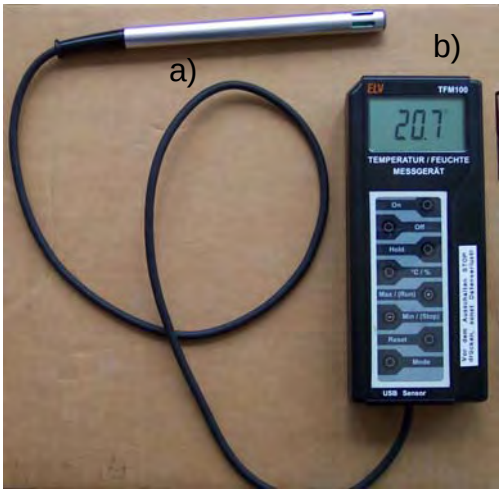

Figure 6.13 Air temperature and the relative air humidity measuring device; a) measuring probe, b) display and control keyboard

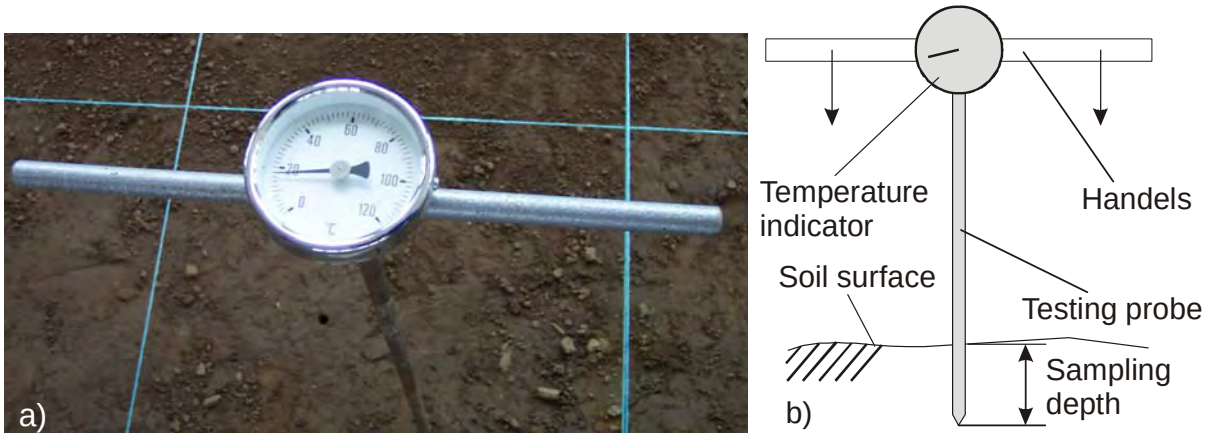

Figure 6.14 Soil temperature sampling probe; a) probe in the soil, b) main parts of the probe and sampling principle

The soil temperature is measured with the sampling probe shown in Figure 6.14. This method of soil temperature measurement gives an approximate temperature data in the upper layer of soil (approximately 15 cm of depth) with the measuring accuracy of ±2° C. This probe delivers the temperature of the sampling depth in the zone of the probe's tip. In Figure 6.14 a) the applied temperature probe in soil is shown, and in Figure 6.14 b) the sampling principle and the main parts.

Experimental object properties

During the laboratory experiments two different types of experimental objects were used:

- *Sugar beets* of cultivar *Belinda* (KWS) of different sizes and shapes without extraordinary attributes grown in the glasshouse conditions at the Teaching and Research Station: *Marhof* of the Agricultural Faculty in Bonn and
- *Reference objects* in the form of aluminium spheres with diameters 60 mm and 120 mm.

The important properties of morphological parts of sugar beets (maximal diameter and root length) were measured according to Figure 6.1. The sugar beets were topped according to Figure 6.2 d). In addition to these properties, the mass of each sugar beet was weighed. The detailed descriptions of sugar beets used during experiments are given in the Chapter 6.5.

The reference objects used during the experiments are shown in Figure 6.15. The Styrofoam spheres are wrapped with aluminium foil forming geometrically and dielectrically unambiguous form needed for the development of the data processing procedures. Since the average diameter of sugar beets is around 100 mm (the average diameter of 1770 measured sugar beets in the year 2004 and 2006 was 102 mm with standard deviation 17 mm), the sizes of 60 mm and 120 mm in diameter of spheres have been chosen. The diameter of the smaller sphere has been selected as unusually small diameter for sugar beets in the time of harvest and as such appropriate for detectability tests.

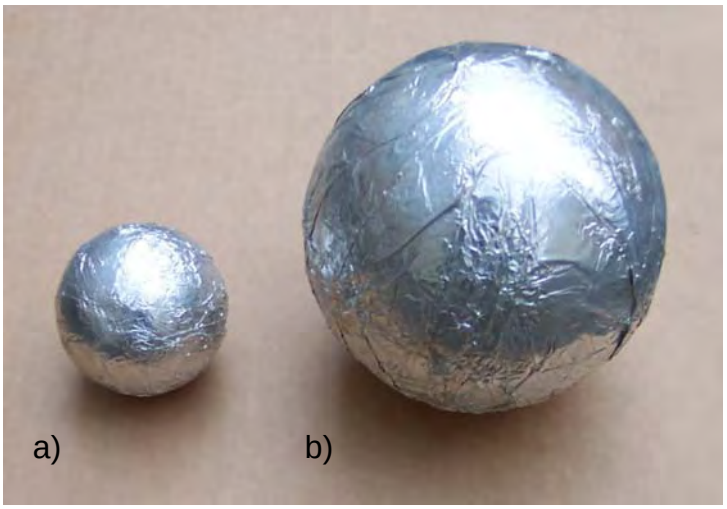

Figure 6.15 Reference objects used for experiments in laboratory conditions; a) aluminium sphere of Ø60 mm, b) aluminium sphere of Ø120 mm

6.3.2 Experimental environment and experimental accessories – field experiments

Features of the experimental field vehicle

The experimental field vehicle shown in Figure 6.16 has been designed in order to comply with radar technology requests. The measuring system carrier allows 6 degrees of freedom; three linear and three angular adjustments of antenna's position, like the one used in laboratory conditions. This allows the repeating of geometrical system parameters tested in the laboratory conditions.

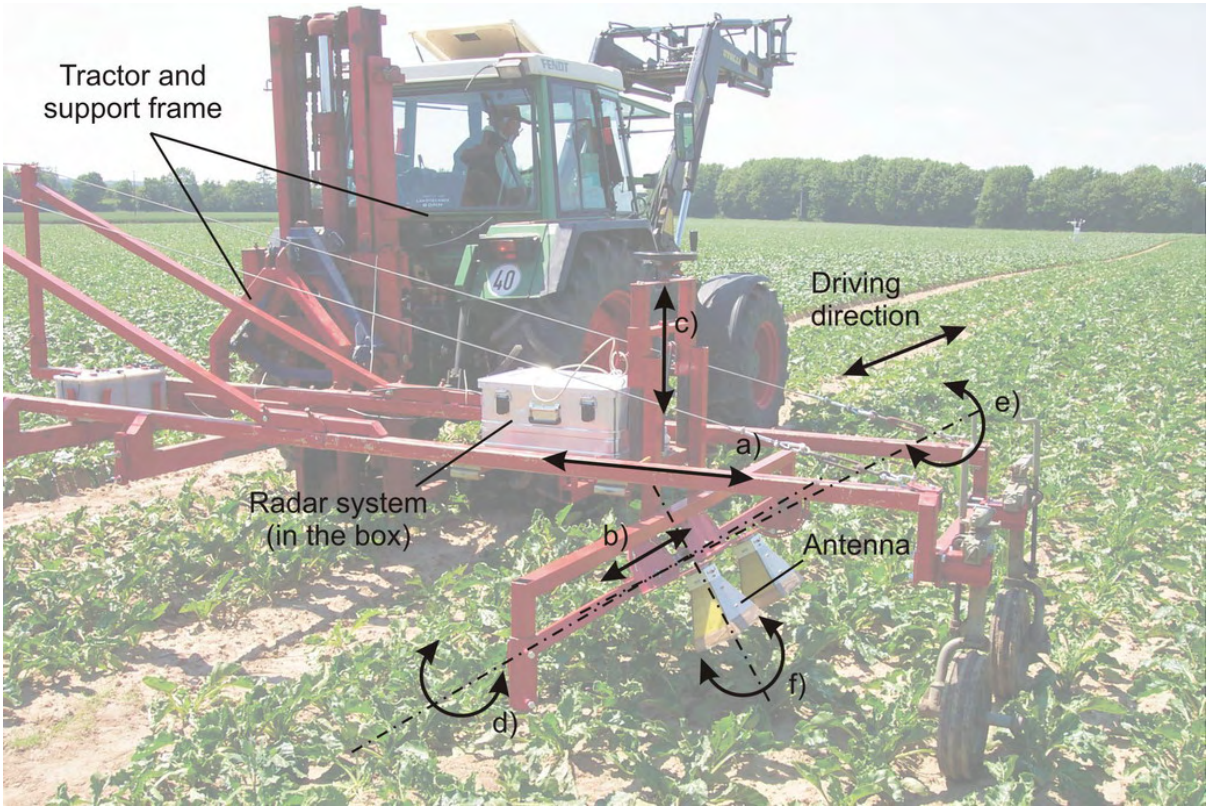

Figure 6.16 Field measuring system carrier and adjustment possibilities of radar antennas; a) perpendicular adjustment of the antenna set – manual during scanning, b) longitudinal adjustment of each antenna separately, c) vertical adjustment of the antennas set, d) antenna set angle adjustment in the perpendicular plane, e) angle adjustment in the longitudinal plane of each antenna separately, f) polarisation adjustment of each antenna separately

Geophysical soil properties

Soil type on the experimental field (Plot *Oberhoicht 23*), similar to the type 2 from the soil box, contains in average 6 ±2% of sand, 18 ±4% of clay, and the rest silt (ca. 75%). The data are shown in the diagram in Figure 6.17. This soil was chosen the experiments in field conditions because it represents typical arable soil.

For the determination of the soil water content, the properties of the soil surface, the soil and air temperature, and the relative air humidity the same experimental accessories are used like in the laboratory conditions.

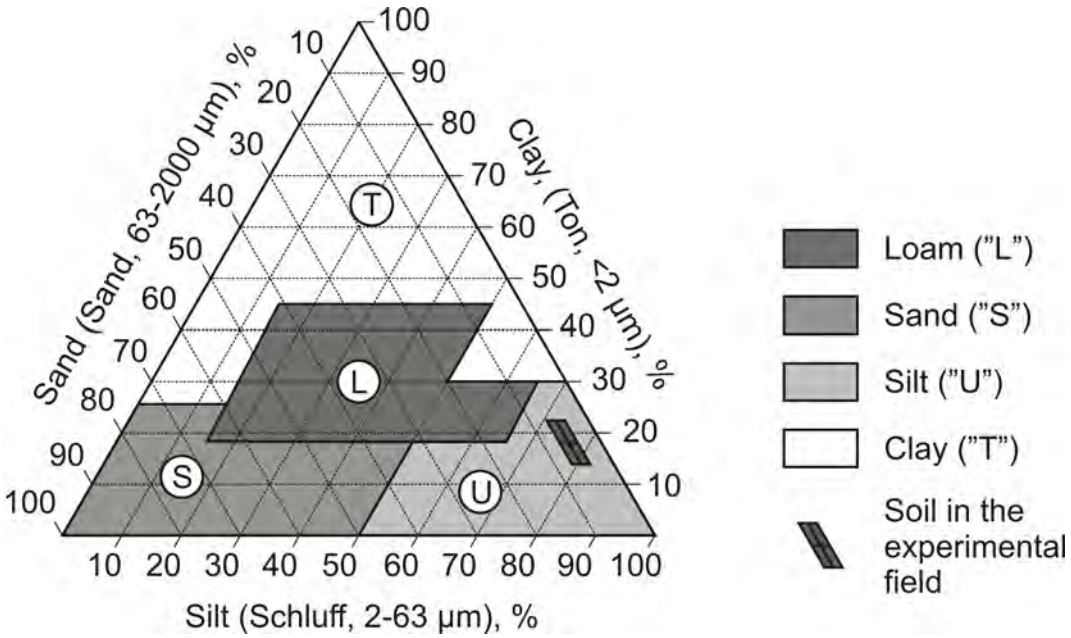

Figure 6.17 Soil type in the experimental field (Plot *Oberhoicht 23*, sand 6±2%, clay ca. 18±4%, the rest silt, ca. 75%)

Experimental object properties

During the field experiments sugar beets of cultivar *Belinda* (KWS) of different size and shape without extraordinary attributes are used. The sugar beets are grown in normal field conditions at the Teaching and Research Station *Klein Altendorf* of the University of Bonn, 15 km south-west from Bonn. The relevant properties of morphological parts of sugar beets (maximal diameter, root length and top height) were measured according to Figure 6.1. The sugar beets were topped according to Figure 6.2 d). In addition to these properties, the mass of each sugar beet was weighed and the distance between sugar beets in the row was measured. The detailed descriptions of sugar beets used during experiments are given in the Chapter 6.5.

6.4 Data acquisition and processing

Data acquisition and signal analysis

Sugar beet detection is an uncommon case in GPR practice, because the target is located in the boundary layer of soil, like in Figure 6.18. During the measurements

the antenna system (one transmitter and one receiver) was moved at a fixed distance from the soil over the sugar beets. The radiated waves are reflected and scattered in different manners and a part of their energy is backscattered to the receiving antenna.

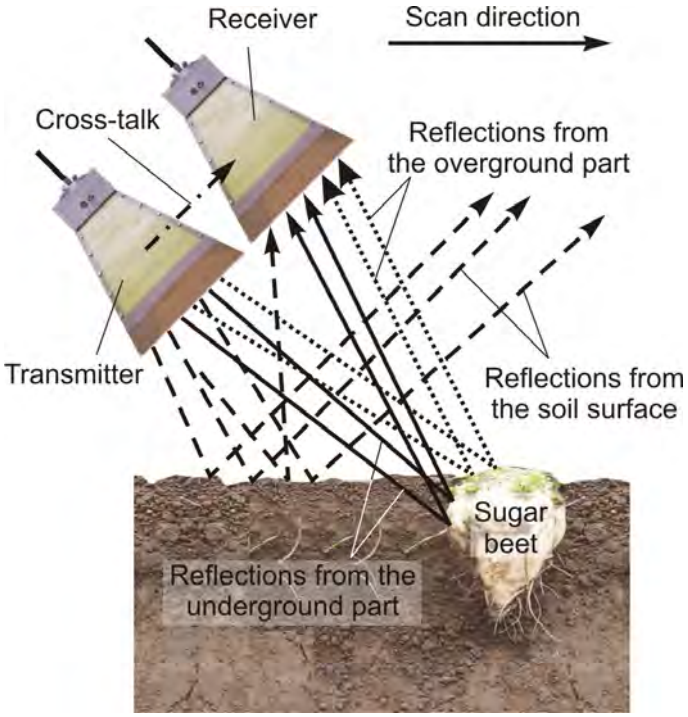

Figure 6.18 Data collection principle (Konstantinović et al. 2005)

The following simplified Equation summarizes the most relevant components of the received signal (Woeckel et al. 2006):

$$b_{tot}(t) = b_{target}(t) + b_{XT}(t) + b_{sf}(t) + b_{nt}(t) + n_{ext}(t) + r_{mult}(t) \qquad 6.2$$

b_{tot} measured signal

b_{target} scattering signal of the target (underground and overground part)

b_{XT} antenna cross talk

b_{sf} reflection from the soil surface

b_{nt} scattering from other objects (stones, soil bumps – usually called clutters)

n_{ext} noise, external disturbance

r_{mult} multiple reflections (antenna-surface, antenna-target, target-soil, etc).

For simplification of morphologic and feature dependent scattering, a model with a point scatterer is established. In this manner all feature-depend signals are correlated to their reference points. The reduction of geometrical objects into point sources is a restriction for simplification and serves to get deeper into the nature and complexity of the target scattering signal. The signal orientated model presented in Figure 6.19 is based on the radar equation and implies far-field conditions. Equation 6.3 represents the complete radar equation in time domain with impulse response functions in free space (only the target); in this equation the polarization is omitted for simplicity (Woeckel et al. 2006).

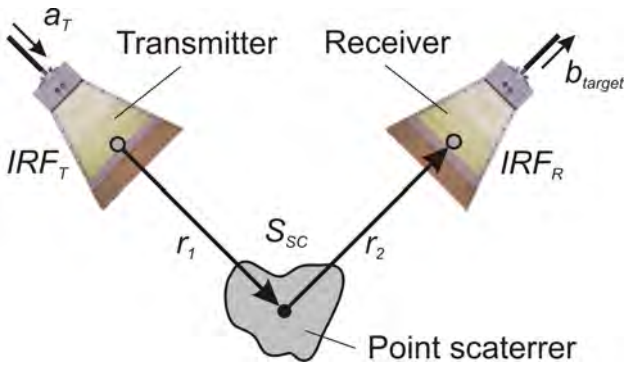

Figure 6.19 System model with point scatterer (Woeckel et al. 2006)

$$b_{target}(t) = \frac{1}{2\pi r_1 r_2} IRF_T(t, \varphi_T, \vartheta_T) * S_{sc}(t, \varphi_T, \vartheta_T, \varphi_R, \vartheta_R) * IRF_R(t, \varphi_R, \vartheta_R) * a_T\left(t - \frac{r_1 + r_2}{c}\right) \quad 6.3$$

a_T transmitted wideband signal

IRF_T IRF of the transmitting antenna

IRF_R IRF of the receiving antenna

S_{sc} scattering IRF

φ, ϑ propagation directions

c propagation velocity of light

r_1, r_2 distances between antennas and object

$*$ symbol which represents operation of convolution.

Even if other influences presented in Equation 6.2 are disregarded, the Equation 6.3 shows the complex and interlaced nature of the scattering IRF in the system signal-antennas-target. The measurable b_{target} has to be analysed in order to extract the IRF of the scatterer S_{sc} (in free space). Considering the Equation 6.3 S_{sc} is disguised by the IRF of the antennas ($IRF_T * IRF_R$) and the transmitted signal a_T. The masking by the transmitted signal a_T is reduced by using UWB radar electronics. To extract the scattering function S_{sc} of the target out of $IRF_T * S_{SC} * IRF_R$, the influence of the antenna has to be removed by the operation of deconvolution (Woeckel et al. 2006).

Data processing and interpretation

Equation 6.2 describes a simple model regarding all scattering effects to be independent from each other. The validity of this assumption is limited but it should be sufficient to extract the scattering of the target out of the measured signal. The goal of the data processing is to extract the IRF of the sugar beet from the collected data in order to determine its physical properties (volume or mass, for example).

The data processing steps are:

1. Extract the backscattered signal of the target b_{target} from the measured signal b_{tot}
2. Clean-up the extracted signal from the influences of antennas by deconvolution
3. Data interpretation in order to recognize important geometrical properties of the test object from its IRF.

1. Extraction of the target signal

For the successful extraction of the target signal it is necessary to prepare and perform the experiments carefully, and to introduce several approximations in the signal analysis. Because of the low variety of other objects than beets on agricultural fields the clutter by unwanted objects $b_{nt}(t)$ is neglected in this analysis. Compared to clutter, the noise $n(t)$ will only cause minor effects. Therefore it will be excluded from further considerations. Additional multiple reflections $r(t)$ between the antenna and the soil can also be neglected because of the far-field conditions. The remaining two

components b_{XT} and b_{sf} from Equation 6.2 can be more or less successfully suppressed or removed by:

a) time gating of short non-overlapping signals (typical examples: antenna cross talk b_{XT} and multiple reflections). Additionally, the antenna cross talk can be suppressed by absorber shielding between the transmitting and receiving antenna and easily be subtracted because of its time stability
b) subtraction of static background reflections
c) reduction of surface reflection by the appropriate (oblique) antenna position and
d) techniques of sliding (moving) background subtraction BS – the calculation methods BS and the size of the moving window were varied to find the best solution for separating the targets' hyperbolas (Woeckel et al. 2006).

2. Deconvolution procedure

The joint antenna IRF presented in Equation 6.4 covers the targets IRF S_{sc} and stretches and expands all signal components by its ringing (post-oscilation). Conventionally, this influence is used to be removed by division of the antenna spectrum in frequency-domain called deconvolution.

$$IRF_T\left(t, \varphi_T = 0, \vartheta_T = 0\right) * IRF_R\left(t, \varphi_R = 0, \vartheta_R = 0\right) \qquad 6.4$$

The deconvolution has two main goals: compression of the impulse length to improve time gating, and the sharpening the radar images (B-scan). In the case of noise and low signal level, the deconvolution produces additional noise. To suppress the influence of noise caused by deconvolution and to suite the signal shape on GPR-demands, a filter with optimized and known filter output is used. The optimized filter output is a synthetic impulse with special time shape. In order to design the pulse shaping filter, the joint antenna IRF has to be known and it is measured by the direct transmission between antennas. It is important that the gain of the transfer function of the impulse shaping filter is small or zero at frequencies where the joint antenna IRF has low SNR (signal to noise ratio). Depending on the purpose, the shape of the impulse can be optimized by different criteria: minimizing side lobes (reduced

ringing), narrow main lobe, symmetric shaping etc. This synthesized impulse can be converted to any type of antenna and it defines the new IRF of the radar system.

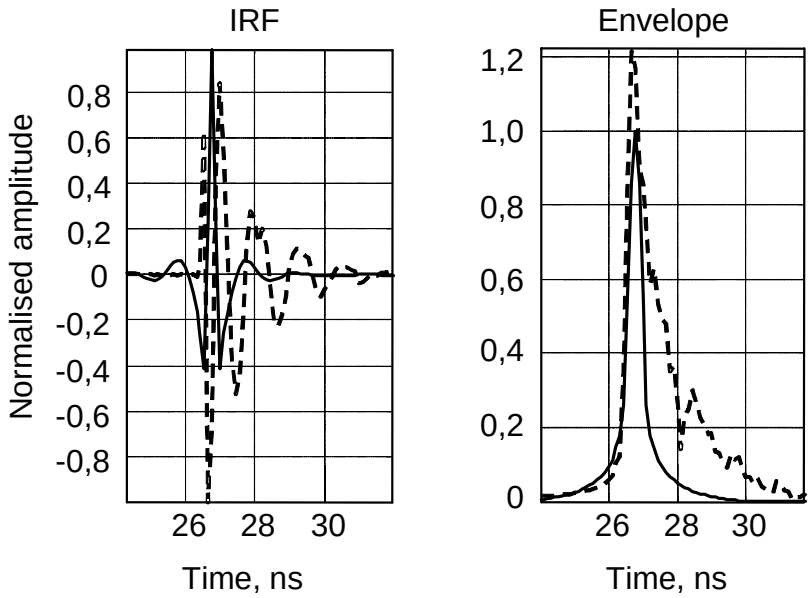

Figure 6.20 Comparison of real joint antenna IRF (dashed line) and synthetic IRF (continuous line) gained with objective function filtering

Figure 6.20 demonstrates an example. The synthetic impulse was adapted for reduction of antenna ringing to achieve a better time resolution for gating of multiple reflections. The effect of impulse compression by objective function filtering reduces the pulse width of the envelope (from 3 ns to 1 ns) and the amplitude of side lobes.

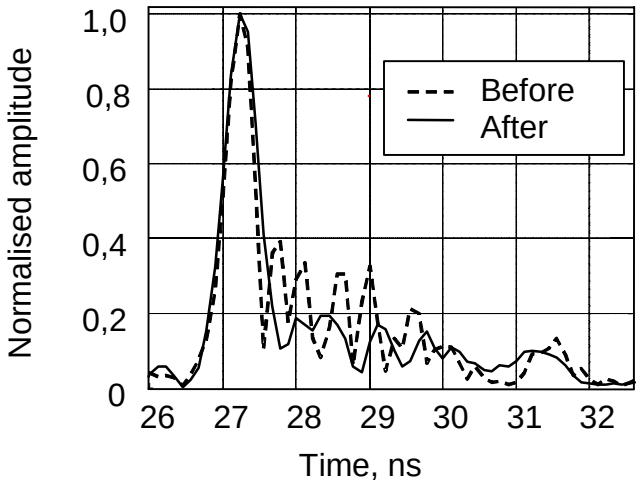

Figure 6.21 IRF of a sugar beet in soil before (dashed line) and after (continuous line) deconvolution procedure

In Figure 6.21 an example of deconvolution procedure applied on the IRF of a sugar beet in soil is shown. The continuous line presents the signal after processing, which shows substantially less ringing than the original signal (dashed line).

3. Data interpretation

The above presented signal processing procedure used within this project is developed at the partner institution. An example of the processing of an acquired radargram and the interpretation principle of the processed date used in the course of project activities is shown in Figures 6.22 and 6.23.

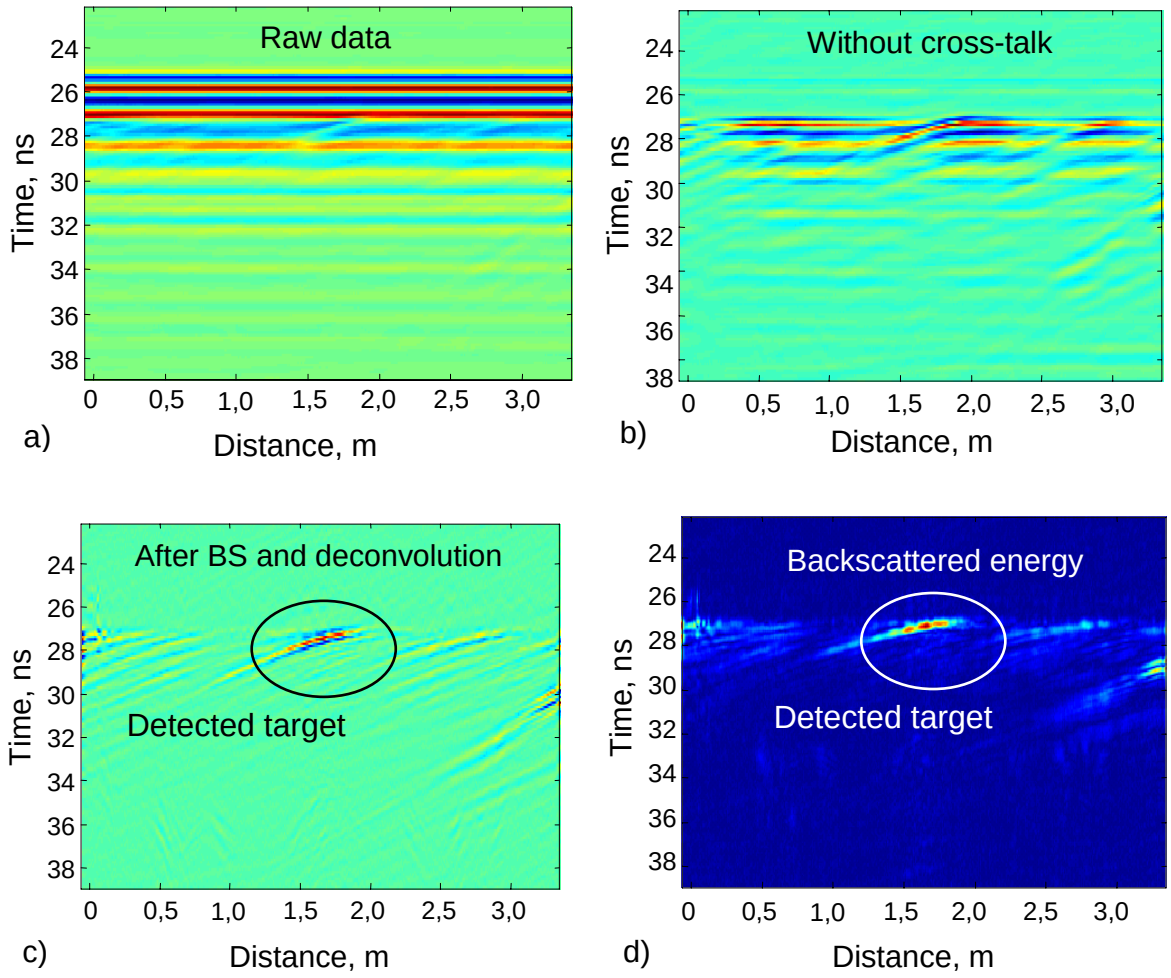

Figure 6.22 Radargram processing procedure and interpretation steps; a) acquired radargram – raw data, b) radargram without cross-talk, c) processed radargram with detected target, d) quadratic absolute value of Hilbert-transformed radargram (time-dependent energy representation)

In Figure 6.22 a) an acquired radargram of raw data is presented which is not possible to interpret. In b) are data without cross-talk, which is removed by time-gating of constant signals, and in c) is shown the processed radargram after background subtraction and deconvolution (described above) with recognisable signal of the detected object.

In Figure 6.22 d) time-dependant quadratic absolute value of Hilbert-transformed radargram is used for representation of amount of backscattered energy from the target. Hilbert-transformation is a linear integral-transformation. The absolute values of this transformation represent the envelope of the real signal. Thereafter energy of the real signal could be calculated according to the following equation.

$$E_{HT} = \int \left| hilbert\left(\left| s(t)^2 \right| \right) \right| dt \qquad 6.5$$

In Figure 6.23 an example of the data processing and interpretation procedure of a sugar beet row scan with 4 sugar beets of different sizes is given. This measuring scenario illustrated in 6.23 a) has been used in the preliminary phase of the project and represents the original idea of sugar beet detection (Konstantinović et al. 2005). In Figures b) and c) the processed data (see Figure 6.22) are presented. The diagram in Figure 6.22 d) represents the same collected backscattered energy presented in an integral form.

According to the presented processed radargrams the following values can be extracted:

- distance of the object from the antennas (travelling time of the wave in ns)
- distance of the object from the beginning of the scan and/or distance between the detected objects (measured with path meter in laboratory conditions, see position 12 in Figure 6.9, and presented in recorded samples and optionally converted into meters in field conditions) and
- the amounts of backscattered energy from the detected objects, which show correlation to the size of objects.

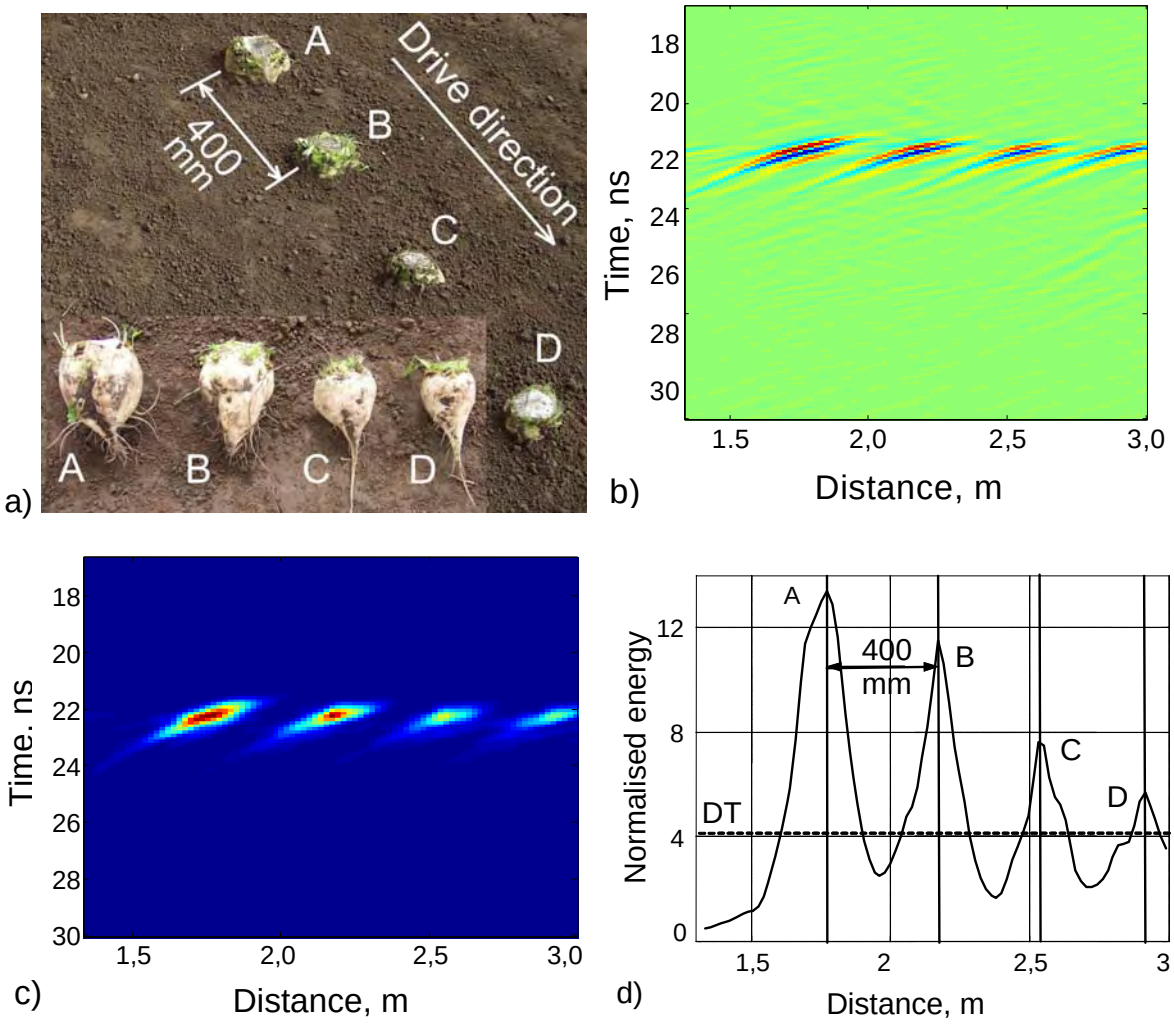

Figure 6.23 Principle of radargram interpretation for sugar beet detection; a) sugar beet row, b) processed radargram, c) time dependant energy representation of backscattered energies, d) threshold detection of sugar beets (DT stands for detection threshold)

The above presented data i.e. radargrams have been acquired in the favourable and controlled conditions in order to test the approximate limits of the developed data processing method and its general capacity for sugar beet detection. The following chapters deal systematically with the experimental determination of the best possible parameters of the measuring system, which would provide sufficient information about field-compatible scenarios.

6.5 Experimental procedures

6.5.0 Boundary conditions determination

Results of preliminary measurements

In the course of preliminary experiments different system configurations were tested in order to minimise large number of possible combinations, most of all: antenna arrangement and antenna polarisation combinations. The measuring system allows coupling of three antennas: one transmitter and two receivers (see Figure 6.3) in various user-defined spatial arrangements. Different antenna arrangements with three antennas were tested and they did not show improvements of the signal quality in comparison to the chosen two-antenna arrangement shown in Figure 6.24. The other possibility, the arrangement with two forward looking antennas saddled over the row did not show significant advantages in data collecting, but it caused technical problems on the measurement system carrier in both laboratory and field conditions and it was not used for further experiments.

The antenna arrangement in Figure 6.24 is geometrically determined with three constrains: α – incident angle of wave propagation, β – angle between antennas and h – height of the starting point of wave propagation and the crossing point of antenna axes on the soil surface. The general demand of any antenna arrangement is to keep the antennas as low as possible because of dissipation losses. In Figure 6.24 d) the special case with parallel antennas is shown, which showed signals of insufficient quality, first of all because of the signal loss – one part of transmitted waves from antenna Tx goes directly into the side of the receiving antenna Rx. This antenna arrangement is used only in preliminary phase of the project.

The adjustment boundaries of the used ranges of antenna angles are shown in Figure 6.25. The angle α is changed from 0° to 60°, where the minimum angle represents the scanning over (directly above) the row, and the angle β from 0° (parallel antennas) to 90°.

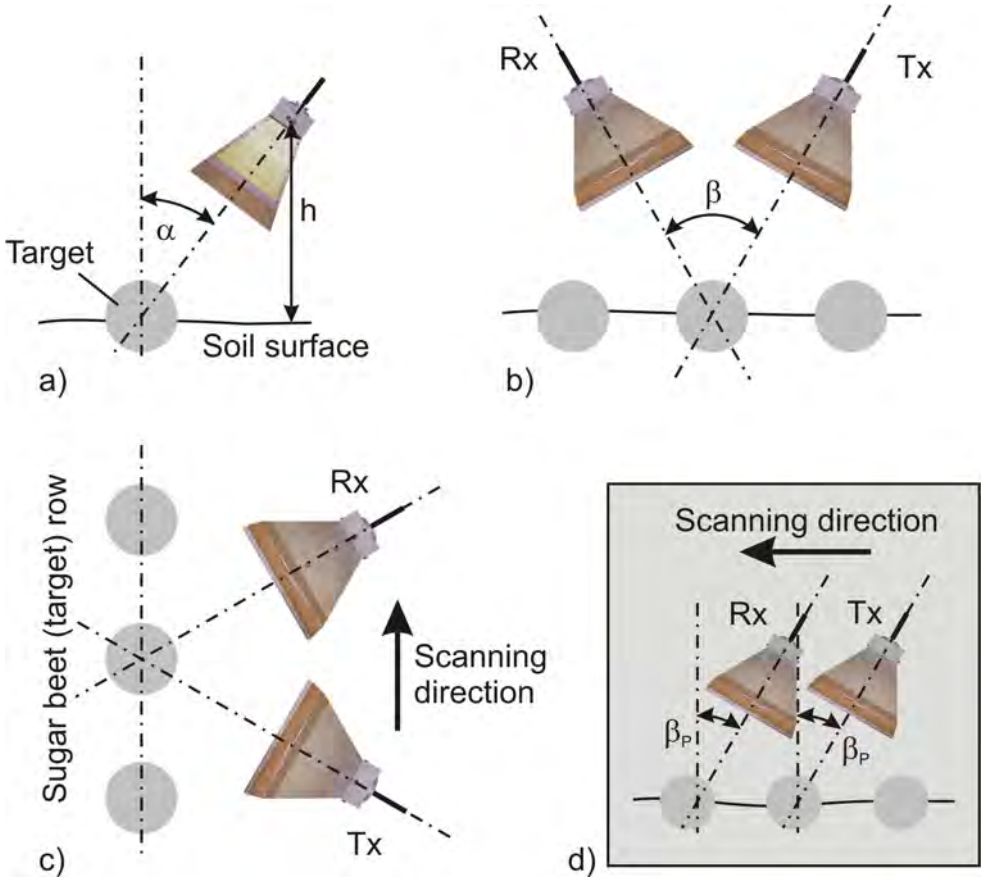

Figure 6.24 Bistatic antennas arrangement with the scanning direction parallel to the row; a) view from above, b) side view, c) view in the scanning direction, d) special case with parallel antennas

There are three polarisation combinations of the antenna system, shown in Figure 6.26. There are two types of polarisations – vertical and horizontal, depending on the direction of the wave propagation (see Figure 2.8), i.e. antenna orientation. If the lone electric vector is oriented in the vertical (horizontal) direction in antenna co-ordinates this polarisation is called vertical (horizontal) linear polarisation. The mode of radar polarisation where the microwaves of the electric field are oriented in the vertical plane for both signal transmission and reception by means of a radar antenna is called VV (vertical-vertical) polarisation (Anonymous 2006o), which also respectively applies for HH (horizontal-horizontal) and VH (vertical- horizontal). The following nomenclature for polarisation combinations of antennas is adopted: VV polarisation in Figure a), HH in Figure b) and VH in c). The first experiences showed that the VH polarisation (cross-polarisation) has no potential for sugar beet detection. From the results of preliminary tests it was concluded that the VV polarisation provides better

signal quality than VH, because of that the VV polarisation was predominantly utilised during the experiments.

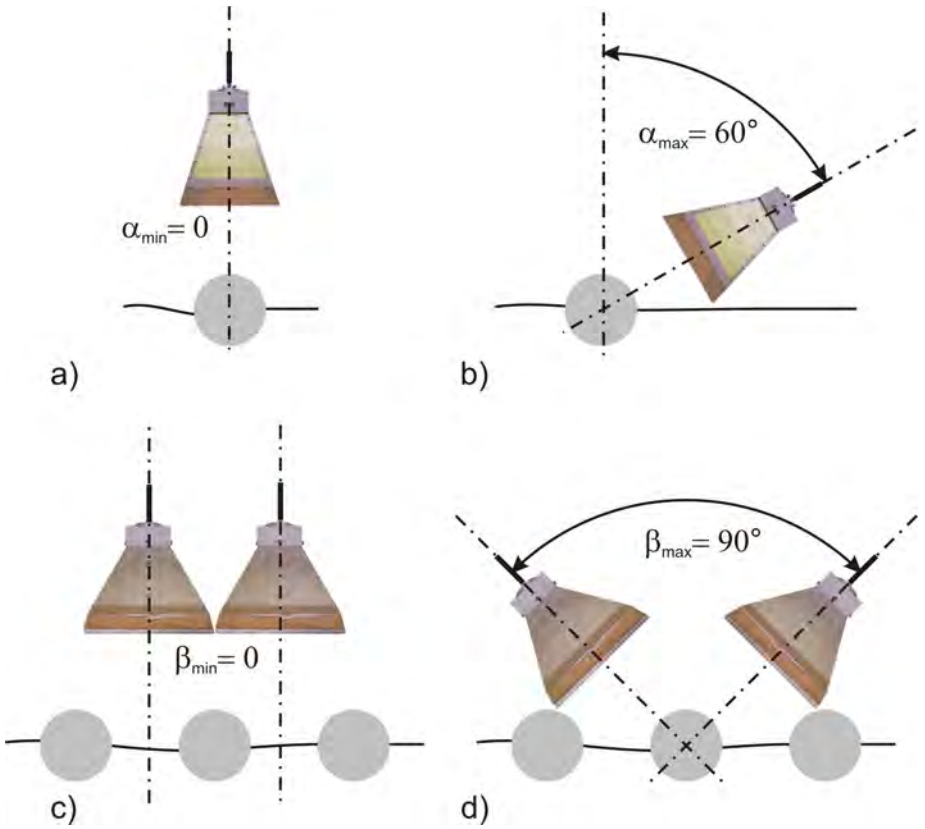

Figure 6.25 Boundaries of antenna adjustment ranges; a) minimum of the incident angle, b) maximum of the incident angle, c) minimum of the angle between antennas, d) minimum of the angle between antennas

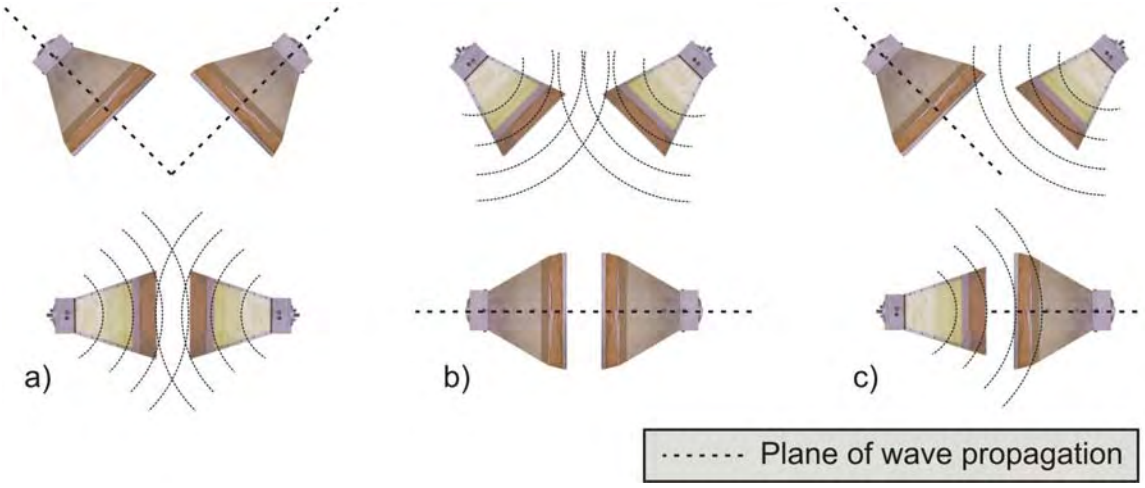

Figure 6.26 Propagation of radar waves – polarisation of antennas; a) VV polarisation, b) HH polarisation, c) VH polarisation

Measurement conditions: soil surface roughness

In order to determine the surface roughness of the soil and to reproduce the effects of surface roughness in all experiments, the standard deviation σ_{sp} of the height profile (referred to an area which corresponds to the antenna footprint) and the maximum diameter d_{sp} of soil bumps were defined and monitored. The height profile of the surface was measured with a laser-scanner with the resolution of 5 x 5 mm (see Figure 6.12). In the laboratory conditions three significantly different levels of soil surface roughness, shown in Figure 6.27, were selected and reproduced according to experimental requirements:

Level 1: Smooth, σ_{sp} = 3 mm, d_{sp} = 5 mm
Level 2: Fine, σ_{sp} = 6 mm, d_{sp} = 20 mm and
Level 3: Rough, σ_{sp} = 13 mm, d_{sp} = 100 mm

a)  b)  c) 

Figure 6.27 Soil roughness levels; a) smooth, b) fine, c) rough

Measurement conditions: soil water content

The soil water content within the test stand is changed using a common garden hose with constant flow, Figure 6.28 a). The equal distribution of water over the whole soil surface during watering has been possible thanks to the even raster, Figure 6.28 b). The soil water content is determined by analysing the probes taken with a soil sample cylinder (see Chapter 6.3.1) from the top soil layer (15 cm), which is the most influential for radar measurements. The soil boxes were covered with plastic sheeting

during the breaks between the experiments, and over the night and the weekends, which successfully preserved constant water content. The water content reduction is achieved by uncovering (without forced evaporation).

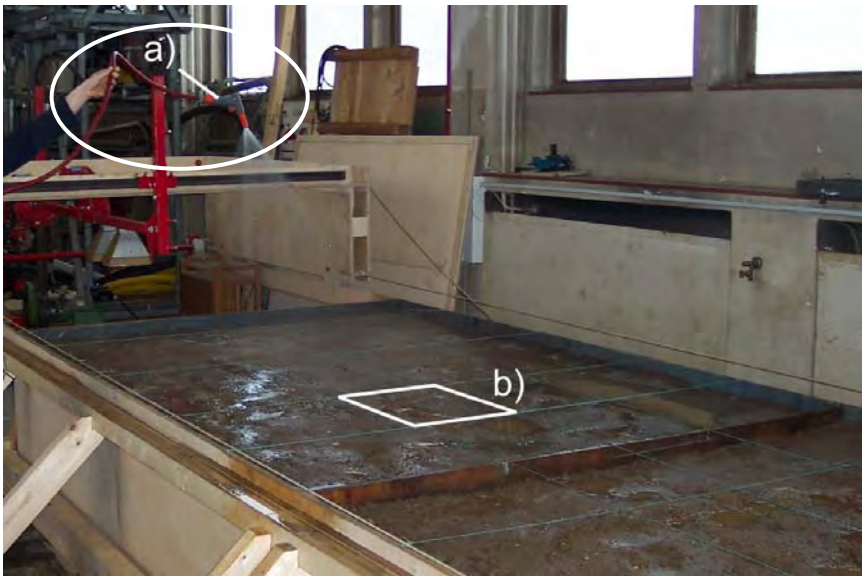

Figure 6.28 Soil water content changing – watering procedure; a) garden hose, b) soil surface divided into even raster

The following levels of soil water content in soil boxes were selected:

Level 1: Moderate wet, 25%vol (± 5%vol)
Level 2: Wet, 30%vol (± 5%vol)
Level 3: Very wet, 35%vol (± 5%vol)

The reason for setting aside the soil water contents below 20%vol was to test the radar measuring system in conditions which resemble the field conditions in the time of harvest (period from September to December). If the radar system is capable to provide useful information in the conditions with higher water contents, it is also able to work in the drier conditions with higher dielectric contrast between the sugar beet and the environment.

In Table 6.4 an overview on monitored and changed features of the measuring environment, measuring radar system and test objects is given.

Table 6.4 Overview on properties and features recorded, or varied and recorded during the experiments

	Property/Feature	Conditions	
		Laboratory	Field
Environmental conditions	Soil type*	●	○
	Soil water content*	●	○
	Soil surface roughness*	●	○
	Soil temperature	○	○
	Air temperature	○	○
	Relative air moisture	○	○
Measuring radar system	Incident angle of the antennas, α*	●	●
	Angle between antennas, β*	●	●
	Scanning speed	○	○
	Distance target-antennas (connected to angles)*	●	○/●
	Wave polarisation*	●	○
Test objects	Material*	●	○
	Size/mass/volume*	●	○
	Shape (e.g. topped and untopped sugar beets)*	●	●
	Position/distribution*	●	○

* highly influential parameter on radar measurements

○ – only recorded, ● – changed and recorded (controlled) values

6.5.1 Laboratory experiments

6.5.1.0 Reference measurements

Goal of the tests

Measurements with reference objects – aluminium spheres shown in Figure 6.15 were used in order to determine the sets of system parameters which allow acquiring of radar signals suitable for successful data processing and interpretation.

Test conditions

For this purpose the measuring scenario with two aluminium spheres (Ø60mm and Ø120 mm) has been arranged as depicted in Figure 6.29 in all three soil boxes. The spheres were at the distance of 1 m from each other, on the prepared surface (0,75 x 2 m) with a certain soil surface roughness level. The regular distance between sugar beets is 20 cm. The distances between objects of 1 m from each other and 1 m from the walls of the soil box have been chosen because it was needed to enable reliable separation of signals, independent of influences of other objects.

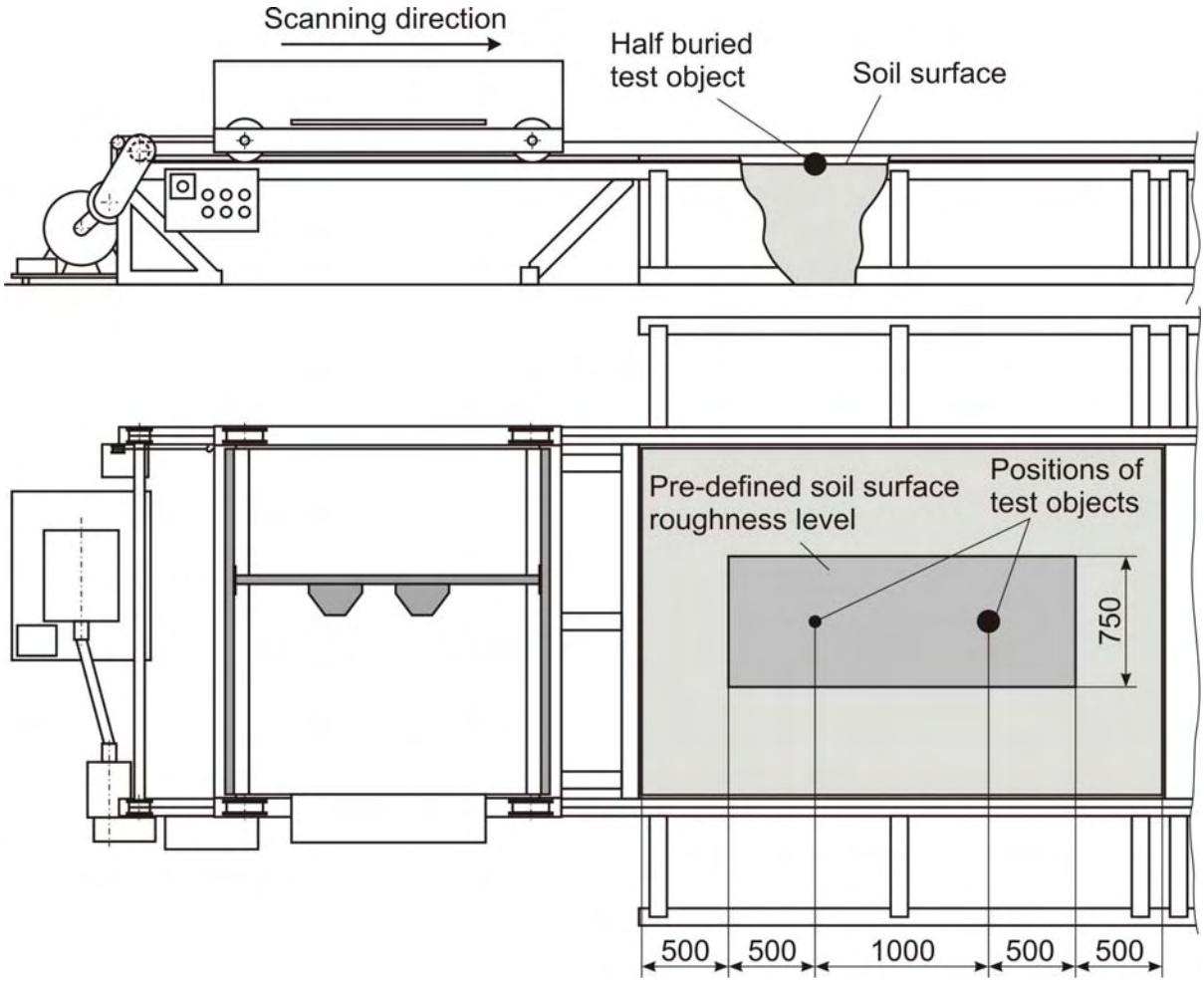

Figure 6.29 Scenario arrangement with aluminium test objects

The radar measuring system features were changed in accordance to the experience from the preliminary experiments presented in the previous chapter. The total of 9 combinations of antenna angles was tested in 27 different scenarios, for each soil

type, soil water content level, and soil surface roughness level combination, see Table 6.5.

Table 6.5 Scenario conditions with aluminium test objects

	Scenario property/feature		*Value/feature*		
Environmental conditions	Soil type, –		Sand	Loam	Clay
	Average soil water contents in upper 10 cm soil layer, %vol	Level 1:	23	26	30
		Level 2:	27,5	29,5	31,5
		Level 3:	31,5	33,5	35
	Average soil surface roughness, level		1, 2 and 3		
	Soil temperature range, °C		16 -19		
	Air temperature range, °C		19 - 22		
	Relative air humidity range, %		25 - 40		
Measuring radar system	Incident angle of the antennas, °		0, 30, 45 and 60 (α in Figure 6.30)		
	Angle between antennas, °		0, 45 and 90 (β in Figure 6.30)		
	Scanning speed, m/s		0,14		
	Wave polarisation, –		VV		
Test objects	Material, –		Aluminium		
	Diameter, mm		60 and 120		
	Distance between test objects, m		1 (Figure 6.29)		

In all cases the antenna beams crossed on the soil surface, in the centre of spheres. A general case (α = 30°, β = 45°) and the boundary case (α = 0°, β = 0°) are presented in Figure 6.30. The vertical polarisation of the incident electromagnetic wave was chosen because it provided better target reflections within preliminary experiments than the horizontal one. The used scanning speed was the lowest driving speed from the range of the driving unit's variable transmission system.

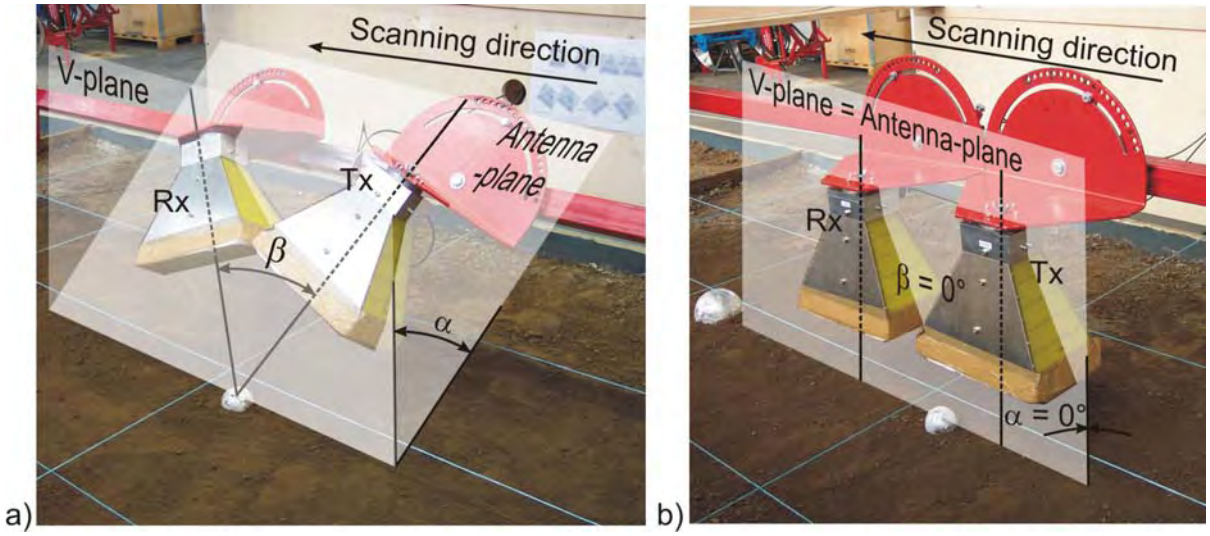

Figure 6.30 Antenna positions in the scenario with aluminium test objects; a) general case, b) boundary case (α = 0°, β = 0°)

6.5.1.1 Experiments with topped sugar beets

Goal of the tests

The experiments with topped sugar beets were used as a comparison and confirmation method for results of experiments with reference objects, most of all for the choice of antenna angles. This part of experimental activities was used to asses the potential of the system in laboratory conditions, most of all the potential of separation and size differentiation of the developed signal processing procedure.

Test conditions

For this purpose the measuring scenario described in the previous chapter has been approximately reproduced. Three sets of sugar beets (maximal diameters: 60 mm and 120 mm) have been arranged like in Figure 6.29 in all three soil boxes. The sugar beets were at the distance of 1 m from each other, on the prepared surface (0,75 x 2 m) with certain soil surface roughness level, Figure 6.31.

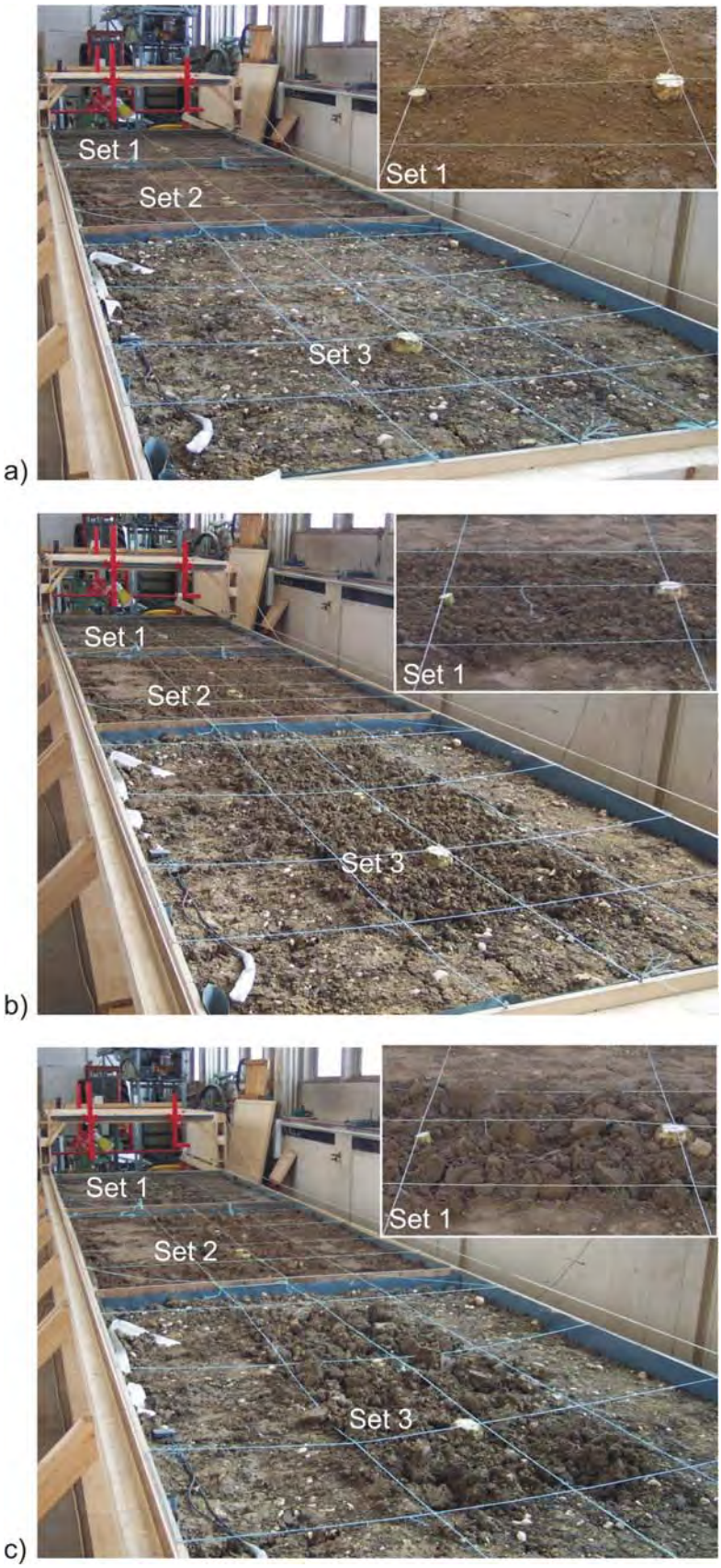

Figure 6.31 Scenario with topped sugar beets; a) soil surface roughness level 1, b) soil surface roughness level 2, c) soil surface roughness level 3

The radar measuring system features were changed in accordance to the experience from the experiments with reference objects. The total number of previously used combinations of antenna angles was reduced and it was tested for each soil type, soil water content level, and soil surface roughness level combination, see Table 6.6. All other conditions were comparable to the conditions during measurements with reference objects.

Table 6.6 Scenario conditions with topped sugar beets

	Scenario property/feature		*Value/feature*		
Environmental conditions	Soil type, –		Sand	Loam	Clay
	Average soil water contents in upper 10 cm soil layer, %vol	Level 1	22	21	25*
		Level 2	26,5	27	32,5
		Level 3	31	32	39
	Average soil surface roughness, level		1, 2 and 3		
	Soil temperature range, °C		20 - 27		
	Air temperature range, °C		21 - 29		
	Relative air humidity range, %		45 - 57		
Measuring radar system	Incident angle of the antennas, °		30 and 45		
	Angle between antennas, °		0 and 45		
	Scanning speed, m/s		0,14 m/s		
	Wave polarisation, –		VV		
Test objects	Material, –		Sugar beets		
	Diameter, mm		60 and 120		
	Average mass**, g		160 and 800		
	Shape, –		Topped		
	Distance between test objects, m		1 (Figure 6.29)		

* The water content level of the clay soil was in upper 3-5 cm very dry (about 15%vol) and below this layer the water content was still high, approximately 25%vol.

** During the tests different sets of fresh sugar beets have been used; smaller sugar beets were between 150 and 180 g and larger between 710 and 930 g

6.5.1.2 Experiments with sugar beets with foliage

Goal of the tests

The experiments with sugar beets with foliage were used to test the potential of radar system to acquire data about sugar beet roots independent on leaves, i.e. the potential to penetrate through the leaves in order to obtain information about roots.

Test conditions

For this purpose the measuring scenario with three sets of sugar beets (maximal diameters: 60 mm and 120 mm) with complete foliage has been arranged like in Figure 6.32 in all three soil boxes according to the experimental arrangement from Figure 6.29. The sugar beets were at the distance of 1 m from each other, on the prepared surface (0,75 x 2 m) with the soil surface roughness level 1.

Figure 6.32 Scenario with three sugar beet sets with foliage

During experiments with foliage, the tested combinations of antenna angles have been reduced because it was only possible to scan the sugar beet row with the incident angle of 45° (see Figure 6.33) in order to partially avoid contact with the leaves. The tests have been conducted with all three soil types, and the first level of soil water content and soil surface roughness, see Table 6.7. All other conditions were comparable to the previously described conditions.

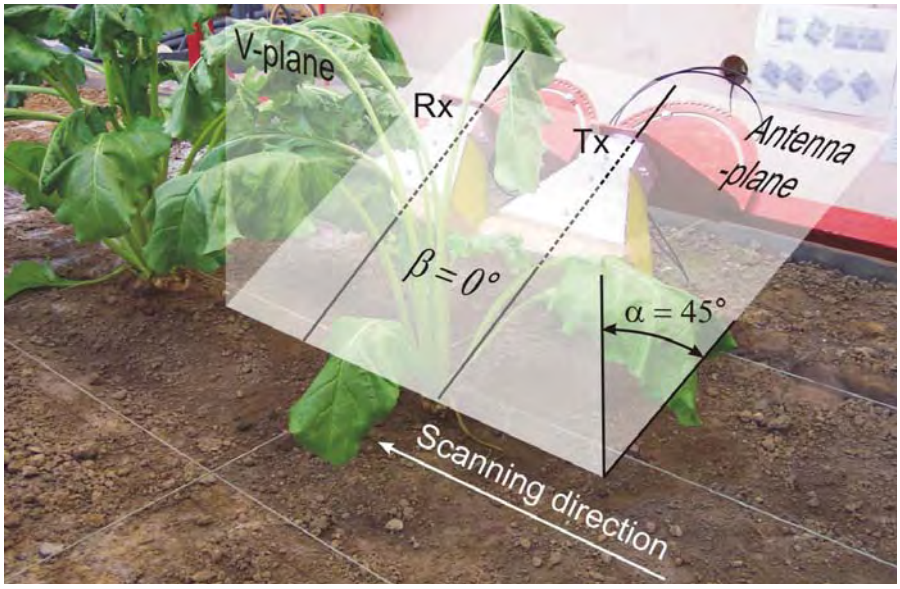

Figure 6.33 Antenna positions with sugar beets with foliage (α = 45°, β = 0°)

Table 6.7 Scenario conditions with sugar beets with foliage

	Scenario property/feature		*Value/feature*		
Environmental conditions	Soil type, –		Sand	Loam	Clay
	Average soil water content in upper 10 cm soil layer, %vol		22	23	25*
	Average soil surface roughness, level			1	
	Soil temperature, °C			19,5	
	Air temperature, °C			21	
	Relative air moisture, %			45	
Measuring radar system	Incident angle of the antennas, °			45	
	Angle between antennas, °			0 and 45	
	Scanning speed, m/s			0,14 m/s	
	Wave polarisation, –			VV	
Test objects	Material, –			Sugar beets	
	Diameter, mm			60 and 120	
	Average mass**, g	Roots		160 and 750	
		Leaves		Was not measured	
	Shape, –			With whole leaves	
	Distance between test objects, m			1 (Figure 6.29 and 6.32)	

* The water content level of the clay soil was in upper 3-5 cm very dry (about 15%vol) and below this layer the water content was still high, approximately 25%vol.

** During the tests three sets of fresh sugar beets have been used; roots of smaller sugar beets were between 150 and 180 g and larger between 710 and 790 g

6.5.1.3 Experiments with leaves brush

Goal of the tests

The experiments with untopped sugar beets, like in Figure 6.2 a), were used to test the influence of the residual biomass on the top of the sugar beet on the backscattered energy amounts and its potential to cause data misinterpretation in comparison to the test with correctly topped sugar beets.

Test conditions

For this purpose the measuring scenario with three sets of sugar beets (maximal diameters: 60 mm and 120 mm) with ca. 40 cm and 20 cm long leave brushes has been arranged like in Figure 6.34 a) and b) respectively in all three soil boxes according to the arrangement from Figure 6.29. The sugar beets with long brushes have been only defoliated, i.e. the stalks have been left in the original size. In the case of 20 cm long brushes, the stalk have been shortened. The sugar beets were at the distance of 1 m from each other, on the prepared surface (0,75 x 2 m) with the soil surface roughness level 1.

a)

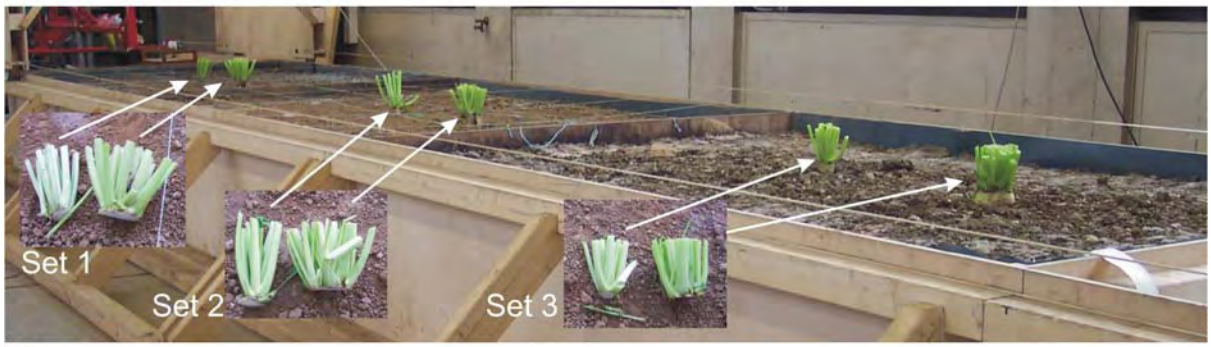

b)

Figure 6.34 Scenario with sugar beets with leaves' brush; a) with long brushes (ca. 40 cm), b) with short brushes (ca. 20 cm)

During these experiments, the same combinations of antenna angles as in the test with correctly topped sugar beets were tested for each soil type, the first level of soil water content, and the first level of soil surface roughness, see Table 6.8. All other conditions were comparable to the previously described conditions.

Table 6.8 Scenario conditions with sugar beets with leaves' brush

	Scenario property/feature		*Value/feature*		
Environmental conditions	Soil type, –		Sand	Loam	Clay
	Average soil water content in upper 10 cm soil layer, %vol		22	23	25*
	Average soil surface roughness, level			1	
	Soil temperature, °C			19,5	
	Air temperature, °C			21	
	Relative air moisture, %			45	
Measuring radar system	Incident angle of the antennas, °			45	
	Angle between antennas, °			0 and 45	
	Scanning speed, m/s			0,14 m/s	
	Wave polarisation, –			VV	
Test objects	Material, –			Sugar beets	
	Diameter, mm			60 and 120	
	Average mass**, g	Roots		160 and 750	
		Brushes (short)***		190 and 450	
	Shape, –			Partially defoliated (with long and short leaves' brushes ca. 40 and ca. 20 cm respectively)	
	Distance between test objects, m			1 (Figure 6.29 and 6.32)	

* The water content level of the clay soil was in upper 3-5 cm very dry (about 15%vol) and below this layer the water content was still high, approximately 25%vol.

** During the tests three sets of fresh sugar beets have been used; smaller sugar beets were between 150 and 180 g with brushes between 160 and 220 g and larger between 710 and 790 g with brushes between 390 and 530 g

*** The masses of long brushes (ca. 40 cm) have not been measured

6.5.1.4 Experiments with different height of sugar beets tops

Goal of the tests

Similar to experiments with leaves' brush in Chapter 6.5.1.2, the tests with different height of sugar beets' tops were conducted in order to research the influence of different height of sugar beets' tops on the backscattered energy amounts and its potential to cause data misinterpretation.

Test conditions

For this purpose the measuring scenario with one topped sugar beet (1 kg mass and 12 cm diameter) in the middle of the soil box with sand soil has been arranged like in Figure 6.35.

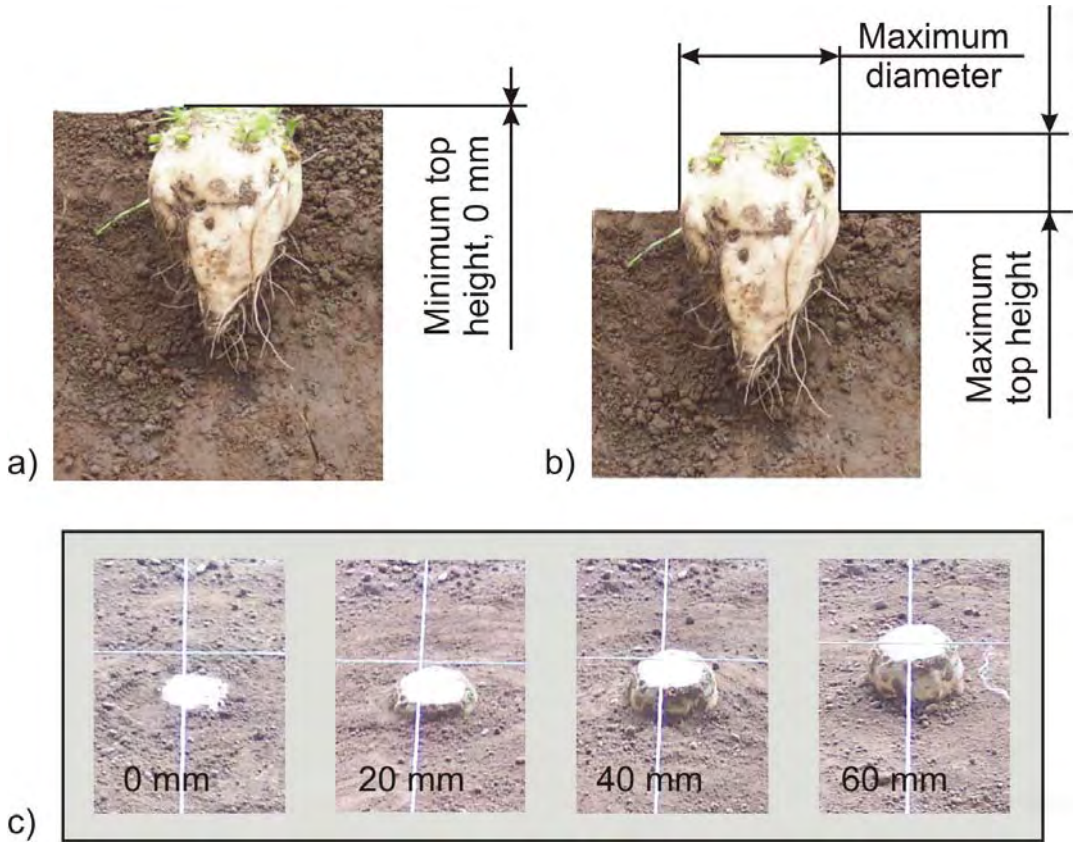

Figure 6.35 Scenario arrangement with different heights of sugar beet top; a) top in the surface level – minimum top height, b) maximum diameter in the surface level – maximum height, c) tested sugar beet top heights

During experiments with different height of sugar beets' tops, the same combinations of antenna angles as within the tests with correctly topped sugar beets were tested in sand soil, with the first level of soil water content and the first level of soil surface roughness, see Table 6.9. All other conditions were comparable to the previously described conditions.

Table 6.9 Scenario conditions with different height of sugar beets' tops

	Scenario property/feature	*Value/feature*
Environmental conditions	Soil type, –	Sand
	Average soil water content in upper 10 cm soil layer, %vol	22
	Average soil surface roughness, level	1
	Soil temperature, °C	25
	Air temperature, °C	29
	Relative air moisture, %	40
Measuring radar system	Incident angle of the antennas, °	30 and 45
	Angle between antennas, °	0 and 45
	Scanning speed, m/s	0,14 m/s
	Wave polarisation, –	VV
Test objects	Material, –	Sugar beets
	Mass, kg	1
	Diameter, mm	120
	Shape, –	Topped
	Top heights (Figure 6.35 c), mm	0, 20, 40 and 60

6.5.1.5 Experiments with different positions of sugar beets in the row

Goal of the tests

The experiments with different positions of sugar beets and different objects in the row were used to test the potential of radar system to distinguish between sugar beets of different sizes with different positions and to recognize either position without a sugar beet (gap in the row) or the position with a foreign object on the position of a sugar beet.

Test conditions

In the scenario in Figure 6.23 four sugar beets of different size have been descending ordered in the row – the largest sugar beet was the first. During these tests four sugar beets, Figure 6.36 a) have been arranged like in Figure 6.36 b) in sand soil with the first level of soil water content and the first level of soil surface roughness, see Table 6.10. The distances between objects of 0,4 m from each other have been chosen because it was needed to enable reliable separation of signals independent of influences of neighbouring objects.

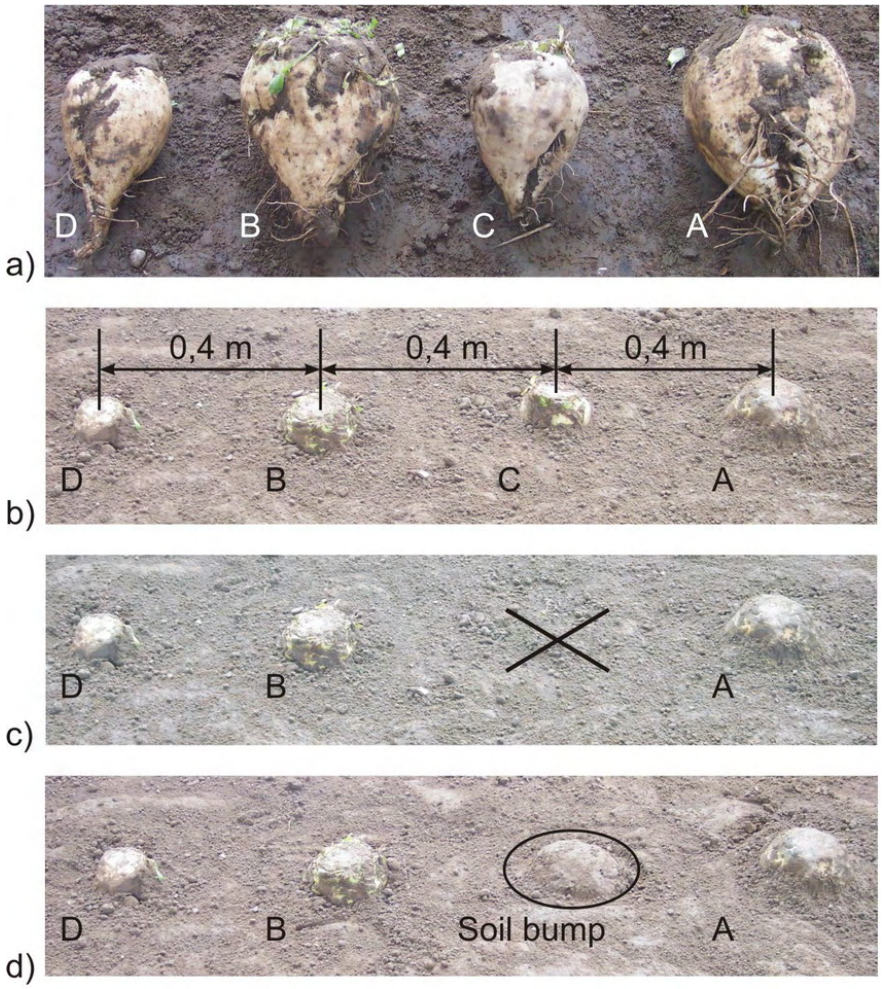

Figure 6.36 Test objects and test arrangement with different positions of sugar beets in the row; a) test objects – sugar beets (A: 1150 g, Ø130 mm, B: 850 g, Ø120 mm, C: 550 g, Ø100 mm, D: 240 g, Ø70 mm), b) scenario with four sugar beets, c) scenario without sugar beet C, d) scenario with three sugar beets and a soil bump

Additionally, the sugar beet C has been removed and the scenario has been scanned without it, Figure 6.36 c), and with a soil bump with about the about same size instead of it, Figure 6.36 d). All other conditions were comparable to the previously described.

Table 6.10 Scenario conditions with different positions of sugar beets in the row

	Scenario property/feature	*Value/feature*
Environmental conditions	Soil type, –	Sand
	Average soil water content in upper 10 cm soil layer, %vol	29
	Average soil surface roughness, level	1
	Soil temperature, °C	23
	Air temperature, °C	27
	Relative air moisture, %	42
Measuring radar system	Incident angle of the antennas, °	45
	Angle between antennas, °	45
	Scanning speed, m/s	0,14 m/s
	Wave polarisation, –	VV
Test objects	Material, –	Sugar beets
	Diameter (A, B, C, D, respectively), mm	130, 120, 100, 70
	Mass (A, B, C, D, respectively), g	1150, 850, 550, 240
	Shape, –	Topped
	Distance between test objects, m	0,4 (Figure 6.23 and 6.36)

6.5.2 Field experiments

Goal of the tests

The field experiments were used to study the potential of the radar measuring system in field conditions with undisturbed soil structure, water content and water content distribution, and soil surface roughness.

The main goals were to observe the data acquisition capabilities of the radar system and the effectiveness of data processing procedure in the scenario with in-field grown

sugar beets in order test the abilities:

1. to detect and localise individual sugar beets and
2. to determine a single sugar beet mass.

Test conditions

For this purpose four sections of a row in the field, each 10 m long have been selected and prepared by topping. The sugar beets have been correctly topped according to Figure 6.2 d). Scanned scenario with a full row with usual distance of 20 cm is presented in Figure 6.37 a), and with a thinned row and increased distance in Figure 6.37 b). The measurements with thinned rows have been conducted because the preliminary experiments showed that the objects which close to each other effect each other and in turn cause data processing difficulties. In that sense, the increase distance between sugar beets was used to enable the test of the single sugar beet detection independent of the surrounding sugar beets.

The rows with normal distance have been scanned on two occasions, during the months of August and October 2006. The rows with increased distance have been scanned only during October 2006. The antenna position combinations and important scenario conditions data are presented in Table 6.11.

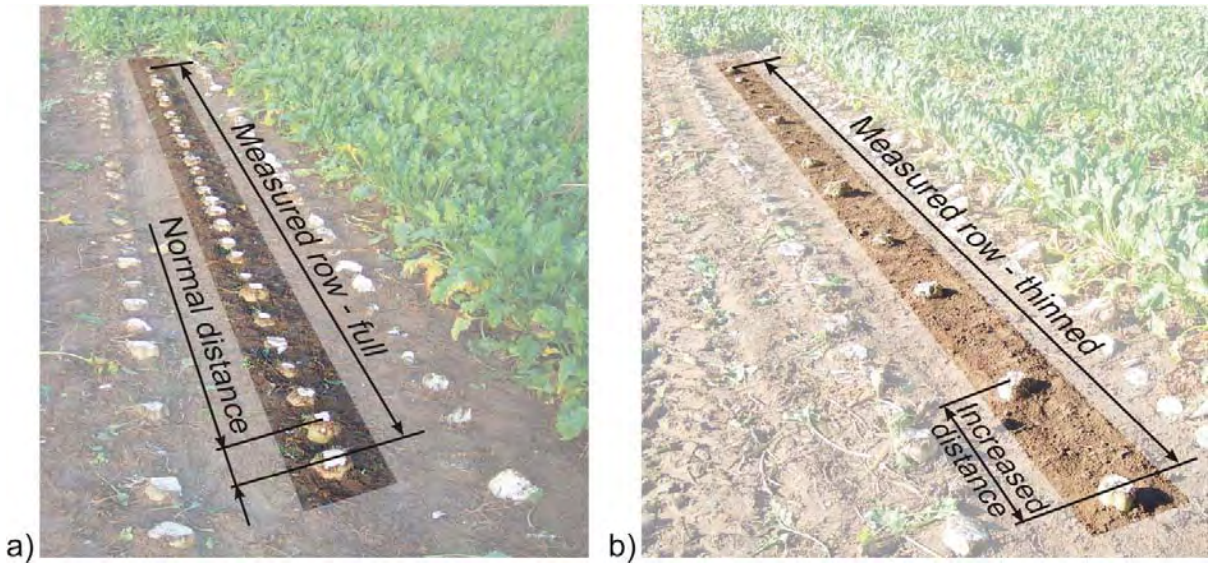

Figure 6.37 Field experiment scenario; a) full row – normal distance between sugar beets, b) thinned row – increased distance between sugar beets

Table 6.11 Scenario conditions in the field

	Scenario property/feature	*Value/feature*			
		August 2006	October 2006		
Environmental conditions	Soil type, –	Loam (Figure 6.17)			
	Average soil water content in upper 10 cm soil layer, %vol (level)	31 (3)	22,3 (1)	28,1 (2)	27,3 (2)
	Standard deviation of average soil water content in upper 10 cm soil layer, %vol	3,8	2,4	3,1	4,2
	Average soil surface roughness, level	From 1 to 2			
	Soil temperature, °C	17	13		
	Air temperature, °C	19	15		
	Relative air moisture, %	66	70		
Measuring radar system	Incident angle of the antennas, °	30 and 45			
	Angle between antennas, °	0 and 45	0		
	Scanning speed, m/s	ca. 0,25 m/s			
	Wave polarisation, –	VV			
Test objects	Material, –	Sugar beets	Sugar beets*		
	Average diameter, mm	97	100 and 104		
	Diameter standard deviation, mm	16	16 and 16		
	Average mass, g	560	747 and 748		
	Mass standard deviation, g	246	309 and 296		
	Shape, –	Topped, one row ca. 12 m long	Topped, three rows, each ca. 10 m long		
	Average distance between objects in the row, cm	23	23 and 64		
	Standard deviation of the distance between objects, cm	8	6 and 6		

* Full row and thinned row respectively

7. Results and discussion

7.1 Laboratory experiments

7.1.0 Reference measurements

During this phase of the research, the measurements have been conducted with reference objects – aluminium spheres shown in Figure 6.15 in the scenario arrangement presented in Figure 6.29. General specification of signals acquired in this scenario is presented in the radargram in Figure 7.1. Recognisable hyperbolical traces in the middle of radargram present two spheres (Ø60 mm and Ø120 mm) at the distance of 1 m from each other and 1 m from the walls on the left and right side of the soil box. The radargram has been acquired in the following scenario conditions: antenna angles α = 30° and β = 0°, in the sand soil with soil water content level 1, soil surface roughness level 1.

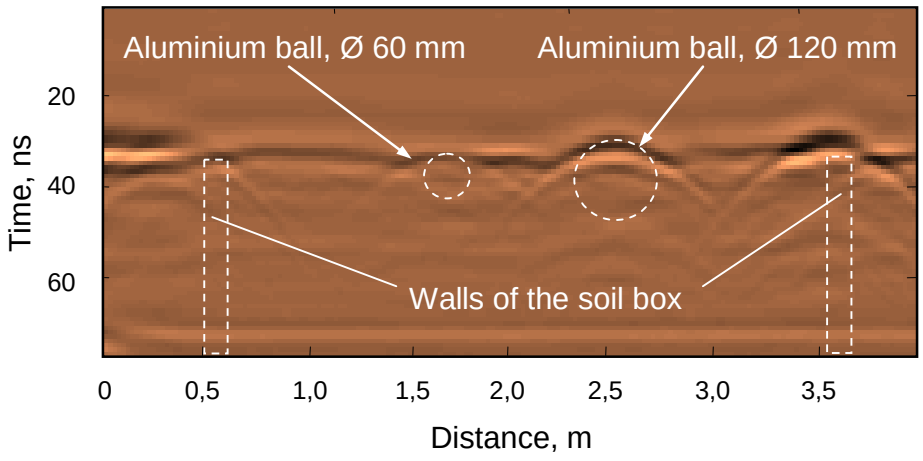

Figure 7.1 Specification of signals in a radargram acquired in the soil box with two aluminium spheres

Analysis of system parameters – antenna position influence and selection of antenna combinations

The basic criterion used in this analysis was to select the sets of antenna angles which allow acquiring of radar signals with

- the sufficient amount of backscattered energy from the target and

- the potential of separation of target signals from the surrounding signals, most of all surface interaction and antenna cross talk

in order to provide successful data processing and interpretation.

In Figure 7.2 radargrams with raw data (with cross talk and background - soil signals) acquired in the sand soil with roughness level 1 and water content level 1 are presented in order to illustrate the influence of antenna positions on target signal intensity. The radargrams for antenna combinations with α = 60° show a very low intensity of target signals (marked target signals in ellipses).

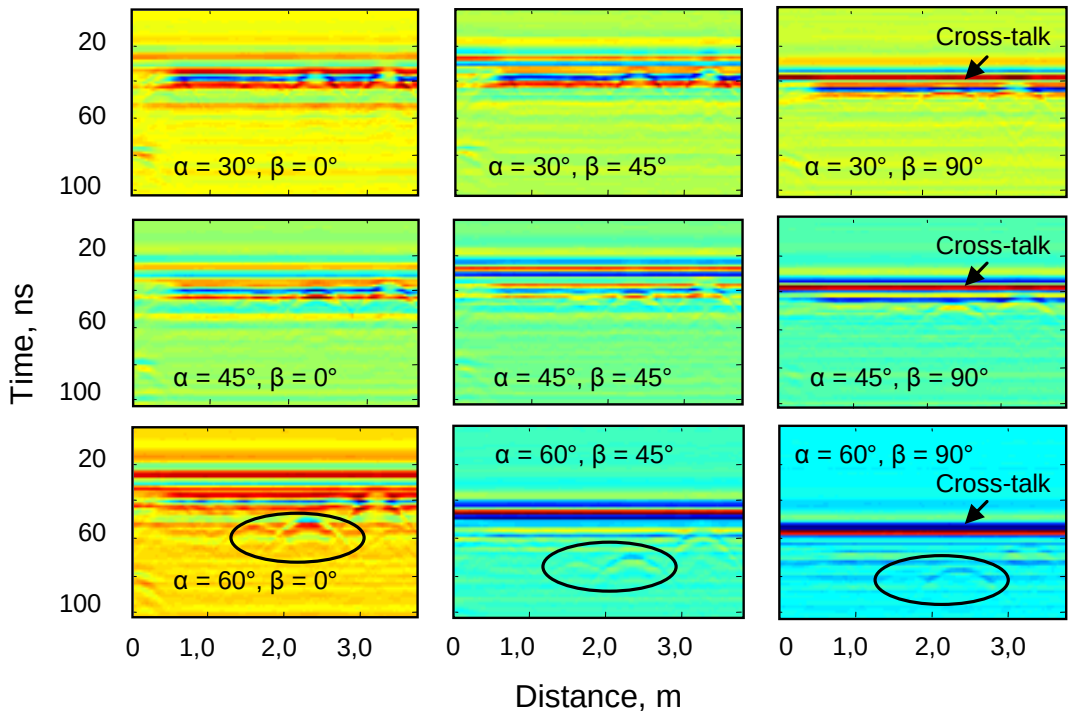

Figure 7.2 Analysis of influence of antenna angle combinations on target signal intensity and using radargrams with raw data (sand soil, roughness level 1, water content level 1)

The explanation of the low intensity signals is given in Figure 7.3. The antenna positions are geometrically determined with three constrains: angles α and β, and height of the starting point of wave propagation (h), which together form the crossing point of antenna axes on the soil surface in the centre of the scanned object, like in Figure 6.24.

In the case of α = 60°, shown in Figure 7.3 a), the reflecting area of the object, so called radar cross-section, is smaller than in the case of α = 30°, Figure 7.3 b). This, together with sharper incident angle, causes lower reflected and received amounts. Additionally, the used radar signals are low-energy signals of about 1 mW radio power, capable to better acquire target information close to the antenna system. In the case of α = 60° the length of the wave path is approximately 60% longer than the length of the path in the case of α = 30°. This difference in the lengths caused higher radar wave losses is the case of α = 60° due to the dissipation effect. The listed phenomena were the reason to omit this value of angle α in the further research.

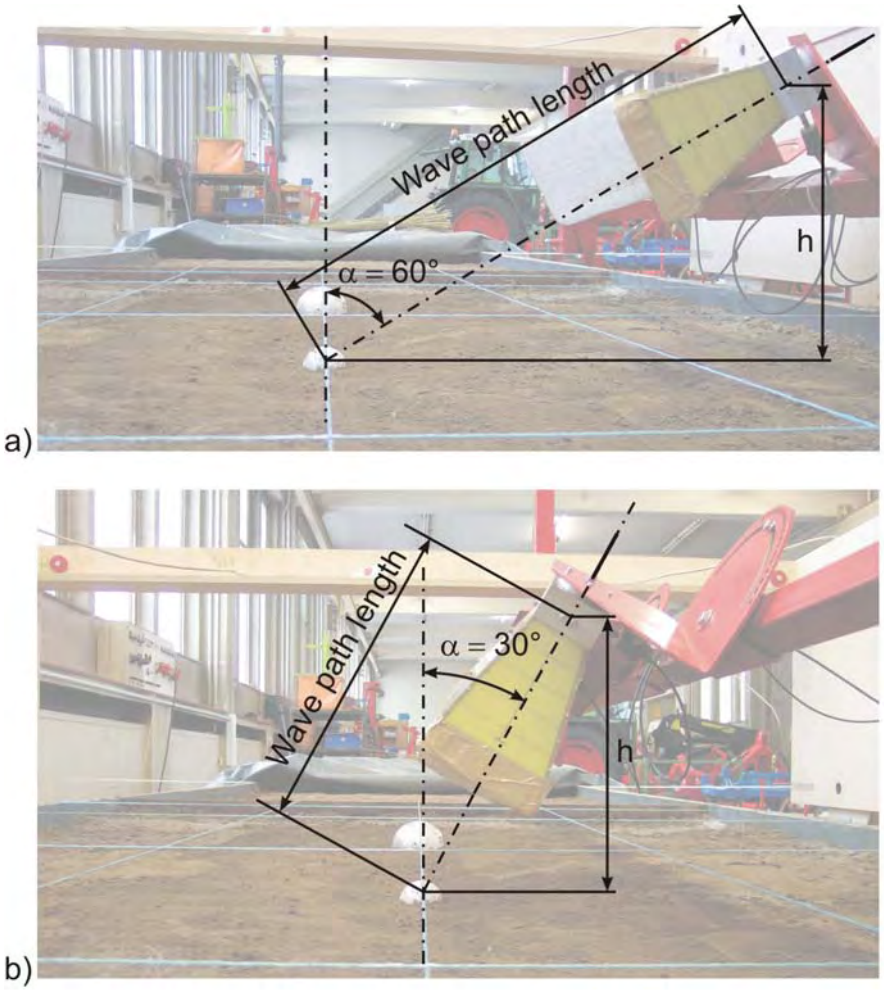

Figure 7.3 Influence of geometrical constrains on the wave path length; a) wave path antenna length in the position α = 60°, b) wave path antenna length in the position α = 30°

In Figure 7.4 approximate paths of transmitted and received waves, and direct waves – cross talk are shown for the case of β = 90°. In this case antennas are turned to each other what causes strong direct signal, also visible as continuous intensive signal in radargrams with raw data in Figure 7.2 (marked with arrows in radargrams in the right column).

The cross-talk partially covers the target signal because the length of *transmitter-target-receiver* path is similar to the length of direct path *transmitter-receiver*. This geometrical similarity is illustrated in Figure 7.4 and it causes the need to introduce additional attenuation of the original signal. This effect, presented it Figure 7.5, generates losses in radar dynamics and in turn less information about the target.

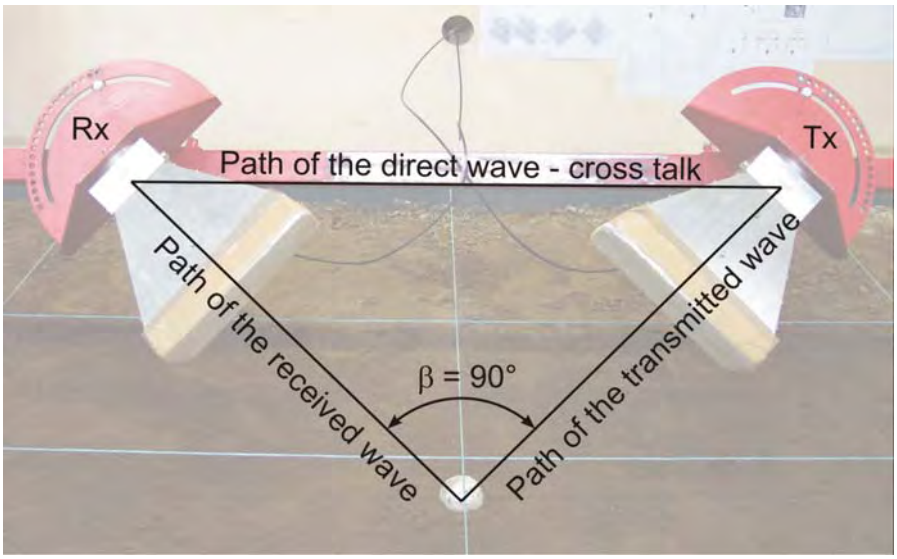

Figure 7.4 Simplified paths of transmitted, received and direct waves for β = 90°

The data in radargrams in Figure 7.5 have been acquired in the scenario with sand soil, lowest water content level and soil surface level 1. The radargrams have been processed according to the method described in Chapter *Data acquisition and processing* in data processing steps shown in Figure 6.22. The data in Figure 7.5 a) are without cross-talk, which is removed by time-gating of constant signals. In Figure 7.5 b) the Hilbert-transformed radargrams are presented in order to illustrate the amounts of backscattered energies from the target and the diagram in Figure 7.5 c) presents the relationship between normalised energy amounts and tested antenna combinations.

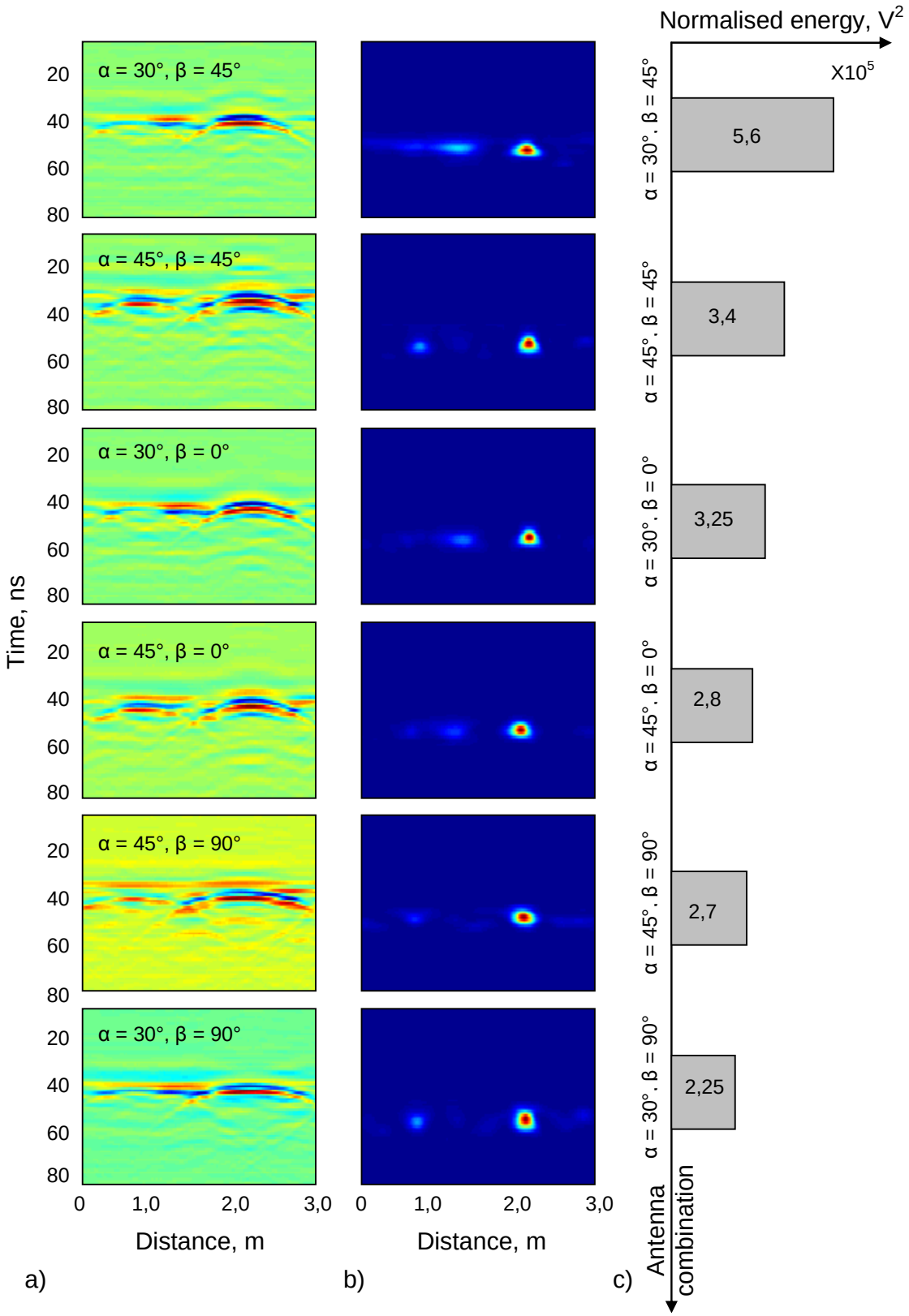

Figure 7.5 Amounts of backscattered energy from aluminium spheres for different antenna combinations; a) processed radargrams, b) backscattered energies, c) normalised energy amounts vs. antenna combinations

The main problem caused by time-gating of cross-talk was the decrease of target's the detectability because of the radar dynamics decrease. In the case of far-field conditions the time gating subtracts a part of the signal, which causes radar dynamics decrease. Further problem are near-field conditions, because in that case the interaction with soil surface changes the behaviour of antennas. In Figure 7.5 b) both targets are visible, but smaller spheres are hardly detectable even in conditions with the lowest soil surface roughness although recognisable in all recorded raw radargrams. In Figure 7.5 c) the amounts of backscattered energies are shown, and the amount for antenna combinations with angle $\beta = 90°$ showed the smallest values, which was the reason to omit this value of angle β in the further research.

In addition to the above analysis, the combinations with angle $\alpha = 0°$, like in the boundary case in Figure 6.30 b), showed insufficiently good results and this angle was also omitted due to strong clutters coming from the direct reflections from soil surface, which covered the target signal after the step of background subtraction even more the in the case of antenna combinations with $\beta = 90°$.

Analysis of the influences of test scenario

The following analysis deals with three influential and mutually interlacing parameters of any agricultural test scenario: soil surface roughness, water content and soil type.

The processed radargrams without cross-talk, and after background subtraction and deconvolution for all antenna combinations are shown in Figure 7.6 in order to illustrate the influence of soil surface roughness on backscattering of radar signals. The presented data have been acquired in the sand soil with the first level of soil water content.

According to the visual analysis, it is possible to distinguish between the hyperbolical traces of sets of targets and the surroundings up to the level 2 of soil surface roughness, Figure 7.6 b). The tests with the level 3 of soil surface roughness delivered data without recognisable pattern, Figure 7.6 c) for all antenna combinations, which is more closely described in the following analyses.

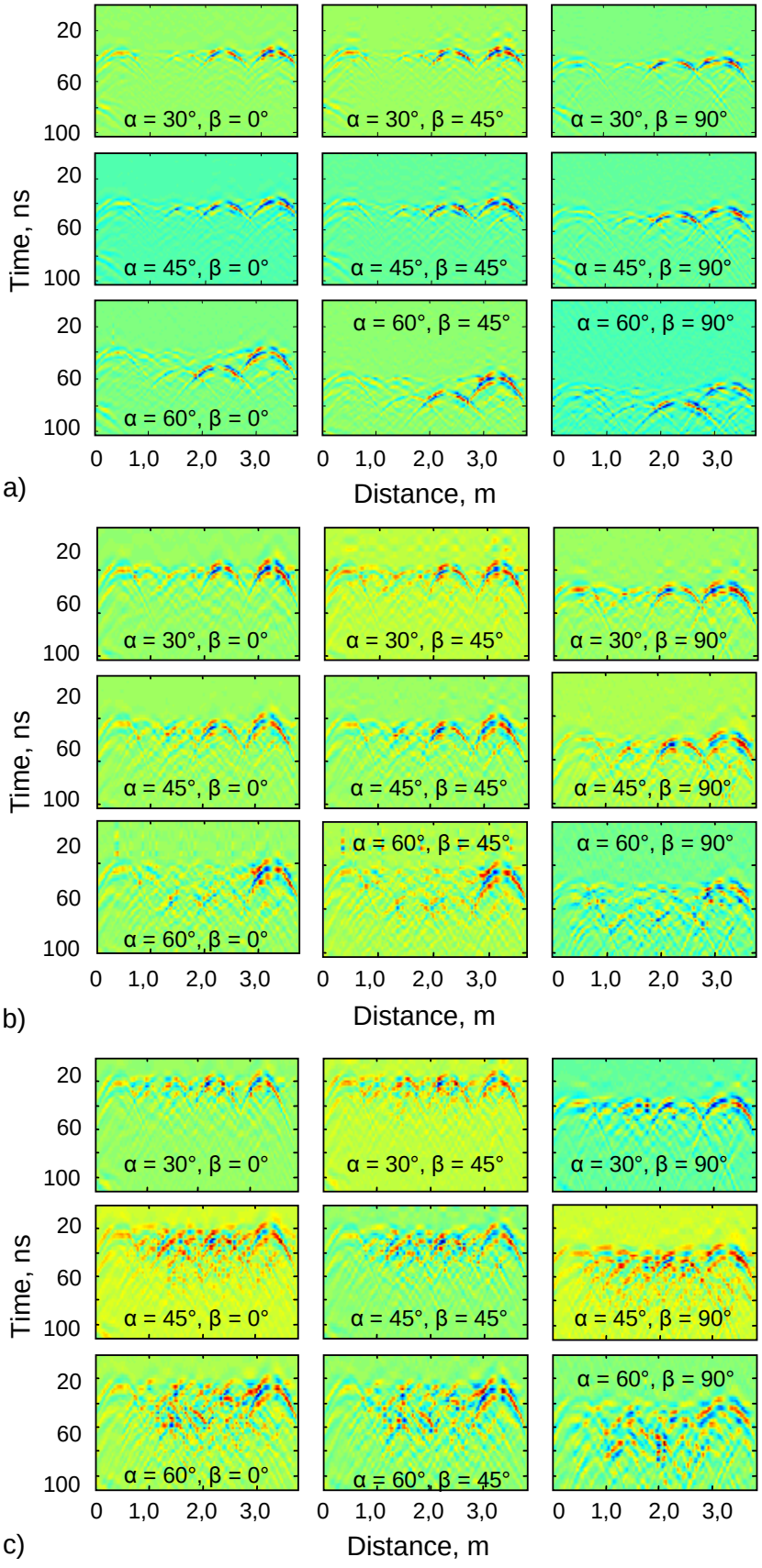

Figure 7.6 Influence analysis of soil surface roughness on backscattered radar signals, a) roughness level 1, b) roughness level 2, c) roughness level 3

A further analysis of the soil surface roughness influence and interconnection to soil type and water content influences has been made for the distribution and consistency of backscattered energy amounts in scenario with each soil surface roughness level, with all three soil types and soil water content levels, and two angle combinations (α = 30°, β = 0° and α = 45°, β = 0°). This analysis has been made on the processed data presented in following figures starting from the surface roughness level 3 (Figure 7.7) and followed with other two in order to test the potential to distinguish the targets from the clutter which is mostly coming from surrounding soil parts, i.e. soil surface. The tests with other two angle combinations (α = 30°, β = 45° and α = 45°, β = 45°) delivered analogous results for all tested conditions.

The real positions of two aluminium spheres in Figure 7.7 are marked with pairs of vertical dashed white lines. According to the visual analysis and as expected, it is not possible to locate any of the smaller spheres (Ø60 mm). The signals of these objects are lost amongst soil parts masked by the soil surface clutter because of high surface roughness for all antenna combinations, soil types and soil water contents.

Bigger spheres (Ø120 mm) could be located and distinguished as energy amounts with good contrast to the background in several cases for different soil types, water contents and antenna combinations, e.g. for α = 30° and α = 45°, and water content level 1 in Figure 7.7 a) and 7.7 b). According to these data, it was not possible to define a general rule of backscattering behaviour. In all radargrams there were energy portions of different size other than spheres (marked with rectangles), which could be recognised as targets, and in some cases, the spheres were completely lost within reflections from soil surface, e.g. for α = 45° and water content level 1 in Figure 7.7 c).

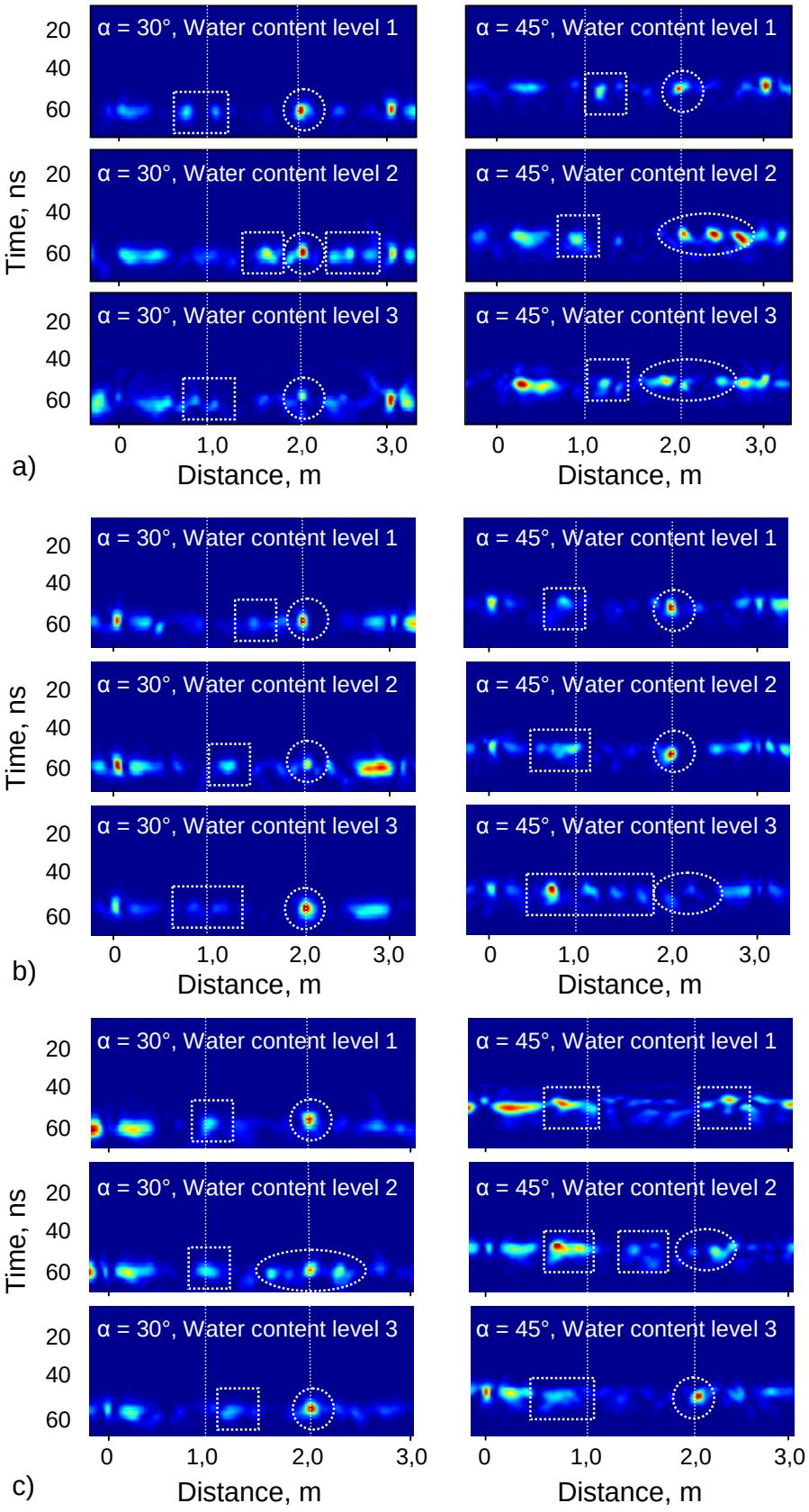

Figure 7.7 Backscattered energies from reference objects acquired in scenario with and soil surface roughness level 3, a) sand soil, b) loam soil, c) clay soil

The previous analysis of the influence of scenario, in this case of soil surface roughness, has been made for data acquired in extreme test conditions (soil surface roughness level 3), which is unusual for field conditions in the time of sugar beet harvest. The expected field conditions of soil surface roughness are from the level 1 up to the level 2, shown in Figure 6.27 a) and b). The analysis of influences the soil water content and the soil type on the amounts of backscattered energies of radar signals is made on data acquired in field-expected conditions shown in Figure 7.8, 7.9 and 7.10. The tests with other two angle combinations (α = 30°, β = 45° and α = 45°, β = 45°) delivered analogous results for all tested conditions.

The data in Figure 7.8 have been acquired in surface roughness of level 2 with all three soil types and water contents using two angle combinations (α = 30°, β = 0° and α = 45°, β = 0°). The real positions of two aluminium spheres are marked with pairs of vertical dashed white lines. The signals from smaller spheres were either lost during data processing steps or ambiguously detectable in all cases in Figure 7.8, although they were to a certain degree visible as hyperbolical traces in radargrams in Figure 7.6 b).

The focused signals of bigger spheres showed good contrast to the background and enabled unambiguous detection and localisation in the expected position of the sphere in all cases. In the case of data acquired with α = 45° in clay soil with water content level 1, Figure 7.8 c) the signal of the sphere was also recognisable, but the amount of clutter was significantly higher in comparison to other data.

The case of strong clutter in radar signals recorded in clay soil with water content level 1 is a phenomenon which repeated itself in measurements with these conditions, see also Figure 7.7 c) and 7.10 c). The explanation of this occurrence lies in the method of soil water content reduction described in Chapter 6.5.0 and its influence on the soil surface structure. In the case of clay soil, the soil surface has been levelled before natural drying because it was not possible to do it in the dry state. This kind of drying induced the forming of very hard and smooth soil surface, which generated the mirror-effect and introduced additional strong clutter disturbances in the backscattered signals.

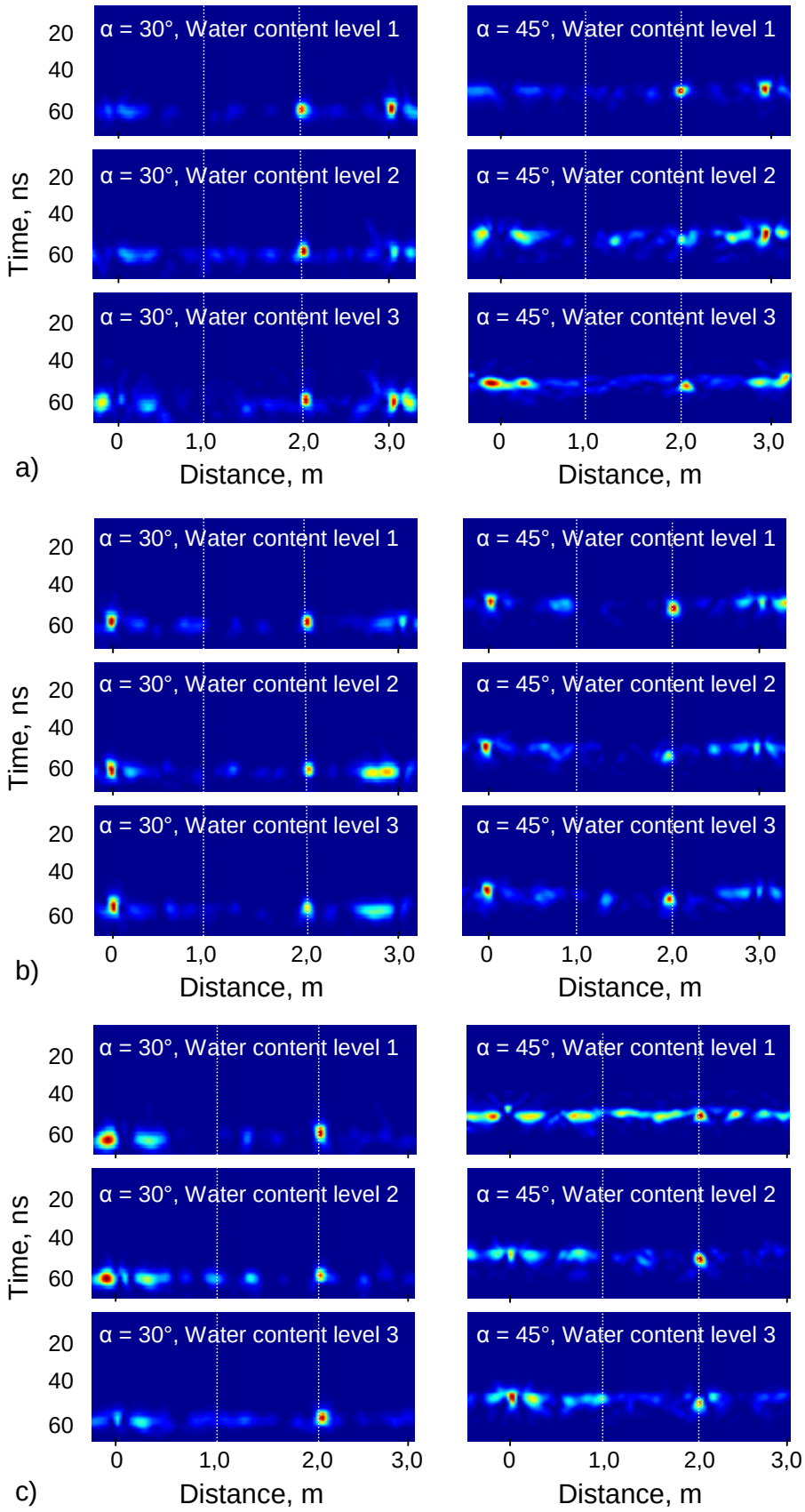

Figure 7.8 Backscattered energies from reference objects acquired in scenario with soil surface roughness level 2; a) sand soil, b) loam soil, c) clay soils

The data in Figure 7.9 and Figure 7.10 have been acquired in the field-expected conditions of soil surface roughness of level 1 with all three soil types and water contents using two angle combinations (α = 30°, β = 0° and α = 45°, β = 0°). The positions of two aluminium spheres are marked with pairs of vertical dashed white lines. The tests with other two angle combinations (α = 30°, β = 45° and α = 45°, β = 45°) delivered analogous results for all tested conditions.

The hyperbolical traces of both spheres are recognisable in all radargrams. The data presented in radargrams in Figure 7.9 have been processed and the amounts of backscattered energies for corresponding system parameters are presented in Figure 7.10.

The signals from smaller sphere could be located in all cases in Figure 7.10, except in the case of data acquired with α = 45° in clay soil with water content level 1, Figure 7.9 c). In this case the signal of the sphere was not recognisable, because it was covered by the clutter of high intensity caused by previously explained phenomenon.

The masking effect that originates from the soil surface clutter increases with increasing water content. This effect is observable throughout Figure 7.10 with the best example for sand soil and angle α = 45°.

The comparison between amounts of backscattered energy from two aluminium spheres is presented in Table 7.1. The amounts of backscattered energy from the smaller sphere have been calculated and presented in percentage from the bigger sphere for each scenario, i.e. the amounts of backscattered energy from the bigger sphere was 100% for each parameter combination. The average value of the calculated percentages was 23,0% with a large standard deviation of 12%. According to the presented data, the angle combinations with α = 45° provided better detectability of the small sphere than with α = 30°, i.e. the amounts of energies backscattered from small spheres were larger (relative to the large sphere) in all cases except for loam soil with moisture content level 2 and 3.

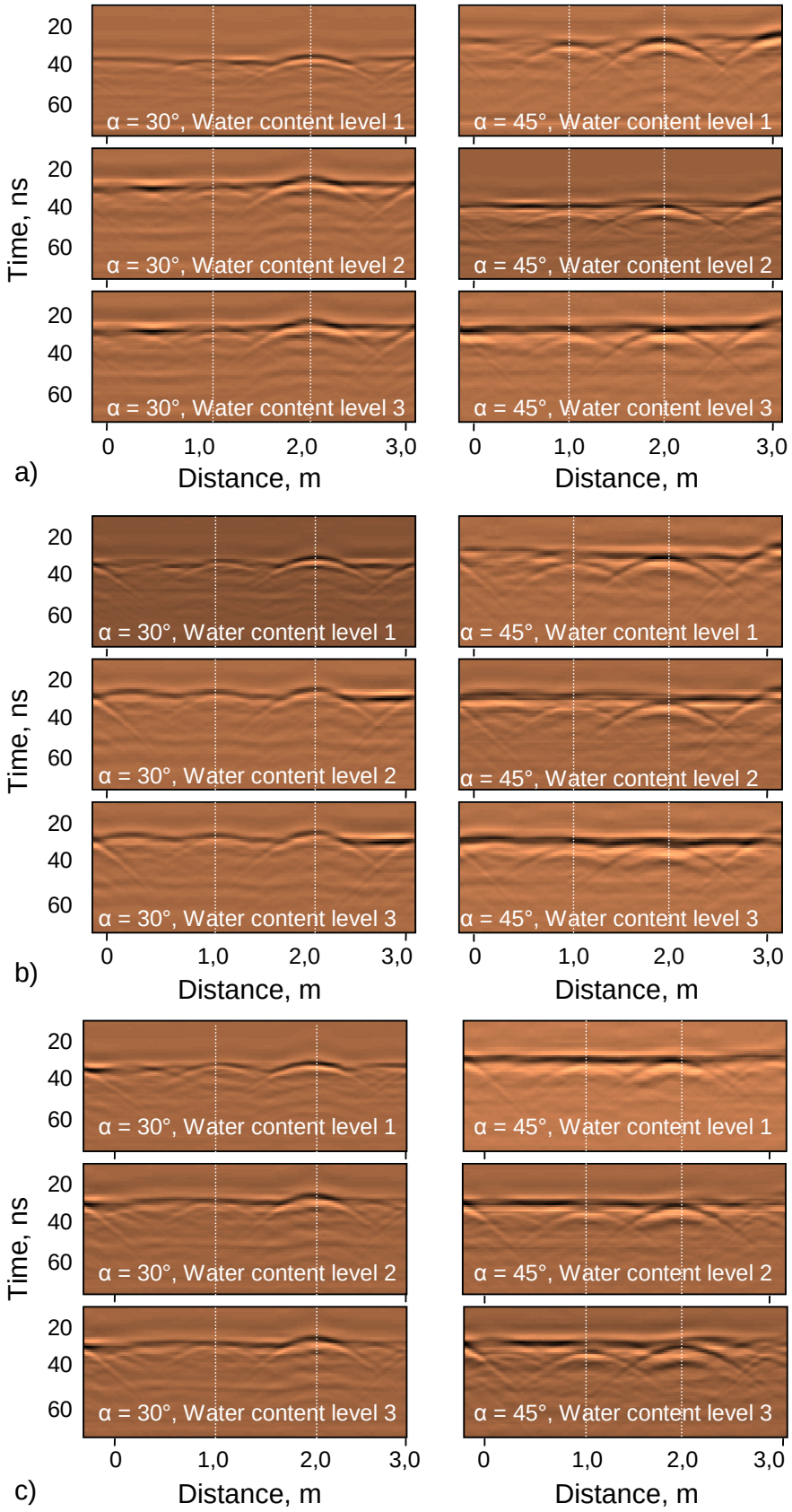

Figure 7.9 Radargrams acquired in scenario with reference objects and with soil surface roughness level 1; a) sand soil, b) loam soil, c) clay soil

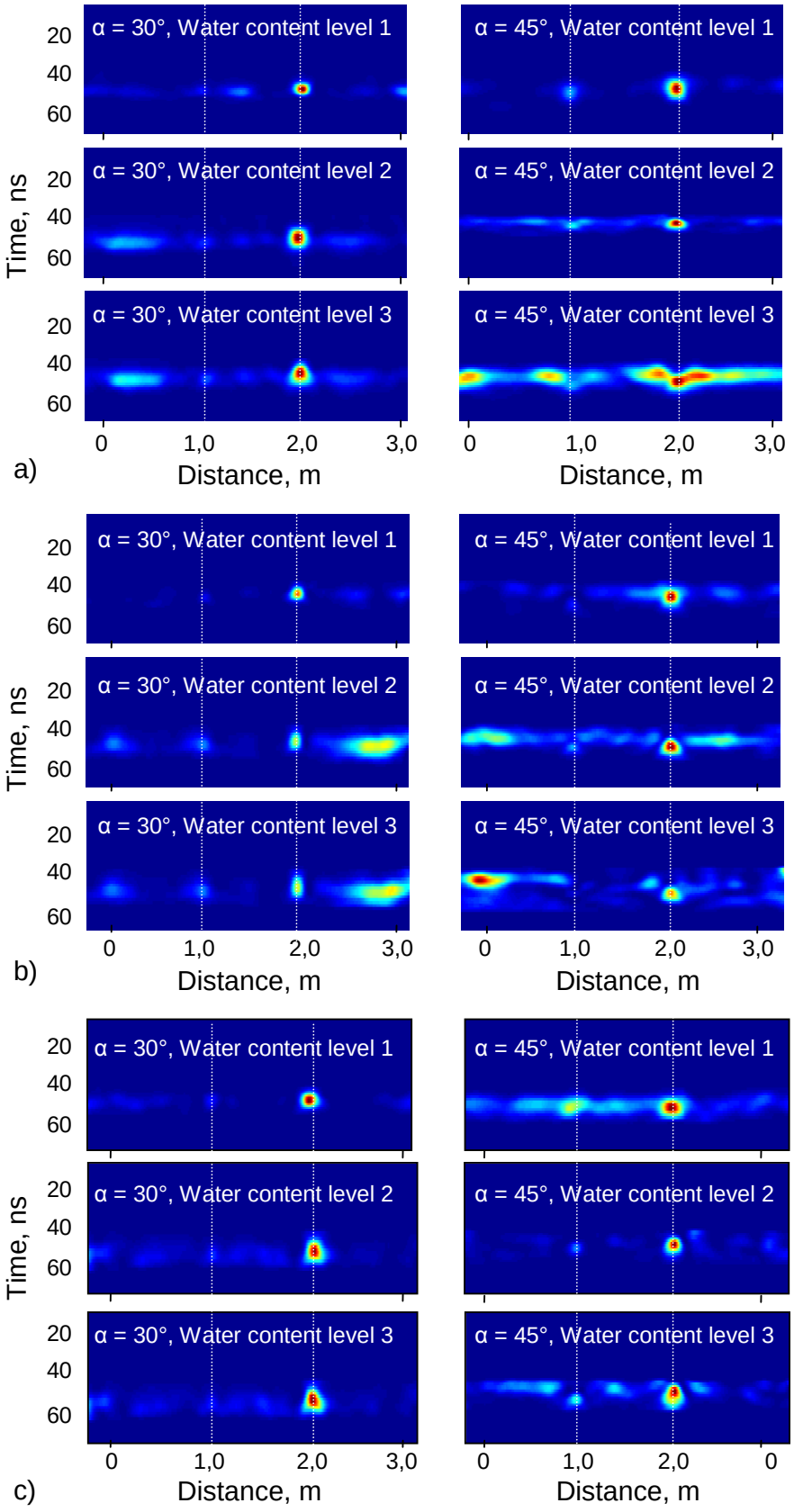

Figure 7.10 Backscattered energy from reference objects acquired in scenario with soil surface roughness level 1; a) sand soil, b) loam soil, c) clay soil

Table 7.1 Comparison between energy amounts backscattered from two aluminium spheres acquired in scenarios with soil surface roughness level 1

Soil type	*Soil water content level*	*Angle α, °*	*Backscattered energy acquired from spheres*		
			Sphere Ø120 mm	*Sphere Ø60 mm*	
			Absolute value, V^2	*Absolute value, V^2*	*Relative to the large sphere, %*
Sand	1	30	389.900	50.520	13,0
	2	30	591.600	84.930	14,4
	3	30	392.800	6.722	1,7
	1	45	343.100	99.720	29,1
	2	45	377.400	156.300	41,4
	3	45	364.800	155.200	42,5
Loam	1	30	461.300	56.470	12,2
	2	30	215.800	94.360	43,7
	3	30	251.900	97.850	38,8
	1	45	399.100	52.000	13,0
	2	45	250.200	76.900	30,7
	3	45	154.700	24.940	16,1
Clay	1	30	529.800	73.980	14,0
	2	30	625.600	96.600	15,4
	3	30	499.600	69.400	13,9
	1	45	451.700	–*	–
	2	45	240.700	51.100	21,2
	3	45	278.600	83.490	30,0
				Average value:	*23,0*

* It was not possible to unambiguously separate the signal of the small sphere

The volume of spheres, V_{Sphere} is directly proportional to the cubic value of its radius ($V_{Sphere} = 4/3 \cdot \pi \cdot r^3$). Hence, the volumes of two spheres with Ø60 mm and Ø120 mm stand in ratio 0,125:1. The area of spheres, A_{Sphere} is directly proportional to the square value of its radius ($A_{Sphere} = 4 \cdot \pi \cdot r^2$). The areas of two spheres with Ø60 mm and Ø120 mm are in ratio 0,25:1 and therefore in almost the same ratio as the calculated energy amounts. This means that the amount of energy backscattered

from the used reference object mainly depended on the surface of the object exposed to the radar waves and not on its volume, which also applies if the high standard deviation of recorded data is taken into account.

Other experimental conditions had shown insignificant impact on the data acquisition, processing and interpretation.

7.1.1 Experiments with topped sugar beets

The experiments with topped sugar beets have been conducted in the scenario shown in Figure 6.31 under experimental conditions from Table 6.6. The data in Figure 7.11 and Figure 7.12 have been acquired in the conditions of soil surface roughness of level 1 with all three soil types and water contents using two angle combinations ($\alpha = 30°$, $\beta = 0°$ and $\alpha = 45°$, $\beta = 0°$). The positions of two sugar beets are marked with pairs of vertical dashed white lines. The tests with other two angle combinations ($\alpha = 30°$, $\beta = 45°$ and $\alpha = 45°$, $\beta = 45°$) delivered analogous results for all tested conditions.

Radargrams acquired in scenarios with sugar beet sets are presented in Figure 7.11. The hyperbolical traces of bigger sugar beets are recognisable in all radargrams. The traces of smaller sugar beets are distinguishable in scenarios with sand and loam soil within data acquired with angle $\alpha = 45°$. The hyperbolas of smaller sugar beets are partially or completely covered in the most of other cases.

The data presented in radargrams in Figure 7.11 have been processed and the amounts of backscattered energies for corresponding system parameters are presented in Figure 7.12. The signals from smaller sugar beets could be located only in several cases with questionable reliability, e.g. for data acquired with $\alpha = 45°$ in sand soil with water content level 1.

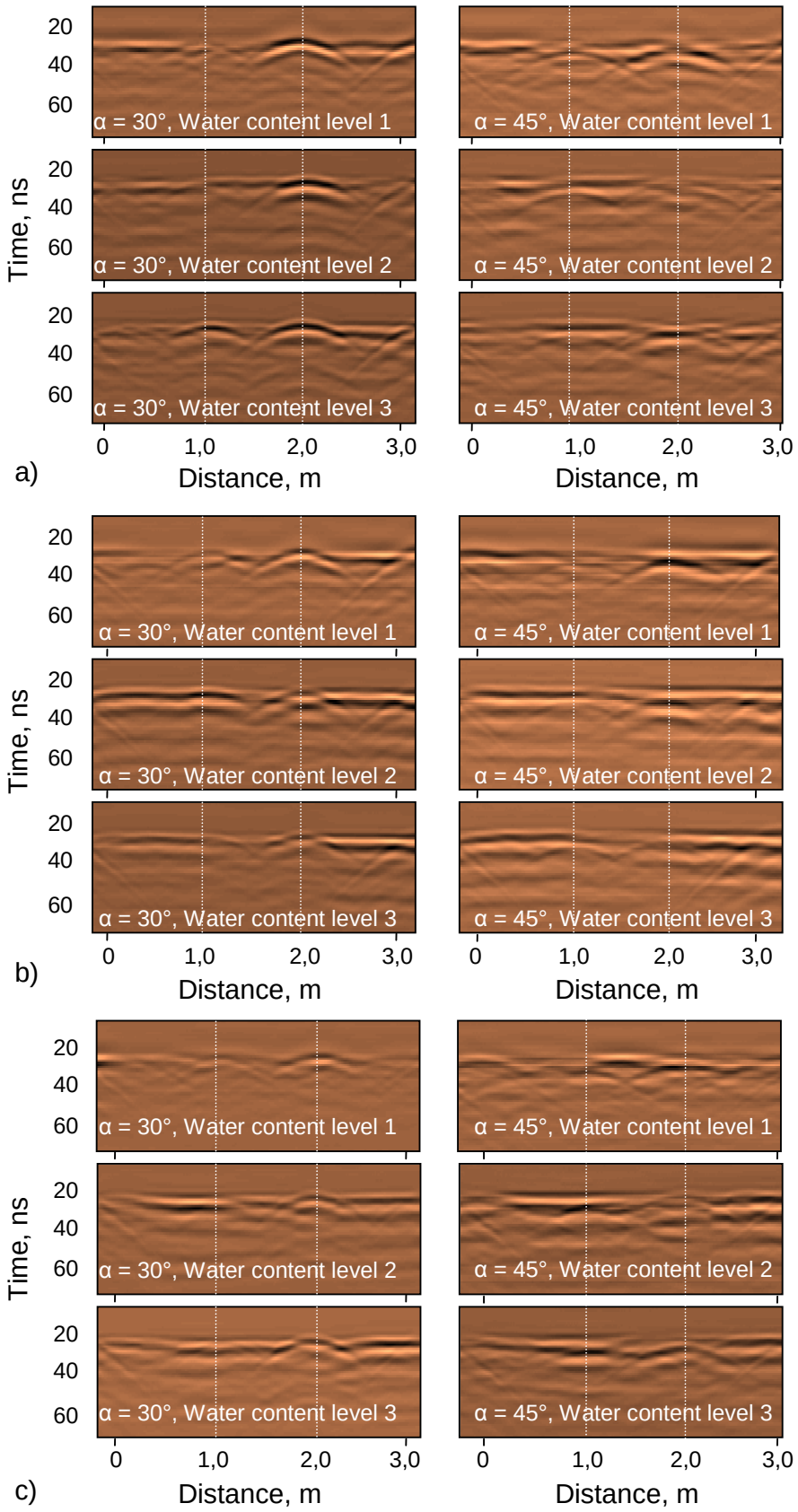

Figure 7.11 Radargrams acquired in scenario with sugar beets and with soil surface roughness level 1; a) sand soil, b) loam soil, c) clay soil

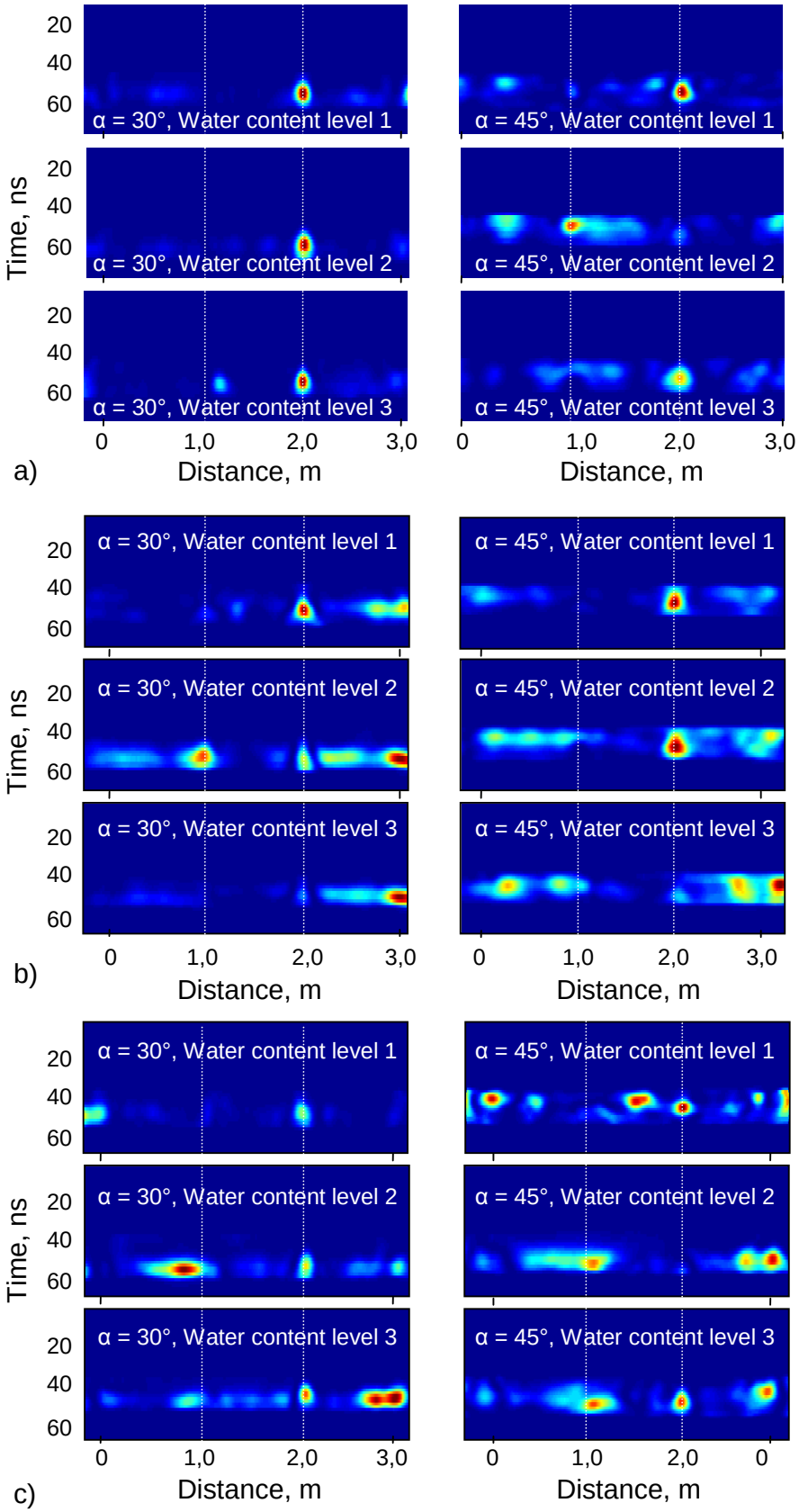

Figure 7.12 Backscattered energy from sugar beets acquired in scenario with soil surface roughness level 1; a) sand soil, b) loam soil, c) clay soil

Table 7.2 Comparison between energy amounts backscattered from large aluminium spheres and energy amounts backscattered from large sugar beet in scenarios with soil surface roughness level 1

Soil type	*Soil water content level*	*Angle α, °*	*Backscattered energy acquired from objects*		
			Sphere Ø120 mm	*Sugar beet Ø120 mm*	
			Absolute value, V^2	*Absolute value, V^2*	*Relative to the sphere, %*
Sand	1	30	389.900	217.700	55,8
	2	30	591.600	37990	6,4
	3	30	392.800	34360	8,7
	1	45	343.100	90880	26,5
	2	45	377.400	2162	0,6
	3	45	364.800	7.140	2,0
Loam	1	30	461.300	117.600	25,5
	2	30	215.800	13150	6,1
	3	30	251.900	16610	6,6
	1	45	399.100	175700	44,0
	2	45	250.200	28330	11,3
	3	45	154.700	6.650	4,3
Clay	1	30	529.800	89.140	16,8
	2	30	625.600	9827	1,6
	3	30	499.600	21580	4,3
	1	45	451.700	64080	14,2
	2	45	240.700	-*	-
	3	45	278.600	14.060	5,0
				Average value:	*14,1*

* It was not possible to unambiguously separate the signal of the sugar beet

Comparable to the previous measurements, the masking effect that originates from the soil surface clutter increases with the increasing water content.

The comparison between the energy amounts backscattered from large aluminium spheres and the energy amounts backscattered from large sugar beet in scenarios with soil surface roughness level 1 is presented in Table 7.2. The amounts of backscattered energy from the large sugar beet have been calculated and presented in percentage from the bigger sphere for each scenario, i.e. the amount of backscattered energy from the bigger sphere was 100% for each parameter

combination. The average value of the calculated percentages was 14,1% with large standard deviation of 15%. This standard deviation is a consequence of very low energy intensities for the second and third soil water content level.

The lower level of backscattered energy amounts is a consequence of the lower dielectric contrast between sugar beets and soil in comparison with the contrast between aluminium spheres and soil. The lowest level of backscattered energy amounts, i.e. dielectric contrast have been recorded for clay soil. The dielectric contrast additionally decreases with the increase of soil water content. Therefore, the amounts of backscattered energy from sugar beets and their detectability also decrease with the increase of soil water content for all scenarios.

The radargrams shown in Figure 7.13 are selected from the data acquired in the conditions of soil surface roughness of level 2 in order to illustrate the feasibility border case of sugar beet detection. The real positions of two sugar beets are marked with pairs of vertical dashed white lines. The tests with other system parameters delivered comparable results for tested conditions up to the soil surface level 2 and water content 2.

Radargrams acquired in above described scenarios are presented in Figure 7.13 on the left side, and the amounts of backscattered energies for corresponding system parameters are presented on the right side. The hyperbolical traces of bigger sugar beets are recognisable in all presented radargrams. The trace of the smaller sugar beet is distinguishable only in scenario with loam soil with the moisture content level 1, although in this case also partially covered with clutter. The hyperbolas of smaller sugar beets are partially of completely covered in the most of other cases.

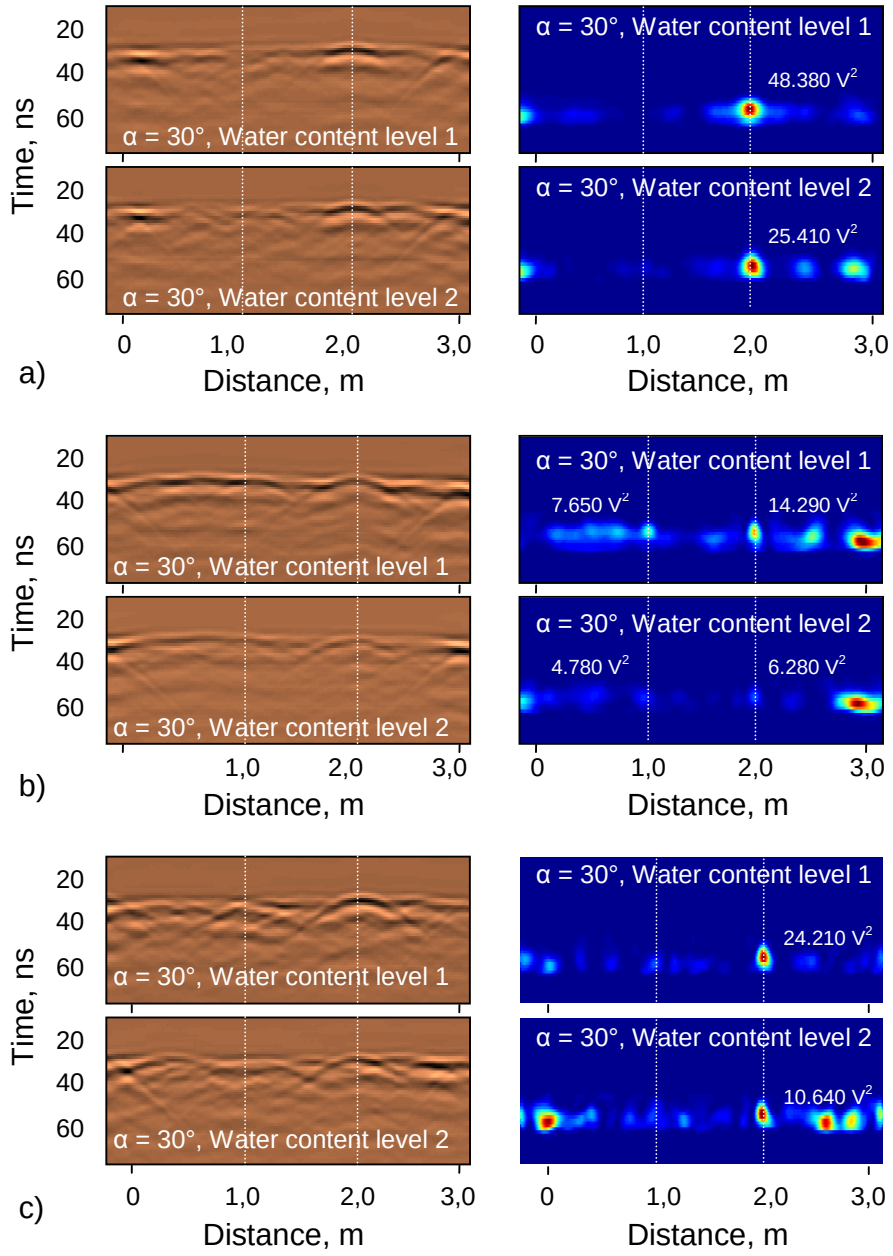

Figure 7.13 Radargrams and backscattered energies from sugar beets acquired in scenario with soil surface roughness level 2 with angles α = 30°and β = 0° ; a) sand soil, b) loam soil, c) clay soil

If the distribution of backscattered energy amounts (values in V^2 shown next to signals in Figure 7.13) is considered, the signals from smaller sugar beets could be located only in two cases, e.g. for data acquired in loam soil with water content level 1 and 2, Figure 7.13 b). The localisation of bigger sugar beets according to the values of backscattered energy amounts is unambiguously possible in all presented

cases; in the case of scenario with loam soil with the water content level 2, the intensity of sugar beet signal is very weak, but with the sufficient contrast to the surrounding soil.

7.1.2 Experiments with sugar beets with foliage

In this segment of the research, the potential of the radar system to acquire data about sugar beet roots through the leaves has been studied. In Figure 7.14, the radargrams acquired in scenario with three sugar beet sets with foliage are presented.

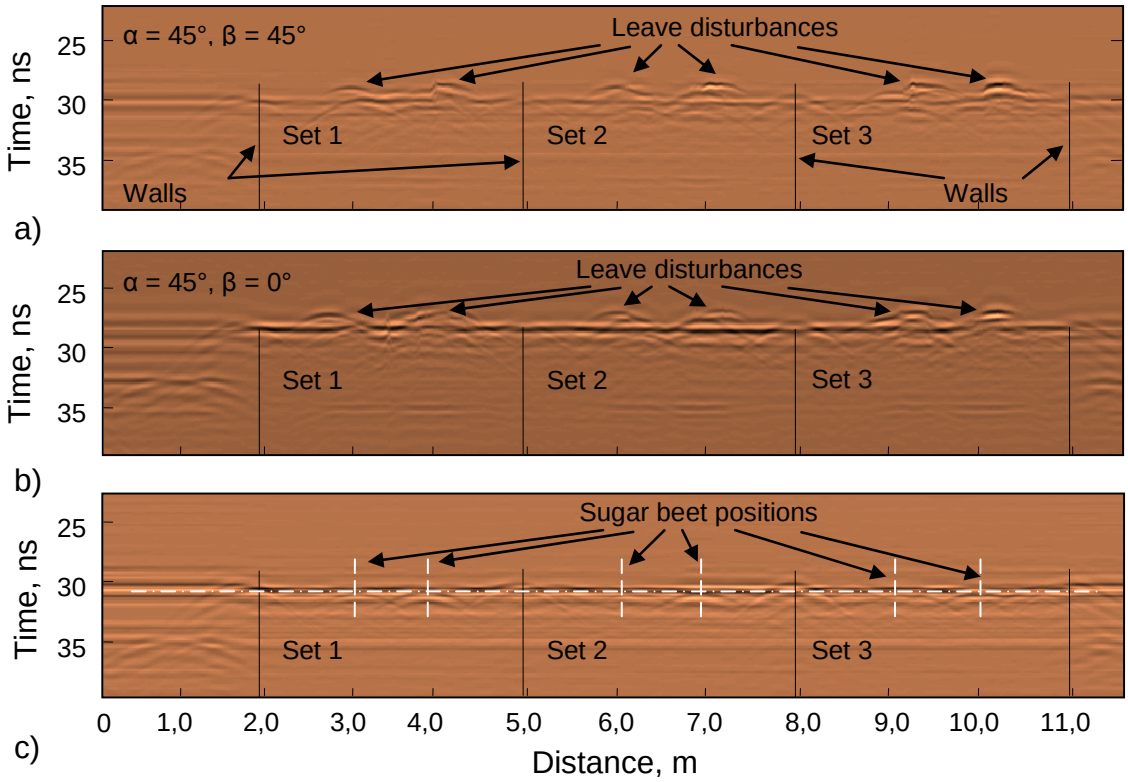

Figure 7.14 Specification of signals in the radargram acquired in scenario with three sugar beet sets with foliage; a) sugar beet sets with foliage acquired with α = 45° and β = 45°, b) sugar beet sets with foliage acquired with α = 45° and β = 0°, c) reference data –with correctly topped sugar beets

The data acquired with angle combinations α = 45°, β = 45° and α = 45°, β = 0° are shown in Figure 7.14 a) and b) respectively. Additionally, a radargram of scenario with the same sugar beets, scanned after topping is presented in Figure 7.14 c), in

order to provide reference data about the sugar beet positions and the shapes of hyperbolical traces of test object sets. In this radargram the sugar beet positions along the scan are marked with vertical white dashed lines. The positions of sugar beet tops are marked with horizontal white dot and dash line.

The radargram recorded with both angle combinations illustrates the same effect: the signals of leaves cover the areas of real positions of sugar beet roots, which are on the level of about 29 ns. This effect is more illustrative presented in Figure 7.15 for the data acquired in the scenario with Set 1.

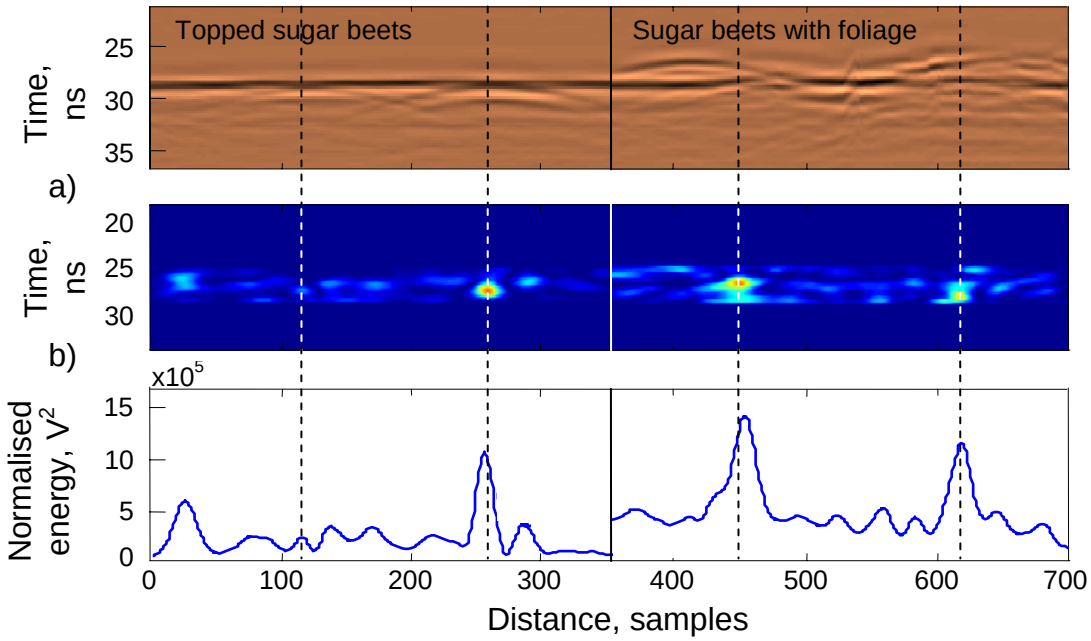

Figure 7.15 Data acquired in scenario with sugar beet with foliage; a) comparison between radargrams *topped sugar beets* vs. *sugar beets with foliage*, b) processed data, c) integrated energies

In Figure 7.15 the data acquired with angle combinations α = 45°, β = 0° in scenario with Set 1 – topped sugar beets (left) and with foliage (right) in sand soil were processed and put next to each other. As expected, the small topped sugar beet was not clearly visible, and it is not possible to be unambiguously distinguished from the neighbouring peaks. The bigger topped sugar beet provided a detectable peak. On the other hand, the backscattered energy from leaves provided even stronger signals

in positions above real positions of sugar beet roots (about 27 ns). Therefore, the effects caused by sugar beets' foliage cover the signals of roots, and consequently make the distinguishing and detecting of single sugar beet roots impossible. This effect is even more visible in the sugar beet row with regular distance of 20 cm between the plants. In that case it is not possible to distinguish between the plants, and only the canopy is recorded. The tests with other angle combinations (α = 45°, β = 45°) delivered analogous results.

7.1.3 Experiments with leaves brush

In this part of the research the potential of radar system to acquire data about sugar beet roots independently on the amount of the leaves' rests has been tested. The radargrams acquired in scenario with three sugar beet sets with long and short brushes and reference data with topped sugar beets are presented In Figure 7.16 a), b) and c) respectively. The data have been acquired with angle combination α = 45° and β = 45°. The tests with other angle combination (α = 45°, β = 0°) delivered analogous results in the tested scenarios.

Similar to scans with foliage, the brushes lead to additional disturbance and clutter that mask the reflection signal from the root. In the case of brushes two separated hyperbolas are visible, Figure 7.16 a): upper one from the brush tops and the lower one from the sugar beets roots. In the case of short brushes, Figure 7.16 b), hyperbolas are overlapped and it is not possible to separate them. This effect causes an increase in reflected energy, more closely visible in Figure 7.17.

In Figure 7.17 the data acquired with angle combination α = 45° and β = 45° in sand soil with set of topped sugar beets (left), sugar beets with long brushes (middle) and sugar beets with short brushes (right) were processed and put next to each other. In these radargrams the real sugar beet positions along the scan are marked with vertical white dashed lines.

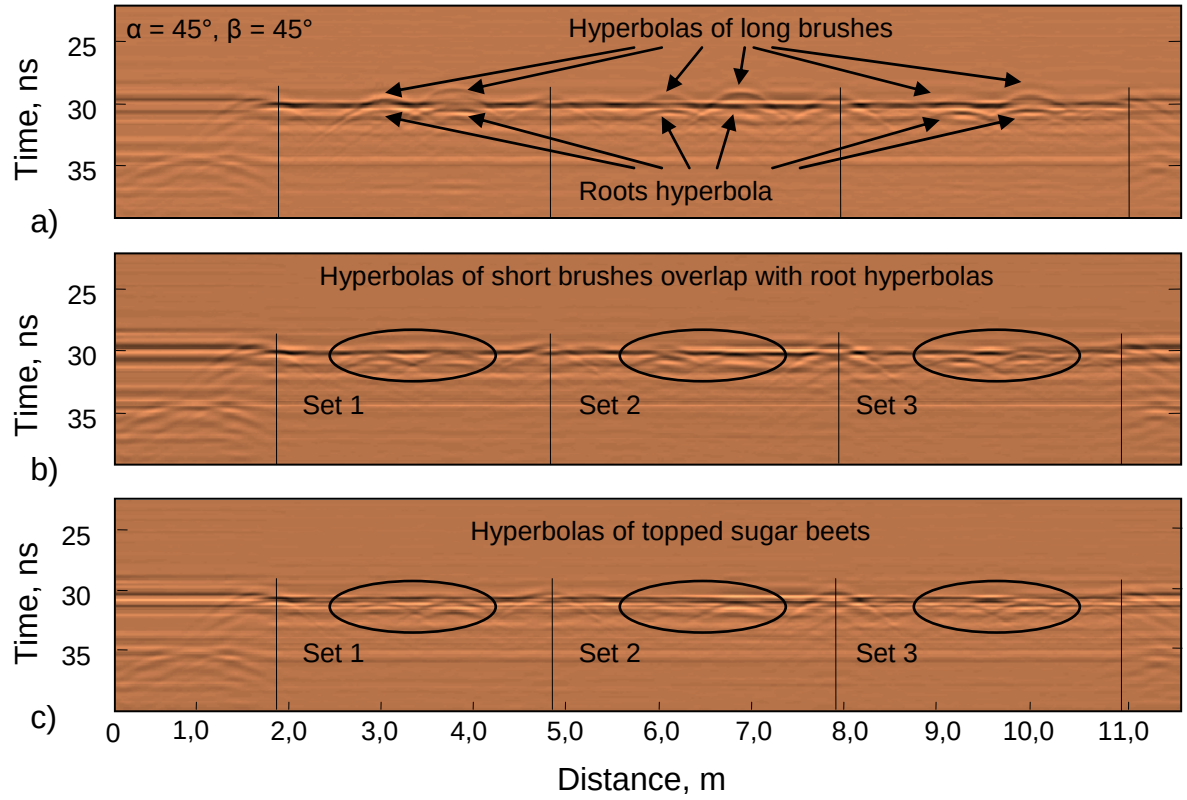

Figure 7.16 Specification of signals in the radargram acquired in scenario with three sugar beet sets with leaves' brush; a) with sugar beets with long brushes (ca. 40 cm), b) with sugar beets with short brushes (ca. 20 cm), c) reference data – with correctly topped sugar beets

As in the previous analysis noticed, the small topped sugar beet was not clearly visible and the bigger one provided a detectable peak. In other two cases the scattering of the hyperbolas caused by both long and short brushes leads to non focused energy amounts, and therefore it could not be separated to a single point – energy amounts marked with ellipses resulted in two and three peaks for larger sugar beet with long and short brushes respectively. In the case of smaller sugar beet with short brush, two hyperbolas: upper from the brush and lower from the root (ca. point 820) lead to two vertically concentrated energy amounts in Figure 7.17 b), causing the highest peak visible in Figure 7.17 c).

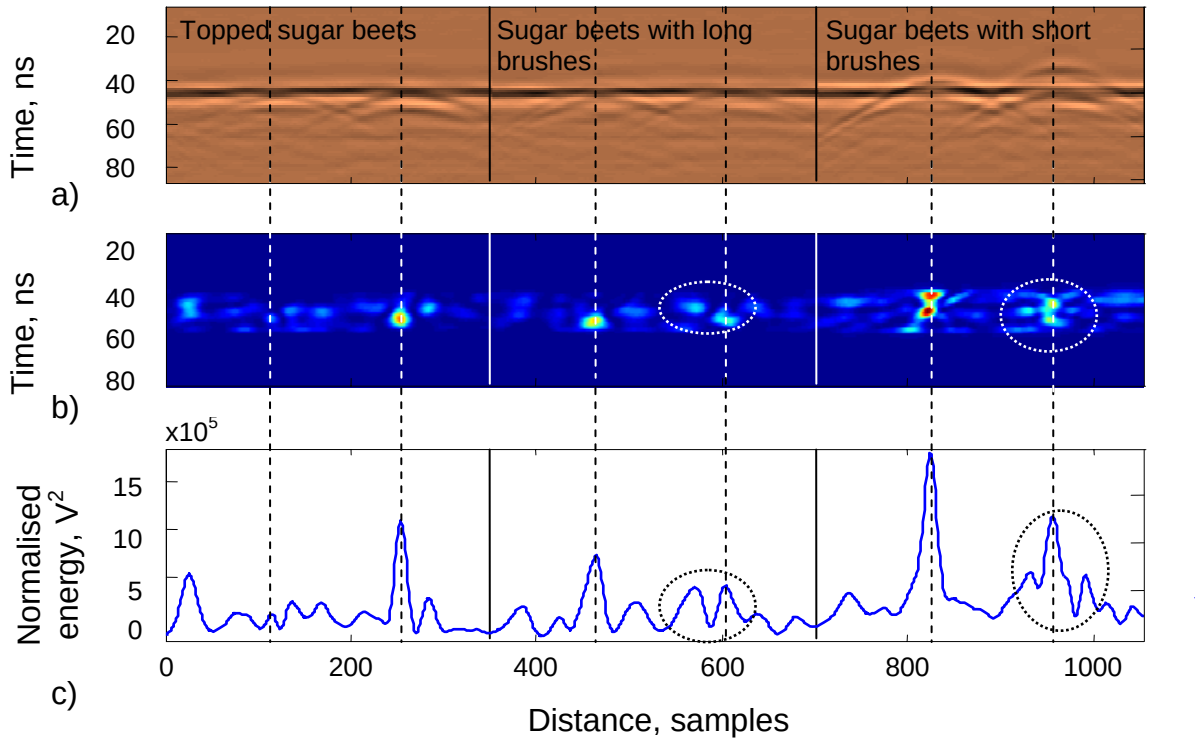

Figure 7.17 Data acquired in scenario with three sugar beet sets; a) comparison between radargrams *topped sugar beets* vs. *sugar beets with long* i.e. *short brushes*, b) processed data, c) integrated energies

7.1.4 Experiments with different height of sugar beets tops

Similar to the experiments with the additional biomass in two previous chapters, the experiments with different heights of sugar beet tops have been conducted in order to test the influence of the height of sugar beet tops on the backscattered energy amounts.

In Figure 7.18 a) the scenario arrangements with different height of sugar beet tops in sand soil with the first levels of soil surface roughness and soil water is shown, from the height 60 mm to 0 mm, from left to right respectively. In Figure b), c), d) and e) acquired radargrams of raw data (up) and processed data in the form of integrated backscattered energy amounts (down) are presented for four tested antenna combinations (α = 30°/β = 0°, α = 30°/β = 45°, α = 45°/β = 0°, and α = 45°/β = 45° respectively). The positions of sugar beets are marked with vertical black dashed lines.

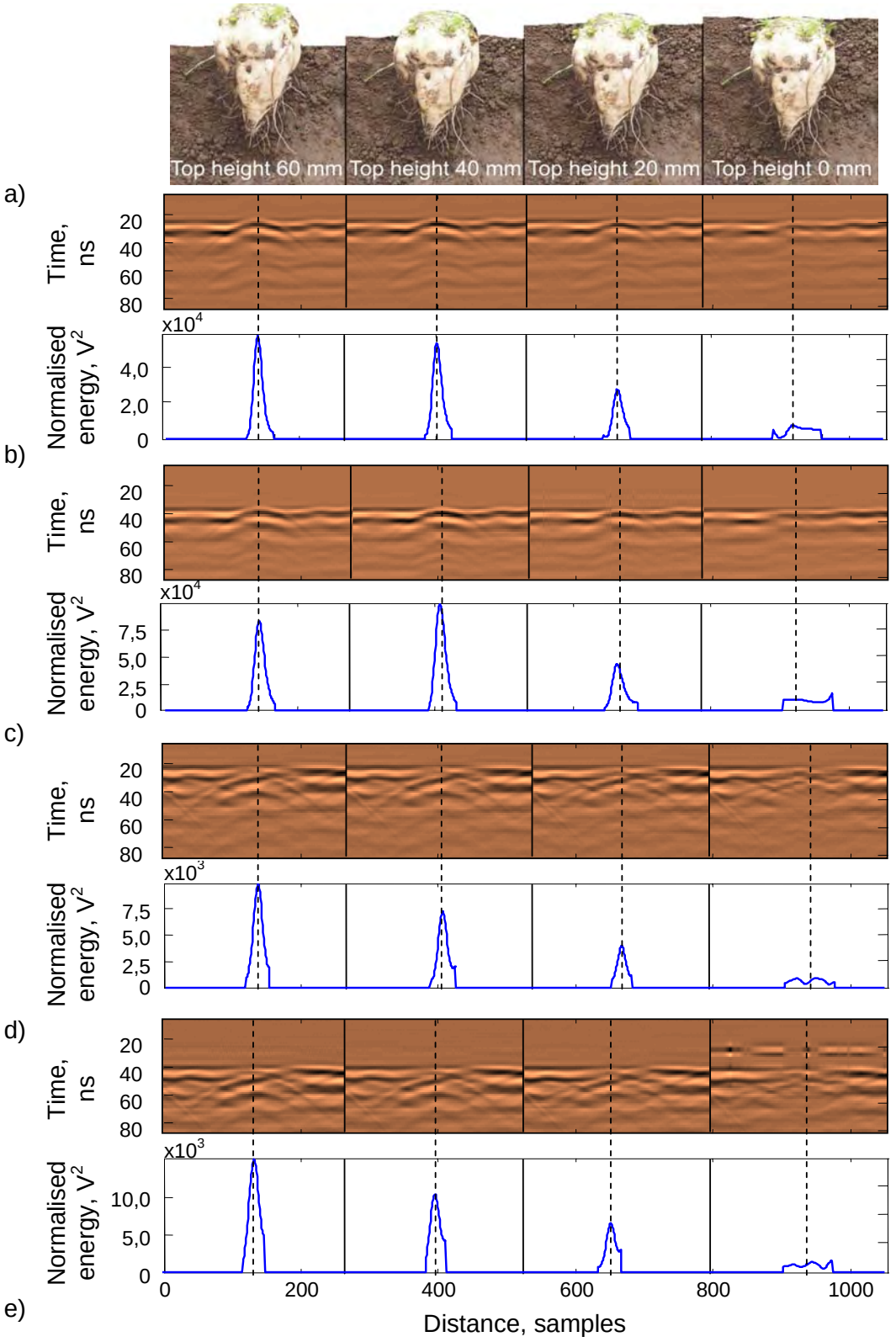

Figure 7.18 Scenario with different height of sugar beet tops; a) scenario arrangements, b), c), d) and e) acquired radargrams (top) and normalised energy amounts (bottom) for: a) α = 30°/β = 0°, b) α = 30°/β = 45°, c) α = 45°/β = 0°, and d) α = 45°/β = 45°

The hyperbolical traces of sugar beets with top heights 20 mm, 40 mm and 60 mm are recognisable in all radargrams. The tests within these scenarios delivered sharp peaks on real sugar beet positions visible in all radargrams in Figure 7.18. The backscattered energy amounts corresponding to the localised peaks are recorded and presented in Table 7.3

The trace of the sugar beet with top height 0 mm is visually distinguishable only in scenario with antenna combination $\alpha = 30°$ and $\beta = 0°$ in Figure 7.18 b). Other hyperbolas are partially covered with clutter effects, with the second best visible trace acquired with antenna combination $\alpha = 30°$ and $\beta = 45°$. Despite this difference noticed during visual detection, the processed data delivered unfocused energy amounts without recognisable peaks for all four tested antenna combinations. The recorded backscattered energy amounts shown in Table 7.3 have been connected to the known sugar beet positions and not to the located peaks belonging to scanned sugar beets.

In Table 7.3 a comparison between the energy amounts backscattered from sugar beets with different top heights and geometrical features of the scanned scenario is presented. The amounts of backscattered energy from sugar beet top heights 0 mm, 20 mm and 40 mm have been calculated and presented in percentage from the sugar beet top with height 60 mm for each parameter combination.

The average energy amount in the case of measurements with top height 40 mm was 88% with the extreme value 119% for antenna combination $\alpha = 30°$, $\beta = 45°$. The standard deviation in that case was 23%. If the extreme value of 119% is omitted, the average energy amount would be 78% with standard deviation of 12%. The recorded data in other scenarios showed more consistency; the standard deviation for measurements with top height 20 mm and 0 mm was in both cases 5%.

The envelope surface area and the volume of scanned overground part of experimental scenario, as the referent geometrical features, have been calculated according to the approximation presented in Figure 7.19 a). In Figure 7.19 a) the

lower part of the overground profile of tested sugar beet has been approximated with a cylinder (Ø120 mm x 20 mm), and the upper part with a spherical calotte (Ø120 mm x 40 mm). The geometrical bodies together represent the shape of the used sugar beet with sufficient accuracy.

In the case of top height 60 mm, both geometrical bodies form the overground profile of scanned scenario, Figure 7.19 b). The profile of the scenario with sugar beet height 40 mm consists only of the spherical calotte, Figure 7.19 c) and in the case of top height 20 mm, the profile consists of the upper 20 mm of the approximated spherical shape, Figure 7.19 d).

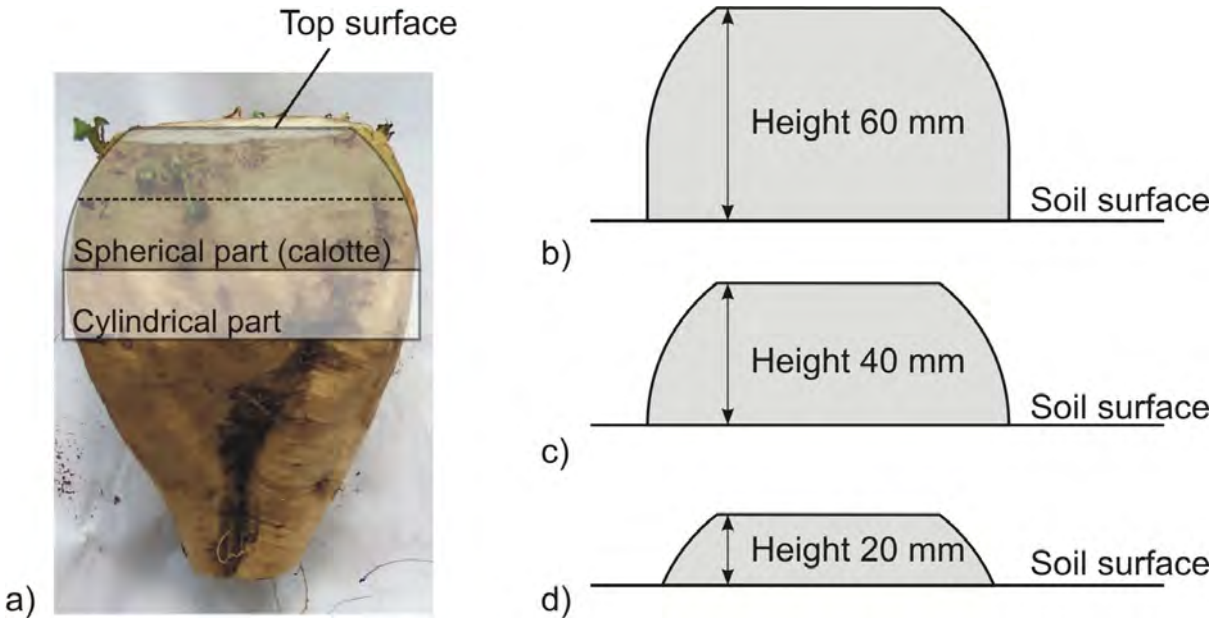

Figure 7.19 Scanned sugar beet and its geometrical approximation; a) sugar beet and approximated geometrical bodies, b), c) and d) scanned profiles with sugar beet top heights 60 mm, 40 mm and 20 mm respectively

The surface areas and volumes of profiles with sugar beet top heights 0 mm, 20 mm and 40 mm presented in Table 7.3 have been calculated and presented in percentages from the values of surface area and volume of the highest profile.

Presented energy amounts show better relationship with the envelope surface areas of scanned profiles than with the volumes, even if the high standard deviation is

considered. The relationship is even closer if the extreme value for top height 40 mm and antenna combination α = 30° and β = 45° is omitted (value shown in Table 7.3 in brackets). These results are in compliance with the results of tests with aluminium spheres; with an exception for the scenario with top height 0 mm.

Table 7.3 Comparison between energy amounts backscattered from sugar beets and geometrical features of the scanned sugar beet

Top height, mm	*Antenna combination α/β, °*	*Backscattered energy amounts from sugar beets*			*Surface area (relative to 60 mm), %*	*Volume (relative to 60 mm), %*
		Absolute value, V^2	*Relative to top height 60 mm, %*	*Average, %*		
60	30/0	56.670	100	100	100	100
	30/45	82.140	100			
	45/0	9.163	100			
	45/45	14.390	100			
40	30/0	52.090	92	88 *(78*)*	74	61
	30/45	98.140	119			
	45/0	6.760	74			
	45/45	9.868	69			
20	30/0	27.150	48	45	48	29
	30/45	41.790	51			
	45/0	3.660	40			
	45/45	6.162	43			
0	30/0	1.148	2	6	22	0
	30/45	1.134	1			
	45/0	1.133	12			
	45/45	1.130	8			

* Average value without the highest amount of measured backscattered energy from sugar beets

The calculated percentage of the amount of backscattered energy in the case of top height 0 mm is significantly lower than the share of 22% of the profile envelope surface area, i.e. top surface marked in Figure 7.19 a). The low percentage of backscattered energy amounts can be explained with the specific behaviour of the data processing step of background subtraction and with the characteristics of the scenario.

The scenario has been arranged with the smoothest soil surface roughness level. The smooth cut on the top of used sugar beet (top surface) was in the same level with soil surface. Despite partially visible hyperbolical trace, the data processing was not successful in preserving and focusing the recorded dielectric contrast within the scenario, which caused energy losses and lower energy level in the case of top height 0 mm.

7.1.5 Experiments with different positions of sugar beets in the row

In Figure 6.23 and in Figure 6.36 two different orders of ascending array of sugar beet have been arranged and scanned. In Figure 7.20 the processed radargrams of three different scenario arrangements are presented.

In Figure 7.20 a) four sugar beets provided four distinguishable signals with energy amounts corresponding to the sugar beet sizes: D: 240 g, Ø70 mm, B: 850 g, Ø120 mm, C: 550 g, Ø100 mm, A: 1150 g, Ø130 mm. In Figure 7.20 b) the sugar beet C has been removed, the empty hole has been filled with soil, and the scenario repeatedly scanned. The data processing provided correct information about the absence of the sugar beet C. In the third case, a soil bump in the shape and size of the sugar beet C has been formed and the scenario scanned once again.

The backscattered energy amount from the soil bump was similar to the energy acquired within the scenario with the sugar beet C. This result confirmed the potential of misinterpretation of the real scenario arrangement if the soil profile provides a soil bump with the shape and the position which comply to the shape and the position of a sugar beet.

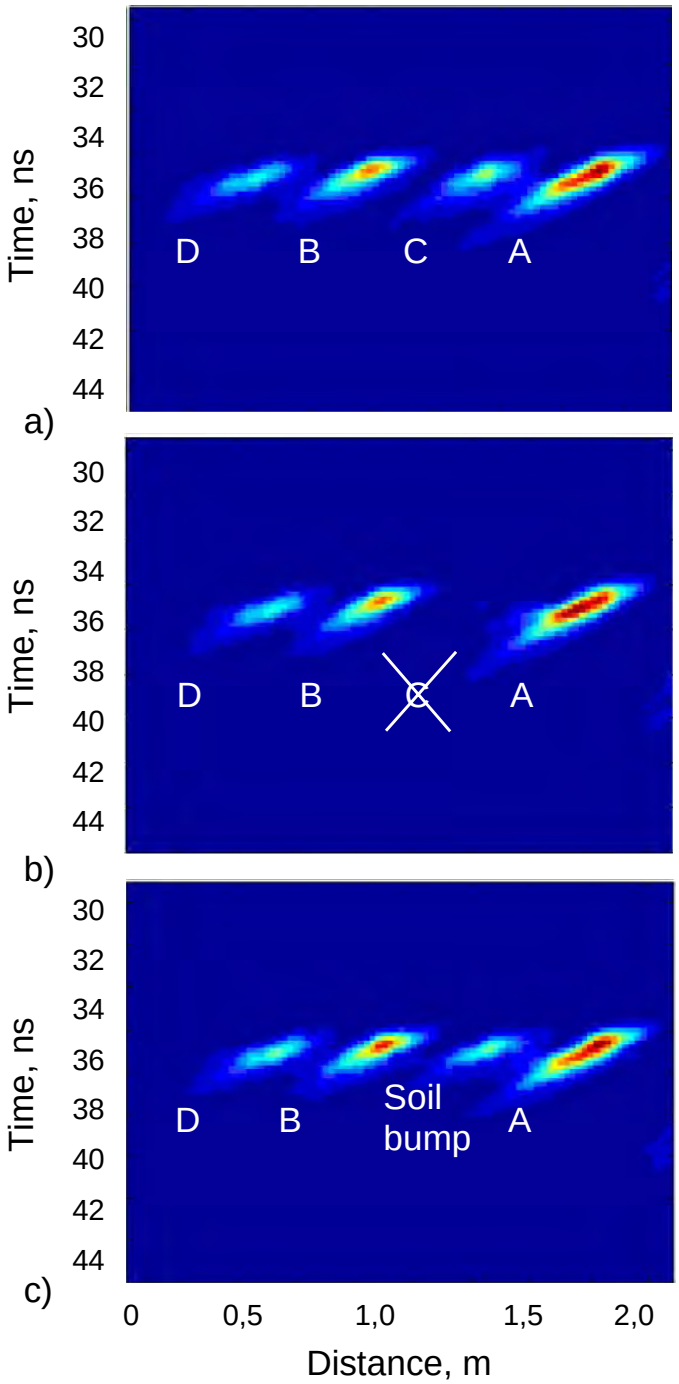

Figure 7.20 Processed data acquired in the scenario with different positions of sugar beets in the row; a) scenario arrangement with four sugar beets, b) scenario arrangement without sugar beet C, c) scenario arrangement with three sugar beets and a soil bump

7.2 Field experiments

The results and discussion on *Field experiments* has been divided into two evaluation steps: analysis of detectability and localisation of sugar beets, and estimation of system's potential to determine single sugar beet mass.

Analogous to the analysis of radar system efficiency and behaviour in general within the chapter *Laboratory experiments*, the analysis of sugar beet detectability has been divided into analysis of influences of: system parameters and scenario properties.

Sugar beet detection and localisation – analysis of system parameters

In Figure 7.21 the comparison between radargrams acquired with two different incident angles, α = 30° in Figure 7.21 a) and α = 45° in Figure 7.21 b), and with the same angle between antennas (β = 0°) in the same scenario conditions are presented, and the influence of this system parameter has been analysed. In both cases the first and the last sugar beet have been marked with the vertical black line. The first sugar beet was in the level of about 90 in both cases, and the last one has been shifted in the case of the scan with α = 30°. This difference occurred as a consequence of different driving speeds during two scans and had no influence on the acquired data.

The scenario conditions were: loam soil (Figure 6.17) with water content 28,1%vol (level 2), prepared row with 45 topped sugar beets with average distance between sugar beets of 22,6 cm, average single sugar beet mass 768 g and average maximal diameter 9,9 cm. The soil surface roughness was predominantly on the level 1, and in some scanned parts up to the level 2. The tests in other row sections delivered comparable results.

In Figure 7.21 a) the data acquired with antenna combination α = 30° and β = 0° is presented with the following steps of data processing procedure: acquired radargram – raw data (up), radargram without cross-talk (second from above), quadratic absolute value of Hilbert-transformed radargram – migrated radargram (third from above) and the integrated values of Hilbert-transformed radargram (down). In the

following figures only the processed data in the form relevant for the analysis are going to be presented.

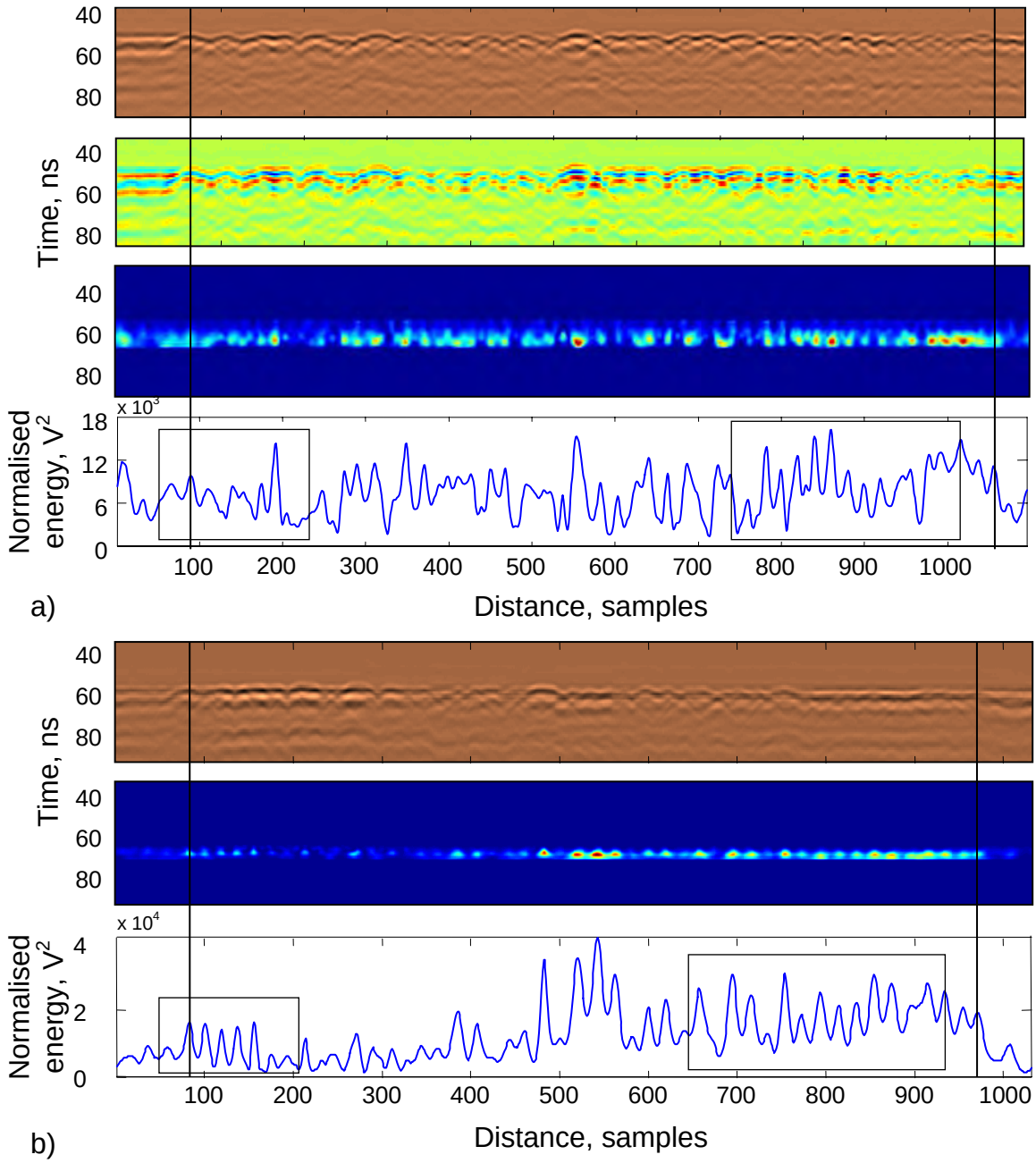

Figure 7.21 Comparison between radargrams of 45 sugar beets in scenario with soil water content 28,1%vol,acquired with two different incident angles and with angle between antennas β = 0° in the same scenario conditions; a) incident angle α = 30° b) incident angle α = 45°

In both cases in Figure 7.21 the raw data look similar. The signal intensity is slightly higher in the radargram with raw data acquired with α = 30°, which is also visible after data processing in the form of unfocused energy amounts. On the other hand, the intensity of obtained peaks was lower, due to less focused data, which resembles the results from previous analyses (see Table 7.1).

The effect of higher intensity and less focused energy amounts could be confirmed on the whole length of diagrams with normalised energies; the effect is particularly visually distinguishable in marked rectangles. In the left rectangle there are 8 sugar beets. In the case of α = 30°, there is a peak left of the rectangle, representing the eighth and non-existing one in the similar intensity level. Other peaks represent existing sugar beets, whereat the peaks obtained with α = 45° show better visual detectability in comparison to the corresponding data acquired with α = 30°; especially for the third sugar beet (double peak for α = 30° at level of sample 150) and the last two small ones (the first small one is still visible, but the peak of the second one is lost). Similar situation is within the area marked with the right rectangle. Other measurements with incident angle α = 30° showed comparable results.

In Figure 7.22 the comparison between radargrams acquired with two different angles between antennas, β = 0° in Figure 7.22 a) and β = 45° in Figure 7.22 b), with the same incident angle (α = 45°) in the same scenario conditions are presented, and the influence of this system parameter has been analysed. In this case also, the scan has been shifted as a consequence of different driving speeds, but this time the difference has been eliminated during the data processing. The tests in other row sections using above described system configuration delivered analogous results.

The scenario conditions were: loam soil (Figure 6.17) with water content 31%vol (level 3), prepared row with 50 topped sugar beets with average distance between sugar beets of 23,3 cm, average single sugar beet mass 563 g and average maximal diameter 9,7 cm. The soil surface roughness was predominantly on the level 1, with maximum value between level 1 and 2.

The real positions of 50 sugar beets are marked with vertical dashed lines. The real positions, i.e. the distance between sugar beets have been recorded according to the Test Procedures for Measuring the Quality in Sugar Beet Production (Anonymous 2004).

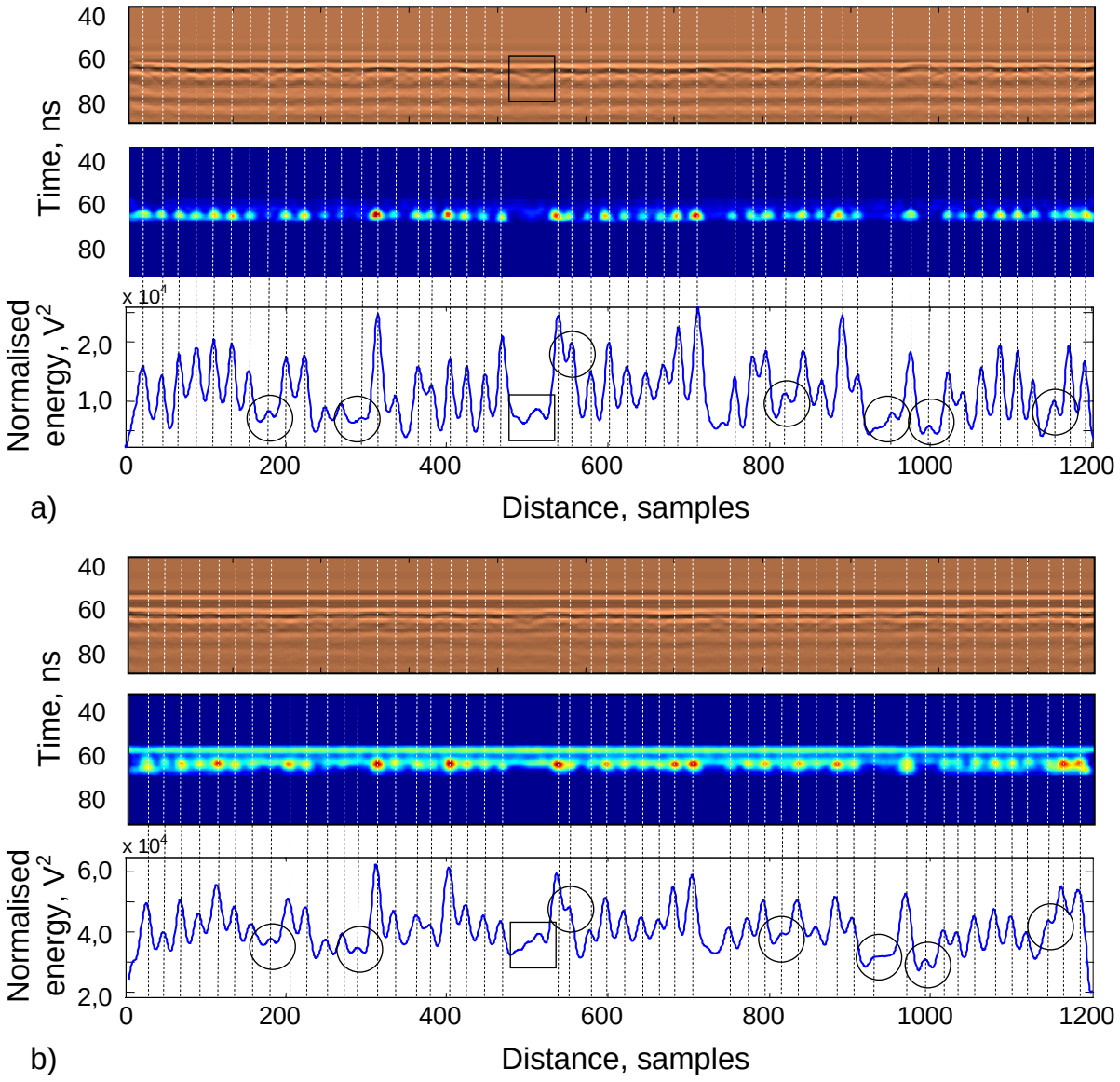

Figure 7.22 Comparison between radargrams of 50 sugar beets in scenario with soil water content 31%vol, acquired with two different angle between antennas with incident angle α = 45° in the same scenario conditions; a) angle between antennas β = 0° b) angle between antennas β = 45°

In Figure 7.22 a) in the radargram with migrated data, single scatterers are visible by focused energy portions. In comparison to the scan in Figure 7.22 b) the energy amounts in Figure 7.22 a) are smaller. However, the large amount of the recorded backscattered energy belongs to the intensive cross talk, which is visible as a horizontal line in the radargram obtained with antenna combination α = 45° and β = 45° (Figure 7.22 b).

Similar to the comparison between scans with α = 30° and α = 45° in Figure 7.21, the data acquired with antenna combination α = 45° and β = 0° deliver more focused energy amounts backscattered from the single sugar beets than data acquired with antenna combination α = 45° and β = 45°. Because of this effect, the separation of single sugar beets is better for antenna combination α = 45° and β = 0°.

This effect is particularly visible for the first 7 peaks in both radargrams. Even better criteria are detectability of extremely small sugar beets and sugar beets close to each other, in both cases marked with circles. All marked peaks with circles are easier to be distinguished and located in Figure 7.22 a), except in the case of the second circle from the left. In this case, the sugar beet of 110 g and 5,5 cm of diameter had higher peak for antenna combination α = 45° and β = 45°. In the third circle from the left there are signals from two sugar beets with the smallest distance in this row (16 cm). In Figure 7.22 a) two peaks are recognisable and the corresponding lower peak in Figure 7.22 b) is almost completely covered by the neighbouring one.

Interesting occurrence was that signals from sugar beets of 120 g to 130 g, with diameters smaller than 6 cm, have been visible in the processed data acquired in field conditions (e.g. signals in the second and the third circle from the right). These diameters were smaller than diameter used as border case during laboratory experiments, which was often undetectable in the laboratory conditions.

The part of the diagram with a peak marked with rectangle does not belong to a sugar beet; neighbouring sugar beets from both sides were at large distance of 68 cm and the energy amount is a result of overlapping of two hyperbolical traces marked with rectangle in the radargram with raw data in Figure 7.22 a).

Both angle combinations from Figure 7.22 are suitable measurement setups for sugar beet detection with advantages and disadvantages. The advantage of antenna combination α = 45° and β = 0° is a small cross talk and deeper penetration into soil, and its disadvantage is that the main signal occurs when the sugar beet is not in the boresight direction (directly in front of antenna). The advantage of antenna combination α = 45° and β = 45° is obtaining the main signal by direct reflection in boresight direction, but the larger cross talk represents the most important disadvantage, which causes a decrease in sensibility.

Sugar beet detection and localisation – analysis of scenario properties

Three most relevant scenario features are soil type, soil surface roughness and soil water content. In field conditions there was no possibility to change the soil surface roughness, and the soil texture was approximately constant within the scanned sugar beet rows. The water content was different from row section to row section. In Figure 7.23 two row sections with different water contents are presented in order to analyse the influence of this scenario feature.

In Figure 7.23 the comparison between radargrams acquired in two scenarios with different water contents: 22,3%vol Figure 7.23 a) and 27,3%vol in Figure 7.23 b), using antenna combination α = 45° and β = 0° are presented. The data in Figure 7.23 a) have been recorded in the following scenario conditions: loam soil (Figure 6.17) with water content level 1, prepared row with 44 topped sugar beets with average distance between sugar beets of 22,5 cm, average single sugar beet mass 678 g and average maximal diameter 9,8 cm. The soil surface roughness was predominantly on the level 1, with maximum value between level 1 and 2. The data in Figure 7.23 b) have been recorded in the following scenario conditions: loam soil (Figure 6.17) with water content level 2, prepared row with 43 topped sugar beets with average distance between sugar beets of 24,1 cm, average single sugar beet mass 795 g and average maximal diameter 10,1 cm with same properties of soil surface.

The real positions of sugar beets are marked with vertical dashed lines. In Figure 7.23 a) in the radargram with migrated data, single scatterers are better focused than in Figure 7.23 b), which is a consequence of the higher dielectric contrast of sugar

beets to the surrounding soil in scenario conditions with lower water content. This effect enables easier separation and localisation of peaks, which is observable in the whole length of radargrams and it was similar to already presented radargram comparative analyses.

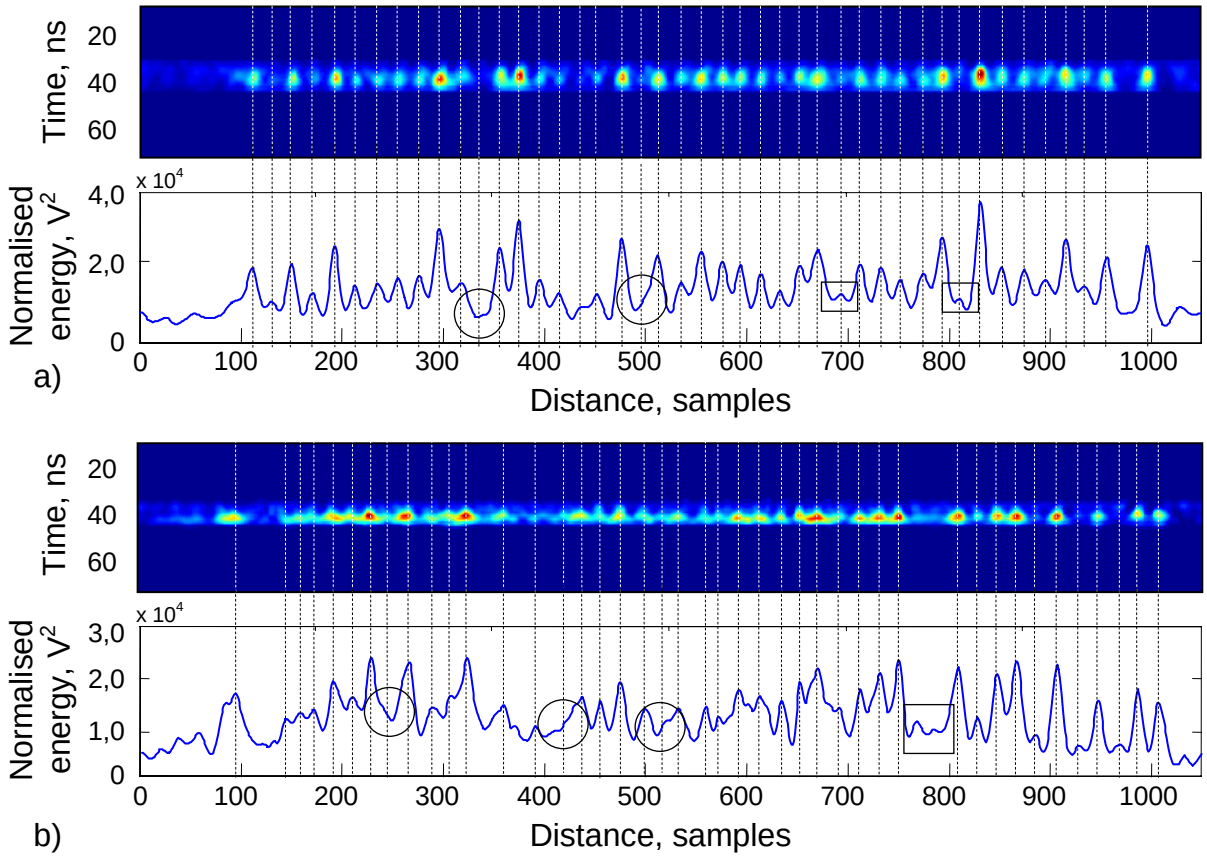

Figure 7.23 Comparison between two scenarios with different water content using antenna combination α = 45° and β = 0°; a) soil water content 22,3%vol, b) soil water content 27,3%vol

In Figure 7.23 a) there were two sugar beet positions without recognisable peak. These two positions are marked with circles. The not-detected sugar beets were smaller than the average value; with mass 400 g and 410 g. On the other hand, two distinguishable peaks marked with rectangles (positions around sample 700 and sample 800) belong to even smaller sugar beets; 370 g and 390 g respectively.

Because of the lower dielectric contrast, the peaks in Figure 7.23 b) are less explicit, but visually still recognisable, except in three case marked with circles. In these three cases the signals of sugar beets (340 g, 470 g and 480 g) were covered with

neighbouring signals. In the position between sample 750 and 800 there were no sugar beets (large gap of 65 cm) and the signal in the rectangle could be interpreted as a sugar beet signal.

Visual vs. threshold detection – normal distance in the row

The potential to visually detect sugar beets according to the backscattered energy amounts has been evaluated. The energy peak positions have been manually selected, i.e. the data have been automatically processed and the peaks have been manually marked, and energies and positions registered.

The number of not detected sugar beets in a row with 40 to 50 sugar beets was between one and four; the visual detectability for all scanned sugar beet rows was from 90% to 96%. All tests of sugar beet position vs. energy peak position showed a correlation of about 99%. The real measured positions of the sugar beet have been successfully detected with an average error from 1,1 cm to 3,6 cm.

In Figure 7.24 the comparison between three simple detection threshold levels is presented. This comparison has been used to evaluate the potential of simple threshold detection shown in Figure 6.23 d). The data used for this analysis have been acquired in the scenario with soil water content 22,3%vol using antenna combination $\alpha = 45°$ and $\beta = 0°$. This data set is one of the best sets considering the quality of focused energy amounts and the success of single sugar beet scatterer separation.

In Figure 7.24 a) the threshold level has been set above the highest saddle on the curve representing normalised energy marked with circle. If this threshold level is used, 14 sugar beets are left below the threshold (marked with rectangles) and these sugar beets are not going to be detected. In counterpart border case the threshold line is situated below the lowest sugar beet peak marked with circle in Figure 7.24 c). In this case 18 sugar beets are not going to be identified, i.e. 26 single sugar beets are going to be recognised as 8 peaks marked with rectangles. In the third situation, the threshold level has been visually selected and put on the level of approximately 50% of the highest peak. The result of the threshold detection is better, but still

unsatisfactory with 9 not detected sugar beets (8 below and one above the threshold).

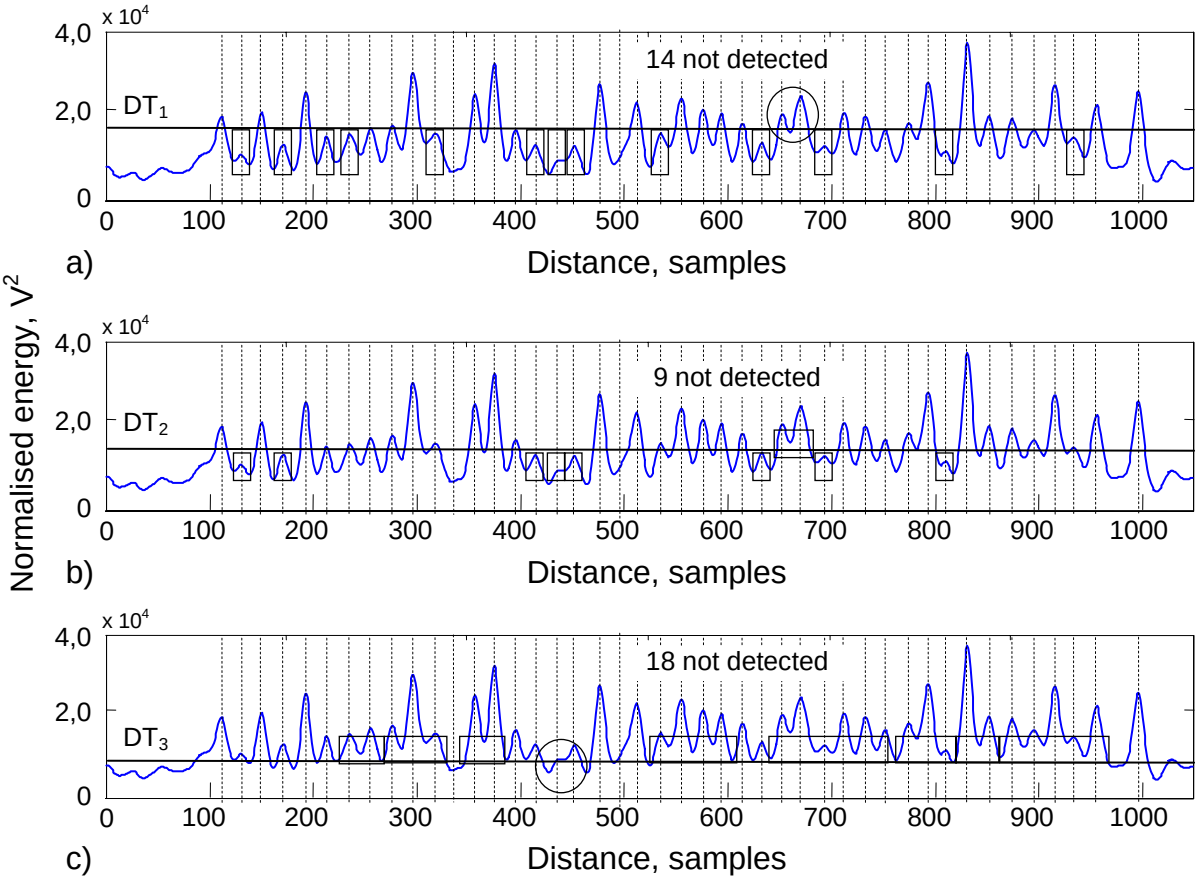

Figure 7.24 Comparison between three simple detection threshold (DT) levels applied for the data acquired in the scenario with soil water content 22,3%vol using antenna combination α = 45° and β = 0°; a) highest detection threshold, b) visually selected detection threshold, c) lowest detection threshold

The tests with other antenna combinations in row sections with less adequate conditions for radar technology, first of all with higher soil water content, delivered comparable results and generally less successful threshold detection results. According to this analysis, the principle of simple threshold detection is insufficiently flexible for data obtained in regular field conditions, i.e. in conditions with normal sugar beet distance of 20 cm.

Visual vs. threshold detection – row with increased distance in the row

Similar analysis of both visual and threshold detection principle has been made for thinned rows – rows with increased distance between sugar beets (see Figure 6.37). All other tests condition concerning system parameters and scenario conditions have been preserved.

All peaks of sugar beets in thinned rows have been identified. The tests of sugar beet position vs. energy peak position showed correlation of about 99%, which is similar to the full row, and the real measured positions of the sugar beet had slightly larger average errors from 1,8 cm to 4,7 cm.

In Figure 7.25 two radargrams acquired in scenarios with different water contents: 22,3%vol Figure 7.25 a) and 28,1%vol in Figure 7.25 b), using antenna combination $\alpha = 45°$ and $\beta = 0°$ are presented and the influence of increased distance with different scenario features has been analysed.

In Figure 7.25 a) the same row presented in Figure 7.24 with increased distance between sugar beets is shown. In this thinned row there were 15 sugar beets with average distance 66,1 cm, with average mass of 619 g and average maximal diameter of 9,9 cm. In Figure 7.25 b) the same row presented in Figure 7.21 with increased distance between sugar beets has been shown. In this row there were 16 sugar beets with average distance of 65,0 cm, with an average mass of 775 g and an average maximal diameter of 10,5 cm.

According to both visual and threshold analysis of all data in Figure 7.25, only several peaks were not distinguishable. In Figure 7.25 a) the first peak marked with a circle was below the line of detection threshold (DT). The neighbouring peaks from both sides of the marked one have similar intensity, which disabled unambiguous detection. On the other hand, the first sugar beet had mass and diameter far under the average values, 260 g and 7 cm respectively.

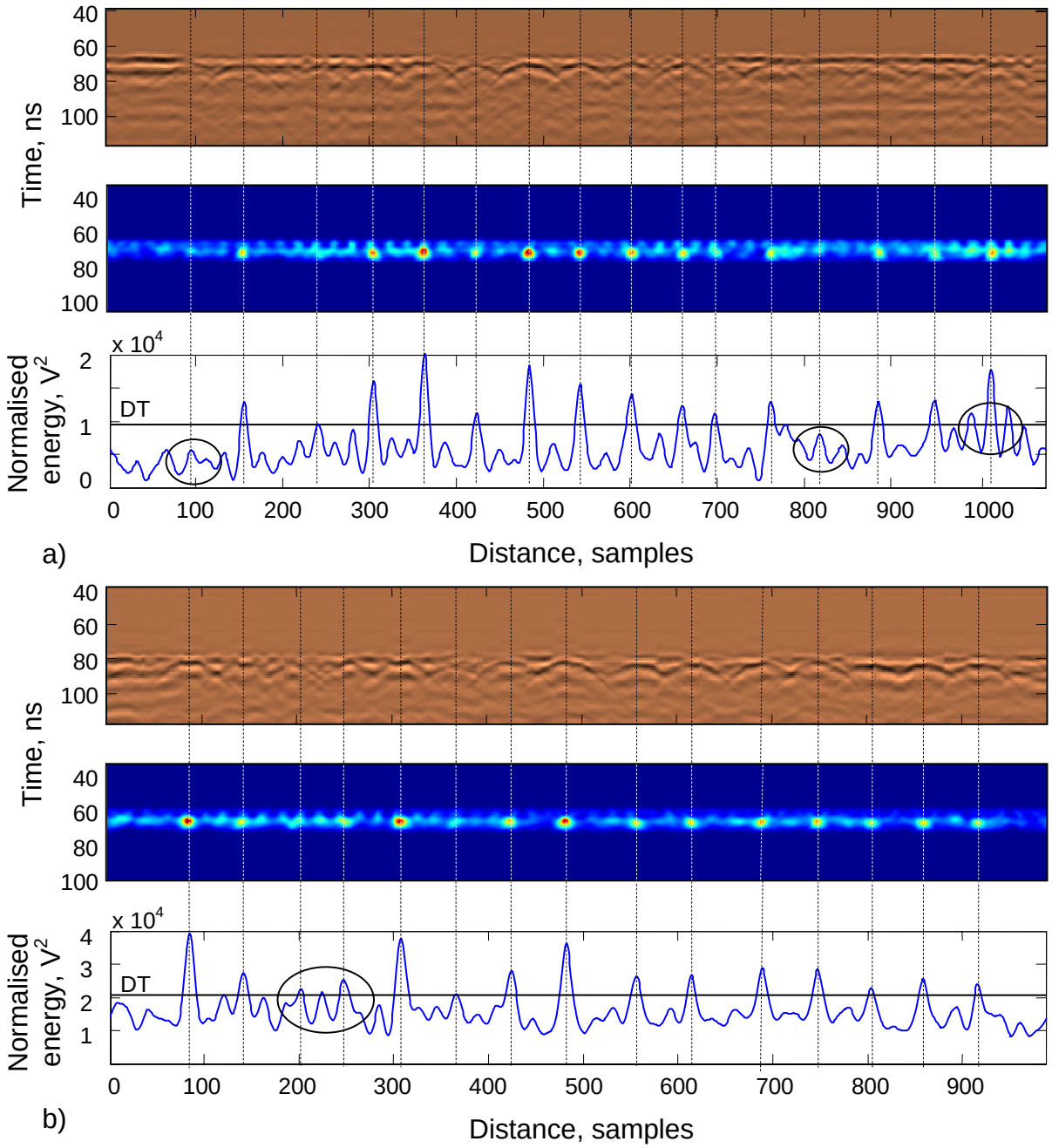

Figure 7.25 Test of threshold detection principle potential on two scenarios with thinned rows and different water content using antenna combination α = 45°, β = 0°; a) water content 22,3%vol, b) water content 28,1%vol

The second signal under DT Figure 7.25 a) marked with circle belonged to the second smallest sugar beet in this row (390 g, Ø8,5 cm). In this case it was visually possible to distinguish the signal from the surroundings. The same was with the last signal in this row, which was distinguishable, but the side disturbances were over DT. Disturbances of the similar shape are recognisable in both diagrams, next to every

sugar beet signal. These disturbances are on the positions of removed sugar beets and originate from the different soil structure on the spots of filled holes, which caused additional reflections.

Similar to the previous analysis, the marked peaks of the third and fourth sugar beet in Figure 7.25 b) were above the DT, just like the side disturbance between them. These two sugar beets were the second and the third smallest in the scanned row, with mass of 380 g and 400 g (the smallest one was the sixth in the row with the smallest peak and mass 340 g).

Although with better and more consistent results in comparison to the full row, the tests with thinned sugar beet rows also showed insufficient flexibility of the threshold detection principle. On the other hand, the visual analysis was easier because of a more recognisable pattern with two side-peaks next to a sugar beet signal.

Sugar beet mass determination

In the following section of the chapter Field experiments, the sugar beet mass determination has been analysed. The first part consists of analysis of three different scenarios with full row, i.e. with regular distance between sugar beets in the row. This part is followed by the analysis of the measuring error and its correction, and by the analysis of two different scenarios with thinned row, i.e. with increased distance in the row.

Analyses of three different scenarios with full rows

The peaks of single sugar beets have been visually detected on diagrams with integrated backscattered energies, and corresponding energy amounts have been registered. These data have been compared to the morphological data of sugar beets. The relevant characteristic data in this case were: distance between sugar beets, maximum diameter, top height and single root mass. These data have been collected according to the Test Procedures for Measuring the Quality in Sugar Beet Production (Anonymous 2004). In the following figures the data series of normalised energy backscattered from single sugar beets have been compared to single sugar

beet masses and correlations between data series are calculated and presented, as well as other relevant relationships of recorded data.

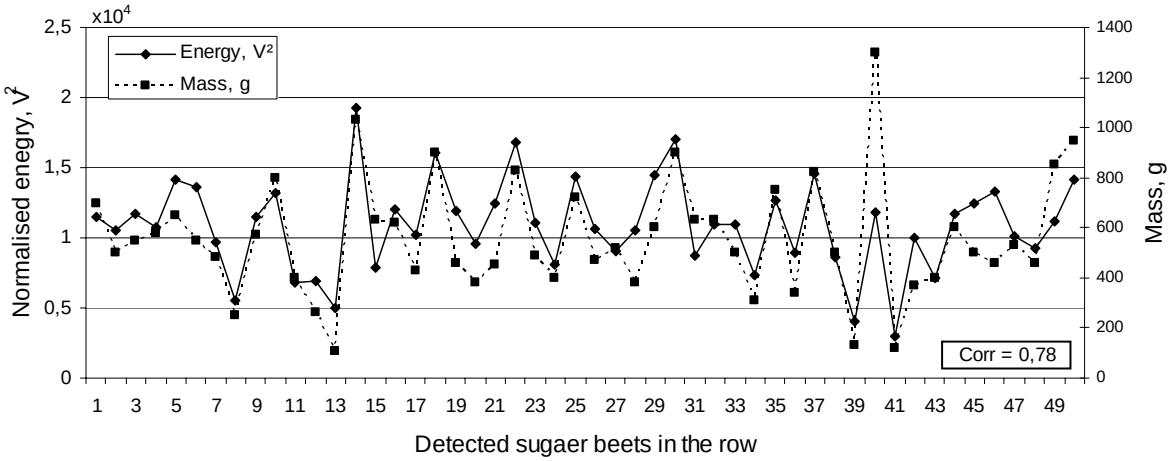

Figure 7.26 Normalised energies backscattered from single sugar beets vs. single sugar beet masses in scenario with soil water content level 3 and low average single sugar beet mass

Table 7.4 Relevant scenario features and data series correlation rates for test in scenario with soil water content level 3 and low average single sugar beet mass

Number of sugar beet in the row		50
Number of detected sugar beets		50
Soil water content, %vol		31 (Level 3)
Average single sugar beet mass, g		563
Average distance between sugar beets, cm		23,3
Average top height, cm		3,7
Average maximum diameter of sugar beets, cm		9,7
Other relevant correlations, %	Mass vs. maximum diameter	87
	Mass vs. top height	78
	Backscattered energy vs. top height	81
	Backscattered energy vs. maximum diameter	74
Correlation mass vs. backscattered energy, %		*78*

In Figure 7.26 the amounts of backscattered energies recorded in the diagram presented in Figure 7.22 a) have been compared to single sugar beet masses. The relevant scenario features and data series correlation rates are presented in Table 7.4. The specific characteristic of this test was low average single sugar beet mass and high soil water content level; this experiment has been conducted in August 2006 with growing sugar beets.

In Figure 7.22 a) the existing peaks of all sugar beets have been identified according to their known positions. The correlation of corresponding energies vs. recorded single sugar beet masses was 78%, despite the small root sizes and the high water content. On the other hand, all significant data series correlate well, 74% or more.

In Figure 7.27 the amounts of backscattered energies recorded in the diagram presented in Figure 7.23 a) have been compared to single sugar beet masses. The relevant scenario features and data series correlation rates are presented in Table 7.5. The characteristic of this test was regular average single sugar beet mass and low soil water content level; this experiment has been conducted in October 2006 with grown sugar beets.

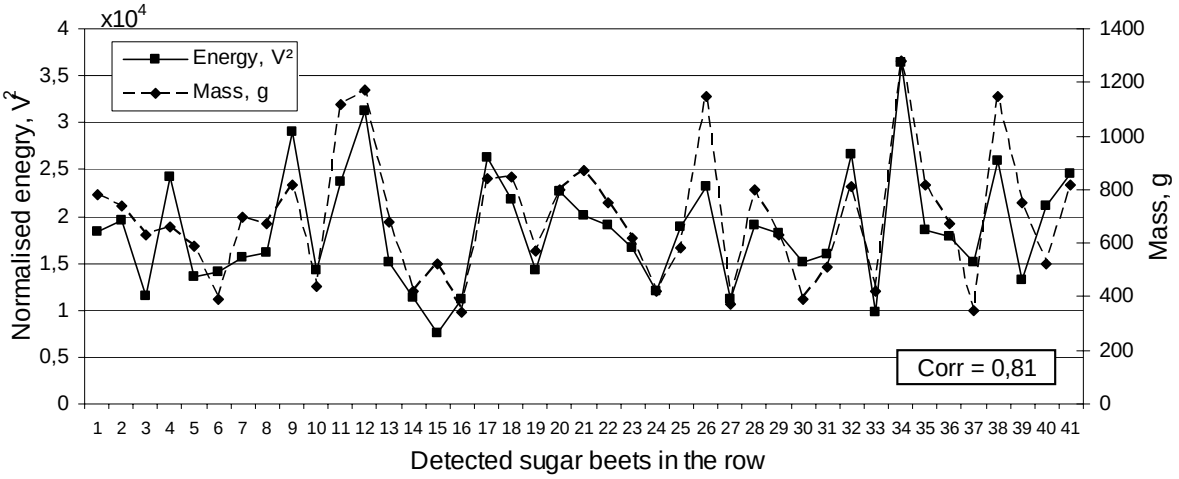

Figure 7.27 Normalised energies backscattered from single sugar beets vs. single sugar beet masses in scenario with soil water content level 1 and regular average single sugar beet mass

In Figure 7.23 a) peaks of 41 from 44 sugar beets have been detected. The correlation of corresponding energies vs. recorded single sugar beet masses was 81%, which is the highest one of all calculated correlations. This result can be explained with convenient test scenario conditions, more of all with the low soil water content.

Table 7.5 Relevant scenario features and data series correlation rates for test in scenario with soil water content level 1 and regular average single sugar beet mass

Number of sugar beet in the row		45
Number of detected sugar beets		41
Soil water content, %vol		22,3 (Level 1)
Average single sugar beet mass, g		678
Average distance between sugar beets, cm		22,5
Average top height, cm		3,4
Average maximum diameter of sugar beets, cm		9,8
Other relevant correlations, %	Mass vs. maximum diameter	71
	Mass vs. top height	61
	Backscattered energy vs. top height	70
	Backscattered energy vs. maximum diameter	50
Correlation mass vs. backscattered energy, %		*81*

In Figure 7.28 the amounts of backscattered energies recorded in the diagram presented in Figure 7.23 b) have been compared to single sugar beet masses. The relevant scenario features and data series correlation rates are presented in Table 7.6. The characteristic of this test was higher average single sugar beet mass and higher soil water content in comparison to the previous experiment. The standard deviation of the water content was 4,2%vol, which is the highest value of all tests. This experiment has been also conducted in October 2006 with grown sugar beets.

In Figure 7.23 b) peaks of 40 of 43 sugar beets have been detected. The correlation of corresponding energies vs. recorded single sugar beet masses was 62%, which is lower than relationships between other morphological features (mass vs. maximum

diameter and mass vs. top height). On the other hand, correlation of 62% is higher than values for other relationships of backscattered energy data. The main reason for lower level of correlation were several peaks (e.g. peak 11, 29 and 30), which were overestimated.

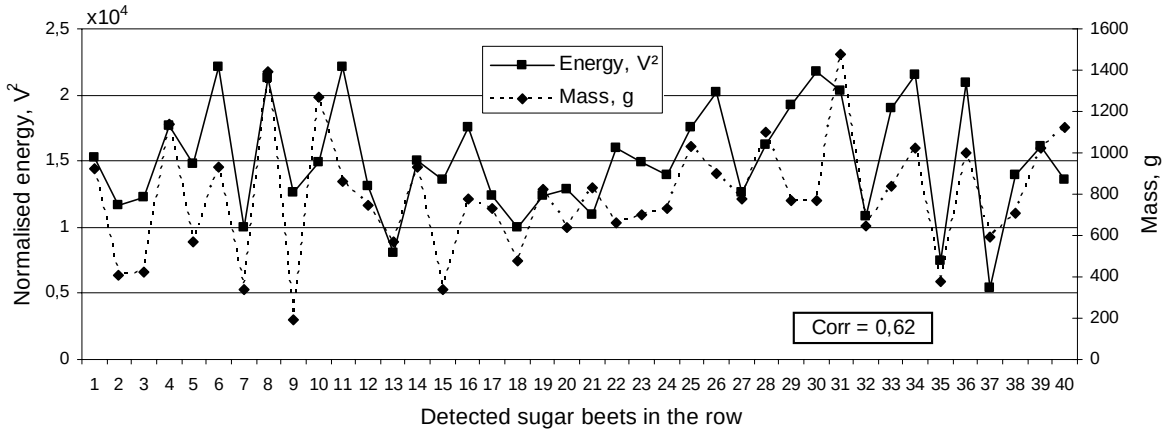

Figure 7.28 Normalised energies backscattered from single sugar beets vs. single sugar beet masses in scenario with soil water content level 2 and regular average single sugar beet mass

Table 7.6 Relevant scenario features and data series correlation rates for test in scenario with soil water content level 2 and regular average single sugar beet mass

Number of sugar beet in the row		43
Number of detected sugar beets		40
Soil water content, %vol		27,3
Average single sugar beet mass, g		795
Average distance between sugar beets, cm		24,1
Average top height, cm		3,1
Average maximum diameter of sugar beets, cm		10,1
Other relevant correlations, %	Mass vs. maximum diameter	83
	Mass vs. top height	78
	Backscattered energy vs. top height	55
	Backscattered energy vs. maximum diameter	56
Correlation mass vs. backscattered energy, %		*62*

Measuring error analysis and its correction

In Figure 7.29 the amounts of backscattered energies recorded in the diagram presented in Figure 7.21 b) have been compared to single sugar beet masses. The relevant scenario features and data series correlation rates are presented in Table 7.7. The characteristic of this test was higher average single sugar beet mass and soil water content in comparison to the previous experiment. The standard deviation of the water content was 3,1%vol. This experiment has been also conducted in October 2006 with grown sugar beets.

In Figure 7.21 b) all 45 peaks of sugar beets have been detected. The correlation of corresponding energies vs. recorded single sugar beet masses was 32%, which is considerably lower than relationships between other morphological features; correlation mass vs. maximum diameter was 85% and mass vs. top height 87%. The correlation of 32% is in the same level with values for other relationships of backscattered energy data.

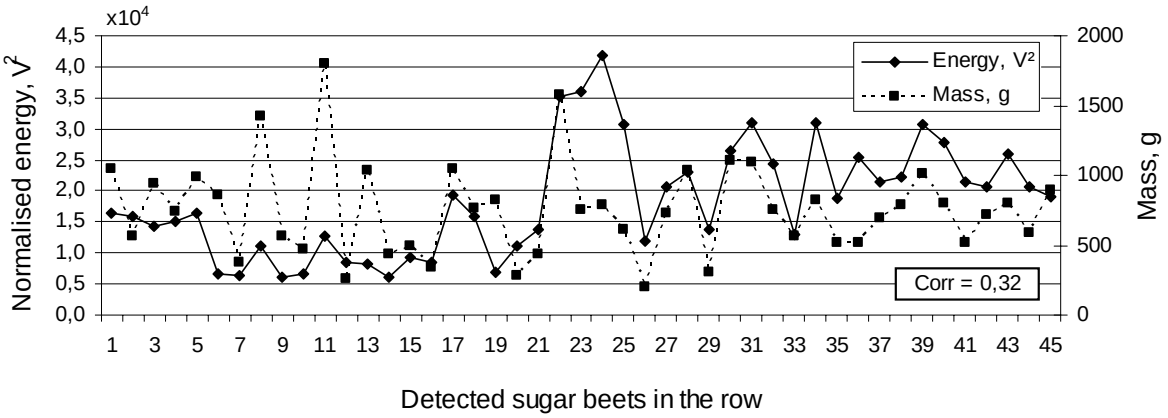

Figure 7.29 Normalised energies backscattered from single sugar beets vs. single sugar beet masses in scenario with soil water level 2 – example of a measuring error

The row section presented in Figure 7.29 showed the worst correlation result of all scanned sections. The next worst calculated correlation coefficient was over 60%, which shows large inconsistency of this data series in comparison to the rest of data. One of the reasons for this might be the automatic data processing procedure

combined with high signal clutter caused by high soil water content. Within this section, the soil water content was the highest of all tests; it averaged 28,1%vol with standard deviation of 3,1%vol. One further reason was not successful separation of single energy amounts, which is especially noticeable for values 8, 11 and 13 (the separated backscattered energy amounts were underestimated) and values 23 and 24 (the separated backscattered energy amounts were overestimated).

Table 7.7 Relevant scenario features and data series correlation rates for test in scenario with soil water content level 2 – example of a measuring error

Number of sugar beet in the row		45
Number of detected sugar beets		45
Soil water content, %vol		28,1
Average single sugar beet mass, g		768
Average distance between sugar beets, cm		22,6
Average top height, cm		3,8
Average maximum diameter of sugar beets, cm		9,9
Other relevant correlations, %	Mass vs. maximum diameter	85
	Mass vs. top height	87
	Backscattered energy vs. top height	44
	Backscattered energy vs. maximum diameter	20
Correlation mass vs. backscattered energy, %		*32*

The lower energy level in the first and the higher energy level in the second half of diagrams in Figure 7.21 and 7.29 show that the antennas were more distant to the row at the beginning of scanning than at the end. This measuring error caused the most significant decrease of the correlation between sugar beet mass and reflected energy. This measuring error originates from the manual steering, i.e. perpendicular adjustment of the antenna set during scanning, see Figure 6.16. According to this observation, values from 23 to 45 have been scaled down; i.e. the values have been multiplied by approximately estimated correctional factor 0,5 and the result is shown in Figure 7.30.

This scaling down of the second half of data fitted two series a lot better and improved the correlation to 54%. Other correlations calculated with the scaled data have been also increased; backscattered energy vs. top height was 53% and backscattered energy vs. maximum diameter was 38%.

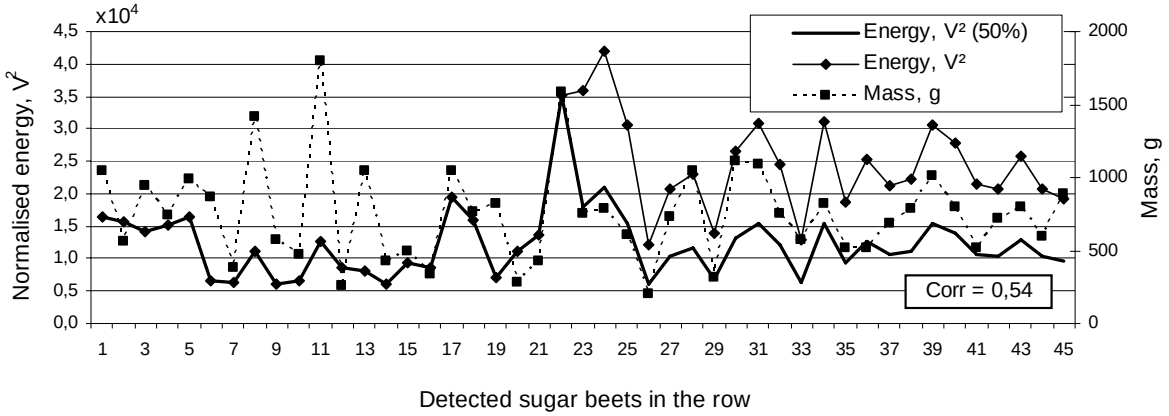

Figure 7.30 Normalised energies backscattered from single sugar beets vs. single sugar beet masses in scenario with soil water level 2 – measuring error correction

Analyses of two different scenarios with thinned rows

The same row analysed in the previous case has been thinned and the distance between sugar beets has been increased. The obtained data are shown in Figure 7.25 b). In Figure 7.31 the amounts of backscattered energies recorded in the diagram from Figure 7.25 b) have been compared to single sugar beet masses. The relevant scenario features and data series correlation rates are presented in Table 7.8.

In Figure 7.25 b) all 15 sugar beet peaks have been detected. The correlation of corresponding energies vs. recorded single sugar beet masses was 83%. Despite the higher soil water content, this result is in the same level with the result presented in Figure 7.27 obtained in more convenient test scenario conditions with the soil water content level 1.

The level of recorded energy amounts is ten times larger than the level of recorded data in the full row, see Figure 7.29. This effect originates from more successful

separation and focusing of the energy amounts within the data processing procedure thanks to the increased distance between scanned objects.

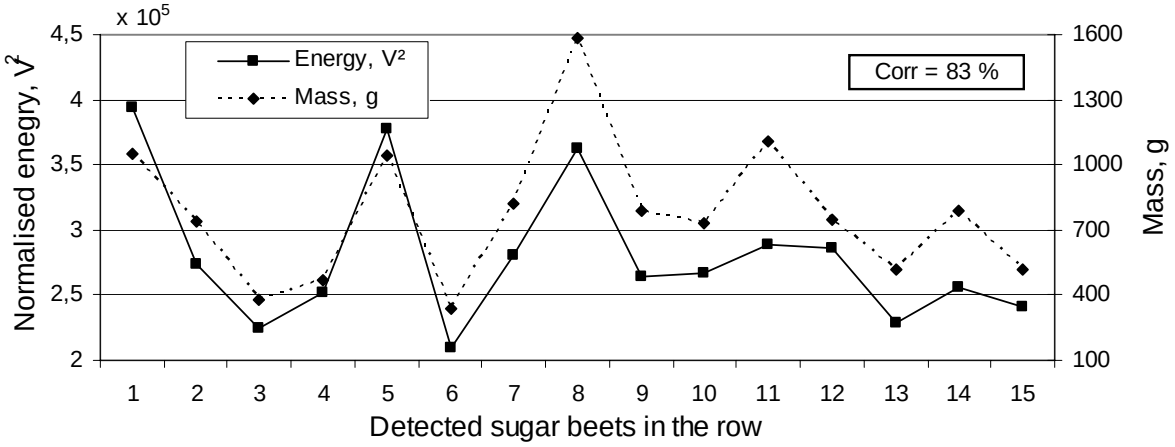

Figure 7.31 Normalised energies backscattered from single sugar beets vs. single sugar beet masses in scenario with thinned sugar beet row and soil water level 2

Table 7.8 Relevant scenario features and data series correlation rates for test in scenario with thinned sugar beet row and soil water level 2

Number of sugar beet in the row		15
Number of detected sugar beets		15
Soil water content, %vol		28,1
Average single sugar beet mass, g		775
Average distance between sugar beets, cm		64,9
Average top height, cm		3,8
Average maximum diameter of sugar beets, cm		10,4
Other relevant correlations, %	Mass vs. maximum diameter	78
	Mass vs. top height	92
	Backscattered energy vs. top height	77
	Backscattered energy vs. maximum diameter	62
Correlation mass vs. backscattered energy, %		*83*

Similar to the previous analysis, the same row analysed in Figure 7.27 has been thinned and the distance between sugar beets has been increased. The obtained

data are shown in Figure 7.25 a). In Figure 7.32 the amounts of backscattered energies recorded in the diagram from Figure 7.25 a) have been compared to single sugar beet masses. The relevant scenario features and data series correlation rates are presented in Table 7.8.

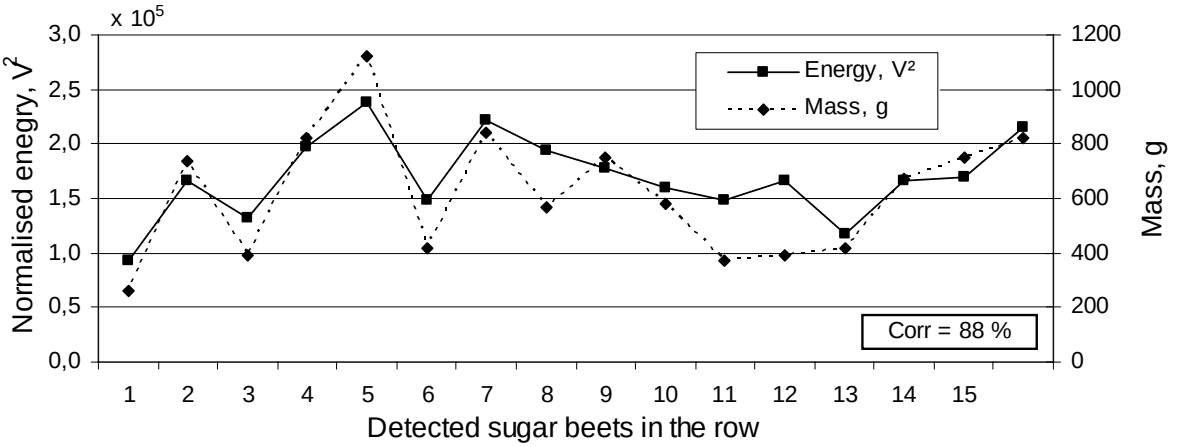

Figure 7.32 Normalised energies backscattered from single sugar beets vs. single sugar beet masses in scenario with thinned sugar beet row and soil water level 1

Table 7.9 Relevant scenario features and data series correlation rates for test in scenario with thinned sugar beet row and soil water level 1

Number of sugar beet in the row		16
Number of detected sugar beets		16
Soil water content, %vol		22,3
Average single sugar beet mass, g		619
Average distance between sugar beets, cm		66,1
Average top height, cm		3,5
Average maximum diameter of sugar beets, cm		9,9
Other relevant correlations, %	Mass vs. maximum diameter	87
	Mass vs. top height	74
	Backscattered energy vs. top height	77
	Backscattered energy vs. maximum diameter	80
Correlation mass vs. backscattered energy, %		*88*

In Figure 7.25 a) all 16 sugar beet peaks have been detected. The correlation of corresponding energies vs. recorded single sugar beet masses was 88%, which represent an increase in comparison to originally obtained correlation for the full row of 81%. The level of recorded energy amounts is in this case also ten times larger than the level of recorded data in the full row, see Figure 7.27.

Similar effect has been noticed for other row sections. The increase of correlation between backscattered energy amounts and single sugar beet masses recorded in thinned row section in comparison to the original full rows was from 8% to 22,5%. The smallest increase of 8% was for the full and thinned row presented in Figure 7.27 and 7.32 respectively. The highest increase of correlation has been recorded for the full row from Figure 7.28; the thinned version of this row section provided correlation of 80%, which represent an increase of 22,5%.

8. Conclusions and prospects

8.1 Hypothesis validation

The hypothesis defined in Chapter 5 have been separately validated:

Hypothesis 1

The measuring system enables the differentiation of sugar beet roots from the soil independent of scenario properties.

Validation

The differentiation of sugar beets from the soil is partially possible, because it is dependent on scenario properties: sugar beet size and soil properties, most of all soil surface roughness.

Hypothesis 2

The measuring system enables identification and counting of

a. sugar beets with foliage
b. sugar beets with leaves brush
c. topped or defoliated sugar beets

in the agricultural soils independent of scenario properties.

Validation

a. The foliage of sugar beets covers the signals of roots, and consequently make the identification of single sugar beet plants impossible.
b. The scanning of sugar beets with both long and short brushes can lead to non focused energy amounts, and therefore it can not be separated to a single point, i.e. single plant, which makes identification of single sugar beets with leaves brush partially possible.
c. The identification and counting of topped or defoliated sugar beets is partially possible, because it is dependent on scenario properties: sugar beet size and soil properties, most of all soil surface roughness.

Hypothesis 3

The measuring system enables root mass determination of

a. sugar beets with foliage
b. sugar beets with leaves brush
c. topped or defoliated sugar beets

in the agricultural soils independent of scenario properties.

Validation

a. The foliage of sugar beets covers the signals of roots, and consequently make the root mass determination of sugar beets impossible.
b. Both long and short brushes lead to additional disturbance and clutter that are masking the reflection signal from the root and therefore make the root mass determination impossible.
c. The root mass determination of topped or defoliated sugar beets is possible up to the certain level of accuracy.

8.2 Conclusions

The system configuration parameters which showed the best results in laboratory conditions during test reference objects were: horn antennas with vertical polarisation (VV) with incident angle $\alpha = 30°$ or $\alpha = 45°$ in combination with angle between antennas $\beta = 0°$ or $\beta = 45°$. The combinations with $\alpha = 45°$ allowed better detectability of targets, and the advantage of antenna combinations with $\beta = 0°$ is smaller cross talk and deeper penetration into soil. In accordance with that, the best results of data acquisition and processing have been achieved with antenna combination $\alpha = 45°$ and $\beta = 0°$.

The laboratory experiments showed that the larger reference test object (aluminium sphere with Ø120 mm) is detectable up to the second level of soil water content of 30 ± 5%vol, and up to the second level of the soil surface roughness determined with the standard deviation of height of the surface profile of 6 mm and maximum diameter of soil parts of 20 mm. The detectability of the smaller reference object (Ø60 mm) was worse, and in this case the influence from the soil surface roughness was

stronger. The small object was detectable up to the same level of soil water content, and up to the soil surface roughness with the standard deviation of height of the surface profile of 3 mm and maximum diameter of soil parts of 5 mm. In comparison to the influences of soil water content level and soil surface roughness level, the influence of soil texture was less significant.

According to the analyses of the ratio of energy amounts, and the ratio of spheres areas and volumes, it can be concluded that the backscattered energy amounts from reference objects depend more on the size of overground surface exposed to radar waves and not on its volume.

The laboratory test with sugar beets showed comparable results in all conditions with worse detectability because of lower dielectric contrast to the surroundings. The differentiation from the surrounding soil of sugar beets with diameter smaller than 60 mm (ca. 100 g) was not unambiguously possible in the tested laboratory conditions. On the other hand, the number of sugar beets of this size is less than 0,5% (determined on a sample of 1770 adult sugar beets) and it represents irrelevant share of the total yield. The unambiguous differentiation of any sugar beet in the scenario with surface roughness level 3 or higher is also impossible.

The parameters chosen during laboratory experiments have been tested in field conditions. The method of visual sugar beet signal positioning confirmed its feasibility for sugar beet detection with the 90% to 96% successfully detected sugar beets in rows with regular distance between the plants. The not detected sugar beets were usually the smallest in the scanned row, but the detecting sensitivity was better than in laboratory conditions, i.e. even the sugar beets with diameter lower than 60 mm have been predominantly successfully detected. All tests of sugar beet position vs. energy peak position showed correlation of about 99%. The real measured positions of sugar beets in a regular row have been successfully detected with an average error from 1,1 cm to 3,6 cm. The detectability of sugar beets in thinned rows was better; in these rows the peaks have been located for every sugar beet with slightly larger average positioning error of 1,8 cm to 4,7 cm. The principle of simple threshold

detection is insufficiently flexible for data obtained in field conditions for both full and thinned row sections.

The results of laboratory experiments conducted with different positions of sugar beets in the row have been confirmed in the field conditions. The reliable localisation of several sugar beets i.e. clutter signals in each scanned row was possible only due to the known sugar beet positions. Although infrequent, the signals which originate from objects in the row other than sugar beets are the permanent possible source of data misinterpretation.

The local conditions during two measuring campaigns in August and October 2006 have been considerably different. The average sugar beet mass in August was 560 g with average diameter of 9,7 cm. The average sugar beet mass in October was more than 30% higher. The soil water content in August was 31%vol in average, and in October between 22,3 and 28,1%vol. Nevertheless, it was not possible to establish a general relationship between local conditions (average sugar beet size and soil water content) and sugar beet detectability. The tests in less favourable conditions in August (smaller average sugar beet mass and higher soil water content) provided similar or in some cases even better results.

The data processing method, on the other hand, delivered several series of reflected energy amounts which poorly correlate with sugar beet mass records. In several cases there were values which strongly deviated from the real mass. One of the reasons for this can be the implemented migration step within processing, which successfully separated single sugar beet signals, but allocated false energy amounts to each detected signal. The second reason can be the local increase of soil water content (standard deviation of soil water content was up to 3,8%vol) or, less probable, the presence of material other than soil or sugar beet. For the rest of the analyzed data series, the correlation between sugar beet mass and reflected energy was above 60% and for the majority over 70%. The best correlation coefficients have been on the level close to 90%. In this case also in was not possible to establish a general relationship between soil water content and average sugar beet size on one side, and correlation coefficients on the other.

Although the laboratory results have shown a strong relationship between height of sugar beet tops and reflected energy, the field tests confirmed the independence of the signal of the used radar system from the influence of top height for sugar beet mass estimation. There are two explanations of this phenomenon. The first is the resemblance of sugar beets within the tested field presumably due to local micro-conditions and similarities within the variety, i.e. good correlation between top height and sugar beet size in the tested cases, which is not a rule. Tests on about 1000 sugar beets from other locations showed correlation from about 30% to 60%. The second difference in comparison to the laboratory experiments was the not disturbed soil structure; the disturbances on positions of different soil structure constantly and unavoidably caused additional reflections in laboratory conditions and provoked worse results.

The tested radar system and the used method of sugar beet yield measuring is not practically usable in this technological stage. The system needs several improvements and further tests in order to confirm its commercial applicability. The main development needs are listed in the following chapter.

8.3 Possible development needs of the tested system

According to the analyses of experimentally acquired results, the following development proposals have been defined:

- Other horn antennas and other antenna types with different propagation behaviour of sounding waves should be tested. Also more appropriate antenna construction for the field conditions is needed.

- Reliable and accurate steering of antennas in field conditions in order to provide the constant distance to the row should be designed. In general, more appropriate antenna carrier construction for the field conditions is needed.

- The signal processing procedure should be improvement in order to provide more accurate separation between-signals and within-signal

- The signal processing procedure has to be automated and tested.

- The development of automated peak detection and positioning is required, since the simple threshold method does not meet established targets.

8.4 Proposals for other possible application of the tested system

The possible utilisation areas in the field of agricultural engineering are connected to the soil properties measurement, e.g. soil texture, soil water content and soil density, or to the procedures associated to the plants species with yielding parts under soil surface, e.g. potato and asparagus.

The soil properties measurements with radar sensing devices have been researched and reported in the last decades and some applications have been described in the chapter State of the art. On the other hand, the detection and/or yield estimation of potatoes, asparagus or similar crops using a radar sensor system have not been researched. Possible applications could be: detecting and positioning of potato nest in order to save energy and increase capacity, and detecting and positioning of adult asparagus in order to simplify and automate harvesting process.

9. References

Allred, B. J., Daniels, J. J., Fausey, N. R., Chen, C., Peters, L. Jr., and Youn, H. 2005. Important Considerations for Locating Buried Agricultural Drainage Pipe Using Ground Penetrating Radar. Applied Engineering in Agriculture, Vol. 21, No. 1, Paper No. 032344, ASAE, St. Joseph, USA. Pg. 71-87 (http://asae.frymulti.com)

Annan, A. P. 2002. GPR - History, Trends, and Future Developments. Subsurface Sensing Technologies and Applications Vol. 3, No. 4, Pg. 253-270

Anonymous 1998. Instruction manual for Laser M5/200. MEL Mikroelektronik GmbH, Eching, Germany (http://www.melsensor.de/info133-153.html).

Anonymous 2001. ASAE Standard: Soil and Water Terminology. S526.2 JAN01, American Society of Agricultural Engineers, St. Joseph, USA (http://asae.frymulti.com)

Anonymous 2004. Test procedures for measuring the quality in sugar beet production - Seed Drillability, Precision Seeders, Harvesters, Cleaner Loaders, 2nd Edition. Ed. Kromer, K.-H. and Bertram, H.-H. Project of the International Institute for Beet Research (IIRB), Agr. Engineering Study Group. Bruxelles, Belgium, 52 pp

Anonymous 2005. Email, phone and personal communication with Dr. S. Pätzold (s.paetzold@uni-bonn.de) from the Institute for Soil Science (Institut für Bodenkunde) in Bonn

Anonymous 2006a. Remote Sensing Tutorial, NASA, USA. Accessed on 13. November, 2006. http://rst.gsfc.nasa.gov/

Anonymous 2006b. Introduction to Soils - A Laboratory Manual Department of Agronomy and Horticulture, New Mexico State University, USA. Accessed on 13. Nov. 2006. http://weather.nmsu.edu/Teaching_Material/soil252/introduction.htm

Anonymous 2006c. Radar Principles by Christian Wolff Accessed on 21. November 2006. http://www.radartutorial.eu/

Anonymous 2006d. Doppler Weather Radar Overview. Accessed on 21. Nov. 2006. http://www.nwas.org/committees/avnwinterwx/doppler_weather_radar_overview.htm/

Anonymous 2006e. Radarsensor Speed Wedge. Accessed on 22. November 2006. http://www.mso-technik.de/sensor/speedwedge.html/

Anonymous 2006f. Driver's Assistant with an Eye for the Essentials. Accessed on 22. November 2006. http://www.daimlerchrysler.com/

Anonymous 2006g. Mobile Geschwindigkeitsmessung. Accessed on 22. November 2006. http://www.robot.de/deutsch/speedophot-ii.php/

Anonymous 2006h. Fundamentals of remote sensing. Accessed on 22. November 2006. http://ccrs.nrcan.gc.ca/resource/tutor/fundam/pdf/fundamentals_e.pdf/

Anonymous 2006i. FGAN-FHR feiert 100 Jahre radar. Accessed on 21. November 2006. http://www.100-jahre-radar.de/

Anonymous 2006j. Ground Penetrating Radar Fundamentals by Jeffrey J. Daniels. Accessed on 21. November 2006. http://www.geology.ohio-state.edu/~jeff/Library/ BASICS.PDF/

Anonymous 2006k. GPR Methodology by Jim Doolittle. Accessed on 24. November 2006. http://soils.usda.gov/survey/geography/maps/GPR/methodology.html#Ground-Penetrating%20Soil%20Suitability%20Maps

Anonymous, 2006l. Ultra Wideband (UWB) Frequently Asked Questions. Accessed on 13. December 2006. http://www.multispectral.com/

Anonymous 2006m. Assessment of Ultra-Wideband (UWB) Technology, Report R-6280, prepared by OSD/DARPA UWB Radar Review Panel (July 1990). Defense Advanced Research Projects Agency, Office of the Secretary of Defense, USA

Anonymous 2006n. ELV Elektronik AG: Temperatur-Feuchte-Messgerät TFM 100. Accessed on 29. January 2006. http://www.elv.de/

Anonymous 2006o. RADAR and SAR Glossary. European space agency. Accessed on 2. February 2006. http://envisat.esa.int/dataproducts/asar/CNTR5-2.htm

Auernhammer, H., Demmel, M., Muhr, T., Rottmeier, J. and Wild, K. 1994. GPS for yield mapping on combines. Computers and Electronics in Agriculture, Vol. 11, No. 1, Pg. 53-68

Barker, P., Fletcher, M. and Bradley, J. 1998. Reflections on the past - Progress in the application of GPR in Archaeology. Proceedings of the Seventh International Conference on GPR. May 27-30, Lawrence, USA

Barrett, T. W. 2000. History of Ultra WideBand (UWB) radar & communications: pioneers and innovators. In: Progress In Electromagnetics Symposium 2000, (PIERS2000), Cambridge, USA

Barrett, T.W. 2001. History of Ultra Wideband (UWB) communications & radar: Part II, UWB radars and sensors. Microwave Journal, Vol.44, No.2, Pg. 22-52

Blackmore, S. 2003. The role of yield maps in Precision Farming. PhD Thesis, National Soil Resources Institute, Cranfield University at Silsoe, England (http://www.cpf.kvl.dk/Papers/), pp. 170

Blume, H.-P., Deller, B., Leschber, R., Paetz, A., Schmidt, S. and Wilke, B. M. 2000. Handbuch der Bodenuntersuchung, Band 6. Beuth Verlag, Wiley-VCH, Berlin, Germany

Blume, H.-P., Felix-Hennigsen, P., Fischer, W. R., Frede, H.-G., Horn, R. and Stahr, H. 1997. Handbuch der Bodenkunde. Ecomed Verlaggesellschaft, Landsbegr/Lech, Germany

Boess, J., Heineke, H.-J. and Kues, J. 2003. Digital soil maps: A requirement for precision agriculture. Book of Joint Conference of ECPA-ECPLF, Berlin. Wageningen Academic Publishers, Nederlands, Pg. 166

Boos, B., Missotten, B., Reybrouck, S. and De Baerdemaker, J. 1998. Mapping and interpretation of sugar beet yield differences. In: Abstracts of the 4th International Conference on Precision Agriculture, July 19-22. St. Paul, USA

Butnor, J. R., Doolittle, J. A., Johnsen, K. H., Samuelson, L., Stokes, T. and Kress, L. 2003. Utility of ground penetrating radar as a root biomass survey tool in forest systems. Soil Science Society of America Journal, Stanford University, USA, Vol. 67, Pg. 1607-1615

Campbell, R. H., Rawlins, S. L., and Han, S. 1994. Monitoring methods for potato yield mapping. ASAE Paper No. 941584, ASAE, St. Joseph, USA (http://asae.frymulti.com)

Chignell, R. J., Dabis, H., Frost, N. and Wilson, S. 2000. The radar requirements for detecting anti-personnel mines. 8th International conference on GPR. Ed. Noon, D. A., Stickley, G F. and Longstaff, D. Proceedings of SPIE, Vol. 4084, Pg. 861-866

Clement, W. P. and Ward, A. L. 2003. Using Ground Penetrating Radar to Measure Soil Moisture Content. ASAE Annual International Meeting, Las Vegas, July 26-30, Paper No. 032275, ASAE, St. Joseph, USA (http://asae.frymulti.com)

Craddock, I. J., McCutcheon, E., Benjamin, R. and Crisp, G.N. 2001. Demonstration of the Detection of Buried Mines with Real-Aperture Radar. Subsurface Sensing Technologies and Applications Vol. 2, No. 3, Pg. 273-283

Da Costa, J. P., Germani, C., Lavialle, O. and Grenier, G.. 2003. Rows detection in high resolution remote sensing images of vine fields. Book of Joint Conference of ECPA-ECPLF, Berlin. Wageningen Academic Publishers, Nederlands, Pg. 182

Damerow, L. 1998. Bodenprofilmessgeräte zur Bewertung der Saatbeetbereitung. 35. Gartenbauwissenschaftliche Tagung, March 4-6, Berlin, Germany

Daniels, D. J. 1998. Ground probing radar techniques for mine detection. Proceedings of the Seventh International Conference on GPR. May 27-30, Lawrence, USA

Daniels, D. J. 2004. Ground-Penetrating Radar, 2nd Edition. Institution of Electrical Engineers, London, United Kingdom

Davidson, M. W. J., Le Toan, Thuy, Mattia, F., Satalino, C., Manninen, T. and Borgeaud, M. 2000. On the characterization of agricultural soil roughness for radarremote sensing studies. Geoscience and Remote Sensing, Vol. 38, No. 2, Part 1, Pg. 630-640

Demmel, M. 1997. Erträge automatisch erfassen. DLZ Agrarmagazin, Special edition 10. BVL Verlaggesellschaft, München, Germany, Pg. 10-12

Demmel, M. and Auernhammer, H. 1998. Lokale Ertragsermittlung bei Kartoffeln und Zuckerrüben. In: Book of Proceedings of the VDI-MEG Conference Agricultural Engineering, Hannover, Germany, Pg. 263-268

Diercks, R. and Heitefuss, R. 1994. Integrierter Landbau. BLV Verlagsgesellschaft, München, Germany

Dittmer, J. 2004. Principles of GPR forensic search. In: Ground-Penetrating Radar, 2nd Edition. Ed. Daniels, D. J. Institution of Electrical Engineers, London, United Kingdom. Pg. 425-429

Doolittle, J. A. and Collins, Mary E. 2004. Suitability of soils for GPR investigations. In: Ground-Penetrating Radar, 2nd Edition. Ed. Daniels, D. J. Institution of Electrical Engineers, London, United Kingdom. Pg. 97-108

Doolittle, J. A., Minzenmayer, F. E., Waltman, S. W. and Benham, E. C. 2002. Ground penetrating radar soil suitability map of the conterminous United States. In: Proceedings of 9th International Conference on Ground Penetrating Radar. Ed. Koppenjan, S. K., and L. Hua. Vol. 4158. 30 April - 2 May. Santa Barbara, USA. Pg. 7-12

Ehlert, D. 1996. Massestrommessung bei Kartoffeln. Landtechnik Vol. 51, No. 1, Pg. 20-21

Ehlert, D. 1998a. Grundlagen zur Ertragskartierung von Kartoffeln. In: Book of Proceedings of the VDI-MEG Conference Agricultural Engineering, Hannover,

Germany, Pg. 269-274

Ehlert, D. 1998b. Grundlagen zur Ertragskartierung von Kartoffeln. Beiträge zur teilflächenspezifischen Bewirtschaftung. Bornimer agrartechnische Berichte, Institut für Agrartechnik, Bornim, Germany, Pg. 59-67

Ehlert, D. 2000. Measuring Mass Flow by Bounce Plate for Yield Mapping of Potatoes. Precision Agriculture, Vol. 2, No. 2. Pg. 119-130

Ehrl, M., Demmel, M., Auernhammer, H., Werner, S., Mauer, W. and Wunderlich, T. 2002. Spatio-Temporal Quality of Precision Farming Applications. ASAE Annual International Meeting/CIGR XV World Congress, Chicago, 28-21 July. Paper No. 023084, ASAE, St. Joseph, USA (http://asae.frymulti.com)

Fisher, S. J., Armstrong, M. J., Jaggard, K. W. and Stafford, J. V. 1997. Precision Farming for Sugar Beet. In: Tagungsband des VDI-MEG Kolloquiums Agraratechnik: Anbau-, Ernte- und Nacherntetechnologie von Zuckerrüben, Vol. 23, 8-10 October, Bonn, Germany. Pg. 164-169

Fontana, R. J. 2000. Recent applications of ultra wideband radar and communications systems EuroEM 2000, Edinburgh, Scotland, In Ultra-Wideband, Short-Pulse Electromagnetics, Kluwer Academic/Plenum Publishers (http://www. multispectral.com/pdf/UWBApplications.pdf)

Fountas, S. 2004. Systems Analysis of Precision Agriculture, PhD Thesis, The Royal Veterinary and Agricultural University, Department of Agricultural Sciences, Section of AgroTechnology, England (http://www.cpf.kvl.dk/Papers/)

Freeland, R. S., Miller, M. L., Yoder, R. E. and Koppenjan, S. K. 2003. Forensic Application of FM-CW and Pulse Radar. Journal of Environmental and Engineering Geophysics, Vol. 8, No. 2, Pg. 97–103

Freeland, R., Yoder, R., and Ammons, J. 1998. Mapping shallow underground features that influence site-specific agricultural production; in Journal Applied Geophysics Vol. 40, Pg. 19-27

Gader, P. D., Keller, J. M. and Nelson, B.N. 2001. Recognition technology for the

detection of buried land mines. IEEE Transactions on Fuzzy Systems, Vol. 9, No. 1 Pg. 31-43

Gogineni, S., Thomasson, J. A., Wooten, J. R., White, J. G., Thompson, P. G. and Shankle, M. 2002. Image-Based Sweetpotato Yield and Grade Monitor. ASAE Annual International Meeting/CIGR XVth World Congress, Chicago, Illinois, July 28-31, Paper No. 021169, ASAE, St. Joseph, USA (http://asae.frymulti.com)

Groenenboom, J. and Yarovoy, A. 2002. Data Processing and Imaging in GPR System Dedicated for Landmine Detection. Subsurface Sensing Technologies and Applications. Vol. 3, No. 4, Pg. 387-402

Harmsen, P. E., Persiani, H. and Torres, Martitza. 2003. Evaluation of Several Dielectric Mixing Models for Estimating Soil Moisture Content in Sand, Loam and Clay Soils. ASAE Annual International Meeting, Las Vegas, July 26-30, Paper No. 032278, ASAE, St. Joseph, USA (http://asae.frymulti.com)

Hien, P. 1994. Konstruktion eines Systems zur Messung des Erdanteils von Zuckerrüben – Haufwerken. Doctoral Dissertation. University of Bonn, Bonn, Germany. Pp. 225

Hoffmann, G. 1991. Methodenbuch, Band 1, Die Untersuchung von Böden, 4th Edition. VDLUFA-Verlag, Darmstadt, Germany

Hofstee, J. W. and Molema, G. J. 2002. Volume Estimation of Potatoes Partly Covered with Dirt Tare. ASAE Annual International Meeting/CIGR XVth World Congress, Chicago, Illinois, July 28-31, Paper No. 021200, ASAE, St. Joseph, USA (http://asae.frymulti.com)

Hofstee, J. W. and Molema, G. J. 2003. Machine Vision Based Yield Mapping of Potatoes. ASAE Annual International Meeting, Las Vegas, July 26-30, Paper No. 031001, ASAE, St. Joseph, USA (http://asae.frymulti.com)

Hook, W. R., Ferré, T. P. A. and Livingston, N. J. 2004. The Effects of Salinity on the Accuracy and Uncertainty of Water Content Measurement, Science Society of America Journal, Stanford University, USA, Vol. 68, Pg. 47-56

Immoreev, I. J. 2002. Main capabilities and features of ultra wideband (UWB) radars. Radio Physics and Radio Astronomy, Vol. 7, No. 4, Pg. 339-344

Immoreev, I. J. 2000. Main features of Ultra-Wideband (UWB) radars and differences from common narrowband radars. In: Ultra-wideband radar technology, Ed. Taylor, J. D. CRC Press. Pg. 1-19.

Isensee, E. and Lieder, W. 2001. Ertragsmessung in der Rübenernte. Landtechnik Vol. 56, No. 4. Pg. 272-273

Konstantinović, M., Woeckel, S., Schulze Lammers P. and Sachs, J. 2005. Yield mapping of sugar beet using ultra wideband radar – Methodology and first research results. In Book of Procedings of the VDI-MEG Conference Agricultural Engineering, Hannover, Germany, Pg. 497-502

Konstantinović, M., Wöckel, S., Schulze Lammers P. and Sachs, J. 2006. Detektionsprinzip von Biomasse mittels UWB Radar am Beispiel von Zuckerrüben. Agrartechnische Forschung (Agricultural Engineering Research), No 12, Pg. 92-100

Kromer, K.-H. 1999. Bestimmung des Erdanteils in Förderströmen landwirtschaftlicher Güter. Patent No. DE 0 938 837 A1

Kromer, K.-H. and Degen, P. 1998. Ertrags- und Durchsatzmessung bei Zuckerrüben. Zuckerrübe Vol. 47, No. 2, Pg. 92-95

Kromer, K.-H., Degen, P., Häfner, M. und Schmittmann, O. 2001. Teilflächenspezifische Ertragsmessung bei Zuckerrüben. Landtechnik, Vol. 56, No. 1, Pg. 26-27

Kühbauch, W. 2002. Fernerkundung – eine Zukunftstechnologie im Präzisionspflanzenbau. In: Proceedings of the Conference: Precision Agriculture – Herausforderung an integrative Forschung, Entwicklung and Anwendung in der Praxis, March 13-15, Bonn. KTBL, Darmstadt, Germany. Pg. 79-84

Leppelmann, S., Cruse., C., Bode, M., Burwick, A. and Heineberg, K. 1998. Einsatz neuronaler Netzwerke zur Bestimmung der äußeren Qualität von Zuckerüben. In:

Tagungsband des VDI-MEG Kolloquiums Agraratechnik: Anbau-, Ernte- und Nacherntetechnologie von Zuckerrüben, Vol. 23, 8-10 October, Bonn, Germany. Pg. 28-41

Ludowicy, C., Schwaiberger, R. and Leithold, P. 2002. Precision Farming – Handbuch für die Praxis. DLG-Verlag, Frankfurt, Germany

Maierhofer, C., Leipold, S. and Woestmann, J. 1999. Strukturuntersuchungen in Beton mit dem Impulsradar, Fachtagung Bauwerksdiagnose - Praktische Anwendun-gen Zerstörungsfreier Prüfungen, Lecture 5, January 21-22, München, Germany (http://www.dgzfp.de/pages/tagungen/berichtsbaende/bb_66-CD/bb66_v05.pdf)

Manacorda, G., Miniati, M., Sarri, A., Consani, M., Penzo, A. 2004. Designing a GPR system for the snow-thickness measurement on mounts everest and karakoram 2. In: Proceedings of the 10th International Conference on Ground Penetrating Radar, GPR 2004. Pg. 167-170

Meier, E., Staubli, P., Müller, B. U., Stünzi, J., Schubert, E., and Dubois, D. 2002. Georadar – der zerstörungsfreie Blick in den Untergrund: Beispiele aus dem Natur-schutzgebiet Zigermoos, Unterägeri/ZG und der Deponie Riet, Winterthur/ZH. Bulletin für angewandte Geologie, VSP/ASP, Zürich, Switzerland Vol. 7, No. 1, Pg. 31-44 (http://www.angewandte-geologie.ch/Dokumente/Archiv/Vol71/7_1Meier-Geo radar.pdf)

National Research Council, Board on Agriculture. 1997. Precision agriculture in 21st century: geospatial and information technologies in crop management. National Academy Press, Washington D.C., USA, pp. 149. (http://www.nap.edu/books/0309058937/html)

National Research Council, Board on Earth Sciences and Resources. 2000. Seeing into the earth/Noninvasive characterization of the shallow subsurface for environmental and engineering applications. National Academy Press, Washington D.C., USA, pp. 129 (http://www.nap.edu/books/0309063590/html/R1.html)

Odhiambo, L. O., Freeland, R. S. and Yoder, R. E. 2004b. Soil Characterization Using Textural Features Extracted from GPR Data. Paper No: 042108, ASAE/CSAE Annual International Meeting, August 1-4, Ottawa, Ontario, Canada (http://asae. frymulti.com)

Odhiambo, L. O., Freeland, R. S., Yoder, R. E. and Hines, J. W. 2004a. Investigation of a Fuzzy-Neural Network Application in Classification of Soils Using Ground-Penetrating Radar Imagery. Applied Engineering in Agriculture, Vol. 20, No. 1, Paper No. 023097, ASAE, St. Joseph, USA. Pg. 109-117 (http://asae.frymulti.com)

Okamura, S. 1999. Microwave Technology for Moisture Measurement. Subsurface Sensing Technologies and Applications Vol. 1, No. 2, Pg. 205-227

Paul, W. and Speckmann, H. 2002. Measuring Crop Density and Soil Humidity by Pulsed Radar. International Conference on Agricultural Engineering, AgEng2002, June 30 – July 4, Budapest, Hungary, Pg. 14-16

Paul, W. and Speckmann, H. 2004a. Radar Sensors - new technologies for precise crop management. CIGR International Conference, October 11- 14 Beijing, China

Paul, W. and Speckmann, H. 2004b. Radarsensoren: neue Technologien zur präzisen Bestandsführung, Teil 1: Grundlagen und Messung der Bodenfeuchte. Landbauforsch Völkenrode, Bundesforschungsanstalt für Landwirtschaft (FAL), Braunschweig, Germany, Vol. 54, No. 2, Pg. 73-86

Paul, W. and Speckmann, H. 2004c. Radarsensoren: neue Technologien zur präzisen Bestandsführung, T. 2, Messung der Bestandsdichte und Ausblick. Landbauforschung Völkenrode, Bundesforschungsanstalt für Landwirtschaft (FAL), Braunschweig, Germany, Vol. 54, No. 2, Pg. 87-102

Persson, D.A., Eklundh, L. and Algerbo, P.−A. 2004. Evaluation of an Optical Sensor for Tuber Yield Monitoring. Transactions of the ASAE, ASAE, St. Joseph, USA, Pg. 1851-1856 (http://asae.frymulti.com)

Petersen, H., Fleige, H., Rabbel, W. and Horn, R. 2005. Anwendbarkeit geo-

physikalischer Prospektionsmethoden zur Bestimmung von Bodenverdichtungen und Supstratheterogenitäten landwirtschaftlich genutzter Flächen. Journal of Plant Nutrition and Soil Science, Wiley-VCH Verlag, Germany, Vol. 168, Pg. 68-79

Raper, R. L., Asmussen, L. E. and Powell, J. B. 1990. Sensing Hard Pan Depth with Ground-Penetrating Radar. Transaction in Agriculture, Vol. 33(1), January-February, Paper No. 881627, ASAE, St. Joseph, USA. Pg. 41-46 (http://asae.frymulti.com)

Rappaport, C. M., Silevitch, M. B., McKnight, S. W., DiMarzio, C. A., Miller, E. L. and Raemer, H. 2001. Multi-Mode Subsurface Sensing and Imaging for Land Mine Detection. Subsurface Sensing Technologies and Applications. Vol. 2, No. 3, Pg. 215-230

Redman, D., Galagedara, L. and Parkin, G. 2003. Measuring Soil Water Content with the Ground Penetrating Radar Surface Reflectivity Method: Effects of Spatial Variability. ASAE Annual International Meeting, Las Vegas, July 26-30, Paper No. 032276, ASAE, St. Joseph, USA (http://asae.frymulti.com)

Rial, W. S. and Han, Y. J. 2000. Assessing Soilwater Content Using Complex Permittivity. Transactions of the ASAE, Paper No. 993114, ASAE, St. Joseph, USA, Pg. 1979-1985 (http://asae.frymulti.com)

Saarenketo, T. 1998. Electrical properties of water in clay and silty soils. Journal of Applied Geophysics, Vol. 40, Pg. 73-88

Sachs, J and Peyersl, P. 2003. Ultra Breitband – Sensoren: Anwendung und Prinzipien. 48. Internationales Wissenschaftliches Kolloquium, Technische Universität Ilmenau, September 22.-25

Sachs, J, Kmec, M., Wöckel, S., Peyerl, P. and Zetik, R. 2005b. Combined Frequency and Time Domain Moisture Sensing by an Ultra Wideband IQ-M-Sequence Approach, 6th International Conference on Electromagnetic Wave Interaction with Water and Moist Substances, May 29 – June 1, Weimar, Germany, Pg. 214-221

Sachs, J. 2004. M-Sequence radar. In: Ground-Penetrating Radar, 2nd Edition. Ed. Daniels, D. J. Institution of Electrical Engineers, London, United Kingdom. Pg. 225-237

Sachs, J., Dvoracek, J., Schneider, A., Friedrich, J. and Zetik, R. 2001. Ultra-Wideband Methods applied for Moisture and Liquid Sensing, Fourth International Conference on Electromagnetic Wave Interaction with Water and Moist Substances, May 13-16, Weimar, Germany

Sachs, J., Kmec, M., Zetik, R., Peyerl, P. and Rauschenbach, P. 2005a. Ultra wideband radar assembly kit. In: Proceedings of Geoscience and Remote Sensing Symposium, IGARSS '05. Seoul, Korea

Sachs, J., Peyerl, P., Rauschenbach, P., Tkac, F, Kmec, M. and Crabbe, S. 2002. Integrated digital UWB-radar. In: Proceedings of AMEREM 2002, June 2-7, Annapolis, USA

Sachs, J., Peyerl, P., Rossberg, M., Rauschenbach, P. and Friedrich, J. 2000. Ultra-Wideband Principles for Surface Penetrating Radar, EUROEM 2000 Conference, UK, May 31- June 2, Edinburgh, Scotland

Sachs, J., Peyerl, P., Zetik, R., and Crabe, S. 2003. M-Sequence Ultra-Wideband-Radar: State of Development and Applications. In: Proceedings of Radar 2003, September 3-5 2003, Adelaide, Australia

Scheers, B. 2000. Laboratory UWB GPR System for Landmine Detection, Eight International Conference on Ground Penetrating Radar, May 23-26, Gold Coast, Australia, Pg. 747-752

Scheffer, F. and Schachtschabel P.. 2002. Lehrbuch der Bodenkunde, 15th Edition. Spektrum Akademischer Verlag, Heidelberg, Berlin, Germany

Schmitt, H. 1986. Einsatz von Radarmessgeräten in der Landwirtschaft. Landtechnik Vol. 41, No. 10. Pg. 434-435

Schmittmann, O. 2002. Teilflächespezifische Ertragmessung von Zuckerrüben in Echtzeit unter besonderer Berücksichtigung der Einzelrübenmasse. Doctoral

Dissertation. University of Bonn, Bonn, Germany. pp. 250

Schmittmann, O. and Hien, P. 2001. Einzelrübenbezogene Ertragsmessung von Zuckerrüben, Landtechnik 56 H1, Pg. 195-197

Schmittmann, O. and Schulze Lammers, P. 2003. Systeme zur Ertragsbestimmung bei Zuckerrüben. Landtechnik 58, H3, Pg. 150 and 195

Schmittmann,O., Schmitz, S. and Kromer, K.-H. 2001. Heterogenity and Site-Specific Yield-Monitoring of Sugar Beets. I.I.R.B.-Meeting 'Plant and Soil & Agricultural' 30. Juni 2001, Lüttewitz, Germany

Schön, H. 1993. Elektronik und Computer in der Landwirtschaft. Eugen Ulmer GmbH, Stuttgart, Germany

Searcy, S. W., Schueller, J. K., Bae, Y. H., Borgelt, S. C., and Stout, B. A. 1989. Mapping of spatially variable yield during grain combining. Transactions of the ASAE, Vol. 32., Paper No. 871533, ASAE, St. Joseph, USA Pg 826-829

Seidl, M. S., Batchelor, W. D. and Paz, J. O. 2004. Integrating Remotely Sensed Images With a Soybean Model to Improve Spatial Yield Simulation. Transactions of the ASAE, Paper No. 003039, ASAE, St. Joseph, USA, Pg. 2081-2090 (http://asae.frymulti.com)

Smith, D. G. and H. M. Jol. 1995. Ground-penetrating radar: antenna frequencies and maximum probable depths of penetration in Quaternary sediments. Journal of Applied Geophysics, Vol. 33, No. 1. Pg. 93-100

Thomas, D. L., Perry, C. D., Vellidis, G., Durrence, J. S., Kutz, L. J., Kvien, C. K., Boydell, B. and Hamrita, T. K. 1997. Development of a load cell yield monitor for peanut. Paper No. 971059, ASAE, St. Joseph, USA

Topp, G. C., Davis, J. L. and Annan, A. P. 1980. Electromagnetic determination of soil water content: measurements in coaxial transmission lines. Water Resources Research, Vol. 16, No. 3, Pg. 574-582

Ulaby, F. T., R.K. Moore, R. K. and Fung, A. K. 1981. Microwave Remote Sensing:

Active and Passive, Vol. 1. Artech House, Norwood

van Deen, J. K. 2004. Soil contamination. In: In: Ground-Penetrating Radar, 2nd Edition. Ed. Daniels, D. J. Institution of Electrical Engineers, London, United Kingdom. Pg. 465-466

Vellidis, G., Perry, C. D., Durrence, J. S., Thomas, D. L., Hill, R. W., Kvien, C. K., Hamrita, T. K. and Rains, G. 2001. The Peanut Yield Monitoring System. Transactions of the ASAE, Paper No. 001128, ASAE, St. Joseph, USA, Pg. 775-785 (http://asae.frymulti.com)

Vrindts, E., Reyniers, M., Darius, P., Frankinet, M., Hanquet, B., Destain, Marie-France and De Baerdemaeker, J. 2003. Analysis of Spatial Soil, Crop and Yield Data in a Winter Wheat Field. ASAE Annual International Meeting, Las Vegas, July 26-30, Paper No. 031080, ASAE, St. Joseph, USA (http://asae.frymulti.com)

Walter, J. D. and Backer, L. F. 2003. Sugarbeet Yield Monitoring for Site-Specific Farming Part I – Laboratory Tests and Preliminary Field Tests. Precision Agriculture, Vol. 4, No. 4, Pg. 421-431

Weiler, K. W., Steenhuis, T. S., Boll, J., and Kung, K.-J. S. 1998. Comparison of ground penetrating radar and time-domain reflectometry as soil water sensors, Science Society of America Journal, Stanford University, USA, Vol. 62, Pg. 1240-1246

Werner, A., Kettner, E., Pauly, J., Reining, E., Roth, R., Kühn, G. J., Selige, T., Bobert, J., Schmidhalter, U. and Hufhnagel, J. 2002. Ertragspotentiale von Teilflächen innerhalb von Ackerschläen als Schlüsselgröße für die Bestandführung von Precision Agriculture. In: Proceedings of the Conference: Precision Agriculture – Herausforderung an integrative Forschung, Entwicklung and Anwendung in der Praxis, March 13-15, Bonn. KTBL, Darmstadt, Germany. Pg. 197-200

Wild, K., Ruhland, S. and Haedicke, S. 2003. Performance of Pulse Radar Systems for Crop Yield Monitoring. ASAE Annual International Meeting, Las Vegas, July 26-30, Paper No. 031038, ASAE, St. Joseph, USA (http://asae.frymulti.com)

Winner, C. 1981. Zuckerrübenbau. DLG-Verlag, München. Pp. 308

Woeckel, S., Konstantinović, M., Sachs, J., and Schulze Lammers, P. 2005. High resolution ultra wideband radar- Principle and technique, Poster at the Agritechnika exibition 2005 in Hannover, Germany

Woeckel, S., Konstantinović, M., Sachs, J., Schulze Lammers, P. and Kmec, M. 2006. Application of ultra-wideband M-Sequence-Radar to detect sugar beets in agricultural soils, 11th International Conference on Ground Penetrating Radar, June 19-22, Columbus Ohio, USA

Yarovoy, A.G., van Genderen, P. and Ligthart, L.P. 2000. Ground penetrating impulse radar for landmine detection. 8th International conference on GPR. Ed. Noon, D. A., Stickley, G F. and Longstaff, D. Proceedings of SPIE, Vol. 4084, Pg. 856-860

Youn, H., Chen, C. and Peter, L. Jr. 2003. Automatic Pipe Detection Using Fully Polarimetric GPR. ASAE Annual International Meeting, Las Vegas, July 27-30, Paper No. 032343, ASAE, St. Joseph, USA (http://asae.frymulti.com)

Zegelin, S. J., White, I., and Russell, G. F. 1992. A Critique of the Time Domain Reflectometry Technique for Determining Field Soil-Water Content. Proceedings of the Symposium: Advances in Measurement of Soil Physical Properties: Bringing Theory into Practice. Ed. G. C. Topp. Soil Society of America, Madison, USA. Pg. 187-208

Ziekur, Regine, and Schuricht, R. 2002. Georadar und sein Beitrag zur teilflächenspezifischen Landwirtschaft. Zeitschrift Angewandte Geologie, No. 3. E. Schweizerbart'sche Verlagsbuchhandlung, Stuttgart, Germany, Pg. 12-15

Appendixes

A. List of abbreviations and symbols

Abbreviations and symbols	*Unit*	*Denotation*
Θ	°	beam width
α	°	incident angle of wave propagation in relation to a target
a	–	empirically determined coefficient
$a(f)$	–	column vector of the received normalised guided waves
A_b	%	absorptance
ADC	–	analog-digital converter
AGC	–	automatic gain control
A_{Sphere}	m^2	area of sphere
a_T	–	transmitted wideband signal
b	–	empirically determined coefficient
B	Hz	bandwidth of the sounding wave
β	°	angle between antennas
β_P	°	angle between parallel antennas
B_u	Hz	usable bandwidth
$b(f)$	–	column vector of the sent normalised guided waves
BEIS	–	Bonner Erdanteil-Informationsystem (Bonn soil tare information system)
b_f	–	*fractional bandwidth*
b_{nt}	–	scattering from unwanted objects
BS	–	background subtraction
b_{sf}	–	surface reflection

b_{target}	–	scattering signal of the target
b_{tot}	–	measured signal
b_{XT}	–	antenna cross talk
c	ms^{-1}	propagation velocity of the wave (in general light velocity)
CCD	–	charge coupled device
CW	–	continuous wave
σ_{sp}	mm	standard deviation of height of the soil profile
d_{DD}	mm	diameter of the single sugar beet in the driving direction
dGPS	–	differential global positioning system
DLO	–	digital local oscillator
d_{max}	mm	maximum diameter of the single sugar beet
DNAPL	–	dense non-aqueous phase liquid
d_{sp}	mm	maximum diameter of soil bumps
DT	–	detection threshold
E	–	electric field
E_{HT}	–	Hilbert-transformed backscattered energy
E_i	–	sounding electromagnetic waves
E_r	–	reflected and measured electromagnetic waves
f_c	Hz	RF-clock
f_l	Hz	lower bound of the occupied spectrum
FMCW	–	frequency modulated continuous wave
FRF	–	frequency response function
f_s	Hz	sampling rate
f_u	Hz	upper bound of the occupied spectrum
g(t)	–	sounding electromagnetic waves
GIS	–	geographic information system

GPR	–	ground penetrating radar
GPS	–	global positioning system
h	m	antenna elevation from the soil surface - starting point of wave propagation
H	–	magnetic field
HF-chip	–	high frequency-chip
HH	–	horizontal-horizontal polarisation
h(t)	–	impulse response function
IRF_R *or* IRF_T	–	impulse response function (of receiver *or* transmitter)
LAN	–	local area network
LNA	–	low noise amplifier
l_{DD}	m	measured length in the driving direction
LED	–	light emitting diode
LNAPL	–	light non-aqueous phase liquid
LTI	–	linear time-invariant
m'	tha^{-1}	yield mass
m_{single}'	kg	empirical mean mass of a single sugar beet for a field
MBC-Radar	–	maximum length binary sequence correlation radar
MLBS	–	maximum length binary sequence
n	–	number of sugar beets
n_{ext}	–	noise, external disturbance in received signal
NIR	–	near infrared
PA	–	precision agriculture
PF	–	precision farming
PRBS	–	pseudo-random binary sequence
PSD	–	position sensing device

R	m	unambiguity range
r_1 *and* r_2	m	distances between antennas and object
R^2	–	square value of the correlation coefficient
RADAR	–	radio detection and ranging
RASOR	–	real aperture synthetically organized radar
R_e	%	reflectance
RF	–	radio frequency
RFID	–	radio frequency identification
r_m	ns^{-1}	measurement rate
r_{mult}	–	multiple reflections in received signal
Rx	–	receiving antenna
S	–	scattering matrix
SNR	–	signal to noise ratio
S_{sc}	–	scattering IRF
s_d	m	distance between sugar beet rows
SiGe	–	silicon germanide alloy (commonly silicon-germanium)
s(t)	–	reflected and measured electromagnetic waves
t	s	time
T	ns	MLBS period
t_c	ns	period of the system clock
T&H-circuit	–	track and hold circuit
TDMA	–	time division multiple access
TDR	–	time domain reflectometry
T_{obs}	s	observation time
T_r	%	transmittance
T_w	s	length of the time window

Tx	–	transmitting antenna
UWB	–	ultra wideband
v_1 *and* v_1	ms^{-1}	incident and refracted wave velocity
v_{max}	ms^{-1}	the maximum displacement speed of the antennas
VH	–	vertical-horizontal polarisation
V_{Sphere}	m^3	volume of sphere
VV	–	vertical-vertical polarisation
WAN	–	wide area network
δ_{cr}	m	cross range
δ_r	m	spatial resolution in range
ε	Fm^{-1}	absolute electrical permittivity of medium
ε	–	real part of complex permittivity
ε_1 *and* ε_2	–	permittivity of host media and encountered object
ε_r	–	relative permittivity of medium
ε_0	Fm^{-1}	absolute electrical permittivity of free space
ε''	–	imaginary part of complex permittivity
ε'_e	–	real part effective permittivity
ε''_e	–	imaginary part of effective permittivity
ϕ_1 *and* ϕ_2	°	incident and refracted wave angle
μ	Hm^{-1}	absolute magnetic susceptibility of medium
μ_r	–	relative magnetic susceptibility
μ_0	Hm^{-1}	absolute magnetic susceptibility of free space
τ	m	half-value width of the pulse envelope
φ and ϑ	–	propagation directions
$*$	–	symbol which represents operation of convolution

B. List of figures

C. List of tables

D. Analysis of soil properties in laboratory conditions

For the planned experiments it was necessary to cover typical soil types. Three boundary soil types were chosen from unlimited palette of different soil types – sand, silt and clay soil from agricultural locations. The choice was made according to similar experimental environments (Harmsen et al. 2003, Daniels 2004). The location of the sand soil was a field north from Cologne (Köln-Worringen) on the bank of the river Rhine, silt soil location was the experimental field Endenich of the Institute for Agricultural Engineering in Bonn and the clay soil location was research station Frankenforst of the Agricultural Faculty in Bonn, near Königswinter.

The accurate data about soil properties were needed in order to replicate it in the laboratory conditions. For this purpose soil probes were taken with the horizontal soil sample cylinder – "Stechtzylinder" of 100 mm^3 volume according to DIN 19671 (Blume et al. 1997*)*. Method number 4 within the Standard: undisturbed sampling the centre of horizon using horizontal soil sampling cylinder (layer thickness <20 cm) was applied and presented in Figure 10.1. Mix-probes for particle size distribution analysis were not taken from the probing location, but later from the test facility, so called sand box.

The cross-section was divided into 6 layers, each 10 cm thick. The depth of the analysed cross-section was determined according to the depth of the soil layer which is influenced by agricultural processes, and is certainly less than 60 cm deep. This depth was also planned to be the minimal depth of the soil layer in the soil box. From every layer 5 soil probes were taken using a horizontal soil sample cylinder. The probes were used to determine two soil properties in the field: dry bulk density according to ISO 11272 (Soil quality; Determination of dry bulk density; 1992.) and soil water content as a volume fraction, according to ISO 11461 (Soil quality; Determination of soil water content as a volume fraction; 2001.) (Blume et al. 2000, Hoffmann 1991, Anonymous 2001). These two soil properties were intended to be repeated in the laboratory conditions.

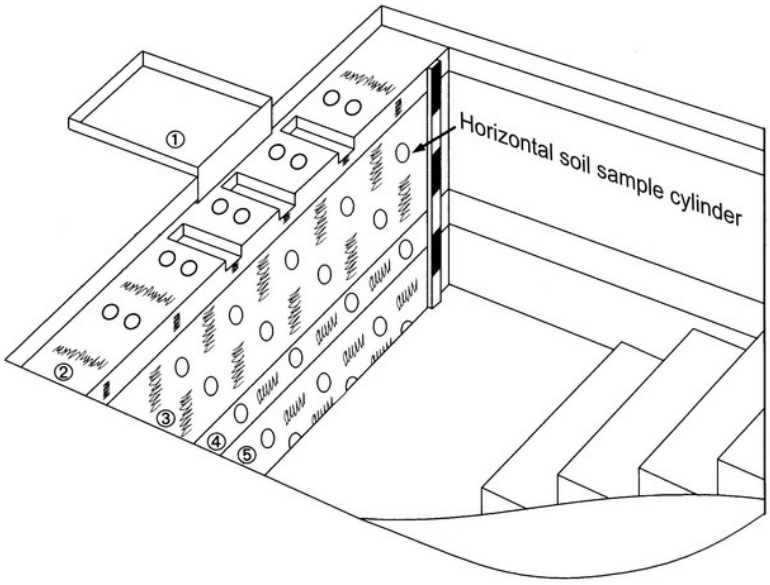

Figure 10.1 Different disturbed and undisturbed soil sampling methods (Blume et al. 1997); 1. surface layer sampling with frame, 2. whole horizon sampling using mix-probes (scraped from the surface) and vertical soil sample cylinder (layer thickness <20 cm), 3. whole horizon sampling using vertical mix-probes (scraped from the surface) and horizontal soil sampling cylinder (layer thickness >20 cm), 4. sampling the centre of horizon using horizontal mix-probes (scraped from the surface) and horizontal soil sampling cylinder (layer thickness <20 cm), 5. sampling the centre of horizon using horizontal mix-probes (scraped from the surface) and horizontal soil sampling cylinder (layer thickness >20 cm)

These two significant physical soil properties, probed on the day of excavating and loading have been measured, statistically processed and presented in Table 10.1. Soil dry bulk density is an expression of the mass to volume relationship for a given material. Soil bulk density measures total soil volume. Thus, bulk density takes into account solid space as well as pore space. Soils that are loose, porous, or well-aggregated will have lower bulk densities than soils that are compacted or nonaggregated. Sandy soils have less total pore than clayey soils, so generally they have higher bulk densities. Bulk densities of sandy soils vary between 1,2 to 1,8 gcm^{-3}. Fine-textured soil, such as clays, silty clays, or clay loams, have bulk densities between 1,0 and 1,6 gcm^{-3} (Anonymous 2006b).

Table 10.1 Soil properties in field conditions on the day of excavating and loading

Soil type	*Depth, cm*	*Water content, %vol*		*Dry bulk density, gcm^{-3}*		*Mean values*		
		Mean value	Standard deviation	Mean value	Standard deviation	Layer, depth	Water content, %vol	Dry bulk density, gcm^{-3}
Sand soil	10	30,8	2,28	1,56	0,04	Upper, 10-30 cm	31,3	1,6
	20	33,4	1,36	1,62	0,04			
	30	29,8	1,99	1,68	0,03			
	40	23,5	1,87	1,58	0,05	Lower, 40-60 cm	24,9	1,5
	50	24,3	1,20	1,53	0,05			
	60	26,9	2,03	1,53	0,02			
Silt soil	10	30,3	1,46	1,40	0,02	Upper, 10-30 cm	28,7	1,5
	20	30,6	1,44	1,51	0,02			
	30	25,3	2,01	1,62	0,03			
	40	20,5	1,08	1,50	0,03	Lower, 40-60 cm	22,0	1,5
	50	21,3	1,01	1,48	0,06			
	60	24,1	0,92	1,48	0,05			
Clay soil	10	40,4	1,96	1,43	0,01	Upper, 10-30 cm	40,1	1,5
	20	40,8	1,72	1,47	0,04			
	30	39,2	3,54	1,50	0,01			
	40	51,9	0,29	1,25	0,06	Lower, 40-60 cm	51,0	1,3
	50	49,3	1,42	1,24	0,05			
	60	51,7	1,66	1,29	0,02			

Farmers often speak of “heavy” and “light” soils in relation to the ease of tillage. “Heavy” soils are clayey and difficult to till, while “light” soils are sandy and easy to till. These terms are misnomers, because “heavy” and “light” actually refer to other physical properties of the soil, such as plasticity, cohesion, adhesion, etc. which determine the soil's ease of tillage. In the technical sense sandy soils are heavier per unit volume than clayey soils (Anonymous 2006b), which is also confirmed within the results in Table 10.1. In Figure 10.2 are shown the cross-sections with graphical illustration of the results from the Table 10.1.

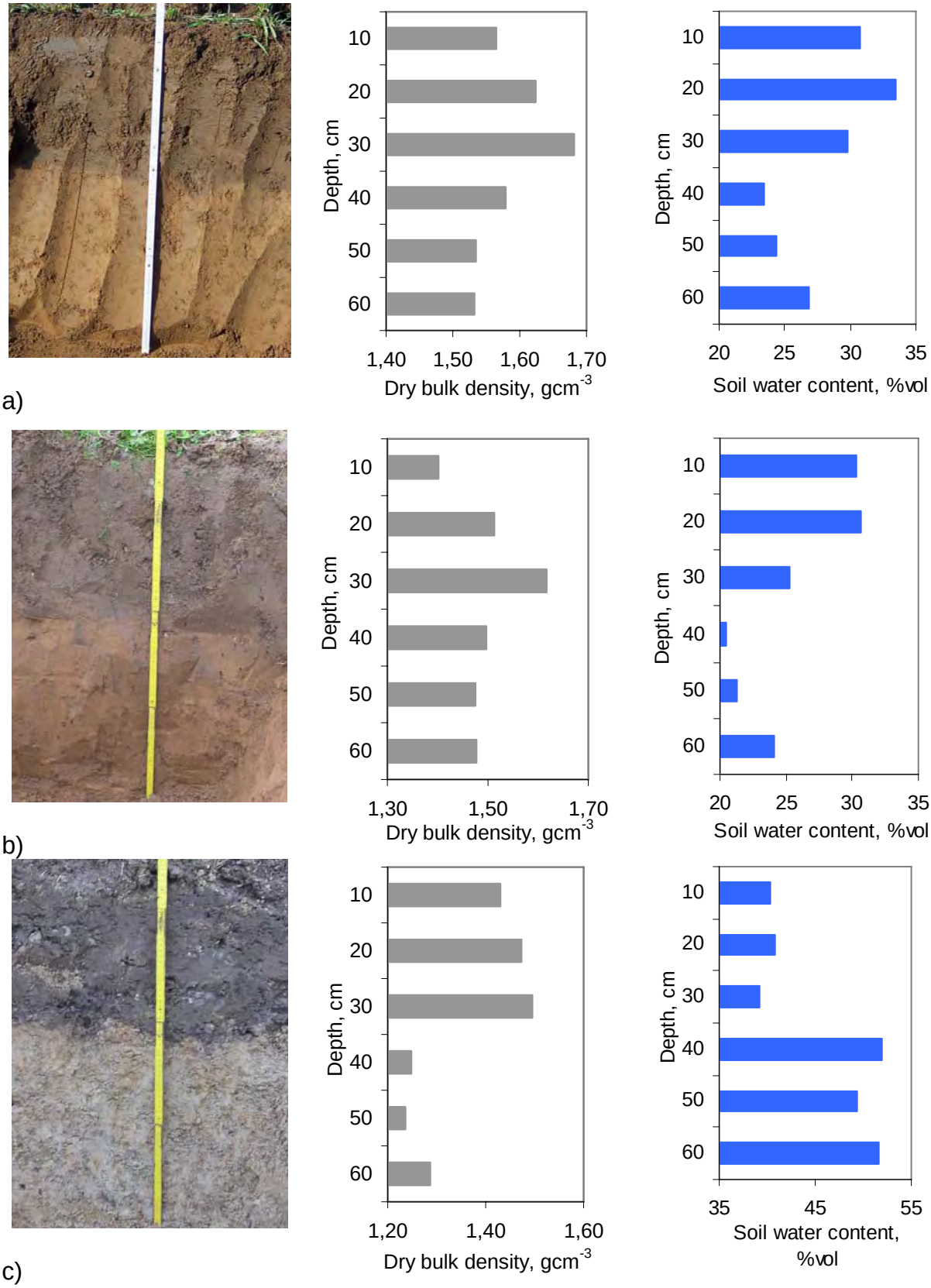

Figure 10.2 Soil profile in the field on the day of excavating and loading, dry bulk density and soil water content as a volume fraction: a) sand soil, b) silt soil, c) clay soil

The probes were taken and the soil was excavated and loaded in the winter and spring 2005. The water content was in range from 20%vol to over 50%vol, with very different values throughout the depth. Since it was needed to replicate natural conditions in the laboratory environment and it was not possible to cut out a soil cube of 4,5 m^3 (2 x 3 x 0,75 m) and to move it to the laboratory, the following method was chosen. The soil layer was divided into two areas, evidently differentiated in the profile on all three locations by different colours by all three soil types in Figure 10.2. The difference in colours was noticed at the depth of 30 cm to 35 cm, which was assumed to provide different soil properties. The upper layer is usually richer in plant residues, mixed by regular agricultural measures and lower layer is less disturbed with less plant residues and moved only rarely by deep ploughing. Thus the upper layer was set at first 30 cm of depth and lower layer at following 30 cm. In Table 10.1 on the right side are shown mean values for in this manner divided layers. The values were supposed to be replicated in the soil box under in order to provide field-near laboratory conditions.

A digger, shown in Figure 10.3 was used for excavating and loading of two different layers into trailers. In Figure 10.3 left the excavating and loading of upper layer is shown, in which the limitation of digging was more the colour of the soil than the depth, although the depth corresponded to the measured depth of 30 to 35 cm. In the same Figure right, further 30 cm deep layer was excavated and loaded into second trailer.

Figure 10.3 Digging and loading of the clay soil at Frankenforst research station, 9th of February 2005: left upper layer, right lower layer

The soil material was transported and reloaded into three soil boxes in two layers, forming the near-field cross-section. The detailed description of the soil boxes, together with the whole test stand is given in Chapter 6.3. The lower layer in the soil box was 40 cm thick consisted of the “lower layer soil” from the field and the upper layer in the soil box, consisted of “upper layer soil” from the field, added 30 cm to the total depth of 70 cm in the soil boxes. This method enabled approximate field conditions shown in Table 10.1, without intention or potential to replicate it entirely.